Award Number:
W81XWH-05-2-0094

TITLE:

Physical and Neuropsychiatric Trauma-Wound Healing and Tissue Preservation

PRINCIPAL INVESTIGATOR:

Michael Weiner, M.D.

CONTRACTING ORGANIZATION:
Northern California Institute for Research and Education, Inc.
San Francisco, CA 94121-1545

REPORT DATE:
October 2008

TYPE OF REPORT:
Annual

PREPARED FOR: U.S. Army Medical Research and Materiel Command
Fort Detrick, Maryland 21702-5012

DISTRIBUTION STATEMENT:

Approved for public release; distribution unlimited

REPORT DOCUMENTATION PAGE				*Form Approved* *OMB No. 0704-0188*
Public reporting burden for this collection of information is estimated to average 1 hour per response, including the time for reviewing instructions, searching existing data sources, gathering and maintaining the data needed, and completing and reviewing this collection of information. Send comments regarding this burden estimate or any other aspect of this collection of information, including suggestions for reducing this burden to Department of Defense, Washington Headquarters Services, Directorate for Information Operations and Reports (0704-0188), 1215 Jefferson Davis Highway, Suite 1204, Arlington, VA 22202-4302. Respondents should be aware that notwithstanding any other provision of law, no person shall be subject to any penalty for failing to comply with a collection of information if it does not display a currently valid OMB control number. **PLEASE DO NOT RETURN YOUR FORM TO THE ABOVE ADDRESS.**				
1. REPORT DATE *(DD-MM-YYYY)* 30-10-2008	**2. REPORT TYPE** Annual			**3. DATES COVERED** *(From - To)* Oct. 1, 2007– Sep 30, 2008
4. TITLE AND SUBTITLE Physical and Neuropsychiatric Trauma-Wound Healing and Tissue Preservation				**5a. CONTRACT NUMBER**
				5b. GRANT NUMBER W81XWH-05-2-0094
				5c. PROGRAM ELEMENT NUMBER
6. AUTHOR(S) Lilly Bourguignon, PhD; Valerie Cardenas-Nicholson, PhD; Wenhan Chang, PhD; Linda L. Chao, PhD; Rajvir Dahiya, PhD; Peter Elias, MD; Grant Gauger, MD; Eric Huang, MD, PhD; Gary A. Jarvis, PhD; Hubert Kim, MD, PhD; Stephen Massa, MD, PhD; Thomas C. Neylan, MD; Norbert Schuff, PhD; Karen Seal, MPH, PhD; William Seaman, MD; Wang Zhan, PhD. robert.obana@ncire.org Michael Weiner, M.D.				**5d. PROJECT NUMBER**
				5e. TASK NUMBER
				5f. WORK UNIT NUMBER
7. PERFORMING ORGANIZATION NAME(S) AND ADDRESS(ES) Northern California Institute for Research and Education, Inc. San Francisco, CA 94121-1545				**8. PERFORMING ORGANIZATION REPORT NUMBER**
9. SPONSORING / MONITORING AGENCY NAME(S) AND ADDRESS(ES) U.S. Army Medical Research & Materiel Command 504 Scott Street Fort Detrick, MC 21702-5012				**10. SPONSOR/MONITOR'S ACRONYM(S)**
				11. SPONSOR/MONITOR'S REPORT NUMBER(S)
12. DISTRIBUTION / AVAILABILITY STATEMENT				
13. SUPPLEMENTARY NOTES				

14. ABSTRACT

The Neuroscience Center of Excellence at San Francisco VA Medical Center is a unique VA/Department of Defense research collaboration with the goal of *predicting*, *anticipating*, and *reducing* the effects of injury on our warfighters and veterans, potentially minimizing veterans' long-term disabilities and their subsequent impact on the health care system. It represents a joint collaborative research effort between SFVAMC, Department of Defense, and NCIRE that combines military knowledge of health impairments to warfighters with VA data and expertise on prediction, prevention, diagnosis, and intervention.

What follows are the individual Progress Reports of the various projects funded by this Program. See each pilot study for individual abstract.

Three of the pilot studies (PI: Rajvir Dahiya, PhD; Stephen Massa, MD, PhD; William Seaman, MD) have been completed in 2008 and final reports are included for these specific pilot studies.

15. SUBJECT TERMS
Traumatic Brain Injury, MRI, Spinal Cord Injury

16. SECURITY CLASSIFICATION OF:			**17. LIMITATION OF ABSTRACT**	**18. NUMBER OF PAGES**	**19a. NAME OF RESPONSIBLE PERSON** usamrc
a. REPORT unclassified	**b. ABSTRACT** unclassified	**c. THIS PAGE** unclassified	unlimited	227	**19b. TELEPHONE NUMBER** *(include area code)*

Standard Form 298 (Rev. 8-98)
Prescribed by ANSI Std. Z39.18

Table of Contents

Three Final Reports for Pilot Studies Completed in FY 2008:

Project Study 1:

Novel Astrocyte Signaling Therapy to Promote Neuronal Regrowth and Suppress Glial Scarring During Traumatic Brain and Spinal Cord Injury

Principal Investigator: Lilly Y.W. Bourguignon, Ph.D., Professor of Medicine

ABSTRACT

Traumatic spinal cord injury (SCI) of combat soldiers can greatly increase morbidity/mortality and significantly delay or prevent their return to normal physical activities. Functional recovery after serious traumatic SCI remains limited. This study focuses on specific aspects of astrocyte functions required for neuronal outgrowth, axonal regeneration and glial scar formation. Results from these proposed studies will provide important novel insights into the mechanism(s) by which selective cellular signaling regulates astrocyte functions, and will offer new approaches to modulate glial scarring processes. In this study we observed that after spinal cord injury (SCI), a glial scar surrounds the lesion and becomes a major obstacle to axonal regeneration. Formation of the glial scar involves astrocyte migration toward the lesion. Matrix metalloproteinases (MMPs), including MMP-9 and MMP-2, govern cell migration through their ability to degrade constituents of the extracellular matrix. Although MMP-9 and MMP-2 are expressed in reactive astrocytes, their involvement in astrocyte migration and glial scar formation is unknown. We also examined the role of these MMPs in astrocyte migration using an *in vitro* scratch wound assay and astrocytes cultured from MMP-9-null, MMP-2-null, and wild-type (expressing MMPs) mice. MMP-9-null astrocytes and wild-type astrocytes treated with an MMP-9 inhibitor exhibited impaired migration relative to untreated wild-type controls. MMP-9-null astrocytes showed abnormalities in the actin cytoskeleton organization and function but no detectable untoward effects on proliferation, cellular viability, or adhesion. In contrast to MMP-9, MMP-2-null astrocytes showed increased migration which could be attenuated in the presence of an MMP-9 inhibitor. Given the prominent role of MMP-9 in astrocyte migration, we evaluated glial scar formation in spinal cord injured, MMP-9 null mice. Consistent with *in vitro* findings, glial scar formation was abrogated in MMP-9-null relative to wild-type mice. Moreover, there was a reduction in the expression of chondroitin sulfate proteoglycans, indicating a more permissive environment for axonal regeneration/plasticity. Collectively, our studies provide the first evidence that MMP-9 plays an important role in cytoskeleton-mediated astrocyte migration and promotes glial scar formation in the injured cord and thus may be a promising therapeutic target to improve recovery after spinal cord injury.

TABLE OF CONTENTS

INTRODUCTION

After spinal cord injury, one of the major causes leading to the regenerative failure of injured axons is the formation of a glial scar. The glial scar, consisting mainly of reactive astrocytes, not only forms a non-permissive physical barrier to the regenerative axons but also expresses inhibitory molecules such as chondroitin sulfate proteoglycans (CSPGs), which chemically arrest the regrowth of injured axons across the lesion (Silver and Miller, 2004). Formation of the glial scar is primarily attributed to astrocyte migration towards the lesion with only a minor contribution resulting from astrocyte proliferation (Ridet et al., 1997; Fitch et al., 1999; McGraw et al., 2001; Matyash et al., 2002). The migratory behavior of reactive astrocytes depends on the dynamics of actin cytoskeleton mediated by small GTPases Rho and Rac1 (Etienne-Manneville and Hall, 2002; Bourguignon et al., 2007), integrity of the intermediate filament including vimentin and glial fibrillary acidic protein (GFAP) (Menet et al., 2003), cell adhesion (Okada et al., 2006), and water fluxes across the plasma membrane (Saadoun et al., 2005).

We have previously shown that matrix metalloproteinases (MMPs), including MMP-2 and MMP-9, are expressed in reactive astrocytes after spinal cord injury (Noble et al., 2002; Hsu et al., 2006), raising the possibility that these MMPs may participate in the formation of the glial scar. Consistent with that possibility, recent studies have shown that astrocyte migration is modulated by MMPs (Ogier et al., 2006; Takenaga and Kozlova, 2006). MMPs are a family of zinc-dependent endopeptidases that can degrade a variety of protein constituents in the extracellular matrix (ECM) and thus remodel the pericellular microenvironment for cell translocation (Sternlicht and Werb, 2001). As such MMPs modulate numerous pathological and tissue repair processes in the nervous system particularly those that require cell migration (Yong et al., 2001). The modulatory effect of MMPs in this context is largely dependent on the temporospatial expression of different MMP subtypes and their cellular sources (Yong, 2005). Thus, in the injured spinal cord, it is likely that MMPs may exert both beneficial and detrimental effects, depending upon which members of the family are involved and when and where they are actively expressed.

In the injured spinal cord, reactive astrocytes are the source of both MMP-2 and MMP-9 (Duchossoy et al., 2001). Contrary to a promotive role of MMP-2 in astrocyte migration *in vitro* (Ogier et al., 2006), we previously demonstrated that mice deficient in MMP-2 develop a more extensive glial scar in the injured spinal cord (Hsu et al., 2006). Interestingly, these mice also show a compensatory increase in MMP-9, raising the intriguing possibility that the more severe glial scar results from the compensatory up-regulation of MMP-9. Here we test the hypothesis that MMP-9 facilitates astrocyte migration and contributes to the formation of a glial scar in the injured spinal cord. To test this hypothesis, we examined the relationship between MMP-9, astrocyte migration *in vitro*, and glial scarring *in vivo*. Our results offer a new insight into the role of MMP-9 in wound healing after spinal cord injury.

BODY

Astrocyte migration is dependent on MMP-9: To determine if MMPs, particularly MMP-9, are involved in astrocyte migration, cultured wild-type astrocytes were exposed to GM6001, a general inhibitor of MMPs, after a scratch-wound. Migration was significantly impaired in astrocytes treated with varying concentrations of GM6001 (Fig. 1A). Similarly, when wild-type astrocytes were treated with an MMP-9 inhibitor, migration was significantly reduced at all concentrations of the inhibitor (Fig. 1B). These findings demonstrate that MMP-9 facilitates astrocyte migration. Notably, astrocyte migration was reduced but not completely blocked with either a general inhibitor or a specific MMP-9 inhibitor, suggesting that MMPs are not the sole modulators of astrocyte migration.

MMP-9 modulates migration in MMP-2-null astrocytes: We have previously demonstrated that MMP-2 null mice manifest a more extensive glial scar along with a compensatory increase in MMP-9 activity in the injured spinal cord compared to the wild-type mice (Hsu et al., 2006). It is unclear if enhanced scarring results from a deficiency in MMP-2 and/or up-regulation of MMP-9. To address this issue, we compared the migratory behavior of MMP-2 null and wild-type astrocytes in the scratch wound assay (Fig. 2). Similar to *in vivo* findings, migration was enhanced in MMP-2 null astrocytes. To determine the dependency of this migration on MMP-9, migration was assayed in the presence of an MMP-9 inhibitor. Migration was significantly reduced in the presence of the MMP-9 inhibitor. These findings, together with those from cultured MMP-9 null astrocytes, support the hypothesis that MMP-9 plays a pivotal role in astrocyte migration *in vitro*.

MMP-9 deficiency alters actin-cytoskeleton organization and reduces astrocyte migration: The actin cytoskeleton participates in the morphological changes and migration of astrocytes (Baorto et al., 1992; Ramakers and Moolenaar, 1998; Etienne-Manneville and Hall, 2002; Holtje et al., 2005; Bourguignon et al., 2007). In particular, Rho GTPases, such as Rac1 are known to play an important role in regulating filamentous actin (F-actin) formation and those activities required for forming astrocyte membrane protrusions and cell migration (Etienne-Manneville and Hall, 2002; Bourguignon et al., 2007).
To determine whether MMPs, specifically MMP-2 and MMP-9, affect the organization of actin cytoskeleton required for astrocyte migration, we assessed the distribution of the actin cytoskeleton in astrocytes using fluorescent phalloidin to label F-actin. F-actin fibers were mostly distributed in the cell body of both wild-type (Fig. 3A-i) and MMP-2 null astrocytes (Fig. 3B-i). In contrast, only cortical actin underlying the plasma membrane and very little cell body F-actin fibers were detected in MMP-9 null astrocytes (Fig. 3C-i). Such a disarrangement of F-actin fibers in MMP-9 null astrocytes suggests that MMP-9 deficiency, but not MMP-2 deficiency, alters F-actin assembly and distribution in astrocytes. Treatments with cytoskeleton inhibitors cytochalasin D (known to impair F-actin formation) or Rac1 inhibitor (a signaling perturbation agent that blocks Rac1 activation) resulted in the disassembly of both cell body F-actin fibers and cortical actin, along with dramatic changes in the cell shape in astrocytes of all 3 genotypes examined (Fig. 3A-, B-, C-ii, iii), suggesting the importance of actin cytoskeleton in maintaining the morphological integrity of astrocytes.
In the scratch wound assay, F-actin-associated membrane protrusions projecting from the wounding edges toward the migration front were evident in both wild-type (Fig. 3D-i) and MMP-2 null astrocytes (Fig. 3E-i), but negligible in MMP-9 null astrocytes (Fig. 3F-i). Treatment with either cytochalasin D or Rac1 inhibitor resulted in F-actin disarrangement, loss of scratch-induced membrane protrusions, and cell rounding in astrocytes of all 3 genotypes (Fig.

3D-, E-, F-ii, iii). Cytochalasin D or Rac1 inhibitor also significantly attenuated astrocyte migration in all 3 genotypes (Fig. 4), suggesting a close relationship between the integrity of actin cytoskeleton, cell morphology, and astrocyte motility. Together, these findings indicate that deficiency in MMP-9, but not MMP-2, is closely associated with aberrant F-actin assembly which contributes to the inhibition of membrane projection formation, migration, and wound closure of astrocytes.

Deficiency of MMP-2 or MMP-9 does not affect astrocyte proliferation, adhesion, and viability: It is possible that deficiency in either MMP-2 or MMP-9 has untoward effects on astrocyte proliferation, adhesion, and viability, which may contribute to the altered migration observed above. Proliferation, defined by BrdU incorporation was studied in cultured wild-type, MMP-2 null, and MMP-9 null astrocytes (Fig. 5A, B, C). Quantitative analysis showed that the number of proliferative astrocytes were comparable among the 3 genotypes (Fig. 5D). Adherence, assessed in these groups one day after the first passage, was similar among genotypes (Fig. 5E). Astrocyte viability, determined by cellular metabolic activity using the MTT assay, revealed no differences between genotypes 1, 2, and 3 days after the first passage (Fig. 5F). These findings suggest that deficiency of MMP-2 or MMP-9 does not differentially affect astrocyte proliferation, adhesion, or viability, parameters that would influence migration.

MMP-9 deficiency reduces glial scarring and the expression of CSPGs in injured spinal cord: Based on *in vitro* findings of hindered migration of MMP-9 null astrocytes, we next determined if MMP-9 deficiency would reduce glial scar formation *in vivo* after spinal cord injury. The severity of glial scarring was compared between wild-type mice and MMP-9 null mice 42 days after a contusive spinal cord injury. Wild-type mice had a remarkably more complicated pattern of glial scarring with prominent bundling of thick astrocytic processes than MMP-9 null mice (Fig. 6A-D). In addition, the intensity of GFAP immunoreactivity appeared higher in wild-type mice as compared to MMP-9 null mice. The severity of glial scar formation was analyzed by a semi-quantitative scale, based on the complexity and extent of the scarring (Fig. 6E-H). MMP-9 null mice had a significantly lower total score than the wild-type mice (136 ± 21 vs 180 ± 35, $p < 0.05$) (Fig. 6F). We further analyzed whether such a lower total score in MMP-9 null mice was a result of less complicated (i.e. lower average score per sector) or less extensive (i.e. fewer sectors scored ≥ 1) glial scarring. We found that the average score per sector was significantly lower in the MMP-9 null mice than in the wild-type mice (2.2 ± 0.1 vs 2.4 ± 0.2, $p < 0.05$) (Fig. 6G), although the number of sectors scored ≥ 1 was comparable between these two groups (63 ± 11 vs 74 ± 9) (Fig. 6H). These findings indicate that MMP-9 null mice have a less complicated pattern of glial scarring than wild-type mice.
Expression of inhibitory molecules CSPGs by reactive astrocytes is known to cause regenerative failure of injured axons in the CNS (Davies et al., 1997; McKeon et al., 1999). Quantitative assessment revealed that MMP-9 null mice had significantly lower CSPG immunoreactivity than the wild-type mice ($2.4 \pm 0.7\%$ vs $3.8 \pm 1.2\%$, $p < 0.05$) 42 days post-injury (Fig. 7A-C). In summary, MMP-9 deficiency results in the formation of a less complex and less inhibitory glial scar.

MMP-9 deficiency does not alter MMP-2 expression: We previously demonstrated that MMP-2 is beneficial to wound healing because spinal cord-injured MMP-2 null mice exhibit a more complex and inhibitory glial scar, reduced white matter sparing, and impaired locomotor recovery (Hsu et al., 2006). Importantly, these MMP-2 null mice also show a compensatory increase in MMP-9. Here we determine if the beneficial effect on reduced glial scarring seen in MMP-9 null mice is due to a compensatory up-regulation of MMP-2. Gelatin zymography

revealed the expression of pro- and active MMP-2 in the injured spinal cords of both MMP-9 null and wild-type mice at 7 day post-injury (Fig. 8), a time point when the expression of MMP-2 peaks in the lesion (Goussev et al., 2003). However, there were no qualitative differences in the expression of MMP-2 between these genotypes. These findings suggest a more direct involvement of MMP-9 in glial scar formation.

Materials and Methods

Animals
These studies were approved by the Institutional Animal Care and Use Committee at the University of California San Francisco and in accordance with the National Institute of Health Guide for the Care and Use of Laboratory Animals. Young breeding pairs on an FVBn background ranged in ages from 3 to 6 months. MMP-2 null, MMP-9 null, and wild-type progeny on an FVBn background were generated by breeding homozygous females and males of respective genotypes. Mice were housed in a controlled environment at 25 °C with a 12 hour light-and-dark cycle. Food and water were provided *ad libitum*. The genotypes of animals were identified by the polymerase chain reaction using tail tissue and specific oligonucleotide primers (Itoh et al., 1997; Itoh et al., 1998; Vu et al., 1998; Ducharme et al., 2000) and confirmed by gel zymography using samples of blood.

Astrocyte culture
Cortical astrocytes were cultured from the cerebral cortex of MMP-2 null, MMP-9 null, and wild-types at postnatal day 1 or 2, based on a previously described protocol with some modifications (Rose et al., 1993). The cerebral cortices were dissected from the brain stem, while the hippocampus, adherent meninges, and blood vessels were removed. The cerebral cortices were triturated repeatedly in 0.05% trypsin and 0.05% DNAse in Ca^{++} and Mg^{++} free Hank's balanced salt solution. Cells were pelleted by centrifugation at 250 rpm for 5 minutes, resuspended, filtered through a 70 μm nylon cell strainer, and plated in a poly-L-lysine-coated flask containing Earle's MEM medium supplemented with 10% fetal bovine serum, 22 mM glucose, and 2 mM GlutaMAX-1 (35050-061; Invitrogen, Carlsbad, CA). After 24 hours of incubation in 5% CO_2 at 37°C, the flask was shaken vigorously to remove debris and unattached cells prior to fresh medium replacement. Shaking was repeated before changing the culture medium at 3, 5, and 7 days after astrocyte isolation and weekly thereafter. The purity of astrocyte cultures was approximately 95% and was determined by the number of cells immunostained with GFAP relative to the total nuclei that had been labeled with Hoechst dye. For all *in vitro* studies described below, three triplicates, each of which consisted of three wells, were examined in each genotype or treatment at any given time point.

Scratch wound assay
Cultured astrocytes were trypsinized and replated into tissue culture-treated, 24-well plates at a concentration of 2×10^5 cells/well after the first passage. Five to seven days later when astrocytes reached confluence, a denuded area was produced by scratching the inside diameter of the well with a 10 μl pipette tip (Bourguignon et al., 2007). After 3 rinses with Earle's MEM medium, fresh culture medium containing 10 μM cytosine arabinofuranoside (C1768; Sigma, St. Louis, MO) was added into each well to inhibit cell proliferation. One digital photograph was taken from each well immediately after the scratch wound was made (0 hour) and at 24, 48, and 72 hours later. The denuded area was gradually covered by migrating astrocytes. With the use of ImageJ image processing program (1.33u; National Institutes of Health, Bethesda, MD), the size of the denuded area was determined at each time point from digital images. The astrocyte-

covered area was obtained by subtracting the denuded area void of astrocytes at any given time point from the original denuded area measured at 0 hour in the same well.

To determine the dependency of migration on MMPs and actin cytoskeleton, astrocytes were treated with the following inhibitors: GM6001, a general inhibitor of MMPs (364205; Calbiochem, San Diego, CA); MMP-9 inhibitor (444278; Calbiochem,); cytochalasin D (20 µg/ml, C8273; Sigma); and Rac 1 inhibitor (50 µM, 553530; Calbiochem). The optimal concentrations for GM6001 and MMP-9 inhibitor were determined by dose-response studies using wild-type astrocytes. GM6001 was dissolved in sterile-filtered dimethyl sulfoxide (DMSO) with final concentrations at 20 µM, 40 µM, and 80 µM. A GM6001 analogue (364210; Calbiochem) was used as the negative control at a concentration of 20 µM. Likewise, MMP-9 inhibitor was dissolved in DMSO at 0.5 µM, 1.0 µM, and 2.0 µM, while the DMSO was used as the vehicle control.

Fluorescence staining of actin cytoskeleton

To test the effects of various inhibitors on the actin cytoskeleton rearrangement, astrocytes cultured from wild-type, MMP-2 null and MMP-9 null mice were treated with 20 µg/ml cytochalasin D, 50 µM Rac1 inhibitor, or no drug for 1 hour at 37°C. Subsequently, a scratch wound was made on the astrocyte monolayer using a 10µl pipette tip as described above. After 24 hours of incubation at 37°C, astrocytes were fixed with 2% paraformaldehyde, permeablized by 90% ethanol, and incubated with Texas Red-conjugated pholloidin (Molecular Probes). Another set of astrocytes without a scratch wound were stained simultaneously. The fluorescence labeled astrocytes were examined with a confocal laser scanning microscope.

Astrocyte proliferation assay

Proliferative astrocytes of different genotypes were identified by 5-bromo-2'-deoxyuridine (BrdU) incorporation. After the first passage, astrocytes were transferred into a 24-well plate at 1 $\times$ 10^5 cells/well with a poly-L-lysine-coated coverslip on the bottom of each well. At approximately 40-50% confluence, astrocytes were rinsed with Earle's MEM medium for 3 times, incubated in non-serum culture medium for 24 hours, and incubated with 30 µM BrdU (B9285; Sigma) in culture medium containing 10% fetal bovine serum for 2 hours. The astrocytes were fixed with cold 70% ethanol at 4°C for 20 minutes, air dried, and rinse with 2 N HCl for 20 minutes for DNA denaturation. After 3 washes with phosphate buffered saline (PBS), astrocytes were reacted with Alexa Fluor 594-conjugated mouse monoclonal anti-BrdU (1:100, A-21304; Molecular Probes, Eugene, OR) diluted in blocking and permeablizing solution containing 2% normal goat serum, 0.2% Triton X-100, and 0.1% bovine serum albumin in PBS for 4 hours at room temperature. Double labeling was performed by using rabbit polyclonal anti-GFAP (1:200, Z0334; Dako Cytomation, Carpinteria, CA) diluted in above blocking and permeablizing solution, followed by FITC-conjugated anti-rabbit secondary antibody. The nuclei of astrocytes were stained with 300 nM 4',6-diamidino-2-phenylindole (DAPI; D3571; Molecular Probes) for 3 minutes and the coverslip was mounted onto a slide. A proliferative astrocyte was defined by positive staining for anti-BrdU, -GFAP, and DAPI. The numbers of proliferative astrocytes were counted using an epifluorescent microscope with a 10× objective within 6 adjacent fields in the center of the coverslip. Proliferative astrocytes were expressed as a percentage of the number of BrdU positive cells relative to the total number of DAPI positive nuclei.

Astrocyte adhesion assay

Astrocytes were replated into a poly-L-lysine-coated 12-well plate at 1 $\times$ 10^5 cells/well after the first passage and incubated for 24 hours. The wells were shaken slightly and rinsed with Earle's

MEM medium for 3 times to remove unattached cells. By using an inverted phase contrast microscope with 20× objective, the number of adherent astrocytes was determined in 8 adjacent fields in the center of the well. Results of MMP-2 and MMP-9 null astrocytes were normalized with that of the wild-type astrocytes.

Astrocyte viability assay
To assess the influence of MMP deficiency on astrocytic viability, the metabolic activity of mitochondria was examined by a quantitative colorimetric assay using [3-(4,5-dimethylthiazol-2-yl)-2,5-diphenyl] tetrazolium bromide (MTT; M2128; Sigma) as previously described (Mosmann, 1983). Briefly, cultured astrocytes were transferred into a 96-well plate after the first passage at a concentration of 1×10^4 cells/100 µl medium/well and incubated for 1, 2, and 3 days. After 10 µl of 0.5% MTT was added into the well, the astrocytes were further incubated for 4 hours. Then the astrocytes were dissolved with 100 µl acidic isopropanol containing 0.04 N HCl. The optical density of the resultant formazan product was measured at 550 nm by a plate reader.

Contusive spinal cord injury
Male MMP-9-null and wild-type mice, weighing 30-35 g (approximately 4-6 months of age), were anesthetized (2.5% tribromoethanol, 0.02 ml/g body weight, i.p., T48402; Sigma) and subjected to a moderate contusion injury to the spinal cord as we described previously (Noble et al., 2002). Body temperature of the mice was maintained at 37°C with a warming pad throughout the surgery and during the recovery from anesthesia. Post-operative care included subcutaneous administration of 1 ml 0.9 % Sulfamethoxazole-Trimethoprim (GensiaSicor, Irvine, CA) and manually voiding the urinary bladder twice a day

Tissue preparation and immunohistochemistry
Animals were deeply anesthetized 42 days post-injury. Ice-cold normal saline was perfused transcardially, followed by 4% paraformaldehyde in 0.1 M phosphate buffer, pH 7.4 for 10 minutes. The spinal cord was removed and immersed in the same fixative at 4°C for 4 hours. Then the spinal cord was transferred into 30% sucrose in 0.1 M PBS for cryoprotection. Cryosections of the spinal cord were cut transversely at 20 µm in a cryostat, mounted onto glass slides, and stored at −20°C for further processing.
The following primary antibodies were used for immunohistochemistry: Cy3-conjugated mouse anti-GFAP (to label astrocytes, 1:400, clone G-A-5, C9205; Sigma) and mouse anti-CSPGs (1:200, clone CS-56, C8035; Sigma). Cryosections were rinsed with 0.01 M PBS 3 times and blocking solution consisting of 2% normal goat serum and 0.1% bovine serum albumin in PBS at room temperature for 5 minutes. Incubation of the primary antibodies, diluted in above blocking solution, was performed in a humidified box at 4°C overnight. Sections immunolabeled by anti-GFAP were rinsed with PBS and coverslipped with ProLong Antifade (P-7481; Invitrogen), whereas those immunolabeled by anti-CSPGs were further incubated with biotinylated goat anti-mouse IgM (1:200, 115-065-075; Jackson ImmunoResearch, West Grove, PA) for 30 minutes. The labeling of anti-CSPGs was visualized by a biotin-avidin peroxidase reaction using a Vectastain Elite ABC kit (PK-6100; Vector Laboratories, Burlingame, CA) in combination with 0.05% diaminobenzidine as the chromogen and 0.001% hydrogen peroxide in 0.01 M PBS. Sections of different genotypes were grouped together and processed simultaneously in the same experimental condition to minimize staining variables for subsequent quantitative analyses. An additional group of sections was processed without using primary antibodies to serve as the negative control.

Assessment of the glial scar
The astroglial scar was visualized by Cy3-conjugated anti-GFAP antibody 42 days post-injury (n = 6 per genotype). The severity of glial scarring was analyzed semi-quantitatively by scoring its complexity and extent as we originally described (Hsu et al., 2006). Briefly, the transverse section of the injured cord was subdivided into 12 sectors by superimposing a grid onto the digitized image of the section using Photoshop 7.0 (Adobe Systems, San Jose, CA). In each sector, the pattern of the glial scar, distribution of astrocytes, organization of astrocytic processes, astrocytic hypertrophy, and the intensity of GFAP immunoreactivity were evaluated and then a score ranging from 0 to 3 was given. A score of 0 indicates no evidence of glial scar formation, whereas a score of 1 to 3 represents increasing complexity of the glial scarring. The total score obtained from all 12 sectors in each transverse section reflected the severity (complexity and/or extent) of glial scar formation. In the lesion, GFAP-quiescent regions were excluded from the analysis because they were composed of non-astrocytic components such as macrophages and tissue matrix. Nine transverse sections, at intervals of 480 μm, were sampled across the entire lesion epicenter in each animal.

Assessment of CSPG immunoreactivity
The intensity of CSPG immunoreactivity in the injured cord was quantified 42 days post-injury (n = 7 per genotype) as we previously described with some modifications (Hsu et al., 2006). Briefly, digital images of the immunostained sections were taken under consistent exposure parameters and were imported to the ImageJ image processing software. The intensity of background staining was evaluated on a reference section, which was approximately 1500 μm rostral to the lesion where there was no evident tissue damage. First, the total number of pixels in the reference section was obtained from the histogram. Then a threshold value was determined so that only 1% of the darkest pixels remained in the reference section. This threshold value, which eliminated 99% of background staining, was applied to the images of 4 to 5 sections sampled from the lesion epicenter of the same animal to reveal the pixels that were darker than the background staining. The number of these dark pixels, which represented the intensity of CSPG immunoreactivity, was counted and the percentage of these pixels over the total pixel number of a section was calculated. All sampled sections in each animal were averaged and the mean of each genotype was reported.

Gel zymography
The gelatinase levels of MMP-2 and MMP-9 in the injured spinal cord were examined 7 days post-injury by gel zymography as we previously described (Noble et al., 2002; Goussev et al., 2003). Injured MMP-9 null and wild-type mice (n = 3 per genotype) were deeply anesthetized and then the spinal cord segments containing the lesion were dissected and homogenized in lysis buffer consisting of 28 mM Tris-HCl, 22 mM Tris-base, pH 8, 150 mM NaCl, 1% Nonidet P-40 (74385; Fluka BioChemika, Ronkonkoma, NY), 0.5% sodium deoxycholate, and 0.1% SDS. In another group of wild-type mice receiving only laminectomy, the matched region of the uninjured spinal cord was used as the sham control. After the protein concentration of the homogenates was determined by the bicinchoninic acid method (BCA protein assay kit, 23225; Pierce, Rockford, IL), equal amounts of protein (5 μg) were loaded on a Novex 10% zymogram gel (EC61752; Invitrogen) and separated by electrophoresis with 120 V (6 mA) at 4°C for 120 minutes. The gel was then incubated with renaturing buffer (LC2670; Invitrogen) at room temperature for 30 minutes to restore the gelatinolytic activity of the proteins. After incubated with developing buffer (LC2676; Invitrogen) at 37°C for 48 hours, the gel was stained with 0.5% Coomassie blue for 60 minutes and then destained with 40% methanol containing 10% acetic

acid until appropriate color contrast was achieved.   Clear bands on the zymogram were indicative of gelatinase activity.

Statistic analysis

Data obtained from *in vitro* studies of cultured astrocytes were examined by the analysis of variance (ANOVA), followed by Bonferroni's *post-hoc* test for multiple comparisons between the means of genotypes, treatments, or time points. Quantitative evaluation of the glial scar and CSPG immunoreactivity were performed by 2 observers who were blinded to the experimental conditions and the means obtained from MMP-9 null and wild-type mice were compared by Student's *t*-test. Data are presented as means ± SD. A statistically significant difference is defined at $p < 0.05$.

KEY RESEARCH ACCOMPLISHMENTS

● Our results revealed that overexpression of matrix metalloproteinases (MMPs) such as MMP-2 and MMP-9 occurs in reactive astrocytes and glial scarring.

● We observed that astrocytes isolated from MMP-9-null (but not MMP-2-null) mice display abnormalities in the actin cytoskeleton organization and function. These findings suggest that MMPs (in particular, MMP-9) and the cytoskeleton are functionally coupled during astrocyte migration and glila scarring formation.

● Our data showed that both glial scar formation and chondroitin sulfate proteoglycan formation are abrogated in MMP-9-null relative to wild-type mice following spinal cord injury (SCI), indicating a more permissive environment for axonal regeneration/plasticity.

● We believe that our studies provide the first evidence that MMP-9 plays an important role in cytoskeleton-mediated astrocyte migration and promotes glial scar formation in the injured spinal cord and thus may be a promising therapeutic target to improve recovery after spinal cord injury (SCI).

REPORTABLE OUTCOMES

Funded Active Grants:

DOD (W81XWH-05-2-0094)	4/18/06-4/30/09
PI: Lilly Y.W. Bourguignon	$142,500 direct/yr1
Title: Novel astrocyte signaling therapy to promote	$285,000 direct/yrs1-2
neuronal regrowth and suppress glial scarring	
during traumatic brain injury.	

RO1CA66163 (PI)	7/1/06-6/30/11
NIH/NCI	$275,000 direct/yr 1
CD44/variant-cytoskeleton in breast cancer progression.	$1,375,000 direct/yrs 1-5

RO1CA78633 (PI)   2/1/03-1/31/09
NIH/NCI $283,000 direct/yr 1
CD44-p185HER2 Interaction in ovarian cancer progression. $1,415,000 direct/yrs 1-5

VA Merit Review Grant (PI)   10/1/03-9/30/09
Department of VeteransAffairs $240,000 direct/yr 1
CD44-EGF receptor signaling in head and neck cancer progression. $1,200,000 direct/yrs 1-5

Research Career Scientist Award (PI)   10/1/04-9/30/09
Department of Veterans Affairs $125,000 direct/yr 1
PI's Salary Support…………………………………………. $561,145 direct/yrs 1-5

2PO1 AR03944-15 (PI-project 2)   8/1/03-7/31/09
NIH $125,000 direct/yr 1
Relationship of keratinocyte function to differentiation . $625,000 direct/years 1-5(PI:
D.D. Bikle). Project 2: Hyaluronan-mediated CD44 signaling in keratinocytes.

Papers:

1.   Bourguignon, Lilly Y.W., K. Peyrollier, E. Gilad and A. Brightman. Hyaluronan-CD44 Interaction with N-WASP Promotes Actin Polymerization and ErbB2-Regulated β-Catenin Nuclear Translocation Leading to Cell Migration and Transcriptional Upregulation in Ovarian Tumor Cells. J. Biol. Chem. 282:1265-1280 (2007).

2.   Wang, Steven J., K. Peyrollier and Lilly Y.W. Bourguignon. The Influence of Hyaluronan-CD44 Interaction on Topoisomerase II Activity and Etoposide Cytotoxicity in Head and Neck Cancer. Arch Otolaryngol Head Neck Surg 133:281-288 (2007).

3.   Bourguignon, Lilly Y.W., K. Peyrollier, E. Gilad, A. Brightman and R.A. Swanson. Hyauronan-CD44 Interaction Stimulates Rac1 Signaling and PKNγ Kinase Activation leading to Cytoskeleton Function and Cell Migration in Astrocytes. J. Neurochem. 101:1002-1017 (2007).

4.   Wang, Steven J., V.B. Wreesmann and Lilly Y.W. Bourguignon. Association of CD44v3-Containing Isoforms with Tumor Cell Growth, Migration, Matrix Metalloproteinase Expression, and Lymph Node Metastasis in Head and Neck Cancer. Head & Neck 29:550-558 (2007).

5.   Bourguignon, Lilly Y.W., E. Gilad and K. Peyrollier. Heregulin-mediated ErbB2-ERK Signaling Activates Hyaluronan Synthases Leading to CD44-dependent Ovarian Cell Growth and Migration. J. Biol. Chem. 282:19426-19441 (2007).

6.   Bourguignon, Lilly Y.W. Hyaluronan-mediated CD44 Activation of RhoGTPase Signaling and Cytoskeleton Function Promotes Tumor Progression. Seminars in Cancer Biology 18:251-259 (2008).

7.   Bourguignon, Lilly Y.W., K. Peyrollier, W. Xia and E. Gilad. Hyaluronan-CD44 Interaction Activates Stem Cell-Specific Nanog Signaling, Stat-3-mediated MDR1 Gene

Expression and Ankyrin-regulated Multidrug Efflux in Breast and Ovarian Tumor Cells. J. Biol. Chem. 283:17635-17651 (2008).

8. Bourguignon, Lilly Y.W. Hyaluronan-mediated CD44 Interaction with Receptor and Non-receptor Kinases Promotes Oncogenic Signaling, Cytoskeleton activation and Tumor Progression. (Robert Stern, ed.), Elsevier Publication Co., San Diego, CA (In Press, 2009).

9. Hsu' JYC, Lilly Y. W. Bourguignon, Christen M. Adams, Karine Peyrollier, Haoqian Zhang, Christine Cun, Zena Werb, and Linda J. Noble-Haeusslein. Matrix Metalloproteinase-9 Facilitates Astrocyte Motility and Glial Scar Formation in the Injured Spinal Cord. J. Neuro Science (In Press, 2008).

10. Bourguignon' Lilly Y.W., Weiliang Xia and Gabriel Wong. Hylauronan-mediated CD44 Interaction with p300 and SIRT1 Regulates β-Catenin Signaling and NFκB -Specific Transcription Activity Leading to MDR1 and Bcl-x$_L$ Gene Expression and Chemoresistance in Breast Tumor Cells (Submitted to J. Biol. Chem. 2008).

Abstracts

1. Bourguignon, Lilly Y.W., Peyrollier, Karine, Gilad, Eli and Brightrman, A. Hyaluronan-CD44 Interaction with N-WASP Promotes Actin Polymerization and ErbB2-Regulated β-Catenin Nuclear Translocation Leading to Cell Migration and Transcriptional Upregulation in Ovarian Tumor Cells. American Association for Cancer Research (2007).

2. Wang, Steven, J, Peyrollier, K. and Bourguignon, Lilly Y.W. Hyaluronan-CD44 Interaction Influences Topoisomerase II activity and Etoposide Cytotoxicity in Head and Neck Cancer. American Association for Cancer Research (2007).

3. Bourguignon, Lilly Y.W., Guanwei Wei, Eli Gilad, Man, M.Q., Crumrine, D., Elias, P.M. Selective Haluronan-CD44 Activation of Keratinocyte Proliferation, Differentiation, Lamellar Body Formation and Secretion in Normal and Aged Epidermis. The Society for Investigative Dermatology (2007).

4. Hsu; J.-Y.C, Peyrollier; K., Bourguignon; Lilly Y.W. and Noble, L.J. Matrix metalloproteinase-9 as a modulator of astrocyte migration. The Society for Neuroscience (2007).

5. Bourguignon, Lilly Y.W., E. Gilad and K. Peyrollier. Heregulin-mediated ErbB2-ERK Signaling Activates Hyaluronan Synthases Leading to CD44-dependent Ovarian Cell Growth and Migration. American Association for Cancer Research (2008).

6. Bourguignon, Lilly Y.W., K. Peyrollier, W. Xia and E. Gilad. Hyaluronan-CD44 Interaction Activates Stem Cell-Specific Nanog Signaling, Stat-3-mediated MDR1 Gene Expression and Ankyrin-regulated Multidrug Efflux in Breast and Ovarian Tumor Cells. American Society for Cell Biology (2008).

CONCLUSION

Our studies demonstrate that MMP-9 facilitates astrocyte migration *in vitro* and glial scar formation in the injured spinal cord. By using cultured mouse cortical astrocytes, we found that MMP-9 deficiency, as a result of either pharmacological blockade or genetic deletion, significantly attenuated astrocyte migration in a scratch wound paradigm. This defective migratory behavior was concomitant with a disarranged actin cytoskeleton. Moreover, spinal cord-injured MMP-9 null mice developed a less severe and less inhibitory glial scar compared with wild-type controls. Such ameliorated glial scarring in MMP-9 null mice was independent of MMP-2 activity, which was comparable to that in the wild-type controls. Together, these findings suggest a promotive role for MMP-9 in glial scar formation through modulation of astrocyte migration.

MMPs and astrocyte migration
Here we show that MMPs and in particular MMP-9 governs astrocyte migration in an *in vitro* scratch wound assay. Pharmacologic blockade of MMPs, with a general inhibitor, as well as specific blockade of MMP-9 reduced migration. Astrocytes, cultured from MMP-9 null mice, likewise showed impaired migration. Our results are consistent with others that MMP-9 contributes to enhanced astrocyte migration (Takenaga and Kozlova, 2006; Hsieh et al., 2008). Such a promotive role in migration is further supported in other cell types where MMP-9 has been shown to facilitate neuronal migration of developing granule cells in the cerebellum (Vaillant et al., 2003) and the outgrowth of oligodendrocytic processes and remyelination (Oh et al., 1999; Larsen et al., 2003) by processing the ECM molecules. Our findings contrast that of Ogier et al. (2006), who reported that astrocyte migration principally depends on MMP-2, but not MMP-9. In their study, astrocytes were embedded in agarose drops and the migration was assessed by the extent of astrocyte migration from the agarose drops. They found that pharmacological blockade of MMP-2 substantially inhibited astrocyte migration and gelatinolytic activity, suggesting the involvement of MMP-2 in promoting astrocyte motility. Moreover, MMP-2 was co-localized with actin-associated motile structures such as filopodia and lamellipodia at the leading edge of migrating astrocytes. This discrepancy is likely resulted from the nature of different assays. Our scratch assay simulates an injury and the subsequent wound closure processes, which may involve different mechanisms of cell migration from those of the agarose drop assay.
How MMP-9 modulates astrocyte migration is not well understood. Astrocytes are known to secrete a variety of ECM molecules such as fibronectin, laminin, and hyaluronan (Yoshida and Takeuchi, 1991; Marret et al., 1994). Cell migration is a dynamic interplay of various processes including cell-ECM adhesion, extension of membrane projection and retraction of the trailing edge. Cell motility is also largely dependent on the organization of the actin cytoskeleton (Lauffenburger and Horwitz, 1996; Mitchison and Cramer, 1996), which is regulated through multiple signaling pathways mediated by the Rho family of small GTPases, including Rho, Rac, and Cdc42 (Hall, 1998). Activation of Rho in reactive astrocytes is associated with astrocyte motility *in vitro* and astrogliosis after spinal cord injury (Dubreuil et al., 2003; Goldshmit et al., 2004; Holtje et al., 2005). We previously demonstrated that Rac1 signaling is activated in astrocytes by the interaction between a transmembrane receptor CD44 and its ligand hyaluronan in the ECM, leading to increased migratory activity *in vitro* (Bourguignon et al., 2007). It has been shown that active MMP-9 can bind to CD44, and their pericellular interactions contribute to tumor cell migration (Bourguignon et al., 1998; Yu and Stamenkovic, 1999), suggesting synergism in the extracellular regulation of cell motility. We show here that Rac1 inhibitor or cytochalasin D significantly reduced astrocyte migration regardless of the genotypes in a scratch

assay, providing evidence for the involvement of the actin cytoskeleton in astrocyte motility. Moreover, MMP-9 null astrocytes exhibited a disorganized actin cytoskeleton. Together, these findings suggest that MMP-9 modulates astrocyte migration through a CD44-dependent process, thereby stimulating intracellular signaling that affects the assembly and distribution of actin cytoskeleton.

MMPs and glial scar formation

MMPs have diverse functions in the CNS (Yong, 2005). It has become increasingly apparent that their involvement is dictated by when and where they are activated and in the context of the injury or disease process. MMP-9 and MMP-2 are both expressed in injured spinal cord but in a temporally specific order. MMP-9 is actively expressed in the acutely injured cord (Noble et al., 2002; Wells et al., 2003), whereas MMP-2 is most prominent between 7-14 days after injury (Goussev et al., 2003) and is concurrent with the emergence of a glial scar. Differences between these MMPs are likely related to their distinct roles in the injured spinal cord. MMP-9, expressed in reactive astrocytes and infiltrating leukocytes, mediates early infiltration of inflammatory cells and disruption of the blood-spinal cord barrier (Noble et al., 2002). Thus, MMP-9 null mice show a significant improvement in locomotor recovery after spinal cord injury. While MMP-2 is also expressed in reactive astrocytes, it may limit the formation of an inhibitory glial scar and supports axonal regrowth as well as locomotor recovery (Hsu et al., 2006; Pastrana et al., 2006). Complimentary to our *in vitro* findings, we provide the first evidence that MMP-9 is also involved in glial scar formation. The glial scar is reduced in the spinal cord-injured MMP-9 null mice. Given its acute expression in reactive astrocytes, we suggest that MMP-9 may facilitate the early migration of astrocytes in the vicinity of the necrotic lesion. Thus, improved locomotor function in injured MMP-9 null mice may not only be due to blockade of early inflammatory cells (Noble et al., 2002) but to a reduction in the glial scar. Previously we found that MMP-2 null mice develop more extensive glial scarring than wild-type mice after spinal cord injury (Hsu et al., 2006). We also found a compensatory increase in MMP-9 in these injured MMP-2 null mice, a condition likewise occurring in experimental autoimmune encephalomyelitis (Esparza et al., 2004). Our results in this study further suggest that their extensive glial scarring and poorer recovery may not only be due to the absence of MMP-2 but to the adverse effects of increased expression of MMP-9.

Convergent evidence indicates that the glial scar, though a barrier to axonal regeneration, is also neuroprotective and beneficial to wound healing particularly at early phases after injury (Sofroniew, 2005). In response to an injury, prompt migration of reactive astrocytes seclude the lesion from uninjured tissue by compacting infiltrated inflammatory cells, resulting in more spared neuronal components and better recovery of function (Penkowa et al., 2003; Okada et al., 2006). Moreover, selective ablation of a subgroup of reactive astrocytes near a lesion in the first week after injury causes widespread inflammation, neuronal degeneration, failure of vascular barrier repair, and demyelination (Bush et al., 1999; Faulkner et al., 2004). In this context, spinal cord-injured MMP-9 null mice might be expected to display more extensive tissue damage due to compromised migration of reactive astrocytes. In fact, this does not occur in MMP-9 null mice, which exhibit restricted inflammation, preserved vascular barrier, and improved motor function relative to the wild-types in the acute stages of injury (Noble et al., 2002). Thus, the detrimental effects of MMP-9 on proteolytic tissue damage apparently outweigh its benefit of promoting astrocyte migration to restrain inflammatory responses early after the injury. In the chronic stages, conversely, MMP-9-dependent astrocyte migration culminates in an inhibitory glial scar that blocks axonal regrowth.

Reactive astrocytes in the glial scar also produce growth-inhibiting CSPGs, which restrain neurite outgrowth (McKeon et al., 1999; Jones et al., 2003; Tang et al., 2003). Enzymatic

treatment of the injured spinal cord with chondroitinase ABC significantly promotes axonal regeneration and recovery of motor function as a result of CSPG degradation (Bradbury et al., 2002; Chau et al., 2004). Similarly, both MMP-9 and MMP-2 are capable of degrading certain CSPGs (Muir et al., 2002; Larsen et al., 2003). In degenerated peripheral nerve, MMP-9 attenuates CSPG activity with a higher proteolytic effectiveness than MMP-2 (Ferguson and Muir, 2000). In spinal cord-injured MMP-9 null mice, nevertheless, we found reduced CSPG immunoreactivity in the lesion by 42 days post-injury. This outcome was not attributable to injury-induced MMP-2 activity, which was essentially comparable between injured MMP-9 null and wild-type mice. We suggest that this finding in MMP-9 null mice reflects a reduction in the over-all complexity of the glial scar (Refer to Figs. 6F, G). As such, a less complex glial scar, concomitant with reduced expression of CSPGs, may foster a more permissive environment that would support better recovery processes seen in spinal cord-injured MMP-9 null mice (Noble et al., 2002). Additional research with MMP conditional knockouts and selective MMP inhibitors will better delineate how temporally-specific modulation of MMP activity will affect wound healing events including the formation of the glial scar.

REFERENCES

Baorto DM, Mellado W, Shelanski ML (1992) Astrocyte process growth induction by actin breakdown. J Cell Biol 117:357-367.

Bourguignon LY, Gunja-Smith Z, Iida N, Zhu HB, Young LJ, Muller WJ, Cardiff RD (1998) CD44v(3,8-10) is involved in cytoskeleton-mediated tumor cell migration and matrix metalloproteinase (MMP-9) association in metastatic breast cancer cells. J Cell Physiol 176:206-215.

Bourguignon LY, Gilad E, Peyrollier K, Brightman A, Swanson RA (2007) Hyaluronan-CD44 interaction stimulates Rac1 signaling and PKN gamma kinase activation leading to cytoskeleton function and cell migration in astrocytes. J Neurochem 101:1002-1017.

Bradbury EJ, Moon LD, Popat RJ, King VR, Bennett GS, Patel PN, Fawcett JW, McMahon SB (2002) Chondroitinase ABC promotes functional recovery after spinal cord injury. Nature 416:636-640.

Bush TG, Puvanachandra N, Horner CH, Polito A, Ostenfeld T, Svendsen CN, Mucke L, Johnson MH, Sofroniew MV (1999) Leukocyte infiltration, neuronal degeneration, and neurite outgrowth after ablation of scar-forming, reactive astrocytes in adult transgenic mice. Neuron 23:297-308.

Chau CH, Shum DK, Li H, Pei J, Lui YY, Wirthlin L, Chan YS, Xu XM (2004) Chondroitinase ABC enhances axonal regrowth through Schwann cell-seeded guidance channels after spinal cord injury. Faseb J 18:194-196.

Davies SJ, Fitch MT, Memberg SP, Hall AK, Raisman G, Silver J (1997) Regeneration of adult axons in white matter tracts of the central nervous system. Nature 390:680-683.

Dubreuil CI, Winton MJ, McKerracher L (2003) Rho activation patterns after spinal cord injury and the role of activated Rho in apoptosis in the central nervous system. J Cell Biol 162:233-243.

Ducharme A, Frantz S, Aikawa M, Rabkin E, Lindsey M, Rohde LE, Schoen FJ, Kelly RA, Werb Z, Libby P, Lee RT (2000) Targeted deletion of matrix metalloproteinase-9 attenuates left ventricular enlargement and collagen accumulation after experimental myocardial infarction. J Clin Invest 106:55-62.

Duchossoy Y, Horvat JC, Stettler O (2001) MMP-related gelatinase activity is strongly induced in scar tissue of injured adult spinal cord and forms pathways for ingrowing neurites. Mol Cell Neurosci 17:945-956.

Esparza J, Kruse M, Lee J, Michaud M, Madri JA (2004) MMP-2 null mice exhibit an early onset and severe experimental autoimmune encephalomyelitis due to an increase in MMP-9 expression and activity. Faseb J 18:1682-1691.

Etienne-Manneville S, Hall A (2002) Rho GTPases in cell biology. Nature 420:629-635.

Faulkner JR, Herrmann JE, Woo MJ, Tansey KE, Doan NB, Sofroniew MV (2004) Reactive astrocytes protect tissue and preserve function after spinal cord injury. J Neurosci 24:2143-2155.

Ferguson TA, Muir D (2000) MMP-2 and MMP-9 increase the neurite-promoting potential of schwann cell basal laminae and are upregulated in degenerated nerve. Mol Cell Neurosci 16:157-167.

Fitch MT, Doller C, Combs CK, Landreth GE, Silver J (1999) Cellular and molecular mechanisms of glial scarring and progressive cavitation: in vivo and in vitro analysis of inflammation-induced secondary injury after CNS trauma. J Neurosci 19:8182-8198.

Goldshmit Y, Galea MP, Wise G, Bartlett PF, Turnley AM (2004) Axonal regeneration and lack of astrocytic gliosis in EphA4-deficient mice. J Neurosci 24:10064-10073.

Goussev S, Hsu JY, Lin Y, Tjoa T, Maida N, Werb Z, Noble-Haeusslein LJ (2003) Differential temporal expression of matrix metalloproteinases after spinal cord injury: relationship to revascularization and wound healing. J Neurosurg Spine 99:188-197.

Hall A (1998) Rho GTPases and the actin cytoskeleton. Science 279:509-514.

Holtje M, Hoffmann A, Hofmann F, Mucke C, Grosse G, Van Rooijen N, Kettenmann H, Just I, Ahnert-Hilger G (2005) Role of Rho GTPase in astrocyte morphology and migratory response during in vitro wound healing. J Neurochem 95:1237-1248.

Hsieh HL, Wu CY, Yang CM (2008) Bradykinin induces matrix metalloproteinase-9 expression and cell migration through a PKC-delta-dependent ERK/Elk-1 pathway in astrocytes. Glia 56:619-632.

Hsu JY, McKeon R, Goussev S, Werb Z, Lee JU, Trivedi A, Noble-Haeusslein LJ (2006) Matrix metalloproteinase-2 facilitates wound healing events that promote functional recovery after spinal cord injury. J Neurosci 26:9841-9850.

Itoh T, Ikeda T, Gomi H, Nakao S, Suzuki T, Itohara S (1997) Unaltered secretion of beta-amyloid precursor protein in gelatinase A (matrix metalloproteinase 2)-deficient mice. J Biol Chem 272:22389-22392.

Itoh T, Tanioka M, Yoshida H, Yoshioka T, Nishimoto H, Itohara S (1998) Reduced angiogenesis and tumor progression in gelatinase A-deficient mice. Cancer Res 58:1048-1051.

Jones LL, Margolis RU, Tuszynski MH (2003) The chondroitin sulfate proteoglycans neurocan, brevican, phosphacan, and versican are differentially regulated following spinal cord injury. Exp Neurol 182:399-411.

Larsen PH, Wells JE, Stallcup WB, Opdenakker G, Yong VW (2003) Matrix metalloproteinase-9 facilitates remyelination in part by processing the inhibitory NG2 proteoglycan. J Neurosci 23:11127-11135.

Lauffenburger DA, Horwitz AF (1996) Cell migration: a physically integrated molecular process. Cell 84:359-369.

Marret S, Delpech B, Delpech A, Asou H, Girard N, Courel MN, Chauzy C, Maingonnat C, Fessard C (1994) Expression and effects of hyaluronan and of the hyaluronan-binding protein hyaluronectin in newborn rat brain glial cell cultures. J Neurochem 62:1285-1295.

Matyash M, Matyash V, Nolte C, Sorrentino V, Kettenmann H (2002) Requirement of functional ryanodine receptor type 3 for astrocyte migration. Faseb J 16:84-86.

McGraw J, Hiebert GW, Steeves JD (2001) Modulating astrogliosis after neurotrauma. J Neurosci Res 63:109-115.

McKeon RJ, Jurynec MJ, Buck CR (1999) The chondroitin sulfate proteoglycans neurocan and phosphacan are expressed by reactive astrocytes in the chronic CNS glial scar. Journal of Neuroscience 19:10778-10788.

Menet V, Prieto M, Privat A, Gimenez y Ribotta M (2003) Axonal plasticity and functional recovery after spinal cord injury in mice deficient in both glial fibrillary acidic protein and vimentin genes. Proc Natl Acad Sci U S A 100:8999-9004.

Mitchison TJ, Cramer LP (1996) Actin-based cell motility and cell locomotion. Cell 84:371-379.

Mosmann T (1983) Rapid colorimetric assay for cellular growth and survival: application to proliferation and cytotoxicity assays. J Immunol Methods 65:55-63.

Muir EM, Adcock KH, Morgenstern DA, Clayton R, von Stillfried N, Rhodes K, Ellis C, Fawcett JW, Rogers JH (2002) Matrix metalloproteases and their inhibitors are produced by overlapping populations of activated astrocytes. Brain Res Mol Brain Res 100:103-117.

Noble LJ, Donovan F, Igarashi T, Goussev S, Werb Z (2002) Matrix metalloproteinases limit functional recovery after spinal cord injury by modulation of early vascular events. J Neurosci 22:7526-7535.

Ogier C, Bernard A, Chollet AM, T LED, Hanessian S, Charton G, Khrestchatisky M, Rivera S (2006) Matrix metalloproteinase-2 (MMP-2) regulates astrocyte motility in connection with the actin cytoskeleton and integrins. Glia 54:272-284.

Oh LY, Larsen PH, Krekoski CA, Edwards DR, Donovan F, Werb Z, Yong VW (1999) Matrix metalloproteinase-9/gelatinase B is required for process outgrowth by oligodendrocytes. J Neurosci 19:8464-8475.

Okada S, Nakamura M, Katoh H, Miyao T, Shimazaki T, Ishii K, Yamane J, Yoshimura A, Iwamoto Y, Toyama Y, Okano H (2006) Conditional ablation of Stat3 or Socs3 discloses a dual role for reactive astrocytes after spinal cord injury. Nat Med 12:829-834.

Pastrana E, Moreno-Flores MT, Gurzov EN, Avila J, Wandosell F, Diaz-Nido J (2006) Genes associated with adult axon regeneration promoted by olfactory ensheathing cells: a new role for matrix metalloproteinase 2. J Neurosci 26:5347-5359.

Penkowa M, Giralt M, Lago N, Camats J, Carrasco J, Hernandez J, Molinero A, Campbell IL, Hidalgo J (2003) Astrocyte-targeted expression of IL-6 protects the CNS against a focal brain injury. Exp Neurol 181:130-148.

Ramakers GJ, Moolenaar WH (1998) Regulation of astrocyte morphology by RhoA and lysophosphatidic acid. Exp Cell Res 245:252-262.

Ridet JL, Malhotra SK, Privat A, Gage FH (1997) Reactive astrocytes: cellular and molecular cues to biological function. Trends Neurosci 20:570-577.

Rose K, Goldberg MP, Choi DW (1993) Cytotoxicity in murine cortical cell culture. In: In vitro biological methods. In: (Frazier JM, ed), pp 46-60. San Diego: Academic.

Saadoun S, Papadopoulos MC, Watanabe H, Yan D, Manley GT, Verkman AS (2005) Involvement of aquaporin-4 in astroglial cell migration and glial scar formation. J Cell Sci 118:5691-5698.

Silver J, Miller JH (2004) Regeneration beyond the glial scar. Nat Rev Neurosci 5:146-156.

Sofroniew MV (2005) Reactive astrocytes in neural repair and protection. Neuroscientist 11:400-407.

Sternlicht MD, Werb Z (2001) How matrix metalloproteinases regulate cell behavior. Annu Rev Cell Dev Biol 17:463-516.

Takenaga K, Kozlova EN (2006) Role of intracellular S100A4 for migration of rat astrocytes. Glia 53:313-321.

Tang X, Davies JE, Davies SJ (2003) Changes in distribution, cell associations, and protein expression levels of NG2, neurocan, phosphacan, brevican, versican V2, and tenascin-C during acute to chronic maturation of spinal cord scar tissue. J Neurosci Res 71:427-444.

Vaillant C, Meissirel C, Mutin M, Belin MF, Lund LR, Thomasset N (2003) MMP-9 deficiency affects axonal outgrowth, migration, and apoptosis in the developing cerebellum. Mol Cell Neurosci 24:395-408.

Vu TH, Shipley JM, Bergers G, Berger JE, Helms JA, Hanahan D, Shapiro SD, Senior RM, Werb Z (1998) MMP-9/gelatinase B is a key regulator of growth plate angiogenesis and apoptosis of hypertrophic chondrocytes. Cell 93:411-422.

Wells JE, Rice TK, Nuttall RK, Edwards DR, Zekki H, Rivest S, Yong VW (2003) An adverse role for matrix metalloproteinase 12 after spinal cord injury in mice. J Neurosci 23:10107-10115.

Yong VW, Power C, Forsyth P, Edwards DR (2001) Metalloproteinases in biology and pathology of the nervous system. Nat Rev Neurosci 2:502-511.

Yong VW (2005) Metalloproteinases: mediators of pathology and regeneration in the CNS. Nat Rev Neurosci 6:931-944.

Yoshida T, Takeuchi M (1991) Expression of fibronectin and laminin by different types of mouse glial cells cultured in a serum-free medium. Cytotechnology 7:187-196.

Yu Q, Stamenkovic I (1999) Localization of matrix metalloproteinase 9 to the cell surface provides a mechanism for CD44-mediated tumor invasion. Genes Dev 13:35-48.
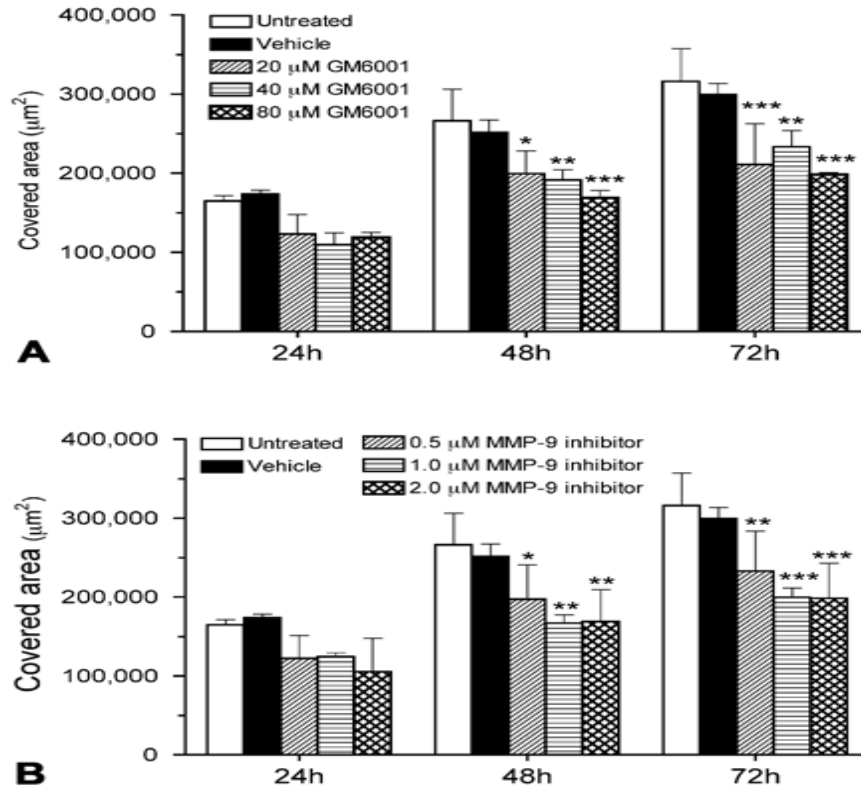
APPENDICES

Figure 1: The effect of various concentrations of GM6001 (A) and an MMP-9 inhibitor (B) on astrocyte migration in the scratch wound assay. The area covered by migrating astrocytes is measured over a period of 72 hours after the scratch is made. All the concentrations examined can effectively inhibit astrocyte migration compared with the untreated group 48 and 72 hours after the scratch. $*p < 0.05$, $**p < 0.01$, $***p < 0.001$, compared with the untreated group of the same time point.
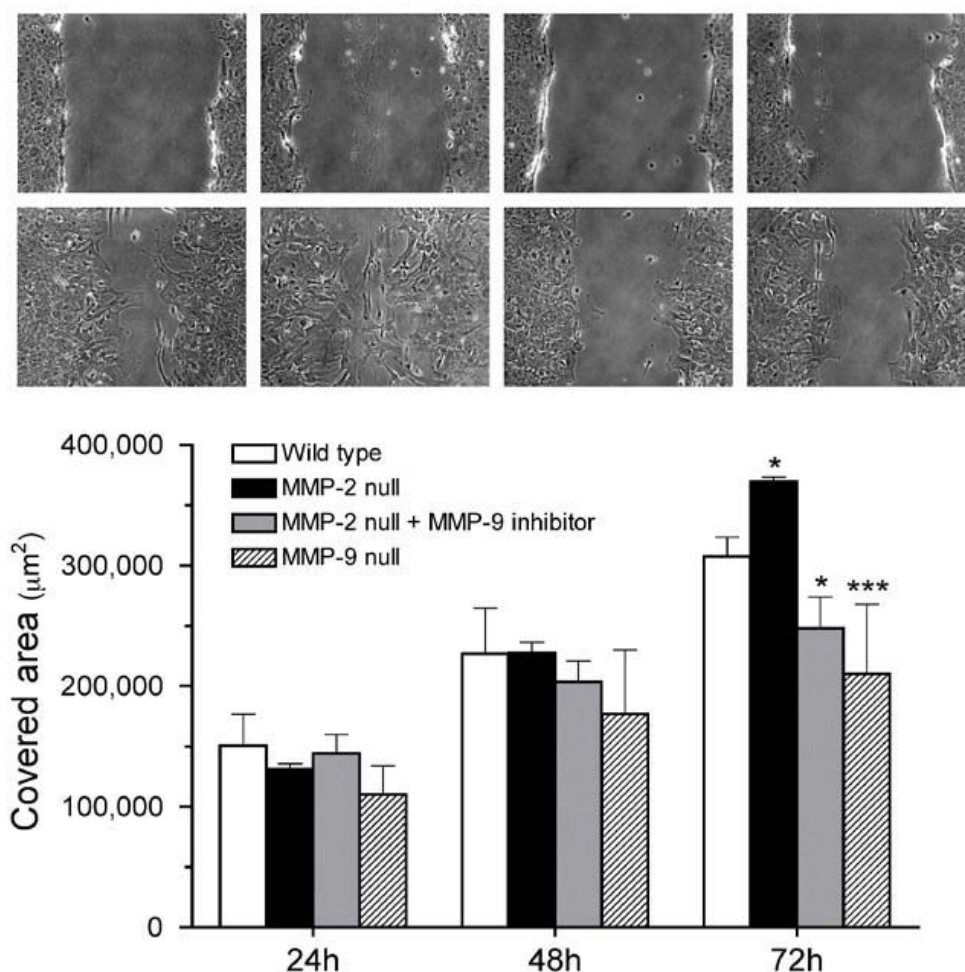
Figure 2: Migration of cultured astrocytes isolated from MMP-2 null, and MMP-9 null mice in the scratch assay. Representative photographs demonstrate the wound closure processes 0 and 72 hours after the scratch is made. Notably, MMP-2-null astrocytes migrate faster and thus cover more denuded area than the wild-type astrocytes 72 hours after the scratching. At the same time point, however, MMP-2-null astrocytes treated with 1.0 μM MMP-9 inhibitor migrate significantly slower than the wild-type astrocytes. A similar outcome of attenuated migration is also observed in MMP-9-null astrocytes. The chart summarizes the quantitative analysis of the area covered by astrocytes at various time points. The results demonstrate that MMP-9 deficiency adversely affects astrocyte migration. $*p < 0.05$, $***p < 0.001$, compared with the wild-type at 72 hours.
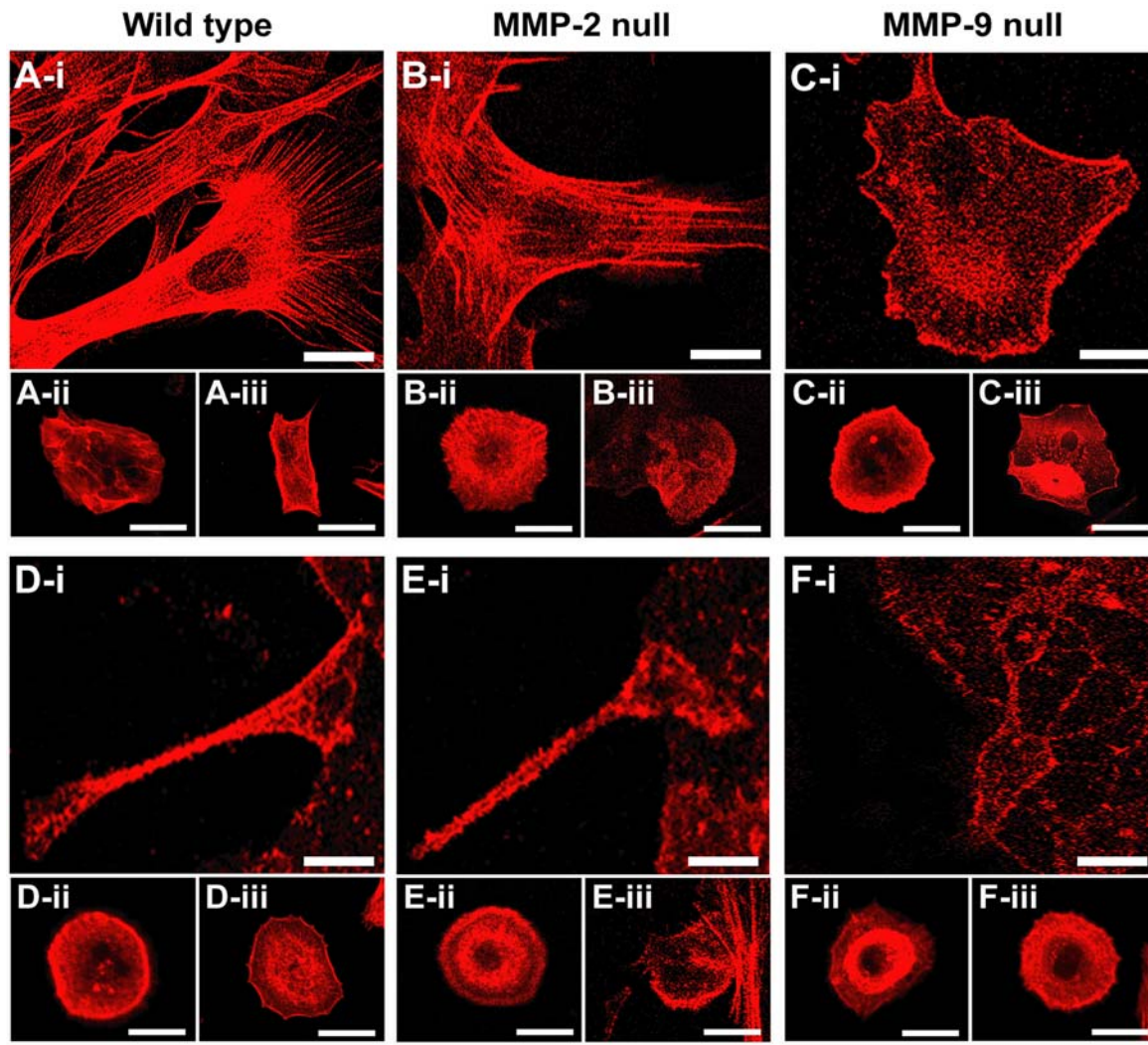
Figure 3: Fluorescence staining of F-actin in cultured astrocytes isolated from wild-type, MMP-2 null, and MMP-9 null mice using Texas Red-conjugated phalloidin. Shown here are astrocytes without cytoskeleton inhibitor (i), treated with cytochalasin D (ii), and treated with Rac1 inhibitor (iii). Before reaching a confluent monolayer (A, B, C), astrocytes without cytoskeleton inhibitor exhibit comparable morphology and F-actin distribution in the wild-type and MMP-2 null groups, whereas MMP-9 null astrocytes lose their stellar profile and show disintegrated F-actin distribution (C-i). After a scratch wound is made on the confluent monolayer (D, E, F), wild-type and MMP-2 null astrocytes, without cytoskeleton inhibitor, at the scratch border extend F-actin-containing membrane protrusions (arrowheads) toward the denuded area (on the left). These membrane protrusions are not observed in MMP-9 null astrocytes (F-i). Regardless of having a scratch wound or not, treatments with cytochalasin D (A~F-ii) or Rac1 inhibitor (A~F-iii) cause abnormal morphology and F-actin distribution in astrocytes of all 3 genotypes. No scratch-induced membrane protrusion is found with these treatments. Scale bars = 25μm in -i, 100μm in -ii, -iii.
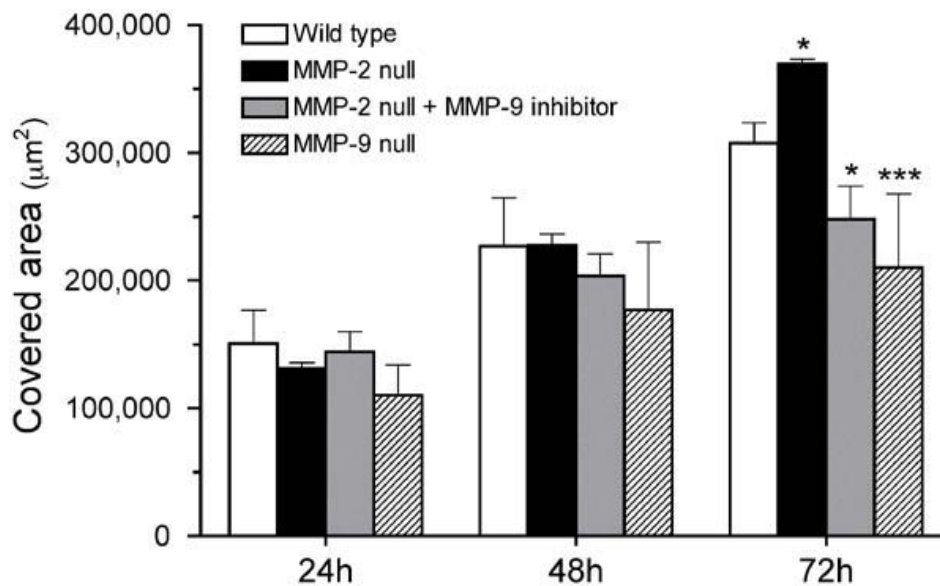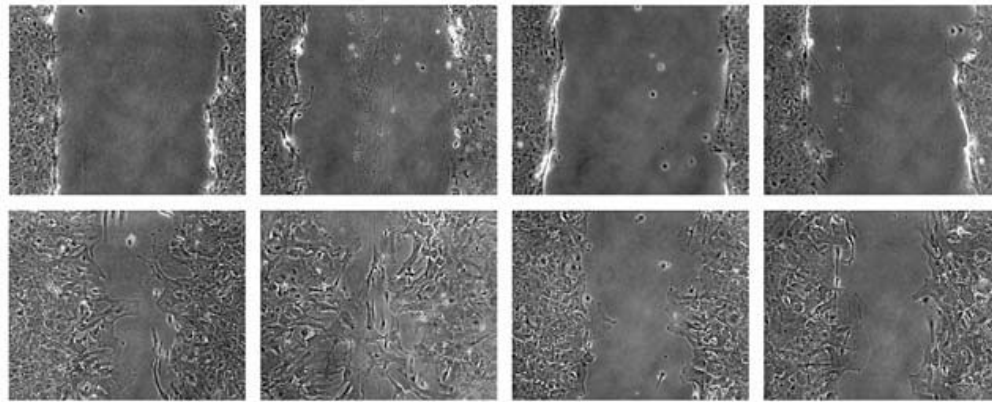
Figure 4: The effects of cytochalasin D and Rac1 inhibitor on astrocyte migration. In the scratch wound assay, both wild-type and MMP-2-null astrocytes migrate faster and cover more denuded area than the MMP-9 null astrocytes 72 hours after the scratch is made (***$p < 0.001$, compared with untreated wild-type). At the same time point, administration of either 20 μg/ml cytochalasin D or 50 μM Rac1 inhibitor significantly slows down astrocyte migration of all 3 genotypes ($^{###} p < 0.001$, compared with respective genotypes in the untreated group).
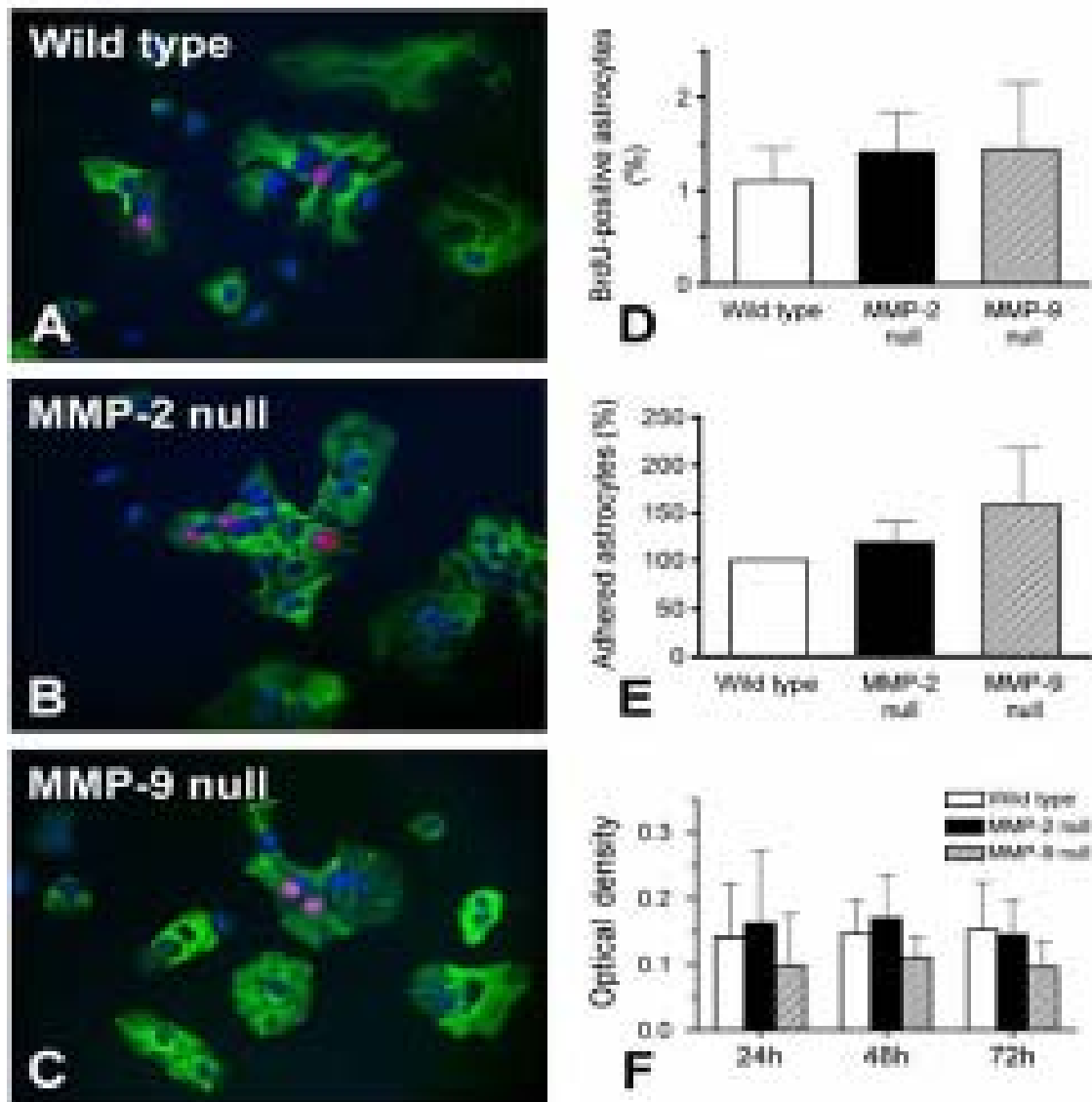
Figure 5: Analyses of proliferation, adhesion, and viability in cultured astrocytes isolated from MMP-2 null, and MMP-9 null mice. Proliferative astrocytes are identified by positive immunolabeling of anti-BrdU (red) and -GFAP (green) along with DAPI nuclear stain (blue) (A, B, C). There is no significant difference in the number of proliferative astrocytes among the 3 groups studied (D). Astrocytes adhering to the poly-L-lysine-coated growth surface are counted 24 hours after the first passage (E), while astrocyte viability is tested by colorimetric MTT assay 1, 2, and 3 days after the first passage (F). There are no significant differences among the 3 groups studied in all these tests. Our findings suggest that knocking out MMP-2 or MMP-9 does not affect astrocytic proliferation, adhesion, and viability. Scale bar = 100 μm
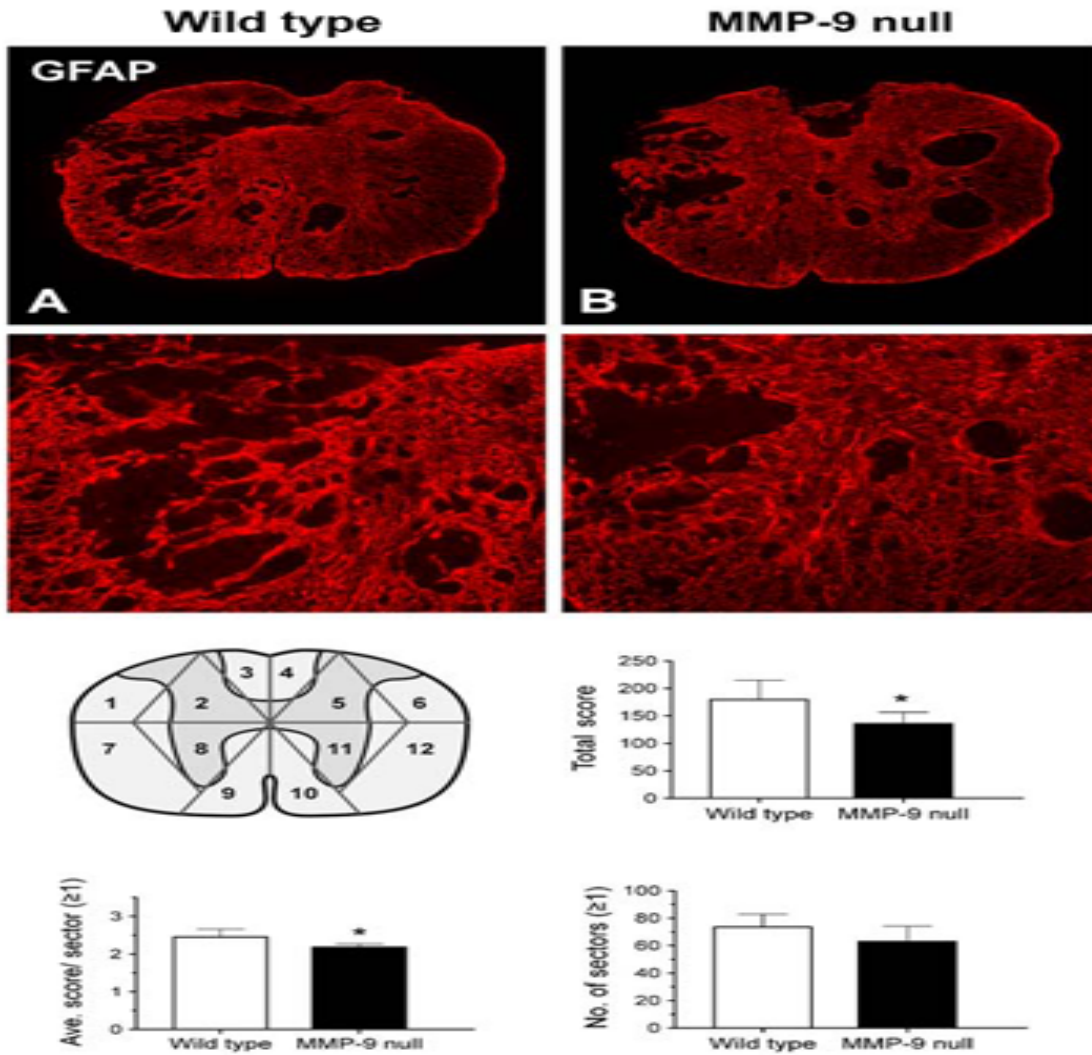
Figure 6: Glial scar formation in MMP-9 null and wild-type mice 42 days post-injury. The wild-type mouse (A) exhibits a more severe glial scar formation in the lesion, evidenced by intricate tangling of astrocytic processes and intense GFAP immunoreactivity, than the MMP-9 null mouse (B). At higher magnification (C, D; taken from boxed area in A and B, respectively), entangled astrocytic processes are densely bundled to form a robust trabecular meshwork in the wild-type mouse, whereas the glial scarring is relatively modest in MMP-9 null mouse. The sampling strategy used in our semi-quantitative analysis of the glial scar is illustrated in the diagram (E). A score ranging from 0 to 3 is given to each of the 12 sectors depending on the severity of glial scarring as described in the Materials and Methods. The total score, obtained from 9 sections in each mouse (n = 6 per genotype), is significantly lower in the MMP-9 null mouse than in the wild-type mouse (F). The average score of each sector that is scored ≥ 1 is also lower in the MMP-9 null mouse than in the wild-type control (G), indicating less complicated glial scarring in the MMP-9 null mouse. The total number of sectors scored ≥ 1 shows no difference between the two groups (H), suggesting the extent of the glial scar is comparable between the two groups. *$p < 0.05$. Scale bars = 250 μm in A, B; 100 μm in C,D.

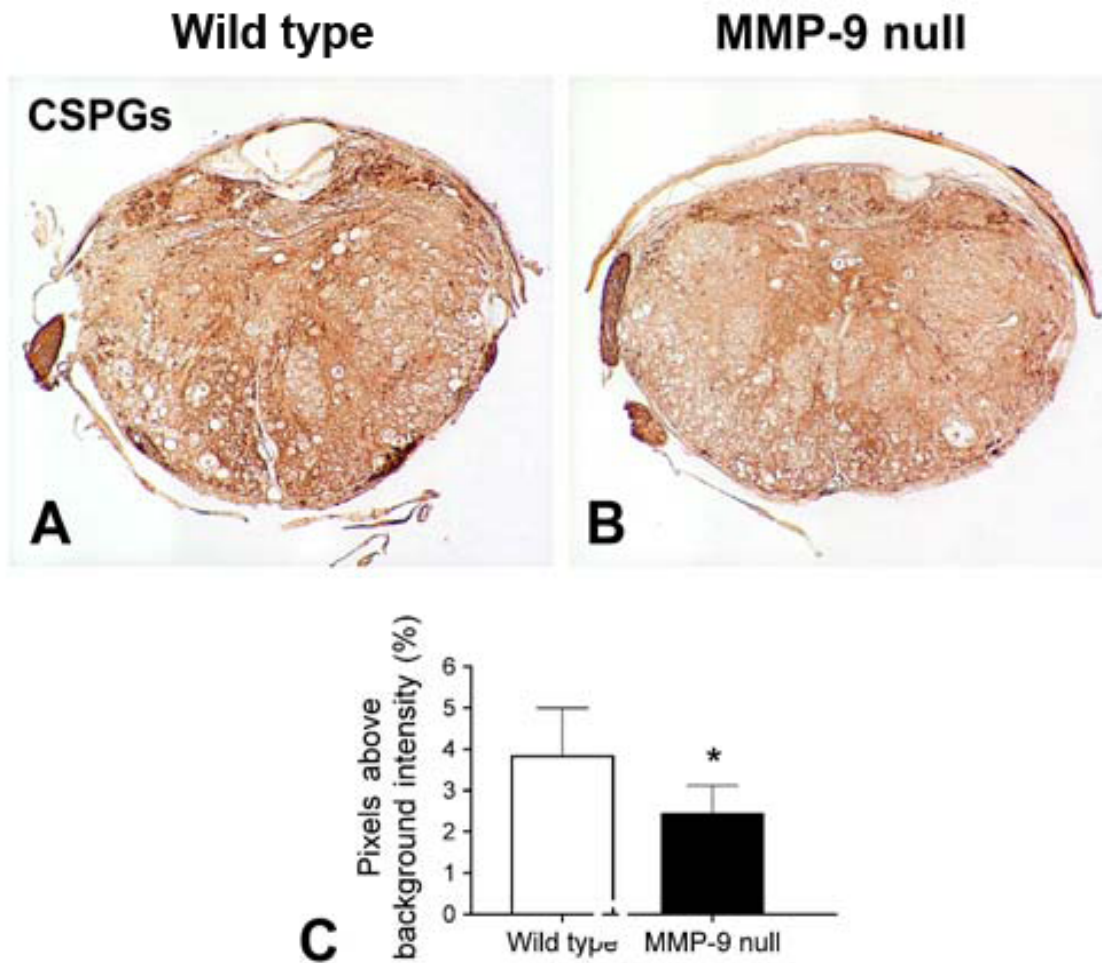**Figure 7.** Comparison of CSPG immunoreactivity (clone CS-56) in the lesion epicenter between MMP-9 null and wild-type mice 42 days after spinal cord injury. The wild-type mouse (A) displays stronger CSPG immunostaining than the MMP-9 null mouse (B). Our quantitative analysis shows that the MMP-9 null mouse has significantly lower CSPG immunoreactivity than the wild-type mouse (n = 7 per genotype) (C). *p < 0.05. Scale bar = 250 μm

Figure 8. Representative gel zymogram showing gelatinase levels in the injured spinal cord at 7 days post-injury. Both MMP-9 and MMP-2 are up-regulated in the wild-type mouse compared with the sham-operated mouse that receives only laminectomy. The intensity of both pro- and active MMP-2 in the wild-type mouse is comparable to that of the MMP-9 null mouse, suggesting the expression of MMP-2 is unaltered in the later.

SUPPORTING DATA
N/A

Pilot Study 2:

Patterns of MRI Brain Atrophy Rate in PTSD

Principal Investigator: Valerie Cardenas-Nicolson, Ph.D. Assistant Adjunct Professor

ABSTRACT

Patients with posttraumatic stress disorder (PTSD) exhibit a wide range of neuropsychological deficits, and atrophy in brain regions such as the hippocampus has been reported. Although there have been numerous magnetic resonance imaging studies of PTSD, most have reported cross-sectional results using region of interest analyses, where only a few anatomical locations of the brain are investigated. Voxel-wise structural image analysis provides a way of looking for anatomical variation without prior hypotheses about the location and extent of the anatomical variation. In this project, we propose to investigate the spatial pattern of longitudinal tissue atrophy in subjects with PTSD compared to normals, and additionally to correlate performance on neuropsychological tests with neurodegeneration. We are uniquely qualified to accomplish these goals, as we have developed novel voxel-wise morphometric methods for automated investigation of spatial patterns of atrophy rate, and because of our access to a sample of longitudinal images and clinical data from patients diagnosed with and without PTSD. The results of this project will lead directly to a better understanding of the temporal course of PTSD and its relation to underlying brain anatomy, which is of great military importance. It is projected that PTSD affects 7.8% of the US population over the course of a lifetime (1). Combat exposure and other severely traumatic experiences dramatically increase the risk of PTSD. Twenty-five percent of men over 55 in the US have been exposed to combat (2). PTSD may effect as many as 28.8% of a combat exposed population (1). More than 90% of the members of ground combat units deployed in Iraq have been shot at, with up to 20% meeting a broad definition of PTSD within 3-4 months after their return from deployment (3). Greater understanding of the longitudinal effects of PTSD on the brain may help in the treatment of these soldiers returning from Iraq, and therefore this project has great military relevance.

TABLE OF CONTENTS

INTRODUCTION

We propose to make use of previously acquired longitudinal images from a cohort of subjects with and without PTSD. These images were acquired as part of several different studies. We plan to create maps of local atrophy rate to use as dependent variables in statistical models examining several candidate independent variables indexing PTSD severity (e.g., tissue volumes, cognitive tests). These models will investigate whether quantitative local volume measures derived from MRI (e.g., local gray matter volume, ERC volume) are better PTSD staging variables and predictors of our atrophy rate maps than cognitive measures (e.g., CAPS score). We also will describe the regional distribution of tissue atrophy over a population during progression of PTSD, and compare maps of atrophy rate between groups. Permutation testing will be used to correct spatial statistics for multiple comparisons (4).
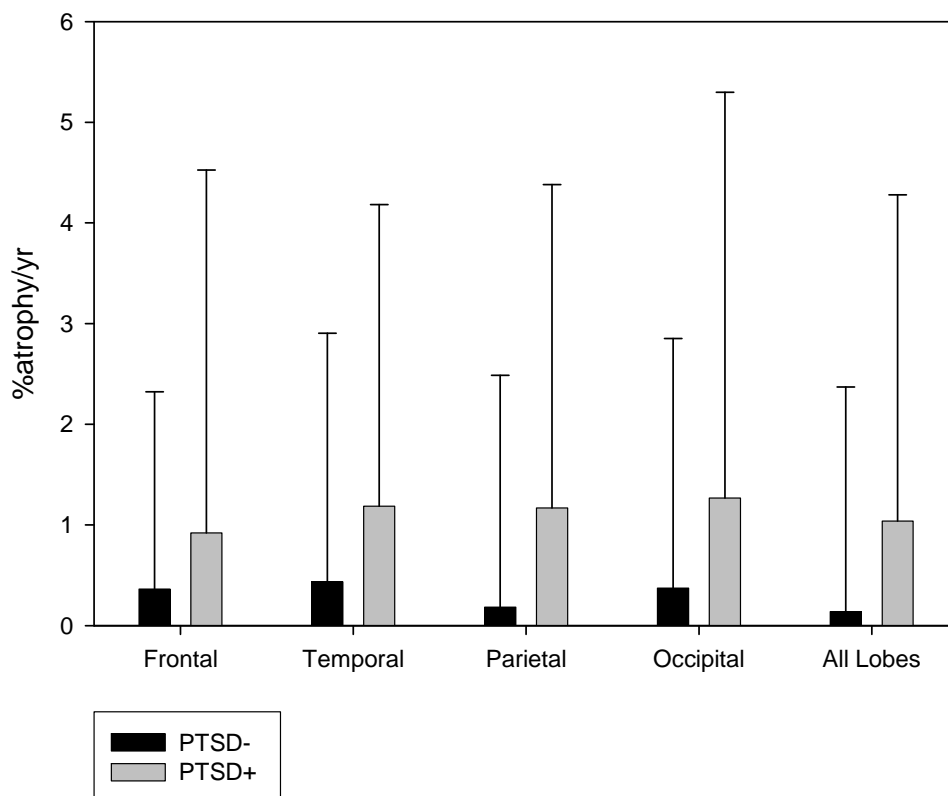
The primary research goal of this project is to describe brain atrophy rate during PTSD. A secondary goal is to determine the extent to which quantitative local volume measures derived from MRI are better than cognitive measures for defining the severity of PTSD and predicting the associated tissue loss over time. A final goal is to describe the distribution of tissue atrophy during PTSD compared to normal aging. Our specific aims are to test the following hypotheses:

    (1) *PTSD+ subjects will show loss of tissue over time (atrophy rate >0), and the magnitude of atrophy rate will vary regionally.*
    (2) *Quantitative imaging measures will better predict atrophy rate than cognitive measures.*
    (3) *The spatial pattern of atrophy rate will differ between subjects with and without PTSD.*

BODY

Tissue Segmentation: This project is a secondary data analysis of imaging datasets collected as part of two different projects. Because of differences in analysis methods used in the two projects, the conventional volumetric tissue segmentation was redone for this project using state-of-the art analysis methods. These volumes have been completed, and will be used as covariates in the analysis of longitudinal maps of deformation. Although not a specific aim of this project, I analyzed whether there were any longitudinal changes observed in these lobar measures of gray matter, white matter, and CSF due to PTSD. There were no significant differences between groups due to large variation within groups, but a greater rate of brain atrophy in PTSD+ was observed in all lobes (as shown), with a concomitant increase in CSF expansion. If the atrophy is spatially localized, lobar measures may be noisy, and deformation morphometry should increase sensitivity to detect group differences. Inclusion of clinical variables using deformation morphometry may also help to explain some of the group variability, increasing our sensitivity to detect group differences.

Rate of Gray Matter Atrophy

Creation of Maps of Baseline Atrophy: The creation of maps of baseline atrophy is a key component of this project that has been completed. An entropy driven B-Spline Free Form deformation algorithm(5, 6) was used to register individual scans to a reference atlas. The Jacobian determinant of this transformation, giving the fractional volume contraction or expansion relative to the reference, characterizes the atrophy at each voxel. These Jacobian maps (i.e., maps of baseline atrophy) will be used as covariates, in order to determine how much variability in atrophy rate can be explained by spatially varying, local baseline atrophy (as opposed to global measures of atrophy, such as whole brain gray matter). Though not part of the original proposal, these maps can also be used as dependent variables in a statistical analysis to examine cross-sectional differences between PTSD+ and PTSD- patients. These maps were created during the first year of the project.

Creation of Maps of Atrophy Rate: The same general approach used to create maps of atrophy state will be used to register and model spatial changes within subject between multiple scans(7). The previously estimated transformation between the initial time point of each subject and the reference anatomy then allows the spatial normalization of annualized pointwise volume change for each subject, yielding relative atrophy rate estimates (tissue volume change in %/yr) at each voxel in standard space. These maps were completed during the reporting year just ended. Figures 1 and 2 show examples of maps of atrophy rate from a PTSD- and PTSD+ subject.
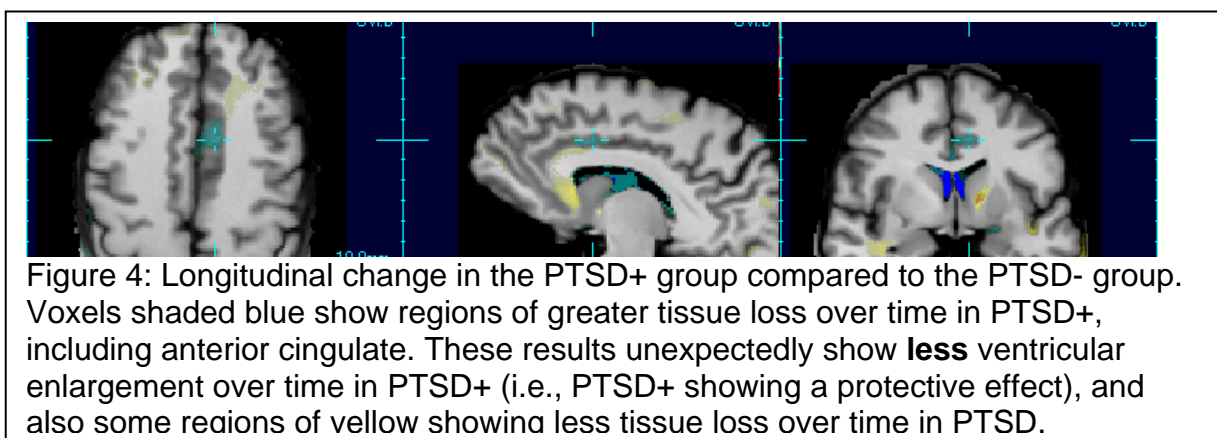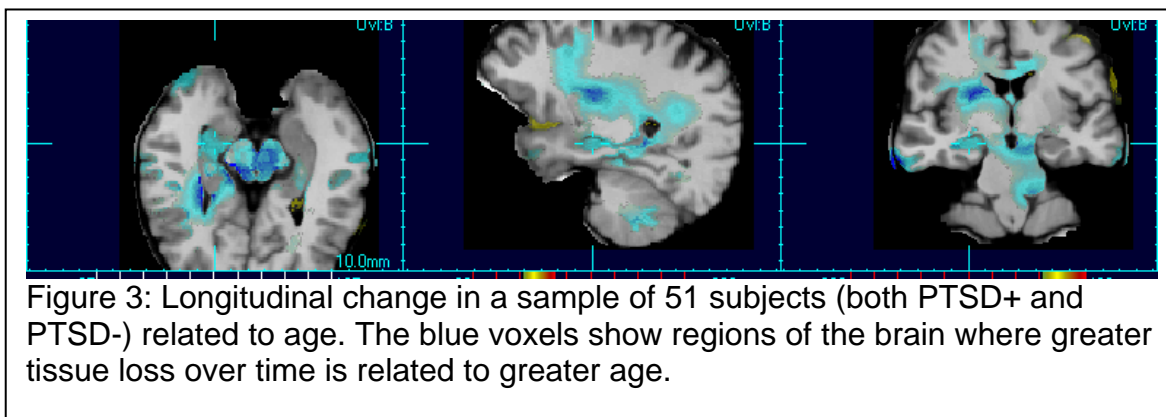
Figure 1: Longitudinal change in a PTSD- subject. Voxels shaded yellow show expansion.

Figure 2: Longitudinal change in a PTSD+ subject. Voxels shaded yellow show expansion, and voxels shaded blue show brain tissue loss over time.

<u>Creation of Measures of clinical/neuropsychological change over time</u>: Measures of clinical/neuropsychological change over time have been created for these subjects. The plan is to use these longitudinal clinical/neuropsychological measures to correlate longitudinal structural change with longitudinal functional change. Kristin Samuelson, a collaborator on the project, recently presented work from this project at the annual meeting of the International Society for Traumatic Stress Studies. She completed a statistical analysis of longitudinal neuropsychological changes observed in these subjects. She reported that PTSD+ subjects declined faster on tests of delayed facial recognition and memory.

<u>Statistical Analysis:</u>
Much of the originally proposed statistical analyses have been completed, and some preliminary results have suggested other statistical comparisons. Figure 3 shows the longitudinal change in a s ample of 51 subject (both PTSD+ and PTSD-) related to age. The blue voxels show regions of the brain where greater tissue loss over time is related to greater age. This figure shows that the hippocampus, brainstem, and regions of white matter seems show accelerated atrophy with greater age.

We have also compared the longitudinal change in the PTSD+ group compared to the PTSD- group (specific aim (3) of the funded proposal), as shown in Figure 4. We unexpectedly found less ventricular enlargement over time in PTSD+, and also some regions showing less tissue loss over time in PTSD+. These results would seem to suggest that PTSD was showing some protection against normal aging, and these results suggested looking at alternative statistical models.

Figure 3: Longitudinal change in a sample of 51 subjects (both PTSD+ and PTSD-) related to age. The blue voxels show regions of the brain where greater tissue loss over time is related to greater age.

Figure 4: Longitudinal change in the PTSD+ group compared to the PTSD- group. Voxels shaded blue show regions of greater tissue loss over time in PTSD+, including anterior cingulate. These results unexpectedly show **less** ventricular enlargement over time in PTSD+ (i.e., PTSD+ showing a protective effect), and also some regions of yellow showing less tissue loss over time in PTSD.
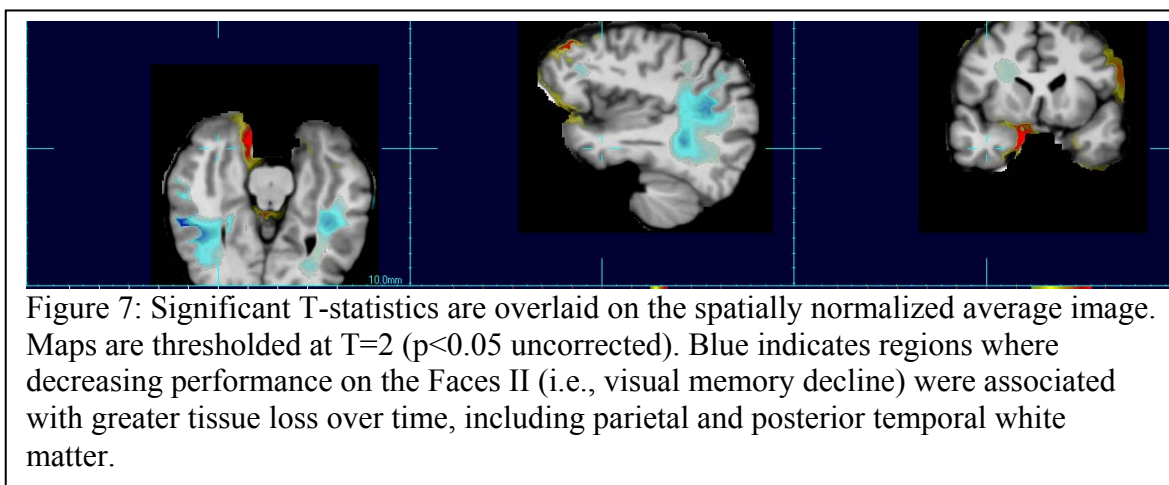
When exploring other statistical models, we began to look at whether the apparent slower aging in the PTSD group could be explained by any clinical or cognitive variables. One natural clinical measure was the change in the CAPS (Clinician Administered PTSD Scale) score over time. Our hypothesis was that patients whose PTSD severity improved over time would show slower than normal aging (i.e., patients with improving disease would show tissue recovery over time). Our results are shown in Figure 5. We observed than longitudinal brain change in the frontal and anterior temporal cortex was related to change in CAPS score; tissue recovery was observed in patients with decreasing PTSD severity and greater tissue loss in patients with increasing PTSD severity.

We also examined the relationship between longitudinal brain change and change scores of verbal, visual and working memory measures (part of specific aim (2) of the funded proposal). Verbal memory decline was related to greater atrophy rate in the region surrounding posterior cingulated (Figure 6), and visual memory decline was related to posterior temporal and parietal white matter regions (Figure 7).

KEY RESEARCH ACCOMPLISHMENTS

1) Creation of maps of longitudinal change.
2) Longitudinal measures of clinical/neuropsychological change over time computed.
3) Statistical analyses accomplished.

Figure 7: Significant T-statistics are overlaid on the spatially normalized average image. Maps are thresholded at T=2 (p<0.05 uncorrected). Blue indicates regions where decreasing performance on the Faces II (i.e., visual memory decline) were associated with greater tissue loss over time, including parietal and posterior temporal white matter.

REPORTABLE OUTCOMES

Sjostrand K, Cardenas VA, Larsen R, and Studholme C (2008): A generalization of voxel-wise procedures for high-dimensional statistical inference using ridge regression. Proc. Of SPIE, Vol. 6914, p. 69140A-1-12.

Samuelson K, Cardenas VA, Marmar C, Neylan T (2007): Longitudinal effects of PTSD on neuropsychological functioning. Symposium presentation at ISTSS 2007.

Cardenas VA, Samuelson K, Studholme C, Lenoci MA, Neylan T, Marmar C, Weiner MW (2008) : Longitudinal brain atrophy and neurocognition in PTSD. Symposium presentation at ISTSS 2008.

CONCLUSION

In conclusion, the project is on track. Although we have not so far shown that PTSD+ patients show greater brain atrophy over time than PTSD- patients, we have demonstrated that 2/3 of our patients showed recovery of symptoms over time, and that symptom recovery is associated with tissue recovery over time. In addition, we have shown several regions where accelerated tissue loss is associated with declining cognitive function.

REFERENCES

1.   Kessler RC, Sonnega A, Bromet E, Hughes M, Nelson CB. Posttraumatic stress disorder in the National Comorbidity Survey. *ArchGeneral Psychiatry* 1995;52:1048-60.
2.   Johnston D. A series of cases of dementia presenting with PTSD symptoms in World War II combat veterans. *J Am Geriatr Soc* 2000;48(1):70-2.
3.   Hoge CW, Castro CA, Messer SC, McGurk D, Cotting DI, Koffman RL. Combat duty in Iraq and Afghanistan, mental health problems, and barriers to care. *N Engl J Med* 2004;351(1):13-22.
4.   Nichols TE, Holmes AP. Nonparametric permutation tests for functional neuroimaging: a primer with examples. *Hum Brain Mapp* 2002;15(1):1-25.
5.   Studholme C, Constable RT, Duncan JS. Accurate alignment of functional EPI data to anatomical MRI using a physics-based distortion model. *IEEE Trans Med Imaging* 2000;19(11):1115-27.
6.   Studholme C, Novotny E, Zubal IG, Duncan JS. Estimating tissue deformation between functional images induced by intracranial electrode implantation using anatomical MRI. *Neuroimage* 2001;13(4):561-76.
7.   Studholme C, Cardenas V, Weiner M. Building Whole Brain Maps of Atrophy Rate from Multi-Subject Longitudinal Studies Using Free-form Deformations. In: *ISMRM*; 2001 Apr; 2001.

APPENDICES

Appendix I

Sjostrand K, Cardenas VA, Larsen R, and Studholme C (2008): A generalization of voxel-wise procedures for high-dimensional statistical inference using ridge regression. Proc. Of SPIE, Vol. 6914, p. 69140A-1-12.

SUPPORTING DATA
N/A

A Generalization of Voxel-wise Procedures for High-Dimensional Statistical Inference using Ridge Regression

Karl Sjöstrand[a], Valerie A. Cardenas[b], Rasmus Larsen[c] and Colin Studholme[b]

[a]EXINI Diagnostics AB, Scheelevägen 17, Beta 3, Lund, Sweden
[b]Center for Imaging of Neurodegenerative Disease, VA Medical Center, University of California San Francisco, San Francisco, USA
[c]Informatics and Mathematical Modelling, Technical University of Denmark, Kgs. Lyngby, Denmark

ABSTRACT

Whole-brain morphometry denotes a group of methods with the aim of relating clinical and cognitive measurements to regions of the brain. Typically, such methods require the statistical analysis of a data set with many variables (voxels and exogenous variables) paired with few observations (subjects). A common approach to this ill-posed problem is to analyze each spatial variable separately, dividing the analysis into manageable subproblems. A disadvantage of this method is that the correlation structure of the spatial variables is not taken into account. This paper investigates the use of ridge regression to address this issue, allowing for a gradual introduction of correlation information into the model. We make the connections between ridge regression and voxel-wise procedures explicit and discuss relations to other statistical methods. Results are given on an in-vivo data set of deformation based morphometry from a study of cognitive decline in an elderly population.

1. INTRODUCTION

Statistical Analysis of extremely high-dimensional data sets have become commonplace in medical image analysis. Tens of thousands to millions of spatial variables must be taken into account while the number of observations (subjects) is typically limited – less than a hundred or a few hundred at most. Traditional statistical analysis of such data sets becomes impossible for computational reasons, but also cannot be expected to yield trustworthy results as the addition of a single new subject risks changing the results of the analysis to a large extent. This makes clear the need to constrain the analysis to lower the variance of the estimates. A popular approach is to divide the analysis into several manageable subproblems. Typically, this division is taken to its extreme, where each problem contains a single spatial variable that is related to a clinical outcome variable, an approach we denote *pointwise regression*, but which is also known as voxel-wise or univariate regression. Each such problem will contain many more observations than variables, and will yield results of low variance. However, a limitation is that any dependencies between spatial variables are neglected. Spatial variables are known to exhibit significant correlations, primarily among neighbors but also extending across the entire anatomy.[1] There is therefore a need for an *aggregate* method that is able to incorporate the correlation structure of the spatial variables, while keeping the variance of the estimates from inflating. This paper presents ridge regression as a viable alternative to pointwise regression. It is shown that the two methods are closely related, but that the use of ridge regression may extend the analysis through gradual introduction of small amounts of correlation structure information. The presentation of the method is given with synthetic data as reference, while the results are given on in-vivo deformation data. The application here is to tensor based morphometry, but the method generalizes to any data set with a single continuous or dichotomous clinical variable that is typically analyzed using pointwise regression.

Ridge regression was introduced by Hoerl and Kennard[2] and Marquardt.[3] Regularization by addition of a constraint on the sum-of-squares of the parameters has been discovered in many different areas of research. In the study of inverse problems, it is known as *Tikhonov regularization*[4] while the neural network community refer

---

Send correspondence to K. Sjöstrand: Karl.Sjostrand@exini.com, Telephone: +46 46 286 54 21

to it as *weight decay*. Its application in statistics has traditionally been to lower the prediction error by careful balancing of its inherent bias-variance properties. The use of ridge regression in problems with more variables than observations is less wide-spread, but has found applications in e.g. neuroimaging[5] and microarray analysis.[6]

There exist several methods for the aggregate analysis of image data arising from e.g. fMRI, PET and morphometric studies. To deal with the great excess of spatial variables produced by such investigations, there are several statistical techniques available such as decomposition, variable selection, regularization and classification.

Variable decomposition is perhaps the most popular of these, where the data are transformed into a smaller set of spatial variables that summarizes the data. Principal component analysis (PCA) is the most well-known such technique. Cootes et al.[7] pioneered the use of PCA to obtain a compact model of anatomy. Friston et al.[8] and Strother et al.[9] used PCA to decompose a set of PET images and used the resulting eigenimages for interpretation. These methods seek to maximize variance in the spatial data without using information from an exogenous clinical variable. Canonical variate analysis (CVA)[10] is one method that may be used to incorporate such information. CVA is a generalization of multiple regression where several dependent variables can be related to several independent variables at once. This results in linear combinations of the spatial and clinical variables that are maximally correlated. A related but non-linear approach is partial least squares (PLS), introduced to neuroimaging by McIntosh et al.,[11] who applied it to functional MR image data. An overview of aggregate methods in neuroimaging is given by Worsley.[12]

Variable selection and regularization techniques (which are often connected) have previously been reported by Valdes-Sosa et al.[5] in a study of functional connectivity.[13] The paper discusses ridge regression as one option for the simultaneous analysis of hundreds of voxels over time, but does not relate the method to pointwise regression nor apply it to studies of morphometry.

Often, the clinical or cognitive variable of interest indicates group belonging. In such cases, classification techniques can be used to characterize anatomical differences. Examples are Lao et al.[14] and Golland et al.[15] who use non-linear support vector machines to identify spatial variables that distinguish between populations.

Differences between pointwise and aggregate analyses were highlighted by Fletcher et al.,[16] who concluded that an aggregate analysis may provide crucial information that might otherwise be lost. Davatzikos[1] and Friston and Ashburner[17] debate the practice of making global inferences from the local analyses of pointwise regression, and agree on the point that aggregate methods are preferable under many circumstances. The use of aggregate techniques, such as PCA-reduced multivariate analysis of covariance and CVA, in studies of deformation based morphometry has previously been reported by e.g. Ashburner et al.[18] The use of pointwise regression in neuroimaging is a thoroughly investigated subject in part due to the development of the Statistical Parametrical Mapping (SPM) software.[19] The general linear modeling approach of SPM enables several types of analyses such as group comparisons and time-series analysis.

The ridge regression method described in this paper is suited for problems where the dependent (clinical) variable is either continuous (e.g. age) or a variable that can be approximated by a continuous variable, such as certain ordered categorical variables. Hastie and Tibshirani[20] note that several statistical methods including a quadratic penalty term on the parameters have similar computational properties to ridge regression, such as penalized logistic and multinomial regression, penalized linear and mixture classification, the Cox model, and neural networks. Although such extensions may be possible, the focus in this paper is on ridge regression. The aim is to point to the possibility of using ridge regression as a *complement* to pointwise regression in the common case where a single clinical variable is related to spatial data.

2. MATERIALS AND METHODS

In the majority of regression analyses performed in medical imaging processing, a linear model is used, and its coefficients are estimated by minimizing the size of the residuals using a quadratic loss function. This is known as ordinary least squares regression and has the following form,

$$\mathbf{y} = \mathbf{X}\boldsymbol{\beta} + \boldsymbol{\varepsilon}, \qquad \min_{\boldsymbol{\beta}} \boldsymbol{\varepsilon}^T \boldsymbol{\varepsilon} = \min_{\boldsymbol{\beta}} \|\mathbf{y} - \mathbf{X}\boldsymbol{\beta}\|^2. \tag{1}$$

Here, $\mathbf{y}$, a vector of n observations, is the dependent variable that is modeled, $\mathbf{X}$ is an $n \times p$ matrix containing the p independent variables, $\boldsymbol{\beta}$ ($p \times 1$) is the vector of regression coefficients, and $\boldsymbol{\varepsilon}$ ($n \times 1$) represents the residuals. Without loss of generality, the variables are assumed to be centered. The intercept is usually not of interest as the focus here is on the sign and strength of each regression coefficient, but can if necessary be added back to the solution. The ubiquitous minimizer of (1) is given by,

$$\boldsymbol{\beta} = (\mathbf{X}^T\mathbf{X})^{-1}\mathbf{X}^T\mathbf{y}, \tag{2}$$

providing that the inverse of the ($p \times p$) *gram matrix* $\mathbf{X}^T\mathbf{X}$ exists. For the gram matrix to be invertible, it must have full rank. In cases where there are more observations than variables ($n > p$), rank deficiencies may occur due to collinearities among the independent variables. In this paper, we focus on the case where $p > n$. In this case, the gram matrix will *always* be ill-conditioned with rank less than or equal to $n - 1$. This motivates the use of regularization in some form, We wish to augment the setup in Equation 1 in some way such that the system of equations has a feasible solution, a solution that should approximate $\mathbf{y}$ as good as possible.

2.1 Pointwise Regression

One approach to regularization is to set the off-diagonal elements of the gram matrix to zero. This corresponds to the assumption that the independent variables are uncorrelated. Unless any of the variables have zero variance, this process will give a gram matrix with positive values along the diagonal and zeros elsewhere,

$$\mathbf{X}^T\mathbf{X} = \begin{bmatrix} \mathbf{x}_1^T\mathbf{x}_1 & & \mathbf{0} \\ & \ddots & \\ \mathbf{0} & & \mathbf{x}_p^T\mathbf{x}_p \end{bmatrix} \tag{3}$$

Such a matrix is positive definite and therefore invertible. Using this augmented gram matrix to solve Equation 2, it is realized that each regression coefficient β_i is a function of the ith variable $\mathbf{x}_i$ and $\mathbf{y}$ alone such that $\beta_i = (\mathbf{x}_i^T\mathbf{x}_i)^{-1}\mathbf{x}_i^T\mathbf{y}$. This represents the pointwise regression approach discussed above.

2.2 Ridge Regression

Pointwise regression is a computationally efficient solution to Equation 1 in cases where $p > n$, and is generally believed to provide sufficiently accurate results in a variety of applications. There is, however, no guarantee that pointwise regression uses the most sensible form of regularization for any application and indeed there exist a number of alternative regularization options. Ridge regression is one such method which both takes the correlation structure of the independent variables into account and is attractive from a computational viewpoint. The method adds a quadratic penalty term on the regression coefficients,

$$\min_{\boldsymbol{\beta}} \|\mathbf{y} - \mathbf{X}\boldsymbol{\beta}\|^2 + \lambda\|\boldsymbol{\beta}\|^2, \tag{4}$$

where $\lambda \geq 0$ is a parameter that controls the amount of regularization. A positive value of λ emphasizes solutions with regression coefficients of smaller absolute size. This shrinkage is strengthened as λ grows, and excessive regularization will drive all coefficients towards zero. Figure 1 shows coefficient values obtained using ridge regression for a range of values of λ on a synthetic data set with 20 observations and 40 variables. Only eight variables are shown for clarity. This type of plot is known as a *ridge trace*. The shrinkage introduces a tendency among the coefficients known as *bias* that is not inferred from the data at hand ($\mathbf{X}$ and $\mathbf{y}$). As given by Equation 1, ordinary least squares regression, when it has a solution, results in the lowest possible training error for any linear model, and the addition of bias in any form will invariably lead to larger residuals. However, the bias introduced by ridge regression has several benefits. In the presence of multicollinearity, where the regression coefficients may vary considerably among strongly correlated variables, the shrinkage helps to fix the coefficient vector at a more even distribution of coefficients. Ridge regression may also improve the *prediction accuracy* – the size of the residuals measured on previously unseen data – and the ability of recovering the true underlying model using a carefully chosen amount of regularization. Finally, and of particular interest in this paper, ridge regression manages to provide a solution in cases where the gram matrix cannot be inverted, especially when
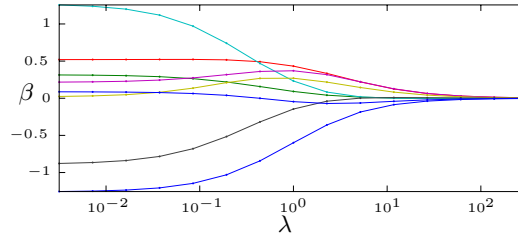
Figure 1. Ridge trace of 8 out of $p = 40$ variables for a synthetic data set with 20 observations. The parameter λ is defined by 15 equidistant points on a logarithmic scale. Coefficients may vary considerably with λ and may even change signs, before being shrunk towards zero.

$p > n$. To see why this is the case, we derive the optimal $\boldsymbol{\beta}_{ridge}$ by differentiating Equation 4, setting to zero and solving for $\boldsymbol{\beta}$,

$$\boldsymbol{\beta}_{ridge} = (\mathbf{X}^T\mathbf{X} + \lambda\mathbf{I})^{-1}\mathbf{X}^T\mathbf{y}, \qquad (5)$$

where $\mathbf{I}$ is the $p \times p$ identity matrix. Here, the computational effect of ridge regression is evident. A small constant is added to the diagonal of the gram matrix, giving it full rank. Further, $\lambda = 0$ gives the ordinary least squares solution, in cases where the gram matrix can be inverted.

Independent variables of different units are commonly standardized to unit length or unit variance to assure fair penalization. In the examples given in this paper, all variables are of equal units and require no standardization. The intercept is excluded and treated separately since we normally do not wish to penalize this variable.

In the analysis of clinical data, there are often a set of external variables that are not of immediate interest to the analysis, but which may influence both dependent and independent variables in unfortunate ways. Examples of such variables are age, gender and head size. These must be included in the analysis to ensure results that are adjusted for these factors. We refer to such variables as *confounding* variables. In standard linear regression, confounders enter the model as independent variables. This is not a suitable strategy for ridge regression, as we normally do not wish to apply shrinkage to these variables. Instead, we suggest factoring out confounding variables in a preliminary step, similarly to the work of Ashburner et al.[18] Letting $\mathbf{G}$ denote the $n \times g$ matrix of g confounding variables, this can be performed by

$$\mathbf{y}_a = \mathbf{y} - \mathbf{G}(\mathbf{G}^T\mathbf{G})^{-1}\mathbf{G}^T\mathbf{y}, \qquad (6)$$

where $\mathbf{y}_a$ is the adjusted dependent variable. In the remainder of this paper, $\mathbf{y}$ is assumed to be suitably adjusted.

2.3 Computation

With the intended applications of this paper, the number of variables p far exceeds the number of observations n. While the regularization provided by ridge regression makes estimation of the regression coefficients possible in theory, the excess of variables poses a computational hurdle. In particular, the estimation involves the inversion of the regularized gram matrix of size $p \times p$.

However, $\mathbf{X}$ has rank k where $k \leq n - 1$; $\mathbf{X}$ therefore has a non-redundant representation in the form of an $n \times k$ matrix $\mathbf{R}$. A particularly useful instance of $\mathbf{R}$ is given by the singular value decomposition (SVD)[21] of $\mathbf{X}$. We differentiate between two types of SVD transforms; let

$$\mathbf{X} = \tilde{\mathbf{U}}_{n \times n}\tilde{\mathbf{D}}_{n \times p}\tilde{\mathbf{V}}_{p \times p}^T \qquad \text{and} \qquad \mathbf{X} = \mathbf{U}_{n \times k}\mathbf{D}_{k \times k}\mathbf{V}_{k \times p}^T \qquad (7)$$

denote the *full* SVD and the *economy size* SVD respectively. Here, $\mathbf{U}$ and $\mathbf{V}$ have orthonormal columns and $\mathbf{D}$ is a diagonal matrix with elements known as singular values d_i. The rank k of $\mathbf{X}$ is the number of non-zero singular values d_i. The two variants are equivalent in that they perfectly reconstruct $\mathbf{X}$. This follows from the fact that the missing $p - k$ columns and $n - k$ rows of the economy size matrix $\mathbf{D}$ are zero.

Now, let $\tilde{\mathbf{R}} = \tilde{\mathbf{U}}\tilde{\mathbf{D}}$ ($n \times p$) and $\mathbf{R} = \mathbf{UD}$ ($n \times k$). For brevity, we use the notation $\mathbf{M}^k$ for the Hadamard (element-wise) product of k matrices $\mathbf{M}$. Further, $\mathbf{M}^{-k}$ denotes the element-wise inversion of $\mathbf{M}^k$ whenever $\mathbf{M}$ is a diagonal matrix. Using the full SVD, the ridge estimate can be written

$$\boldsymbol{\beta}_{ridge} = (\mathbf{X}^T\mathbf{X} + \lambda\mathbf{I})^{-1}\mathbf{X}^T\mathbf{y} = (\tilde{\mathbf{V}}\tilde{\mathbf{R}}^T\tilde{\mathbf{R}}\tilde{\mathbf{V}}^T + \lambda\mathbf{I})^{-1}\tilde{\mathbf{V}}\tilde{\mathbf{R}}^T\mathbf{y} = \tilde{\mathbf{V}}(\tilde{\mathbf{D}}^2 + \lambda\mathbf{I})^{-1}\tilde{\mathbf{R}}^T\mathbf{y}, \tag{8}$$

noting that $\mathbf{I} = \tilde{\mathbf{V}}\tilde{\mathbf{V}}^T$ and that $\tilde{\mathbf{V}}^{-1} = \tilde{\mathbf{V}}^T$. The advantage with this formulation is that $\tilde{\mathbf{D}}^2 + \lambda\mathbf{I}$ is a diagonal matrix and as such, easy to invert. However, through careful inspection of the final expression in Equation 8, in particular using the fact that the last $p - k$ columns of $\mathbf{R}$ are zero, an equivalent expression is seen to be

$$\boldsymbol{\beta}_{ridge} = \mathbf{V}(\mathbf{D}^2 + \lambda\mathbf{I})^{-1}\mathbf{R}^T\mathbf{y}, \tag{9}$$

where $\mathbf{I}$ is now of size $k \times k$. The benefit of this simplified formulation is significant as the inversion now involves a diagonal $k \times k$ diagonal matrix, and $\mathbf{V}$ is of a more manageable size. Hastie and Tibshirani[20] note that the complexity of this formulation is $\mathcal{O}(pk^2)$ rather than $\mathcal{O}(p^3)$ of the original setup. The derived complexity is dominated by the SVD of $\mathbf{X}$. Predictions enjoy particularly low complexity for ridge regression as

$$\hat{\mathbf{y}} = \mathbf{X}\boldsymbol{\beta}_{ridge} = \mathbf{R}(\mathbf{D}^2 + \lambda\mathbf{I})^{-1}\mathbf{R}^T\mathbf{y} = \mathbf{Hy}, \tag{10}$$

where $\mathbf{H}$ is the $n \times n$ hat matrix.

2.4 Inference

In order for a method to be of clinical value, we need a method to assess its statistical accuracy. Although general methods such as the bootstrap[22, 23] exist for this purpose, we prefer a classical parametric approach because of its simplicity and efficiency. Specifically, we require a way of determining whether a single voxel carries information of a significant deformation of the brain, a question that corresponds to testing whether a single regression coefficient is significantly different from zero. In principle, we go about this in the same fashion as for OLS estimation, each regression coefficient is normalized into a *standardized score z* through division by its standard deviation and compared to the distribution of the z-score under the null hypothesis. To this end, we require an estimate of the variance of the regression coefficients resulting from ridge regression. An expression for the variance-covariance matrix of $\boldsymbol{\beta}$ is easily derived[24] using the fact that $\mathbf{X}$ and λ are considered fixed and y is stochastic,

$$\text{var}(\boldsymbol{\beta}_{ridge}) = \text{var}((\mathbf{X}^T\mathbf{X} + \lambda\mathbf{I})^{-1}\mathbf{X}^T y) = (\mathbf{X}^T\mathbf{X} + \lambda\mathbf{I})^{-1}\mathbf{X}^T\mathbf{X}(\mathbf{X}^T\mathbf{X} + \lambda\mathbf{I})^{-1}\text{var}(y), \tag{11}$$

the latter can be derived from the identity $\text{var}(ay + b) = a^2\text{var}(y)$. The variance of y is considered to be due to the errors $\boldsymbol{\varepsilon}$ in the model and is usually measured by the mean squared error σ_ε^2 (MSE). For OLS the usual MSE estimate is $\sigma_\varepsilon^2 = \boldsymbol{\varepsilon}^T\boldsymbol{\varepsilon}/(n - p)$ where $\boldsymbol{\varepsilon} = \mathbf{y} - \mathbf{X}\boldsymbol{\beta}$ and where the denominator represents the number of degrees of freedom of the residuals. Such a measure is clearly inappropriate for ridge regression; consider for instance the $p > n$ case where the residual variance would become negative. A regularized model such as ridge regression becomes less flexible as more regularization is applied, and this must be taken into account for accurately estimating the number of degrees of freedom. For linear models such as ridge regression, a measure known as the *effective number of parameters* has been proposed to replace p as the number of degrees of freedom. This measure, here denoted $d_f(\lambda)$, becomes a function of λ for ridge regression and has a particularly convenient form,

$$d_f(\lambda) = \text{trace}(\mathbf{H}) = \text{trace}(\mathbf{R}(\mathbf{D}^2 + \lambda\mathbf{I})^{-1}\mathbf{R}^T) = \sum_{i=1}^{k}\frac{d_i^2}{d_i^2 + \lambda}, \tag{12}$$

where d_i is the ith diagonal element of $\mathbf{D}$ and $\mathbf{H}$ is the hat matrix of Equation 10. The effective number of parameters is discussed by Moody[25] and more recently by Hastie et al.[26] Armed with this measure of model complexity, a revised measure of MSE for ridge regression is

$$\sigma_\varepsilon^2 = \frac{\boldsymbol{\varepsilon}^T\boldsymbol{\varepsilon}}{n - d_f}. \tag{13}$$
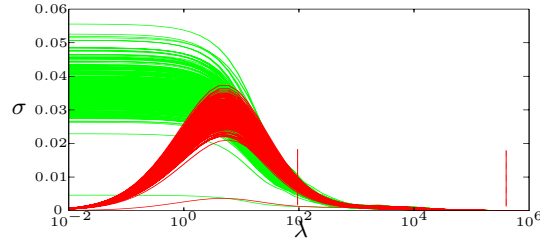
Figure 2. Standard deviation of $\boldsymbol{\beta}$ coefficients. The graph shows the characteristics of the parametric ridge regression estimates (red curves) versus bootstrap estimates (green curves) as functions of λ for a synthetic data set with $n = 45$ observations and $p = 6000$ variables. At a reasonably well defined point, shown by the left vertical dashed line, the bootstrap and parametric estimates become equivalent and parametric inference may be performed. The right vertical dashed line depict the point where solutions are considered to be equivalent to pointwise regression ($\epsilon = 0.01$).

For very large p, the entire variance-covariance matrix is intractable, however, we are usually only interested in the variance of the estimates. These values are placed along the diagonal of the matrix var($\boldsymbol{\beta}$) and can be efficiently calculated by,

$$\sigma_{\boldsymbol{\beta}}^2 = \mathbf{V}^2 \text{diag}(\mathbf{D}^2(\mathbf{D}^2 + \lambda\mathbf{I})^{-2})\frac{\boldsymbol{\varepsilon}^T\boldsymbol{\varepsilon}}{n - d_f}. \tag{14}$$

In our experience, the use of Equation 14 to estimate the variance of the regression coefficients is satisfactory in cases where $n > p$, while the $p > n$ case requires some care. Complications arise in such cases for weakly regularized models. As λ approaches zero, so does the sum-of-squared residuals and therefore also the variance $\sigma_{\boldsymbol{\beta}}^2$. This behavior is counter-intuitive since we expect the variance to grow as less regularization is applied. However, empirical evidence suggest that the variance estimation is correct for sufficiently large values of λ. Figure 2 shows characterizes this property. The graph is based on a synthetic data set with $p = 6000$ and $n = 45$, where green and red lines represent bootstrapped and parametric estimates respectively. Assuming the bootstrapped estimates are reasonably accurate, it is seen that they coincide with the parametric estimates when sufficient regularization is applied. Identification of the critical point λ_{min} where $\sigma_{\boldsymbol{\beta}}^2$ coincides with the bootstrapped estimates is important, as this tells us the range of λ where parametric inference can be safely used. A formal expression for the variance of z_i, which could be used to obtain a rigorous expression for λ_{min}, is a complicated expression of $\mathbf{y}$. Intuitively, however, the behavior of the curves in Figure 2 is related to the values of the diagonal matrix $\mathbf{D}^2$. One expression for λ_{min} that has proved to be a sufficiently accurate estimate in a variety of applications is

$$\lambda_{min} = \frac{1}{n}\sum_{i=1}^{n} d_i^2, \tag{15}$$

but we have yet to prove its validity. This point is shown by the left vertical dashed lines in Figure 2. Estimation for values of λ below this point should not be carried out using the parametric approach described above. Instead, we suggest resorting to bootstrap methods in such cases. However, we anticipate that interesting solutions are found for relatively large values of λ, since the variance of the estimates increase quickly as λ becomes smaller in cases where $p \gg n$.

An important question is whether there is a natural connection between ridge and pointwise regression. The presentation of the two methods in Section 2.1 and 2.2 indicates their similarities, both methods focus on the variance of the variables rather than their covariance. Can this relation be expressed more formally? It turns out that as λ grows, the significance of the ridge solutions approach those of pointwise regression. Looking at the ridge trace in Figure 1, it is seen that the $\boldsymbol{\beta}$ coefficients are shrunk as λ grows, and therefore depart from the coefficients of pointwise regression. However, the corresponding z-statistics behave differently, and turn out to be equal to those of pointwise regression in the limit. We state this finding in the following theorem.

THEOREM 2.1. *In the limit $\lambda \to \infty$, the z-statistics of ridge regression and pointwise regression are equivalent.*

Proof. Let $\boldsymbol{\Omega} = (\mathbf{X}^T\mathbf{X} + \lambda\mathbf{I})^{-1}$ and let $\boldsymbol{\omega}_i$ be the ith column of $\boldsymbol{\Omega}$. The ith z-statistic resulting from ridge

regression is then

$$z_i(\lambda) = \frac{\beta_i(\lambda)}{\sigma_{\beta_i}(\lambda)} = \frac{\boldsymbol{\omega}_i^T \mathbf{X}^T \mathbf{y}}{\sigma_{\boldsymbol{\varepsilon}} \sqrt{\boldsymbol{\omega}_i^T \mathbf{X}^T \mathbf{X} \boldsymbol{\omega}_i}} \tag{16}$$

We note that $\boldsymbol{\Omega} \to \mathbf{I}/\lambda$ as $\lambda \to \infty$. This means that $\boldsymbol{\omega}_i$ simplifies to a zero vector with the ith entry equal to $1/\lambda$. The expression for $z_i(\lambda)$ becomes

$$\lim_{\lambda \to \infty} z_i(\lambda) = \frac{\frac{1}{\lambda} \mathbf{x}_i^T \mathbf{y}}{\frac{1}{\lambda} \sigma_{\boldsymbol{\varepsilon}} \sqrt{\mathbf{x}_i^T \mathbf{x}_i}} = \frac{(\mathbf{x}_i^T \mathbf{x}_i)^{-1} \mathbf{x}_i^T \mathbf{y}}{\sigma_{\boldsymbol{\varepsilon}} \sqrt{(\mathbf{x}_i^T \mathbf{x}_i)^{-1}}} \tag{17}$$

This expression is equivalent to the pointwise estimation of z_i. ☐

   This property of ridge regression is characterized in Figure 3. In this case $n > p$ which means that solutions range from ordinary least squares regression for $\lambda = 0$ to pointwise regression for $\lambda \to \infty$.
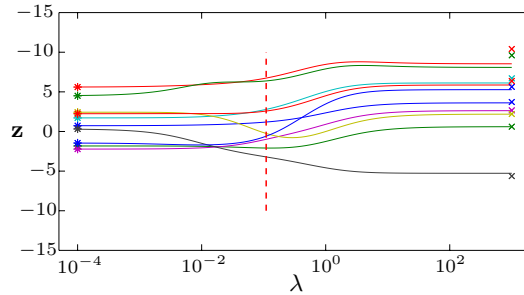

Figure 3. Plot showing the z-scores of each regression coefficient as a function of λ for a small regression problem with $p = 10$ and $n = 442$. For $\lambda = 0$ the full OLS solution is obtained (no bias, high variance), marked by the left set of crosses. For λ sufficiently large, the results converge to those of pointwise regression (high bias, low variance), marked by the right set of crosses. The remaining difference between the methods at this location has to do with the estimation of the error variance σ_{ε}.

   Theorem 2.1 points to an important connection between the two methods; pointwise regression is a special case of ridge regression. It also motivates the use of ridge regression in cases where pointwise regression is normally used; it is unlikely that the amount of bias introduced in pointwise regression yields the lowest error rate. Instead, consideration of cases with slightly less bias, where correlation information is introduced to some extent, may be beneficial. The results also makes clear that values of λ over a certain threshold are uninteresting, as the ridge solutions have converged to pointwise regression at that point. This enables the calculation of an upper limit of λ, in addition to the lower limit of Equation 15. This limit can be defined in terms of the value $d_{max} = \max_i d_i$ as

$$\lambda_{max} = d_{max}^2 \frac{1 - \epsilon}{\epsilon}. \tag{18}$$

For this choice of λ, the elements of the matrix $(\mathbf{D}^2 + \lambda \mathbf{I})^{-1}$ will deviate at most 100ϵ % from the matrix $\mathbf{I}/\lambda$, where ϵ again is a small number $0 < \epsilon < 1$. Equations 15 and 18 now provide suitable choices of endpoints for the range of regularization. The upper limit is represented by the right vertical dashed line in Figure 2.

   The derivation in Theorem 2.1 assumes that the error variance σ_{ε}^2 is measured in the same way for both methods. This is usually not the case. Equation 13 gives this estimate for ridge regression while the estimate for pointwise regression is $\sigma_{\varepsilon}^2 = \boldsymbol{\varepsilon}_i^T \boldsymbol{\varepsilon}_i / (n - p)$ where $p = 2 + g$ and g is the number of confounding variables, if any. However, performing the same asymptotic analysis as above for the error variance for ridge regression gives,

$$\lim_{\lambda \to \infty} \sigma_{\varepsilon}^2(\lambda) = \frac{(\mathbf{y} - \mathbf{X}\boldsymbol{\beta}(\lambda))^T (\mathbf{y} - \mathbf{X}\boldsymbol{\beta}(\lambda))}{n - d_f(\lambda)} = \frac{\mathbf{y}^T \mathbf{y}}{n} = \text{var}(\mathbf{y}), \tag{19}$$

a measure of the error variance that is known to be reasonably close to $\boldsymbol{\varepsilon}_i^T \boldsymbol{\varepsilon}_i / (n - p)$.

At the other end of the spectrum where $\lambda = 0$, what regression problem is ridge regression solving? With the formulation of Equation 5, $\lambda = 0$ is clearly not a valid choice, however, the matrix $\mathbf{D}^2$ of Equation 9 has full rank and is thus invertible. In this case and with no regularization, the solution is readily seen to correspond to a principal component regression (PCR) using all non-zero basis vectors.

An interesting question is how ridge regression relates to multiple comparisons issues. In particular, the multiple testing performed with pointwise regression lead to overly optimistic significance values which must be corrected.[27] At first sight, ridge regression appears to offer a remedy to this complication. All p coefficients are estimated in a single analysis, and multiple comparison adjustment should therefore not be necessary. However, we have just seen that pointwise regression is a special case of ridge regression. There appears to be a conflict here; ridge solutions bridge OLS estimates, where adjustment for multiple comparisons is not commonly considered, and pointwise regression where adjustment is clearly necessary. The key realization is that *the assessment of a single regression coefficient is one test*, regardless of whether it has been estimated via a separate regression equation or is part of a larger regression analysis. If a series of regression coefficients are estimated in a single analysis, and a single one of those is subsequently assessed for its statistical relevance, multiple comparisons correction is not necessary. But as soon as more than one regression coefficient is *interpreted*, adjustment should be carried out. This is naturally of great importance in ridge regression of brain data, where a million regression coefficients might be estimated and all of them are interpreted. There are a range of methods available for adjustment for multiple comparisons. In this paper, we employ methods for adjustment based on non-parametric permutation testing.[27] Specifically, two tests are considered, one where the z-values for each voxel are compared to the empirical distribution function (EDF) of a *maximal statistic*, built from the set of maximal z-values over the entire image for a large number of permutations, and one where the maximal size of the clusters (contiguous z-values) over the image is compared to the EDF of maximal cluster sizes under permutations.

2.5 Model Selection

The choice of the regularization parameter λ is crucial for the estimation of a coefficient vector $\boldsymbol{\beta}$ that is as close as possible to the true (unknown) model. Generally, most model selection algorithms work by estimating some measure of performance for a number of different choices of λ, and then picking the model with the highest score. Here, we let n_λ be the number of candidate models, where λ is specified at equidistant points on a log-scale. Generic methods to estimate an optimal λ include Akaike's information criterion (AIC),[28] the Bayesian information criterion (BIC),[29] Mallow's C_p statistic[30] and cross-validation and bootstrap methods.[22] For a Gaussian model such as ridge regression, BIC is proportional to AIC, and AIC is equivalent to C_p.[26] The C_p (or AIC) criterion for the ridge model is

$$C_p(\lambda) = \boldsymbol{\varepsilon}^T \boldsymbol{\varepsilon} + 2\frac{d_f}{n}\sigma_\varepsilon^2, \tag{20}$$

where $\boldsymbol{\varepsilon}$ denote the residuals as before, $d_f(\lambda)$ are the effective number of parameters and σ_ε^2 is the estimate of the residual variance from Equation 13, estimated from a low-bias model.[26,31] The first term measures the training error, an increasing function of λ. The second term is monotonically decreasing and measures the flexibility of the model, a quantity known as the *optimism* of the training error. The idea is that the minimum of $C_p(\lambda)$ corresponds to a value of λ that balances the two terms in a suitable fashion.

Leave-one-out cross-validation is another technique which can be used for model selection. This can be computed efficiently for ridge regression[32] by

$$CV_{(n-\text{fold})}(\lambda) = \frac{1}{n}\sum_{i=1}^{n}\left(\frac{y_i - \mathbf{H}_i \mathbf{y}}{1 - H_{ii}}\right)^2, \tag{21}$$

where $\mathbf{H}_i$ is the ith row of $\mathbf{H}$ and H_{ii} is the ith diagonal element of $\mathbf{H}$.

3. RESULTS

Three-dimensional T1-weighted MRI images (matrix size $138 \times 148 \times 103$, voxel size $1 \times 1 \times 1.5$ mm) were obtained from 38 subjects with mild cognitive impairment (78 ± 6 years of age, 16 women, MMSE 28.3 ± 1.5) and 7

controls (71 ± 4 years of age, 3 women, MMSE 29.6 ± 0.9). Parallel to image acquisition, neuropsychological testing was carried out with repetition after one year. Testing included the clinical dementia rating (CDR) and parts of the California Verbal Learning Test (cf. e.g. Elwood[33]). The latter included memory tests where the subject is asked to remember a set of items from a typical shopping list after either a short or a long delay. Hints in the form of category cues may be given resulting in four variants of the test; Short Delay Free Recall (SDFR), Short Delay Cued Recall (SDCR), Long Delay Free Recall (LDFR) and Long Delay Cued Recall (LDCR). Longitudinal change scores were computed as (score$_{baseline}$ − score$_{(1\,year)}$)/(test interval (years)), where *a positive score indicates cognitive decline.* A thorough description of the test protocol along with clinical interpretation of the results is deferred to a later paper. Preliminary clinical results on the present data set using pointwise regression with adjustment for multiple comparisons are presented by Cardenas et al.[34]

Images were spatially normalized with respect to a common reference using a B-spline-based algorithm for non-rigid registration.[35] A single subject was used as a reference. For each subject, the procedure results in a continuous representation of the transformation that maps the reference to the subject. This transformation describes both global properties, such as differences in position between the subject and reference, as well as local transformations. To obtain a positioning-invariant representation of anatomy suitable for morphometric analysis, the deformation field is differentiated along each axis, resulting in a (3×3) Jacobian matrix of derivatives at each image coordinate, measuring the rate at which the deformation field changes in each direction. The determinant of the Jacobian matrix gives a single measure of local volume change – a contraction or an expansion.[36] This measure was estimated at each reference voxel location for each subject, rendering $n = 45$ images of local expansions and contractions relative to the reference anatomy.

The assumption of pointwise regression that voxels are not significantly correlated across the brain must be violated if the application of ridge regression is to lead to an improvement of the analysis. Figure 4 provides a hint of the typical correlation patterns found in this type of data. Correlation coefficients are calculated for each voxel in relation to a single reference voxel which approximate location is evident from the figure. The correlation pattern is seen to be focused around the seed voxel, but extends throughout the brain with varying sign and strength.

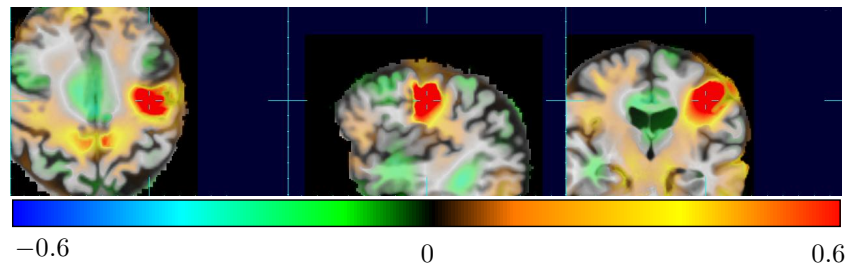$$-0.6 \qquad\qquad 0 \qquad\qquad 0.6$$

Figure 4. Correlation structure for the spatial data in reference to a single voxel. Correlations are significant and extend throughout the entire brain, motivating the use of an analysis method that takes this information into account.

Separate regression analyses were carried out for the test interval normalized change scores of SDFR, SDCR, LDFR, LDCR and CDR. The set of confounding variables were age, group (normal/control), test score at baseline, and head size, approximated by the average determinant-of-Jacobian value of each subject. For pointwise regression, spatial variables were used as dependent variables while change scores and confounding variables made up the set of independent variables. This is a convenient construction as the data matrix stays the same between analyses. With ridge regression, change scores were dependent variables and all spatial variables entered the model simultaneously as independent variables. Confounding variables were factored out prior to the analysis using the method described in Section 2.2. All results given below are uncorrected for multiple comparisons. Adjusting the results for multiple comparisons using the methods discussed in Section 2.4 did not yield significant results on this data set. The analysis is restricted to intracranial voxels, determined from simple thresholding of the average anatomy. This results in a total of $p = 860\,368$ voxels/variables.

Figures 5, 6 and 7 show examples of how the significance patterns resulting from ridge regression (top rows) are distributed over the average anatomy, compared to pointwise regression (bottom rows). Positive values correspond to areas where either significant contraction lead to smaller cognitive change scores, or where

significant expansions lead to increase change scores. Conversely, negative values correspond to areas where significant contractions lead to increased scores, i.e. greater cognitive decline, while expansions relate to decreased scores. Typically, one may see positive values in areas with cerebrospinal fluid (CSF) where expansion due to contraction of surrounding tissue is related to greater cognitive decline, and negative values in gray and white matter where contraction due to tissue atrophy is related to cognitive decline.

None of the proposed model selection criteria provided reliable information for accurate model selection, a problem which we discuss below. Values of the regularization parameter where set to $\lambda = 75766$ for SDFR, $\lambda = 99791$ for LDFR, and $\lambda = 109386$ for LDCR. Parametric inference was used, and all values of λ were well within the interval suggested in Section 2.4.

Figure 5. Axial, sagittal and frontal views of the average anatomy with significant areas overlaid for the SDFR test using ridge regression (top row) and pointwise regression (bottom row).
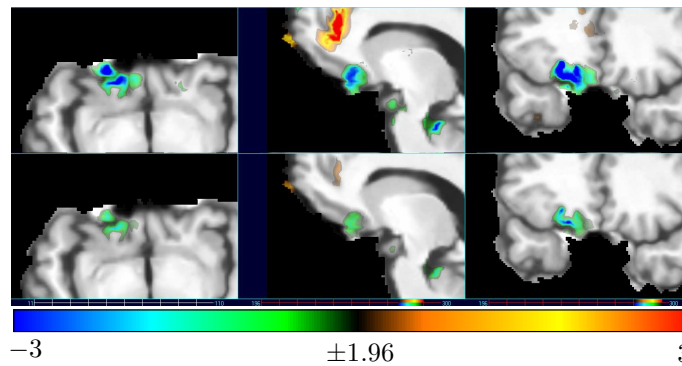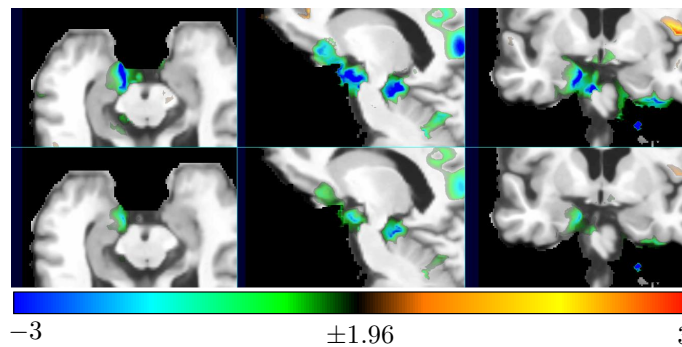

Figure 6. Axial, sagittal and frontal views of the average anatomy with significant areas overlaid for the LDFR test using ridge regression (top row) and pointwise regression (bottom row).

Figure 7. Axial, sagittal and frontal views of the average anatomy with significant areas overlaid for the LDCR test using ridge regression (top row) and pointwise regression (bottom row).

4. DISCUSSION

The central point of this paper is to clarify the connection between pointwise regression and ridge regression, and to show how the latter can be used as a generalization of the former. Careful introduction of covariance information from the spatial data may result in more accurate results. This means that significance levels for individual variables may both rise and fall, in part due to effects known as *supression* and *redundancy*.[37] Figures 5, 6 and 7 all show a general increase in significance for the chosen values of λ. In contrast, the significance levels for CDR generally decreased. This variation of the significance levels, and ultimately the clinical interpretation of the results, makes determination of a proper value of λ crucial. We note that resorting to pointwise regression, which corresponds to a particular choice of λ, is no solution to this problem.

As mentioned in Section 3 above, none of the investigated criteria for model selection proved reliable in extreme cases where $p \gg n$. The C_p-criterion of Equation 20 contains a measure of the error variance σ_ε^2 for a low-bias model, which proved difficult to estimate. Using Equation 13 with $\lambda \to 0$ for this purpose results in $\sigma_\varepsilon^2 \to 0$. The resulting expression for C_p becomes a function of the training error only and does not provide any information for selecting a suitable model. Generalized cross-validation does not suffer from this complication. However, in the authors' experience on a variety of problems where $p \gg n$, cross-validation and bootstrap methods do not provide enough information to confidently choose an appropriate model. A reasonable explanation for this is that the cross-validation estimates become highly variable as modifications to the relatively small set of observations cause considerable differences in the much larger set of regression coefficients.

Inference for $p \gg n$ ridge regression models is less troublesome but also calls for further investigation. Two interesting questions arise. The first regards the accuracy and reliability of bootstrap estimates of the variance of the regression coefficients. Is the bootstrap accurate enough to act as ground truth in this case? Carefully designed experiments on synthetic data may provide a partial answer. The second question regards the lower limit of the interval of λ-values suggested for parametric inference. What is the rationale for using this estimate?

5. CONCLUSIONS

This paper has presented the use of ridge regression as a generalization of pointwise regression, a common approach for analyzing very high-dimensional data sets such as those resulting from non-rigid registration of three-dimensional image data. A detailed revision of the mathematical properties of ridge regression was provided, along with theoretical and empirical findings on inference, model selection and adjustment for multiple comparisons. The central issue of selecting a suitable amount of regularization, consisting of picking a suitable value of the regularization parameter λ out of a set of candidates, was discussed. A suggestion for a suitable lower limit of λ, where parametric inference becomes possible, was given in Equation 15. While this choice is admittedly *ad hoc*, a more rigorous choice of an upper limit of λ was suggested in Equation 18, a point where the difference between ridge regression and pointwise regression becomes negligible. Within this interval, the value of λ that gives the lowest prediction error and allows for the most relevant clinical interpretation is difficult to determine for models with $p \gg n$. The method was applied to a set of whole-brain deformation maps, consisting of a measure of contraction/expansion in each voxel. The results were shown to correspond well to those of the pointwise approach, but also showed characteristic differences that were suggestive of the potential of the method.

Acknowledgments

REFERENCES

1. C. Davatzikos, "Why voxel-based morphometric analysis should be used with great caution when characterizing group differences," *NeuroImage* **23**(1), pp. 17–20, 2004.

2. A. Hoerl and R. Kennard, "Ridge regression: Biased estimation from nonorthogonal problems.," *Technometrics* **12**(1), pp. 55–67, 1970.

3. D. Marquardt, "Generalized inverses, ridge regression, biased linear estimation, and nonlinear estimation," *Technometrics* **12**(3), pp. 591–612, 1970.

4. P. Hansen and D. O'Leary, "The use of the l-curve in the regularization of discrete ill-posed problems," *SIAM Journal on Scientific Computing* **14**(6), pp. 1487–1503, 1993.

5. P. Valdes-Sosa, J. Sanchez-Bornot, A. Lage-Castellanos, M. Vega-Hernandez, J. Bosch-Bayard, L. Melie-Garcia, and E. Canales-Rodriguez, "Estimating brain functional connectivity with sparse multivariate autoregression," *Philosophical Transactions of the Royal Society - Ser B - Biological Sciences* **360**(1457), pp. 969–982, 2005.

6. M. West, "Bayesian factor regression models in the "large p, small n" paradigm," 2002.

7. T. Cootes, D. Cooper, C. Taylor, and J. Graham, "Trainable method of parametric shape description," *Image and Vision Computing* **10**(5), pp. 289–294, 1992.

8. K. Friston, C. Frith, F. Liddle, and R. Frackowiak, "Functional connectivity: The principal-component analysis of large (PET) data sets," *Journal of Cerebral Blood Flow and Metabolism* **13**, pp. 5–14, 1993.

9. S. Strother, I. Kanno, and D. Rottenberg, "Principal component analysis, variance partitioning, and functional connectivity," *Journal of Cerebral Blood Flow and Metabolism* **15**(3), pp. 355–360, 1995.

10. K. Friston, J. Poline, A. Holmes, C. Frith, and R. Frackowiak, "A multivariate analysis of PET activation studies," *Human Brain Mapping* **4**, pp. 140–151, 1996.

11. A. McIntosh, F. Bookstein, J. Haxby, and C. Grady, "Spatial pattern analysis of functional brain images using partial least squares," *NeuroImage* **3**(3), pp. 143–157, 1996.

12. K. Worsley, "An overview and some new developments in the statistical analysis of PET and fMRI data," *Human Brain Mapping* **5**(4), pp. 254–258, 1997.

13. K. Friston, "Functional and effective connectivity in neuroimaging: A synthesis," *Human Brain Mapping* **2**, pp. 56–78, 1995.

14. Z. Lao, D. Shen, Z. Xue, B. Karacali, S. Resnick, and C. Davatzikos, "Morphological classification of brains via high-dimensional shape transformations and machine learning methods," *NeuroImage* **21**(1), pp. 46–57, 2004.

15. P. Golland, W. Grimson, M. Shenton, and R. Kikinis, "Detection and analysis of statistical differences in anatomical shape," *Medical Image Analysis* **9**(1), pp. 69–86, 2005.

16. P. C. Fletcher, R. J. Dolan, T. Shallice, C. D. Frith, R. S. J. Frackowiak, and K. J. Friston, "Is multivariate analysis of PET data more revealing than the univariate approach? evidence from a study of episodic memory retrieval," *NeuroImage* **3**(3), pp. 209–215, 1996.

17. K. Friston and J. Ashburner, "Generative and recognition models for neuroanatomy," *NeuroImage* **23**(1), pp. 21–24, 2004.

18. J. Ashburner, C. Hutton, R. Frackowiak, I. Johnsrude, C. Price, and K. Friston, "Identifying global anatomical differences: Deformation-based morphometry," *Human Brain Mapping* **6**(5-6), pp. 348–357, 1998.

19. K. Friston, A. Holmes, K. Worsley, J. Poline, C. Frith, and R. Frackowiak, "Statistical parametric maps in functional imaging: A general linear approach," *Human Brain Mapping* **2**, pp. 189–210, 1995.

20. T. Hastie and R. Tibshirani, "Efficient quadratic regularization for expression arrays," *Biostatistics* **5**(3), pp. 329–340, 2004.

21. G. Golub and C. Van Loan, *Matrix Computations*, The Johns Hopkins University Press, 3rd ed., 1996.

22. B. Efron and R. Tibshirani, *An introduction to the bootstrap*, Monographs on statistics and applied probability (57), Chapman and Hall, 1993.

23. A. Davison and D. Hinkley, *Bootstrap Methods and Their Application*, Cambridge University Press, 5th ed., 2003.

24. W. Fu, "Penalized regressions: The bridge versus the lasso," *Journal of Computational and Graphical Statistics* **7**(3), p. 397, 1998.

25. J. Moody, "Note on generalization, regularization and architecture selection in nonlinear learning systems," *Neural Networks for Signal Processing [1991]., Proceedings of the 1991 IEEE Workshop* , pp. 1–10, 1991.

26. T. Hastie, R. Tibshirani, and J. Friedman, *The Elements of Statistical Learning*, Springer, 2001.

27. T. Nichols and A. Holmes, "Nonparametric permutation tests for functional neuroimaging: A primer with examples," *Human Brain Mapping* **15**(1), pp. 1–25, 2002.

28. H. Akaike, "Information theory and an extension of the maximum likelihood principle," in *Second International Symposium on Information Theory*, pp. 267–281, 1973.

29. G. Schwartz, "Estimating the dimension of a model," *Annals of Statistics* **6**, pp. 461–464, 1979.

30. C. L. Mallows, "Some comments on Cp," *Technometrics* **15**(4), pp. 661–675, 1973.

31. S. Walker and C. Page, "Generalized ridge regression and a generalization of the cp statistic," *Journal of Applied Statistics* **28**(7), p. 911, 2001.

32. G. Golub, M. Heath, and G. Wahba, "Generalized cross-validation as a method for choosing a good ridge parameter.," *Technometrics* **21**(2), pp. 215–223, 1979.

33. R. Elwood, "The california verbal learning test: Psychometric characteristics and clinical application," *Neuropsychology Review* **5**, pp. 173–201, October 1995.

34. V. Cardenas, L. Chao, C. Studholme, S. Buckley, N. Cashdollar, N. Schuff, and M. Weiner, "Regions of brain atrophy that predict cognitive decline," in *Alzheimer's Association 10th International Conference on Alzheimer's Disease and Related Disorders*, **2 (3 Suppl 1)**, p. 350, (Madrid, Spain), July 2006.

35. C. Studholme, V. Cardenas, R. Blumenfeld, N. Schuff, H. Rosen, B. Miller, and M. Weiner, "Deformation tensor morphometry of semantic dementia with quantitative validation," *NeuroImage* **21**(4), pp. 1387–1398, 2004.

36. C. Davatzikos, M. Vaillant, S. Resnick, J. Prince, S. Letovsky, and R. Bryan, "A computerized approach for morphological analysis of the corpus callosum," *Journal of Computer Assisted Tomography* **20**(1), pp. 88–97, 1996.

37. J. Cohen and P. Cohen, *Applied multiple regression / correlation analysis for the behavioral sciences*, John Wiley & sons, 1975.

Pilot Study 3:

    Interactions of the Calcium-sensing Receptor (CaR) and GABA-B Receptor (GABA-B-R) in Neuronal Function after Ischemia and Neurotrauma

Principal Investigator: Wenhan Chang, Ph.D.,
                      Assistant Professor, Medicine, VAMC, UCSF

ABSTRACT

Traumatic brain injury (TBI) is a major health problem in the US affecting both civilians and military personnel. One of the major sources of central nervous system (CNS) injury after trauma is from ischemia/hypoxia to brain tissue and especially to neurons. Death of axons and neurons resulting from ischemic injury leads to sensory and motor deficits and alterations in cognitive and emotional functioning clinically. Patients with TBI and with other forms of ischemic/hypoxic cerebral insults often suffer from post-traumatic epilepsy (PTE). The molecular and cellular changes in neurons after TBI include hyperexcitability and cell death (or apoptosis) in affected brain regions and progress to tissue scarring (gliosis) and the reorganization of neuronal networks. These changes eventually generate persistent epileptic foci and chronic seizures. Histological studies of brain tissues from patients with epilepsy and from animals with brain injury indicate that neuronal death is closely correlated with decreased expression of metabotropic or type B GABA receptors (GABA-B-Rs). Furthermore, GABA-B-R1 knockout mice display recurrent seizures and die shortly after birth. This suggests a close linkage between GABA-B-R expression, neuronal excitability and survival, and seizures.

In the brain, GABA-B-Rs are co-expressed with Ca^{2+}-sensing receptors (CaRs). CaRs couple changes in the extracellular $[Ca^{2+}]$ ($[Ca^{2+}]_e$) to signaling pathways controlling secretion, growth, and differentiation in many cell types. In neurons and neuroglia, raising $[Ca^{2+}]_e$ opens membrane ion channels, releases Ca^{2+} from intracellular stores, and enhances cell excitability via the activation of CaRs. Our recent studies showed that CaRs form heteromeric complexes with GABA-B-R1s, and the interactions between these receptors lead to reduced CaR expression and signaling. In cultured mouse hippocampal neurons, where CaRs and GABA-B-Rs are co-localized and co-immunoprecipitate, blocking the expression of GABA-B-R1s increased the expression of CaRs and promoted apoptosis. We hypothesize that increased expression and signaling of CaRs are central components of the cellular response to reduced GABA-B-R1 expression and signaling in neurons after brain injury. To test this hypothesis, we propose two aims. Aim 1: To determine whether increased CaR expression promotes a state of Ca^{2+} overload and increases apoptosis in neurons lacking the GABA-B-R1 and in neurons subjected to ischemia in vitro and whether knockout of CaR gene blocks ischemia-induced Ca^{2+} overload. Aim 2: To determine the role of CaRs in brain injury in vivo by comparing ischemia-induced changes in the hippocampus of wild-type (WT) vs CaR knockout mice and by testing whether CaR antagonists reduce neuronal death induced by ischemia. Successful completion of these studies will provide novel insights into molecular and cellular changes involving CaRs and GABA-B-Rs that result in altered signal transduction, gene expression and apoptosis in neurons after brain injury. These mechanisms may explain key aspects of TBI and PTE. Finally, these studies may identify a potential therapeutic target to protect neurons exposed to ischemic injury.

TABLE OF CONTENTS

INTRODUCTION

This pilot project addresses the hypothesis that increased expression and signaling of the extracellular Ca^{2+}-sensing receptors (CaRs) are central components of the cellular response to reduced GABA-B-R1 expression and signaling in neurons after brain injury. Two specific aims are proposed. In Aim 1, studies of cultured neurons will be carried out to determine whether increased CaR expression promotes a state of Ca^{2+} overload and increases apoptosis in neurons lacking the GABA-B-R1 and in neurons subjected to ischemia in vitro and whether knockout (KO) of CaR gene blocks ischemia-induced Ca^{2+} overload. In Aim 2, mouse models will be generated and studied to determine the role of CaRs in brain injury in vivo by comparing ischemia-induced changes in the brains of wild-type (WT) vs neuron-specific CaR knockout mice and by testing whether CaR antagonists reduce neuronal death induced by ischemia.

Only 3 months have passed since the award was granted on July 1, 2008, however, substantial progress has been made toward these goals.

BODY

In order to perform in vitro and in vivo ablation of the CaR gene in neurons, we made floxed-CaR mice, which carry loxP sequences flanking the CaR gene. These mice not only provide floxed-CaR neurons that permit in vitro excision of the CaR gene by infecting the cells with adenoviruses expressing Cre recombinase (Ad-Cre) but also allow gene ablation in neurons in vivo by breeding the floxed-CaR mice with mice expressing Cre recombinase under the control of neuron-specific gene promoters.

To validate our gene targeting strategy, we bred the floxed-CaR mice with mice expressing Cre under the control of a parathyroid hormone (PTH) promoter (*1*) to produce mice with parathyroid cell-specific KO of CaR (PTH-CaR-KO), as the function of CaR in parathyroid cells has been extensively documented. The PTH-CaR-KO mice developed severe hyperparathyroidism, hypercalcemia, hypophostemia, and growth retardation. These phenotypes recapitulate the phenotypes of a generalized CaR KO mouse model developed previously by Ho and colleagues (*2*). We also generated mice with CaR KO targeted to chondrocytes and bone cells. The latter mice showed severe retardation of embryonic and postnatal bone growth, respectively, supporting a critical role for the CaR in skeletal development. Detailed phenotypes of the above conditional knockout mice have been published in the *Science Signaling* (*3*). These data together validate our gene knockout strategy.

For Aim 2, we bred floxed-CaR mice and mice expressing Cre recombinase under the control of the nestin gene promoter (Nes-Cre) to generate neuron-specific CaR knockout mice (Nes-CaR-KO). The nestin gene is specifically expressed in neurons in the central nervous system (*4*). Preliminary observations indicate that both homozygous and heterozygous Nes-CaR-KO mice are viable. However, their body sizes are smaller by ≈10% than their WT littermates. Histology is underway to assess the impact of CaR KO on the brains of these mice. In the coming months, the KO mice and their WT littermates will be subjected to ischemia using vessel-occlusion techniques to determine whether ablation of CaR expression protects the neurons from Ca^{2+}-overload and apoptosis.

For Aim 1, we have begun to isolate and culture hippocampal and cerebral cortex neurons from floxed-CaR mice. Preliminary observations indicate that the cells are viable and differentiate well like WT cells. We have also prepared stocks of Ad-Cre viruses. We will soon infect floxed-CaR neurons with the viruses to ablate CaR expression and incubate the infected

cells under standard ischemic conditions to test whether CaR KO protects the cells from ischemia-induced Ca^{2+}-overload and apoptosis in vitro.

KEY RESEARCH ACCOMPLISHMENTS

- We have generated all animal models needed for the experiments proposed in Aim 2.
- We have established neuron cultures for experiments proposed in Aim 1.

REPORTABLE OUTCOMES

- We have reported the generation and characterization of the floxed CaR mice in an article in the *Science Signaling* in September 2008.

CONCLUSION

During the first 3 months of the funding period, we have successfully obtained mouse models and established cell culture systems required for the proposed experiments. Preliminary studies showed growth retardation in Nes-CaR-KO mice, suggesting that CaR KO might have produced neurological disorders that lead to blunted growth. In addition to pathological assessment of the brains in the KO mice, we will determine whether secretion of growth hormone and other growth factors that are produced by neuroendocrine tissues were also affected. This information will be important in interpreting the outcomes of the mice after they are exposed to ischemic conditions. We cannot rule out the possibility that potential changes in levels of hormonal factors in the Nes-CaR-KO mice could prevent a clear conclusion regarding the effect of CaR KO on ischemia-induced changes in the brain, but we think it is unlikely as proper controls are included. If this becomes an issue, we will turn to another neuron-specific CaR KO mouse model (CamK-CaR-KO) bred from mice expressing Cre under the control of the CamKIIa gene promoter (*5*). The CamKIIa is specifically expressed in subregions of the hippocampus where the CaR is also expressed (*6*). We could, therefore, use this mouse model to study the impact of CaR KO on ischemia-induced changes in hippocampal neurons.

REFERENCES

1. S. K. Libutti *et al.*, *Cancer Res* 63, 8022 (Nov 15, 2003).
2. C. Ho *et al.*, *Nat Genet* 11, 389 (1995).
3. W. Chang, C. Tu, T. H. Chen, D. Bikle, D. Shoback, *Sci Signal* 1, ra1 (2008).
4. F. Tronche *et al.*, *Nat Genet* 23, 99 (Sep, 1999).
5. J. Z. Tsien *et al.*, *Cell* 87, 1317 (Dec 27, 1996).
6. S. Yano, E. M. Brown, N. Chattopadhyay, *Cell Calcium* 35, 257 (Mar, 2004).

APPENDICES
Appendix I (PDF reprint attached)
W. Chang, C. Tu, T. H. Chen, D. Bikle, D. Shoback, *Sci Signal* 1, ra1 (2008), Vol.1, Issue 35 ra1,1-13
The Extracellular Calcium-Sensing Receptor (CaSR) Is a Critical Modulator of Skeletal Development.

SUPPORTING DATA
N/A

DEVELOPMENT

The Extracellular Calcium-Sensing Receptor (CaSR) Is a Critical Modulator of Skeletal Development

Wenhan Chang,*† Chialing Tu,* Tsui-Hua Chen, Daniel Bikle, Dolores Shoback

(Published 2 September 2008)

The extracellular Ca^{2+}-sensing receptor (CaSR) plays a nonredundant role in the functions of the parathyroid gland (PTG) and the kidney. Severe hyperparathyroidism, premature death, and incomplete gene excision in $Casr^{-/-}$ mice have precluded the assessment of CaSR function in other tissues. We generated mice with tissue-specific deletion of $Casr$ in the PTG, bone, or cartilage. Deletion of $Casr$ in the PTG or bone resulted in profound bone defects, whereas deletion of $Casr$ in chondrocytes (cartilage-producing cells) resulted in death before embryonic day 13 (E13). Mice in which chondrocyte-specific deletion of $Casr$ was induced between E16 and E18 were viable but showed delayed growth plate development. Our data show a critical role for the CaSR in early embryogenesis and skeletal development.

INTRODUCTION

Changes in the concentration of extracellular Ca^{2+} ($[Ca^{2+}]_e$) modulate diverse biological activities, such as secretion, neurotransmission, muscle contraction, and coagulation (1–3). To maintain systemic Ca^{2+} homeostasis, land-dwelling tetrapods developed skeletons to serve as Ca^{2+} reservoirs, which, together with complex hormonal systems to transport Ca^{2+} into and out of bone, meet the body's demands for Ca^{2+}. Parathyroid cells (PTCs) are the first responders in the control of systemic Ca^{2+} homeostasis. When the $[Ca^{2+}]_e$ falls below a certain threshold, PTCs rapidly release parathyroid hormone (PTH), which increases bone resorption, releasing Ca^{2+} from the bone matrix into the circulation, and promotes renal Ca^{2+} reabsorption. Both actions tend to restore the serum $[Ca^{2+}]$ to normal. Chronically, PTH increases 1,25-dihydroxyvitamin D_3 production to enhance intestinal Ca^{2+} absorption. When the $[Ca^{2+}]_e$ increases, the release of PTH and the transcription of its gene are suppressed, and the above responses are muted.

The extracellular Ca^{2+}-sensing receptor (CaSR), a guanine triphosphate (GTP)–binding protein (G protein)–coupled receptor (GPCR), couples changes in $[Ca^{2+}]_e$ to signaling responses in PTCs (2, 3). Heterozygous and homozygous inactivating mutations in $Casr$ cause familial benign hypocalciuric hypercalcemia (FBHH) and neonatal severe hyperparathyroidism (NSHPT), respectively (1, 2, 4). Patients with these disorders have mildly to severely elevated serum PTH concentrations [hyperparathyroidism (HPT)] and high serum $[Ca^{2+}]$ (hypercalcemia) depending on gene-dosage effects. Despite hypercalcemia, patients with FBHH and NSHPT have inappropriately low urinary $[Ca^{2+}]$ (hypocalciuria), confirming that renal CaSRs are required for appropriate Ca^{2+} excretion in response to hypercalcemia. Patients with NSHPT have severe skeletal demineralization at birth, which is thought to be due to severe HPT. The presence of CaSRs in bone and cartilage has, however, raised the question of whether defective signaling of CaSRs in bone cells, chondrocytes, or both may contribute to the skeletal phenotype in NSHPT.

Studies in vitro implicate a role for high $[Ca^{2+}]_e$ in enhancing the differentiation of osteoblasts (5, 6) and growth plate chondrocytes (GPCs) (7, 8). CaSRs are found in both cell types (9), but it has been difficult to show a role for these receptors in skeletal development in vivo. Although generalized $Casr$ knockout (KO) mice ($Casr^{-/-}$) (10) exhibit severe rickets and growth retardation (11), this phenotype is rescued when the $Casr^{-/-}$ mice are bred with mice lacking parathyroid glands (PTGs) (12) or with mice with an inability to synthesize PTH (13). This finding led to the idea that HPT alone causes the skeletal abnormalities in $Casr^{-/-}$ mice and that the absence of CaSRs in bone and cartilage does not contribute to skeletal pathology (12, 13).

A critical aspect of $Casr^{-/-}$ mice that has come to light is that knockout of the receptor is incomplete because of the alternative splicing of $Casr$. In the growth plate (14), skin (15), and kidney (15) of these mice, an alternatively spliced $Casr$ transcript, which lacks exon 5, is generated. The neomycin-resistance gene cassette was inserted into exon 5 to disrupt $Casr$ expression in this model. RNA splicing allows for the expression of a truncated CaSR lacking 77 amino acid residues in its extracellular domain, which are encoded by exon 5 (14). Our studies (14) support the hypothesis that this spliced receptor compensates for the absence of full-length CaSRs in tissues such as bone and cartilage in $Casr^{-/-}$ mice and that this renders this knockout incomplete. Whether the compensation is partial or full has not been established. To determine definitively the role of CaSRs in skeletal development, we generated conditional knockouts of $Casr$ in parathyroid, bone, and cartilage cells. Our findings support a requirement for the CaSR in bone growth and mineralization by modulating functions of PTCs, osteoblasts, and GPCs.

RESULTS

Generation of a floxed $Casr$ mouse

We first produced mice with loxP sites flanking exon 7 of $Casr$, which are referred to hereafter as floxed $Casr$ mice. Exon 7 encodes the seven transmembrane domains and four intracellular loops of the CaSR. The targeting strategy used to introduce loxP sequences into 129/SvJae embryonic stem (ES) cells and the generation of floxed $Casr$ mice are described in Materials and Methods (Fig. 1A). The complete integration of the loxP sites into the genome of the ES cells before blastocyst injections and the generation of the resulting floxed $Casr$ mice were confirmed by

Endocrine Research Unit, Department of Veterans Affairs Medical Center, Department of Medicine, University of California, San Francisco, CA 94121, USA. *These authors contributed equally to this work.
†To whom correspondence should be addressed. E-mail: wenhan.chang@ucsf.edu

polymerase chain reaction (PCR) analyses of genomic DNAs with three different sets of primers (Fig. 1B; see table S1 for primer sequences). To confirm that Cre recombinase could excise exon 7, genomic DNAs were incubated with bacteriophage P1 Cre recombinase in vitro. As confirmed by PCR analyses, the enzyme efficiently excised floxed *Casr* alleles in DNA from ES cells and from heterozygous and homozygous floxed *Casr* mice (Fig. 1C).

Although this knockout strategy enabled the transcription of exons 1 to 6, which encode the extracellular domain (amino acid residues 1 to 577) of the CaSR, this truncated protein (ΔExon7-CaSR) does not activate phospholipase C (PLC) as assessed by the inability of human embryonic kidney (HEK) 293 cells expressing ΔExon7-CaSR complementary DNA (cDNA) to produce [^{3}H]inositol phosphates (InsPs) from [^{3}H]inositol-labeled membrane polyphosphoinositides. The ΔExon7-CaSR receptor fails to increase total InsP production in response to increasing $[Ca^{2+}]_e$ to 20 mM when compared with cells expressing the full-length [also referred to as wild-type (WT)] CaSR (fig. S1). Expression of the ΔExon7-CaSR cDNA also does not interfere with the function of the full-length CaSR. When HEK 293 cells separately transfected with cDNAs encoding full-length CaSR or ΔExon7-CaSR were subsequently mixed, cultured together, and then tested for InsP responses, there was no alteration in the sensitivity or magnitude of these responses to high $[Ca^{2+}]_e$ in cells expressing full-length CaSRs (fig. S1).

To confirm the physiological role of the CaSR in PTCs, which was demonstrated previously in *Casr*$^{-/-}$ mice (*10*), and to examine the contribution of HPT mediated by PTC-specific deletion of *Casr* to skeletal development

in vivo, we bred floxed *Casr* mice with mice expressing Cre recombinase cDNA under the control of the *PTH* promoter (*PTH-Cre*) (*16*) to produce PTC-specific *Casr* KO mice. Heterozygous ($^{PT}Casr^{WT/\Delta flox}$, PT-Het) and homozygous KO ($^{PT}Casr^{\Delta flox/\Delta flox}$, PT-KO) mice were born in the expected Mendelian ratios. Control littermates had one or two floxed *Casr* alleles and no *PTH-Cre* transgene. Whereas PT-Het mice developed normally, the growth of PT-KO mice was severely blunted, and they died within 2 weeks of birth, with weights about 45% of those of control and PT-Het mice (Fig. 2A and Table 1). Analyses of genomic DNA confirmed that the genotypes were correct (Fig. 2B) and that excision of exon 7 (ΔExon 7) was restricted to PTGs and had not occurred in bone, cartilage, or other tissues (Fig. 2C). Western blotting showed that the abundance of full-length CaSR protein had been reduced by about 70% in PTGs from PT-Het mice and by more than 95% in PTGs from PT-KO mice compared with that in control mice (Fig. 2D). A band of about 90 kD corresponding to the ΔExon7-CaSR protein was detected in PT-Het and PT-KO PTGs, but not in the PTGs of control littermates (Fig. 2D).

Quantitative real-time PCR (qPCR) performed with primers targeted to the junction of exons 6 and 7 of *Casr* confirmed strong knockdown of *Casr* messenger RNA (mRNA) (by about 90%) in the PTGs of PT-KO mice (Fig. 2E). We observed a greater (about twofold) abundance of *Casr* mRNA in the PTGs of PT-Het mice compared with that in control mice, which is indicative either of an increased rate of *Casr* transcription or of the stabilization of *Casr* mRNA in response to hypercalcemia or another biochemical abnormality in these mice. This is further supported by the increased abundance of ΔExon7-CaSR mRNA in the PT-KO
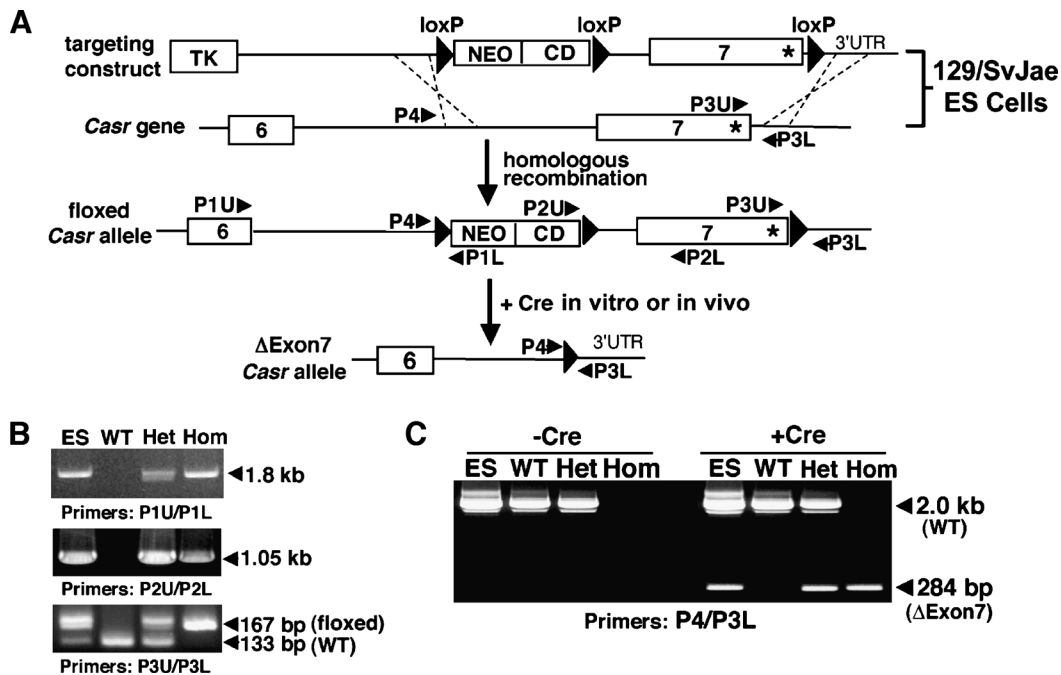
Fig. 1. Generation of floxed *Casr* mice. (**A**) The gene-targeting strategy used to introduce loxP sequences to flank exon 7 of *Casr* required a construct containing three loxP sites flanking exon 7 of the *Casr* gene and the cytidine deaminase (CD)–neomycin (NEO) gene cassette. This construct was transfected into 129/SvJae ES cells to allow homologous recombination with endogenous *Casr* alleles. The resulting floxed *Casr*-containing ES cells were injected into C57/BL6 blastocysts to produce chimeric mice that were bred to obtain heterozygous (*Casr*$^{wt/flox}$) and homozygous (*Casr*$^{flox/flox}$) mice.

(**B**) PCR analyses of genomic DNAs from floxed *Casr*-containing ES cells before blastocyst injection and from the tails of *Casr*$^{wt/wt}$ (WT), heterozygous *Casr*$^{wt/flox}$ (Het), and homozygous *Casr*$^{flox/flox}$ (Hom) mice were performed with specific primers (see Materials and Methods) to confirm integration of the targeting sequences. (**C**) PCR analyses of genomic DNAs from (B) after incubation with (+Cre) or without (−Cre) bacteriophage P1 Cre recombinase in vitro for 30 min. The 284-bp band represents the DNA fragment due to excision of exon 7 (ΔExon7).

mice, as detected by qPCR with primers specific for the junction of exons 2 and 3 of *Casr* (Fig. 2E). Despite the increased abundance of mRNA, the abundance of ΔExon7-CaSR protein in PTGs of PT-KO mice was about 10% of that of full-length CaSR protein in the PTGs of control mice (Fig. 2D), which suggests that the truncated protein has a reduced half-life compared with that of the full-length protein.

The abundance of PTH mRNA in PTGs from PT-Het and PT-KO mice was significantly increased compared with that of control mice (Fig. 2E), compatible with the elevated concentrations of serum PTH and serum Ca^{2+} observed in vivo (Table 1). There was a clear effect of

gene dosage as evidenced by the occurrence of mild HPT in PT-Het mice and severe HPT in the PT-KO mice (Table 1). In contrast to the hypocalciuria of $Casr^{-/-}$ mice (10), PT-Het and PT-KO mice had urinary $[Ca^{2+}]$ about 25% and 380% higher than that of control mice, respectively (Table 1). As expected, intact renal CaSRs promoted Ca^{2+} excretion in the normal physiologic response to hypercalcemia.

Knockout of *Casr* in PTCs retards skeletal development

Whole-mount alizarin red (AR) and Alcian blue (AB) staining of 2-week-old mice showed that PT-KO mice had multiple rib and tibial
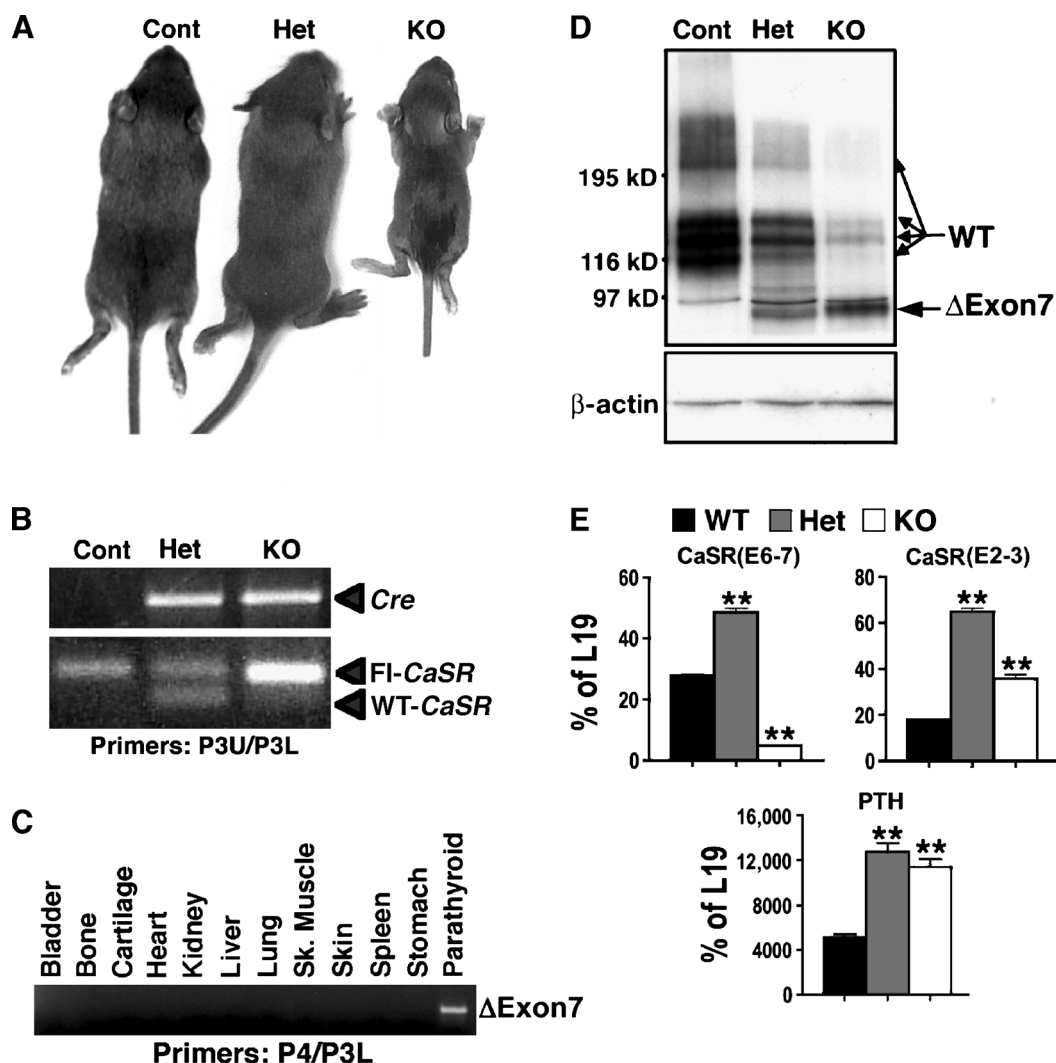

Fig. 2. Heterozygous and homozygous deletion of the *Casr* gene in parathyroid cells (PTCs) produces mild and severe hyperparathyroidism (HPT), respectively. (**A**) Two-week-old PT-KO (^{PT}CaSR$^{Δflox/Δflox}$) mice showed severe growth retardation, with body weights about 45% of that of their control and PT-Het (^{PT}CaSR$^{WT/Δflox}$) littermates. (**B**) PCR analyses of genomic DNAs confirmed the expression of the *Cre* transgene and floxed *Casr* alleles in PT-Het and PT-KO mice. The control mice used in this experiment were CaSR$^{flox/flox}$, which do not express *Cre*. (**C**) PCR analyses of genomic DNAs from tissues of PT-KO mice confirmed the deletion of exon 7 only in PTGs. (**D**) Western blotting of

PTG lysates showed the decreased abundance of full-length CaSR protein (WT, 120 to 250 kD) by ~70% and >95% in the PT-Het and PT-KO mice, respectively, compared with control littermates. PTG lysates from PT-Het and PT-KO mice contained the ΔExon7-CaSR (ΔExon7) protein (about 90 kD), which was encoded by exons 1 to 6. (**E**) qPCR analyses with primers flanking the junctions of either exons 6 and 7 (E6-7) or exons 2 and 3 (E2-3) of *Casr* and primers specific for PTH mRNA were presented as the percentage of expression of the gene encoding the mitochondrial ribosomal protein L19 (**P < 0.01, n = 4 to 6 mice).

Table 1. Concentrations of serum PTH, serum Ca²⁺, and urinary Ca²⁺ and weights of PT-KO (KO), PT-Het (Het), and control (Cont) littermates.

	Cont (*n* = 19 mice)	Het (*n* = 13 mice)	KO (*n* = 11 mice)
Serum [PTH] (pg/ml)	52.7 ± 1.6	170 ± 27.4[*]	959 ± 122[*]
Fold over control		+2.3	+17.2
Serum [Ca²⁺] (mg/dl)	11.6 ± 0.1	13.4 ± 0.2[*]	16.4 ± 0.5[*]
% Change over control		+16	+40
Urine [Ca²⁺] (mg/dl)	2.8 ± 0.4	3.5 ± 0.5[*]	13.4 ± 2.9[*]
% Change over control		+25	+380
Body weight (g)	8.7 ± 0.3	8.4 ± 0.5	3.8 ± 0.4[*]
% Change vs. control			–56

[*]$P < 0.01$.

fractures and smaller and severely undermineralized skeletons compared with those of control and PT-Het littermates (Fig. 3A). To further confirm the reduced mineral content of their skeletons, we performed micro-computed tomography (μCT) on the femurs of PT-KO mice to quantify precisely the amount of mineral present by measuring the density of hydroxyapatite, the dominant form of bone mineral. Three-dimensional (3D) reconstructed images from the μCT scans revealed poorly mineralized matrix and the lack of secondary ossification centers in the epiphyses (tracing in red) compared with the femurs of control mice (Fig. 3B). Histological analyses of bone sections after von Kossa (VK) staining (to detect phosphate-containing minerals) and safranin O (SO) counterstaining (to detect proteoglycan) showed substantially reduced mineral deposition in trabecular (Tb) and cortical (Ct) bones in PT-KO mice compared with those in control mice (Fig. 3C). Goldner trichrome staining of adjacent sections revealed excessive undermineralized osteoid (pink) mixed with mineralized matrix (green) in PT-KO mice (Fig. 3C), which was suggestive of defective bone formation.

To determine whether these defects were due to delayed osteoblast differentiation, function, or both, we examined the expression of genes encoding osteoblast-specific markers and regulators of differentiation. The expression of both early and late osteogenic genes, including *osterix* (*OSX*), *type I collagen* [*Col(I)*], *alkaline phosphatase* (*ALP*), *dentin matrix protein 1* (*DMP1*), *osteocalcin* (*OCN*), and *sclerostin* (*SOST*), was profoundly decreased in the bones of 14-day-old PT-KO mice compared with those of control mice (Fig. 3D), indicating a delay in osteoblast differentiation. We found that the expression of *Casr* mRNA was more than 70% lower in the bones of PT-KO mice than in those of control mice (Fig. 3D), despite our inability to document any excision of *Casr* in bone (Fig. 2C). These data suggest that the severe HPT and hypercalcemia that were due to PTC-specific knockout of *Casr* affected early skeletal development. This likely occurred because of increased PTH receptor signaling that was accompanied by reduced *Casr* expression in the bones of the PT-KO mice.

The bones of PT-Het mice were indistinguishable from those of control mice at 2 weeks of age, as assessed by whole-mount staining, μCT scans, and qPCR analyses. The abundance of *Casr* mRNA in the bones of PT-Het mice was equivalent to that of control mice. Mild osteopenia (reduced bone mineral density) was, however, evident in PT-Het mice by 6 months of age, as demonstrated by μCT of Tb bone in the distal femur and of Ct bone at the tibia–fibula junction (TFJ) (Fig. 3, E and F). The trabecular bone volume (BV), an index of the amount of bone mineral present in a given tissue volume (TV), was significantly decreased when expressed as the ratio of Tb.BV to TV (Fig. 3F). Tb thickness (Th) and Tb numbers (N) were also reduced. These findings could be due to decreased bone formation by osteoblasts, increased bone resorption by osteoclasts, or a combination of the two. Tb connectivity density (CD) and Tb spacing (Sp), which reflect the state of the Tb microarchitecture, in the PT-Het mice were not significantly different from those of control mice (Fig. 3F). In the other bone compartment, namely, Ct bone, Ct. TV, Ct.BV, and Ct.Th were also significantly decreased in PT-Het mice compared with those of control mice (Fig. 3F), indicating that the smaller bones of the PT-Het animals had thinner cortices. Thus, long-term albeit mild HPT has cumulative, age-dependent effects on skeletal homeostasis.

Impaired postnatal growth and skeletal development in mice with osteoblasts deficient in *Casr*

To determine the role of the CaSR in osteoblasts, we generated osteoblast-specific *Casr* KO mice by breeding floxed *Casr* mice with mice expressing the *Cre* transgene driven by the 2.3-kb *Col(I)* α₁ subunit promoter [2.3Col(I)-*Cre*], which is expressed in the early- and late-stage cells of the osteoblast lineage (*17*). Genomic analyses by PCR confirmed the excision of exon 7 of *Casr* in bones from either heterozygous (Col-BoneCasr^WT/Δflox, COL-Het) or homozygous KO (Col-BoneCasr^Δflox/Δflox, COL-KO) mice, but not from those of control littermates (fig. S2).

COL-Het mice grew and developed similarly to their control littermates. Deletion of both alleles of the *Casr* gene in osteoblasts, however, profoundly blocked postnatal growth and skeletal development in the COL-KO mice. This was evident by 3 days of age, and by day 20, the body weights of COL-KO mice were about 30% of those of control and COL-Het littermates (Fig. 4A). Whole-mount AR and AB staining showed that the COL-KO mice had smaller and severely undermineralized skeletons compared with those of control mice, which was visible by 5 days (Fig. 4B).

The skeletons and body weights of COL-Het mice were comparable with those of control littermates through the first 3 weeks of age (Fig. 4, A and B). Most COL-KO mice had rib and long bone fractures and died within 3 weeks of birth. Undermineralization of the skull (Fig. 4C, arrowheads), vertebrae (double arrows), and long bones (arrows) of COL-KO mice was confirmed by µCT analyses. The latter studies showed markedly decreased Tb.BV, Tb.BV/TV, Tb.Th, and Tb.N in the distal femurs of COL-KO mice compared with those of control mice, which suggests the impaired

ability of osteoblasts to form bone in the skeletons of COL-KO mice. This was supported by the finding of a decreased Tb.CD and increased Tb.Sp, hallmarks of osteopenia and a weakened Tb architecture or structure, in the COL-KO mice. In addition, the reduction in cortical parameters (Ct.TV, Ct. BV, and Ct.Th) at the TFJ in COL-KO mice compared with control mice (Fig. 4D) indicated that the impact of *Casr* knockout was general and evident at different skeletal sites and different types of bone. Consistent with the µCT data was the histological staining for mineralization, which
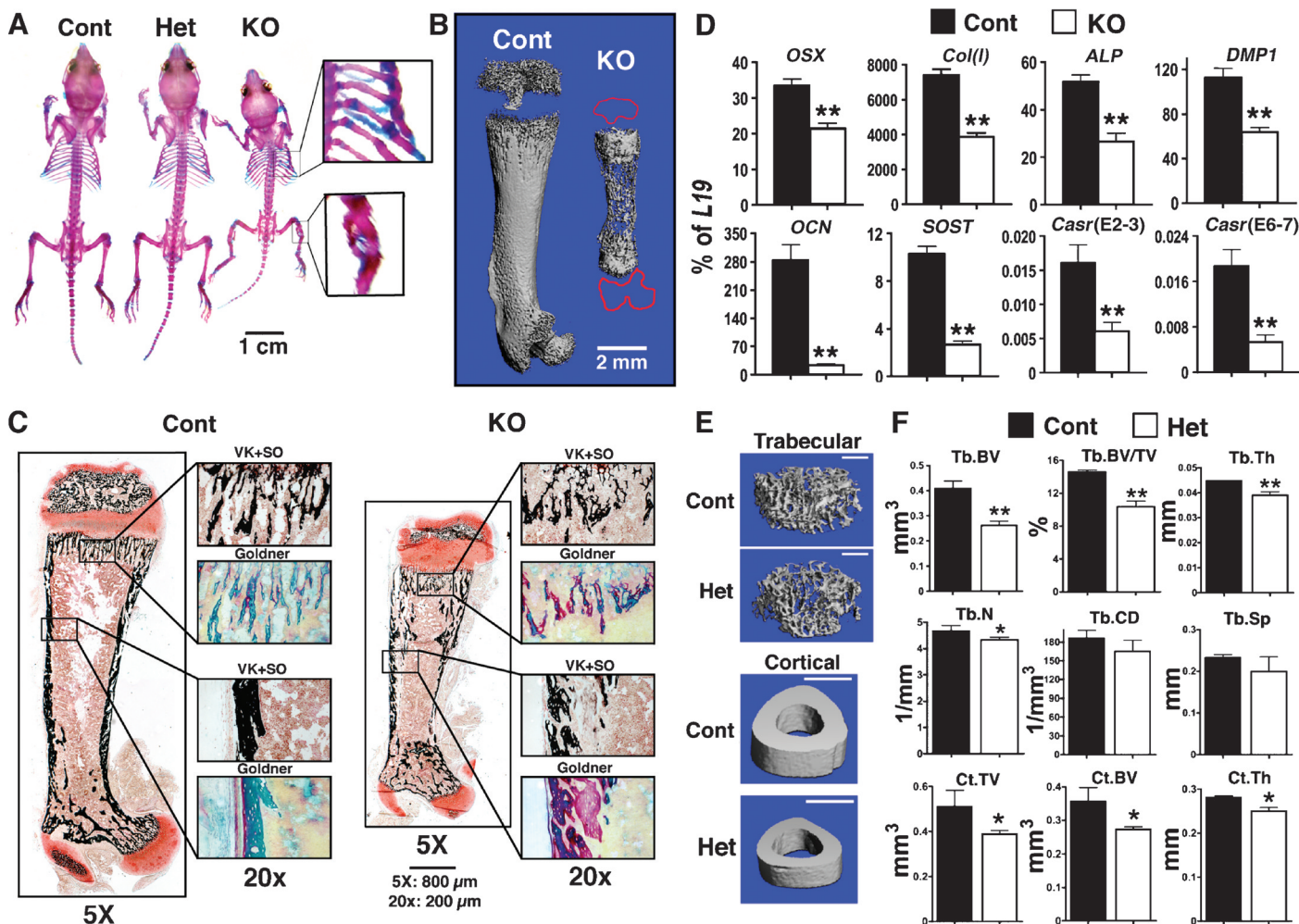

Fig. 3. Knockout of *Casr* in PTCs impedes skeletal development. (**A**) Whole-mount AR and AB staining showed a smaller skeleton with fractures in the ribs and tibiae (see insets) of 14-day-old PT-KO ($^{PT}Casr^{\Delta flox/\Delta flox}$) mice, but not in PT-Het ($^{PT}CaSR^{WT/\Delta flox}$) or control mice. (**B**) Reconstructed 3D µCT images of femurs from 14-day-old PT-KO mice showed severely undermineralized matrix compared with those of control mice. (**C**) Histological analyses of femurs from PT-KO mice showed reduced mineralization and osteoid accumulation. Consecutive plastic-embedded femur sections from 14-day-old control and PT-KO mice stained with VK reagents and counterstained with SO or Goldner reagents were visualized at 5× magnification. Boxes in the right panels are enlarged regions of interest (reproduced at 20×). Scale bars: 800 µm at 5×; 200 µm at 20×. (**D**) Gene expression studies indicated the delayed differentiation of osteoblasts in bones from PT-KO mice compared with that of control mice.

qPCR analyses of genes encoding osteoblast markers were performed on RNA isolated from humeral cortices (no marrow) of 14-day-old mice. All measurements of gene expression are presented as the percentage of *L19* expression (*$P < 0.05$, **$P < 0.01$; $n = 6$ to 8 mice). Expression of *OSX*, *Col(I)*, *ALP*, *DMP1*, *OCN*, and *SOST* in PT-KO mice was reduced by 36%, 48%, 48%, 43%, 91%, and 74%, respectively, compared with that in control mice. PCR analyses with primers flanking the junctions of exons 6 and 7 (E6-7) or exons 2 and 3 (E2-3) of *Casr* showed reductions in both transcripts in bone in which the *PTH-Cre* transgene was not expressed. (**E**) Reconstructed 3D µCT images of Tb bone in distal femurs and Ct bone at the TFJ of 6-month-old control and PT-Het mice. Scale bars: 1 mm for all panels. (**F**) µCT parameters assessed were BV, BV/TV, Th, N, CD, and Sp for Tb bone and TV, BV, and Th for Ct bone (defined in Results; *$P < 0.05$, **$P < 0.01$; $n = 6$ to 8 mice).
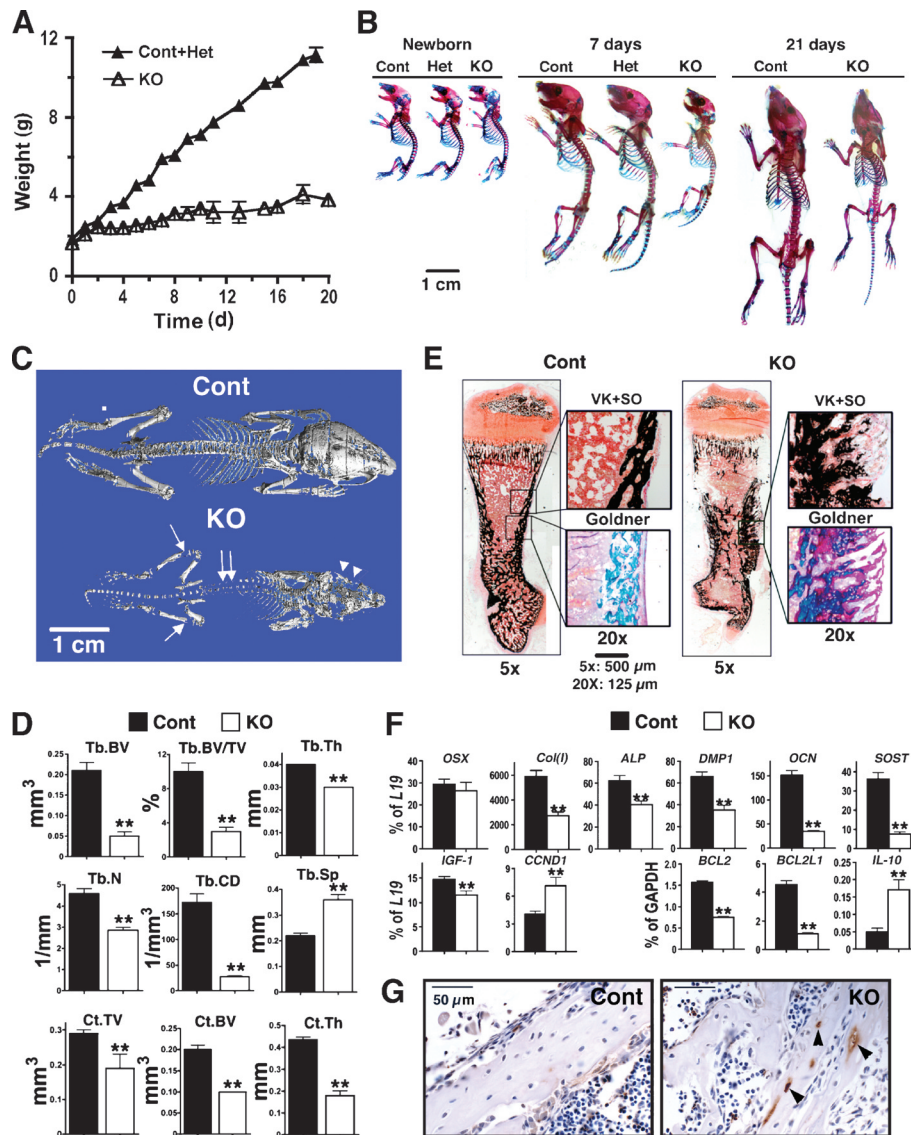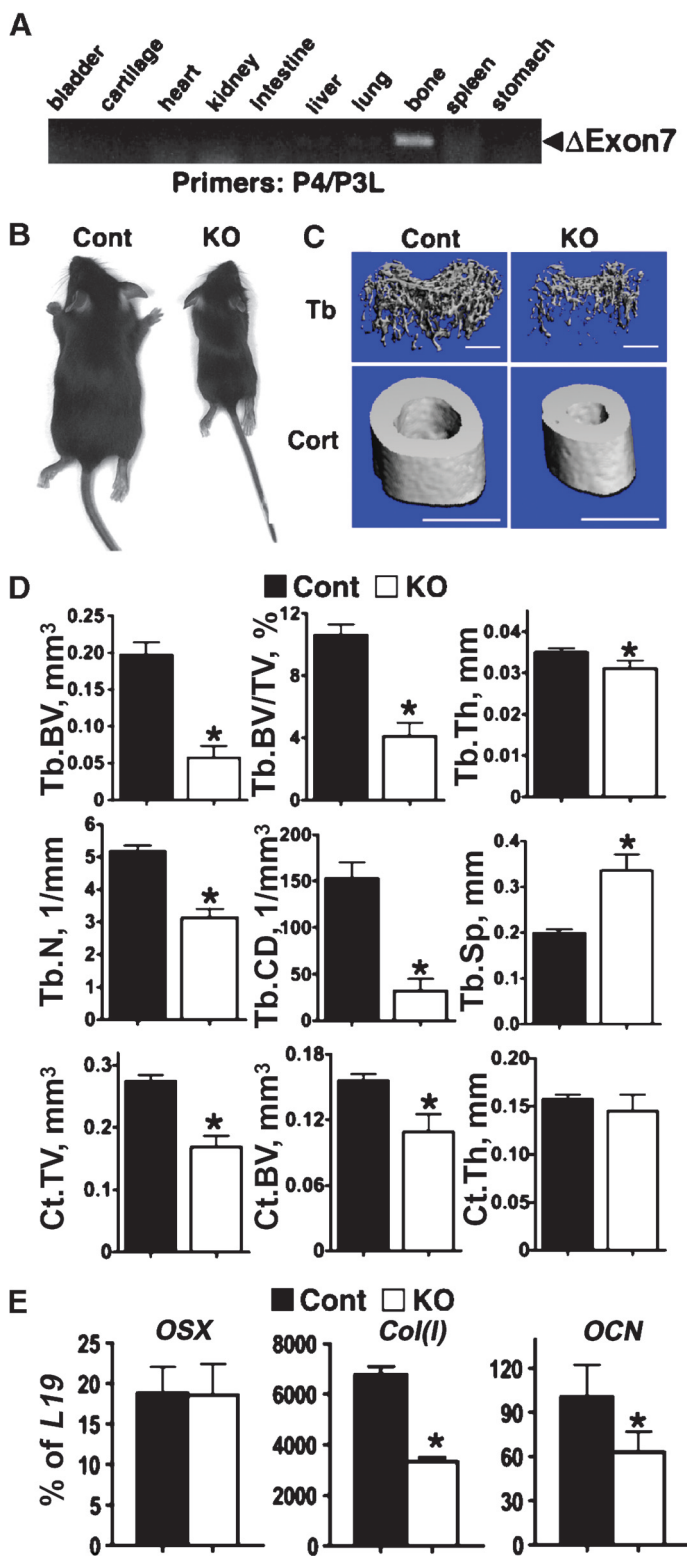
Fig. 4. Knockout of *Casr* in osteoblasts, driven by 2.3*Col(I)*-Cre, blocked growth and skeletal development. (**A**) Body weights of control (*n* = 8), heterozygous (^Col-Bone^*Casr*^WT/Δflox^, COL-Het, *n* = 12), and homozygous KO (^Col-Bone^*Casr*^Δflox/Δflox^, COL-KO, *n* = 9) mice from birth until postnatal day 20. Because the weights of control and Het mice were indistinguishable, they were combined and are presented as Cont+Het. COL-KO mice exhibited growth retardation, which was evident by postnatal day 3. (**B**) Whole-mount AR and AB staining showed that the skeletons of COL-KO mice were smaller than those of control and heterozygous mice at postnatal day 5. (**C**) Reconstructed 3D μCT images of skeletons from 20-day-old mice showed severe undermineralization in COL-KO mice, evident in the skull (arrowheads), vertebrae (double arrows), and long bones (arrows). (**D**) μCT parameters of Tb bone in the distal femur (Tb.BV, Tb.BV/TV, Tb.Th, Tb.N, Tb.CD, and Tb.Sp) and Ct bone at the TFJ (Ct.TV, Ct.BV, and Ct.Th) of 20-day-old control and COL-KO mice showed statistically significant reductions in all parameters except Tb. Sp, which was markedly increased—all of which were confirmatory of reduced bone mass and microarchitecture (**P < 0.01; *n* = 6 mice). (**E**) Histological analyses of femurs from COL-KO mice showed poor

mineralization and osteoid accumulation compared with those of control mice. VK+SO and Goldner staining were performed on consecutive plastic-embedded sections from 7-day-old control and COL-KO femurs and visualized at 5× magnification. Boxes in the right panels are enlarged regions of interest (reproduced at 20×). Scale bars: 500 μm (5×); 125 μm (20×). (**F**) The expression of genes encoding osteoblast markers indicated delayed differentiation in COL-KO mice compared with that in control mice. qPCR analyses of samples isolated from humeral cortices (no marrow) from 14-day-old mice with primers specific for *OSX*, *Col(I)*, *ALP*, *DMP1*, *OCN*, *SOST*, *IGF-1*, *CCND1*, *Bcl-2*, *Bcl-2L1*, and *IL-10* were performed. Results are presented as the percentage of expression of *L19* or *glyceraldehyde 3-phosphate dehydrogenase* (*GAPDH*) (**P < 0.01; *n* = 6 to 9 mice). Reductions (percent decrease in COL-KO mice compared with control mice) of 54%, 35%, 47%, 77%, 79%, and 22% were seen in the expression of *Col(I)*, *ALP*, *DMP1*, *OCN*, *SOST*, and *IGF-1*, respectively. (**G**) TUNEL staining of femoral cortex from 7-day-old control and KO mice with hematoxylin counterstaining. TUNEL-positive cells are indicated by brown DAB stain (arrowheads) (*n* = 8 sections from four mice).

showed that bones from COL-KO mice contained large quantities of undermineralized osteoid (pink by Goldner staining), which was mixed with

normally mineralized matrix (green by Goldner, black by VK staining) (Fig. 4E).

Consistent with poor mineralization, as assessed by histological analyses, qPCR showed the markedly decreased expression of genes encoding both early and late markers of osteoblast differentiation, such as *Col(I)*, *ALP*, *DMP1*, *OCN*, and *SOST*, in bones from 7-day-old COL-KO mice compared with those of control mice (Fig. 4F). However, *OSX* expression in the COL-KO mice was comparable with that of control mice, indicating that the changes due to deletion of *Casr* occurred after the expression of *OSX*. Similar changes in gene expression as well as bone histology were also evident in newborn mice (<1 day old) (fig. S3), which suggests that skeletal defects developed prenatally. In addition to changes in the abundance of markers of differentiation, *Casr* knockout in osteoblasts significantly suppressed the expression of the gene encoding insulin-like growth factor 1 (IGF-1) (Fig. 4F), a growth factor critical for osteoblast survival and differentiation, suggesting that the CaSR may modulate osteoblast differentiation by altering the local abundance of IGF-1. Although *cyclin D1* (*CCND1*) expression was significantly increased in COL-KO mice compared with that in control mice, the expression of the genes encoding the prosurvival factors B cell lymphoma/leukemia 2 (Bcl-2) and Bcl-2–like 1 (Bcl-2L1) (*18*, *19*) was profoundly suppressed. We also found increased expression of *interleukin-10* (*IL-10*), an inducer of apoptosis in other cells (*20*), in COL-KO compared with that in control mice (Fig. 4F). These observations suggested the increased occurrence of apoptosis, which was confirmed by the detection of enhanced terminal deoxynucleotidyl transferase–mediated deoxyuridine triphosphate nick end labeling (TUNEL) staining in apoptotic osteoblasts and osteocytes in sections from COL-KO mice compared with those from control mice (Fig. 4G).

Because the expression of *Col(I)* is low in tissues such as liver, skin, testis, ovary, and kidney (*17*), we considered the possibility that the early death of the COL-KO mice might be due to reduced *Casr* expression in other tissues. To address this, we used a different targeting strategy to generate osteoblast-specific *Casr* KO mice. We bred floxed *Casr* mice with mice expressing the *Cre* transgene controlled by an *OSX* promoter [*OSX-Cre*] (*21*). *OSX* expression is restricted to osteoblasts and their precursors and occurs before the expression of *Col(I)* but after that of *Runx2* (*21*). The *OSX-Cre* construct induces Cre-lox recombination in osteoblasts during embryonic development and early postnatal life (*21*).

Genomic DNA analyses showed that excision of exon 7 of *Casr* in heterozygous ($^{Osx-Bone}Casr^{WT/\Delta flox}$, OSX-Het) and homozygous KO ($^{Osx-Bone}Casr^{\Delta flox/\Delta flox}$, OSX-KO) mice occurred only in bone and not

Fig. 5. Knockout of floxed *Casr* in osteoblasts by *OSX-Cre* results in retarded growth and altered gene expression. (A) PCR analyses of genomic DNAs confirmed that deletion of exon 7 occurred only in bone from homozygous $^{Osx-Bone}Casr^{\Delta flox/\Delta flox}$ (OSX-KO) mice and not in other tissues. (B) One-month-old OSX-KO mice were growth-retarded compared with control mice. (C) μCT images of trabecular (Tb) and cortical (Ct) bones in the distal femur and TFJ, respectively, showed severely undermineralized matrix in 4-week-old KO mice compared with that in control mice. Scale bars: 1 mm for all panels. (D) μCT parameters assessed included BV, BV/TV, Th, N, CD, and Sp for Tb bone and TV, BV, and Th for Ct bone in 4-week-old control and OSX-KO mice. (*$P < 0.01$; $n = 6$ for KO and $n = 12$ for control mice). (E) Analysis of gene expression by qPCR in samples isolated from humeral cortices (no marrow) of newborn mice indicated delayed differentiation of osteoblasts in OSX-KO mice compared with that of control mice, with 55% reduced expression of *Col(I)* and 35% reduced expression of *OCN*. Results are presented as the percentage of *L19* expression (*$P < 0.05$, $n = 4$ to 6 mice).

in other tissues (Fig. 5A) and did not occur in bone from control mice. As was seen in COL-KO mice, knockout of both *Casr* alleles in OSX-KO osteoblasts profoundly blocked postnatal growth and skeletal development (Fig. 5, B to D). Reduced bone formation and mineralization, confirmed by the alterations in μCT parameters, were evident in both Tb and Ct bones in 4-week-old OSX-KO mice. They showed decreased Tb.BV, Tb.BV/TV, Tb.Th, Tb.N, and Tb.CD and increased Tb.Sp in the distal femur and decreases in Ct.TV and Ct.BV at the TFJ (Fig. 5, C and D). Phenotypic abnormalities were also evident in newborn mice (<1 day old) with decreased expression of the genes encoding the osteoblast markers *Col(I)* and *OCN* in bones from newborn OSX-KO mice by qPCR (Fig. 5E). Taken together, these data support a role for the CaSR in modulating the growth and differentiation of osteoblasts, a paradigm essential for orderly postnatal skeletal development.

Delayed growth plate development and embryonic death following GPC-specific deletion of *Casr*

Studies with mouse GPCs support roles for high $[Ca^{2+}]_e$ and the CaSR in promoting differentiation (*8, 14*). To determine the role of CaSR in the growth plate in vivo, we targeted chondrocytes by breeding floxed *Casr* mice with mice expressing the *Cre* transgene under the control of the *type II collagen α₁ subunit* [*Col(II)*] (Cart) promoter [*Col(II)-Cre*] (*22*). No homozygous knockout ($^{Cart}Casr^{\Delta flox/\Delta flox}$, Cart-KO) mice were born alive from 35 litters (~350 pups). In addition, no Cart-KO mouse embryos were detectable at E14 to E16 from 8 litters or at later time points. In 56 embryos from 6 litters at the E12 to E13 stage, only two Cart-KO embryos of confirmed genotype were found, indicating that most of these embryos died earlier (fig. S4). Skeletons from the two surviving E12.5 Cart-KO embryos were shorter than those of control and heterozygous ($^{Cart}CaSR^{WT/\Delta flox}$, Cart-Het) littermates and had poorly mineralized rib cages, calvariae, and long bones (as demonstrated by lack of AR staining) (Fig. 6A). These data suggest that blocking *Casr* expression in *Col(II)*-expressing cells severely impedes viability beyond E12 to E13 and inhibits early steps in cartilage and bone mineralization.

Because knockout of *Casr* in *Col(II)*-expressing cells is lethal, we developed a tamoxifen (Tam)-inducible knockout model [$^{Tam-Cart}Casr^{\Delta flox/\Delta flox}$, Tam-Cart-KO] to examine the role of CaSR at later stages of embryonic and postnatal development of GPCs. We used transgenic (^{Cart}Cre-ER^{Tam}) mice that express a fusion protein (Cre-ER^{Tam}) of the Cre recombinase fused to a mutated ligand-binding domain of the estrogen receptor (ER^{Tam}) under the control of a mouse *Col(II)* promoter (*23*). In this model, translocation of the Cre-ER^{Tam} protein to the nucleus, an essential step for Cre-lox recombination, only occurs when Tam, or its derivative 4OH-Tam, is administered to the mice (*23*). The ability of Tam to specifically induce *Cre* activity in cartilage has been confirmed previously (*23, 24*). We bred the ^{Cart}Cre-ER^{Tam} mice with *Casr*$^{flox/flox}$ mice to obtain ^{Cart}Cre-ER$^{Tam(+/-)}Casr^{flox/flox}$ mice, which were viable and fertile in the absence of Tam. We next crossed the ^{Cart}Cre-ER$^{Tam(+/-)}Casr^{flox/flox}$ mice with *Casr*$^{flox/flox}$ mice to obtain experimental animals: ^{Cart}Cre-ER$^{Tam(+/-)}Casr^{flox/flox}$ (~50%) and *Casr*$^{flox/flox}$ (~50%) mice. Both sets of mice were treated with either 4OH-Tam or vehicle, which resulted in the generation of three strains of mice: induced homozygous *Casr* KO mice ($^{Tam-Cart}Casr^{\Delta flox/\Delta flox}$, Tam-Cart-KO) and the controls, *Casr*$^{flox/flox}$ mice exposed to 4OH-Tam and ^{Cart}Cre-ER$^{Tam(+/-)}$ *Casr*$^{flox/flox}$ mice exposed to vehicle (Fig. 6B).

To delete *Casr* before birth, pregnant mice were injected with a single dose of 4OH-Tam (1.5 mg) or vehicle at E16 to E17, and the embryos were analyzed 48 to 72 hours after injection. The genotypes of ^{Cart}Cre-ER$^{Tam(+/-)}$ *Casr*$^{flox/flox}$ and *Casr*$^{flox/flox}$ mice and the ability of 4OH-Tam to induce excision of exon 7 in the former mice were confirmed by genomic DNA analyses (Fig. 6B). Whole-mount AR and AB staining showed a ~10% reduction

in the overall length of the skeletons of 4OH-Tam–treated Tam-Cart KO mice compared with those of treated *Casr*$^{flox/flox}$ control mice, which included shorter humeri, femurs, and tibiae (Fig. 6C). Immunohistochemical analyses confirmed a marked reduction in the abundance of the CaSR in the hypertrophic zones of tibial growth plates of 4OH-Tam–treated Tam-Cart-KO mice compared with that of treated control mice (Fig. 6D), which was indicative of prompt (within 48–72 hours) knockdown of *Casr* expression.

Further evidence of *Casr* knockdown was provided by qPCR analysis, which showed the decreased expression of full-length *Casr* mRNA in growth plates from 4OH-Tam–treated Tam-Cart-KO growth plates (Fig. 6F). In cartilage sections stained by VK and SO reagents, there was ~20% expansion of the hypertrophic zone and decreased mineral deposition in that zone in 4OH-Tam–treated Tam-Cart-KO mice compared with that in treated control mice (Fig. 6E). qPCR analyses of epiphyseal growth plates showed decreased expression of *type X collagen* [*Col(X)*], *RUNX2*, and *osteopontin* (*OPN*), which are markers of mature and terminally differentiated chondrocytes, in Tam-Cart-KO compared with control mice (Fig. 6F). The expression of genes encoding early differentiation markers, such as *aggrecan* (*AGG*) and *Col(II)*, was unchanged (Fig. 6F), supporting a selective delay in chondrocyte maturation and terminal differentiation in Tam-Cart-KO mice.

Insulin-like growth factor 1 signaling is a critical pathway that promotes chondrocyte differentiation (*25*). We examined whether this pathway was affected by the knockout of *Casr* in the GPCs of Tam-Cart-KO mice. Immunohistochemical and qPCR analyses showed significant reductions in the expression of *IGF-1* and *IGF-1 receptor* (*IGF-1R*) mRNAs (Fig. 6F) and in the abundance of their protein products (Fig. 7A) in the growth plate of Tam-Cart-KO mice compared with those of control mice. To test whether reduced IGF-1R signaling affected the differentiation of GPCs, we performed in vitro knockout of *IGF-1R* by infecting GPCs from floxed *IGF-1R* mice with adenoviruses expressing Cre recombinase (Ad-Cre) or empty vector (Ad-Cont). Knockdown of *IGF-1R* mRNA and loss of IGF-1R protein in the Ad-Cre–infected GPCs were confirmed by qPCR (Fig. 7B) and Western blotting (Fig. 7C), respectively. These changes were accompanied by a significant reduction in the expression of *Col(X)* mRNA (Fig. 7B) and in mineral deposition (Fig. 7D) in the Ad-Cre–infected cells compared with that in Ad-Cont–infected cells. These data support the concept that knockdown of *Casr* delays GPC differentiation in Tam-Cart-KO mice, at least in part by the reduction of IGF-1R signaling in these cells.

DISCUSSION

CaSRs are broadly present in bone, brain, gut, skin, and endocrine glands, and changes in $[Ca^{2+}]_e$ alter cell function in these tissues. Whether the CaSR is the mediator of all aspects of Ca^{2+}-sensing in these tissues in vivo has not been easy to address because of the lack of suitable animal models. The floxed *Casr* mouse strain that we have developed is the first model that permits tissue-specific deletion of *Casr*.

We showed that Cre recombinase excised floxed *Casr* alleles in three tissues critical to Ca^{2+} homeostasis and skeletal development. The PTC-specific *Casr* KO mouse provided proof of concept for the gene-targeting strategy we used, because these mice showed severe HPT and hypercalcemia, despite having normal renal responsiveness to Ca^{2+}. Heterozygous and homozygous PTC-specific *Casr* KO mice showed the expected mild and severe HPT, respectively, with a clear gene dosage effect, similar to the phenotype of generalized *Casr*$^{-/-}$ mice (*10*). We noted that the degree of HPT in PTC-specific *Casr* KO mice appeared to be more severe than that of the generalized KO model (*10*), with serum PTH concentrations in PT-Het and PT-KO mice that were ~2- to 3- and 17-fold higher, respectively, than those of control littermates (Table 1). In contrast, the abundance of serum PTH in generalized *Casr*$^{+/-}$
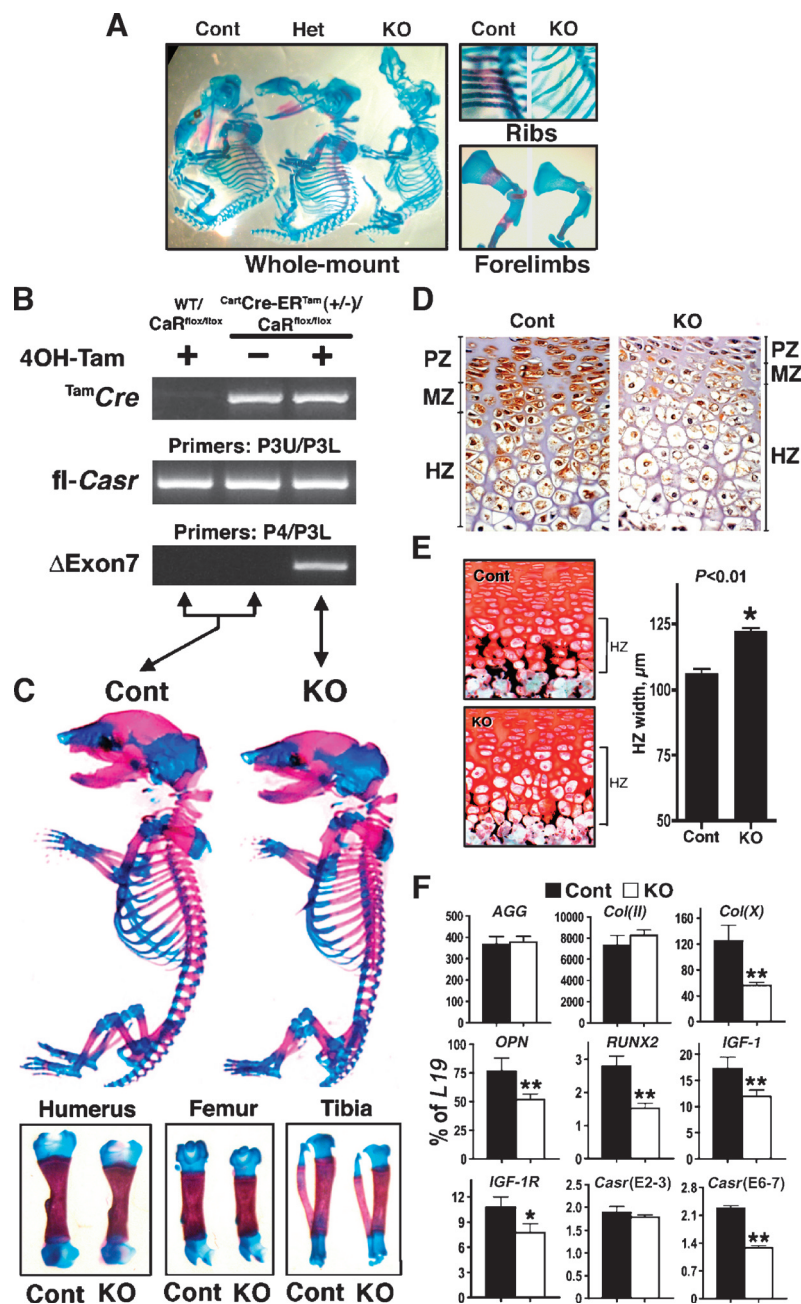
Fig. 6. Knockout of *Casr* in chondrocytes blocks embryonic development and cartilage maturation. (**A**) Whole-mount AR and AB staining shows that the skeletons of Cart-KO ($^{Cart}Casr^{\Delta flox/\Delta flox}$) mice are smaller and undermineralized compared with those of their heterozygous ($^{Cart}Casr^{WT/\Delta flox}$) and control littermates at E12.5. (**B** to **F**) Tamoxifen (Tam)-induced knockdown of the *Casr* in cartilage produces small, undermineralized skeletons in E18-19 $^{Tam-Cart}Casr^{\Delta flox/\Delta flox}$ (Tam-Cart-KO) embryos. (**B**) PCR analysis of genomic DNAs from embryos with (+) or without (−) exposure to 4OH-Tam for the expression of the ^{Tam}Cre transgene, homozygous floxed *Casr* (fl-*Casr*) alleles, and sequences lacking exon 7 (ΔExon7). (**C**) Whole-mount AR and AB staining of E19 embryos showed smaller skeletons, including humeri, femurs, and tibiae in Tam-Cart-KO compared with those of control mice. (**D**) Immunohistochemical staining of CaSR, de- picted by brown DAB staining, in the proximal tibial growth plates from E18 to E19 Tam-Cart-KO and control mice. PZ, proliferation zone; MZ, matura- tion zone; HZ, hypertrophic zone. (**E**) VK and SO staining of plastic sections of proximal tibial growth plates from E18 to E19 Tam-Cart-KO and control mice. The histogram presents HZ widths in proximal tibial growth plates from control and Tam-Cart-KO mice (*$P < 0.01$; $n = 4$ mice). (**F**) Gene profiling in the epiphyseal growth plates indicates a delay in cell maturation and differentiation in Tam-Cart-KO mice compared with that in control mice. qPCR was performed on epiphyseal growth plate samples from E18 to E19 Tam-Cart-KO and control mice with primers specific for early [*AGG* and *Col(II)*] and late [*Col(X)*, *OPN*, and *RUNX2*] chondrocyte markers and for *IGF-1*, *IGF-1R*, and *Casr*. Results are presented as the percentage of *L19* expression (*$P < 0.05$, **$P < 0.01$; $n = 6$ mice).

and $Casr^{-/-}$ mice was only ~0.5- and 9.5-fold higher, respectively, than that of control mice (10). This raises the possibility that the alternatively spliced $Casr$ mRNA, which lacks exon 5, might also be expressed in PTCs in the generalized $Casr^{-/-}$ mouse (10) and so mediate some degree of Ca^{2+}-sensing (10). To confirm this will require direct comparison of the responsiveness of PTCs to Ca^{2+} in these two mouse models, which will be challenging. Alternatively, different breeding conditions, diets, mouse strains, and PTH assays may explain the differences in the biochemical phenotypes.

Data from experiments performed in PT-KO mice confirmed that severe HPT impeded bone growth and mineralization, as was seen in generalized $Casr^{-/-}$ mice (10). We further show that this is accompanied by the reduced expression of genes encoding markers of osteoblast differentiation. This recapitulates the effects of continuous PTH treatment on both the differentiation of osteoblasts and the formation of mineralized nodules in culture (26, 27). In contrast, the milder HPT observed in PT-Het mice produced osteopenia later in life, which is similar to the classic presentation of primary HPT in humans. The molecular basis for the effects of HPT on skeletal development remains to be elucidated. PTH mediates signaling through the receptor activator of nuclear factor κB ligand (RANK-L)/RANK/osteoprotegerin (28, 29) and Wnt (30) pathways, obvious candidate pathways to interrogate in the future.

We unexpectedly observed a marked reduction in the abundance of the CaSR in the bones of PT-KO mice, which suggests that loss of CaSR signaling in that tissue may also contribute to skeletal pathology. This idea is supported by the presence of skeletal defects in both models of $Casr$ KO in osteoblasts (COL-KO and OSX-KO). As well as blocking differentiation, deletion of $Casr$ in the bones of COL-KO mice reduced the expression of $IGF-1$ and increased the expression of $IL-10$ compared with that in control mice. Because IGF-1 signaling in osteoblasts is critical for cell survival and because $IL-10$ is proapoptotic, changes in the abundance of these factors in bone would be expected to promote cell death, particularly in cells of the osteoblast lineage. This was confirmed by the presence of increased TUNEL staining in osteoblasts and osteocytes from COL-KO mice compared with that in control mice. Taken together, these data suggest that CaSR signaling modulates the proliferation, survival, and differentiation of osteoblasts, potentially by altering growth and survival factors elaborated by bone.

The embryonic lethality of the chondrocyte-specific $Casr$ KO mouse was unexpected. Generalized $Casr^{-/-}$ mice (10), which were developed by a different targeting strategy, live for several days postnatally and survive for a longer period if HPT is prevented (12, 13). This has been interpreted as evidence that the CaSR is not critical for embryonic development. In light of data from the Cart-KO mouse, we suspect that alternatively spliced $Casr$
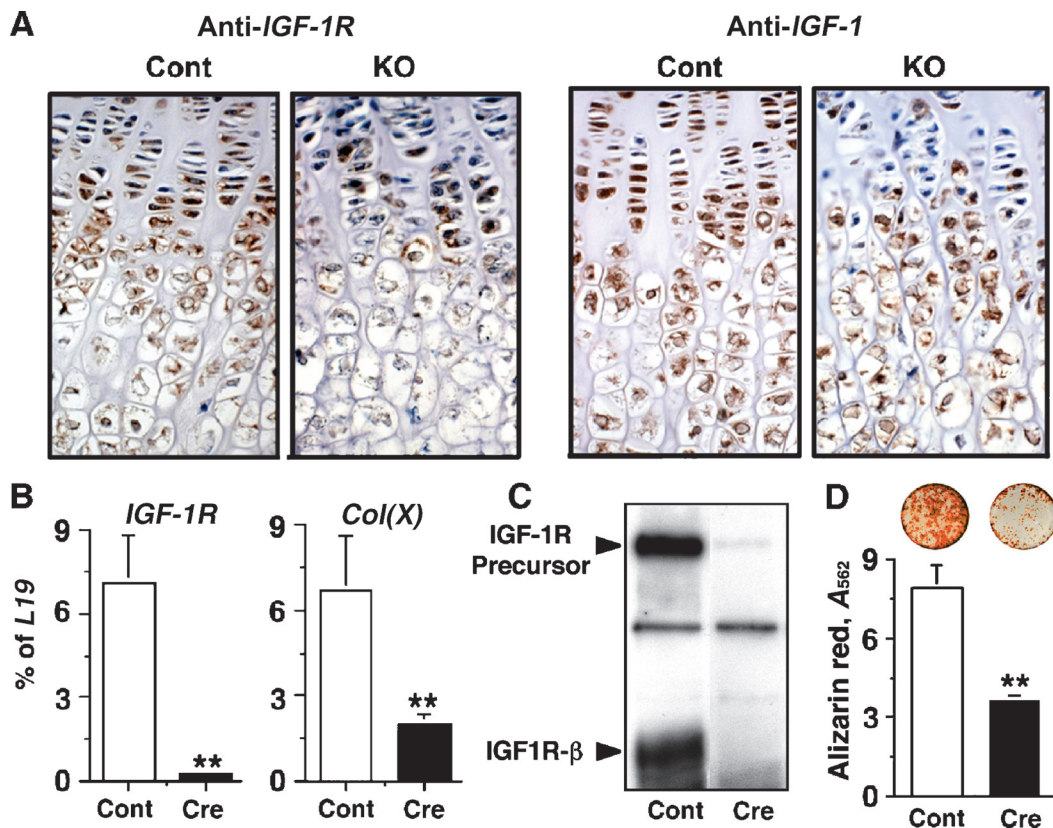
Fig. 7. Knockout of $Casr$ in chondrocytes blocks the expression of $IGF-1$ and $IGF-1R$ and delays cell differentiation. (**A**) Immunohistochemical staining of IGF-1 and IGF-1R, depicted by brown DAB staining, in the proximal tibial growth plates from E18 to E19 Tam-Cart-KO and control mice. (**B**) In vitro knockout of $IGF-1R$ was performed by infecting floxed $IGF-1R$-containing GPCs with Ad-Cre (Cre) or, as a control, Ad-Cont (Cont) viruses (16 PFU/cell). Expression of $IGF-1R$ and $Col(X)$ mRNAs was assessed by qPCR 72 hours postinfection. (**C**) Western blots were incubated with antisera against the β subunit of IGF-1R to confirm the knockdown of IGF-1R in GPCs infected with Ad-Cre (Cre) compared with that in Ad-Cont (Cont) viruses. (**D**) AR staining was performed and quantified by absorbance to assess mineralization in cultures infected with Ad-Cre (Cre) or Ad-Cont (Cont) viruses and grown in media containing 2.0 mM Ca^{2+} for 14 days (**$P < 0.001$; $n = 3$).

mRNAs, which lack exon 5, are present in the generalized $Casr^{-/-}$ mice and can compensate for as yet undefined functions of CaSRs in the embryo. The delayed cartilage maturation and mineralization observed in the two E12.5 Cart-KO embryos we studied support a role for the CaSR in the early stages of growth plate formation. It has been reported that Col(II) is transiently expressed in heart valves in mice between E10.5 and E14.5 (31). Thus, knockdown of *Casr* at that site might affect cardiac development and function and lead to embryonic death, but this remains to be determined.

Because Cart-KO embryos were nonviable, we turned to an inducible KO model. Tam-induced KO of the expression of *Casr* in GPCs produced a rickets-like phenotype with expansion and reduced mineralization of the hypertrophic zone and the decreased abundance of markers of mature, terminally differentiated chondrocytes within 2 to 3 days of exposure to Tam. These observations are consistent with work by us and others that show that high $[Ca^{2+}]_e$ promotes chondrocyte differentiation and that suppressing *Casr* expression with antisense or dominant-negative cDNA constructs blocks this effect (9, 32, 33). Furthermore, our data indicate that reduced local IGF-1R signaling plays at least some part in delaying GPC differentiation in the KO mice. Taken together, these data are the first to definitively establish a role for the CaSR in Ca^{2+} sensing in GPCs.

In summary, this study provides the first evidence supporting the direct involvement of CaSR signaling in the differentiation of osteoblasts and GPCs and skeletal development in vivo and suggests that inhibition of *Casr* expression in bone in states of HPT may be part of the mechanism underlying the skeletal defects in this disorder. These floxed *Casr* mice will enable future definitive assessment of CaSR function in other tissues.

MATERIALS AND METHODS

Construction of the gene-targeting vector and production of floxed *Casr* mice

The targeting construct contained three loxP sites flanking exon 7 of *Casr* and the cytidine deaminase (CD)–neomycin (NEO) gene cassette (Fig. 1A). The targeting construct was transfected into 129/SvJae ES cells to allow homologous recombination with endogenous *Casr* alleles, and cells were selected with G418 and fialuridine. The resulting floxed *Casr* ES cells were injected into C57/BL6 blastocysts and implanted into pseudo-pregnant CD1 mice to produce chimeric mice (University of California San Francisco Transgenic Core Facility). Chimeras were bred with C57/BL6 mice to produce heterozygous floxed *Casr* ($Casr^{wt/flox}$) mice through germline transmission. $Casr^{wt/flox}$ mice were interbred to produce homozygous floxed *Casr* ($Casr^{flox/flox}$) mice. Integration of the targeting construct into the genome of floxed *Casr* ES cells before blastocyst injections and the genotypes of the resulting $Casr^{wt/flox}$ and $Casr^{flox/flox}$ mice were confirmed by PCR with three sets of primers targeting different regions of the construct (Fig. 1A; see table S1 for primer sequences), P1U/P1L, P2U/P2L, and P3U/P3L, which amplified cDNAs with sizes of ~1800, 1050, and 167 bp, respectively, from the floxed *Casr* allele. All mice were maintained under standard conditions with free access to food and water under protocols approved by the Animal Care Subcommittee, San Francisco Department of Veterans Affairs Medical Center.

Generation and genotyping of conditional *Casr* knockout mice

Mice with KO of *Casr* specifically in PTCs, osteoblasts, or chondrocytes were generated by breeding $Casr^{flox/flox}$ mice with transgenic mice expressing *Cre*-recombinase under the control of the appropriate promoter: the *PTH* promoter (PTH-Cre, The Jackson Laboratory) for PTCs, the 2.3-kb fragment of the rat *Col(I)* promoter [2.3Col(I)-Cre; gift

of Dr. Barbara Kream, University of Connecticut, Farmington] or the *OSX* promoter [OSX-Cre, gift of Dr. Andrew McMahon, Harvard University (21)] for osteoblasts, and the mouse *Col(II)* promoter [Col(II)-Cre, The Jackson Laboratory] for chondrocytes. To generate Tam-inducible *Casr* knockout in cartilage, we bred the floxed *Casr* mice with transgenic mice [^{Cart}Cre-ER^{Tam}; a gift of Dr. Susan Mackem, National Institutes of Health (NIH)] expressing a fusion protein (Cre-ER^{Tam}) of Cre recombinase and a mutated ligand-binding domain of the estrogen receptor (ER^{Tam}) under the control of a mouse *Col(II)* promoter and enhancer. The inducibility of Cre activity by Tam and the specific expression of the construct in cartilage has been previously confirmed (23, 24). Mouse genotypes were determined by PCR analyses of genomic DNAs from tail snips with primers for the *Cre* transgene (Cre-1/Cre-2; see table S2), which amplified a ~500-bp cDNA and the P3U and P3L primer set for the loxP sequence at the 3′ end of exon 7, which amplified a 133-bp DNA fragment from wild-type alleles and a 167-bp DNA from floxed *Casr* alleles. To verify tissue-specific gene excision, genomic DNA was isolated from the tissues specified and was then subjected to PCR analysis with the P4/P3L primer set, which amplified a 284-bp DNA fragment from the *Casr* gene allele after the excision of exon 7.

Whole-mount AR and AB staining

Mice were skinned, eviscerated, and fixed in ethanol (95%) for 2 to 5 days. Tissues were then defatted in acetone for 2 days, stained in AR/AB solution [AB (0.015%), AR (0.005%), acetic acid (0.05%), and ethanol (75%)] for 5 days, cleared in KOH (1%) in glycerol (gradually increased from 0% to 20%, 50%, and 80% with 2-day intervals between steps), and stored and visualized in 100% glycerol (34).

Von Kossa and Goldner staining

Femurs and tibiae were isolated, fixed in 10% phosphate-buffered formalin, dehydrated, defatted, and embedded in plastic (methyl methacrylate, Sigma, St. Louis, MO). For detection of phosphate-containing minerals, 4-μm sections were stained with VK reagents by a standard protocol (35) [silver nitrate (1%) in H_2O for 10 min in the dark; a mixture of sodium carbonate (5%) and formaldehyde (10%) in H_2O for 2 min; and a mixture of sodium thiosulfate (10%) and potassium ferricyanide (0.05%) in H_2O for 20 s; with washes in tap water between steps], followed by counterstaining with SO (0.01%) in H_2O for 20 min. To distinguish between mineralized matrix and unmineralized osteoid, sections were stained with Goldner trichrome reagents [in H_2O, picric acid (1%) at 37°C for 2 hours; fuchsin (1%) for 15 min; phosphomolybdic acid (6%) for 5 min; and light green (4%) for 15 min; with washes in tap water between steps].

Cell culture, transfection, and [³H]InsP assay

HEK 293 cells were cultured and transfected with WT-CaSR-green fluorescent protein (GFP), ΔExon7-CaSR-GFP, WT-CaSR, ΔExon7-CaSR, or empty pcDNA3.1 vector cDNAs (10 μg/construct) as described (36). Twenty-four hours after transfection, cells were replated on coverslips for confocal microscopy, six-well dishes for [³H]InsP assays, and 10-cm dishes for protein lysates and cultured for an additional 48 hours. For coculture experiments, cells separately transfected with WT-CaSR or with ΔExon7-CaSR cDNAs were mixed in a 1:1 ratio and cocultured for 48 hours before the start of InsP assays. Twenty-four hours after replating, HEK 293 cells expressing WT-CaSR or ΔExon7-CaSR cDNAs and a mixture of cells expressing each of these constructs were labeled with [³H]myoinositol (2 μCi/ml) for 18 to 24 hours (36). Cells were exposed to conditions of differing $[Ca^{2+}]_e$ for 60 min at 37°C after pretreatment for 10 min with 10 mM LiCl. Total [³H]InsP was quantified after anion-exchange chromatography and is presented as the fold in-

crease over the basal amount of [^{3}H]InsP under conditions of 0.5 mM Ca^{2+} and 0.5 mM Mg^{2+}.

Immunocytochemistry and Western blotting

For fluorescent microscopy, HEK 293 cells transfected with WT-CaSR-GFP or ΔExon7-CaSR-GFP and grown on coverslips were fixed with 4% paraformaldehyde, mounted on glass slides with Gel Mount (Biomeda, Foster City, CA), and examined with a Leica TCS confocal microscope (Laboratory for Cell Imaging, San Francisco Department of Veterans Affairs Medical Center). Tibiae from E18 to E19 Tam-Cart-KO and control embryos were dissected, fixed in 4% paraformaldehyde in phosphate-buffered saline (PBS), decalcified in 10% EDTA in PBS for 24 hours, and cut into 4-μm sections. Immunoreactivity in these sections was detected with a custom-made rabbit polyclonal anti-CaSR antibody (100 nM) raised against an intracellular epitope of the receptor (36) and horseradish peroxidase (HRP)–conjugated goat antirabbit immunoglobulin G antisera, and signals were developed by a 3,3′-diaminobenzidine (DAB) substrate. Sections were counterstained with aqueous hematoxylin. Proteins from total cell lysates of HEK 293 cells expressing WT-CaSR-GFP or ΔExon7-CaSR-GFP and from concentrated culture media bathing the cells were electrophoresed on SDS–polyacrylamide gel electrophoresis gels and transferred to nitrocellulose membranes (36). Membranes were incubated with anti-GFP (50 nM) antibody and the appropriate HRP-conjugated secondary antibodies. Signals were detected with a SuperSignal chemiluminescence substrate and developed on Kodak x-ray film.

Microcomputed tomography

To quantify the amount of mineral deposited by mature osteoblasts in the bone matrix, we performed μCT scans at two anatomical sites: the distal femur, a site rich in Tb bone, and the TFJ, a site rich in Ct bone, as described (35). Femurs and tibiae were isolated, fixed in 10% phosphate-buffered formalin for 24 hours, and then switched to 70% ethanol. Bones were then scanned in a tube containing 70% ethanol by a Scanco vivaCT 40 scanner (Scanco Medical, Basserdorf, Switzerland). To assess Tb bone in the distal femoral metaphysis, 100 serial cross-sectional scans (1.05 mm) of the secondary spongiosa were obtained from the end of the growth plate, extending proximally with 10.5-μm voxel size and 55-kV x-ray energy. For the Ct bone scans, 100 serial cross sections (1.05 mm) of the tibia were obtained from the TFJ, extending proximally with 10.5-μm voxel size and 55-kV x-ray energy. For analysis of μCT images, thresholds were applied to segment or separate the mineralized bone matrix from soft tissue. Linear attenuation was calibrated with hydroxyapatite as the standard. Image analysis and 3D reconstructions were performed with the manufacturer's software (SCANCO Medical AG, Bassersdorf, Switzerland).

Quantitative real-time PCR assays

RNA samples isolated from the PTGs of 2-week-old mice, from the humeral cortices of 14- and 21-day-old mice after the bone marrow was flushed out, or from epiphyseal growth plates from E18 to E19 embryos were reverse-transcribed into cDNA and subjected to qPCR (7, 8). Expression of the following genes was determined: *Casr* and *PTH* for PTGs; osteogenic markers [*OSX*, *Col(I)*, *ALP*, *DMP1*, *OCN*, *SOST*] and *Casr* and the growth regulatory factors *IGF-1*, *CCND1*, *Bcl-2*, *Bcl-2L1*, and *IL-10* for bone; and chondrogenic markers [*AGG*, *Col(II)*, *Col(X)*, *OPN*, and *RUNX2*] and *IGF-1*, *IGF-1R*, and *Casr* for cartilage. Taqman assay–based sets of primers and probes for mouse *Casr* (spanning exons 6 and 7), *PTH*, *CCND1*, *DMP1*, and *SOST* were obtained from Applied Biosystems (Foster City, CA). Cyber green–based sets of primers and probes for *Bcl-2*, *Bcl-2L1*, *IL-10*, and *GAPDH* were purchased from SuperArray (Frederick,

MD). Taqman-based sets of primers and probes for *OSX*, *Col(I)*, *ALP*, *OCN*, *Casr* (spanning exons 2 and 3), *AGG*, *Col(II)*, *Col(X)*, *IGF-1*, *IGF-1R*, *RUNX2*, *OPN*, and *L19* were custom-made by Integrated DNA Technologies (Coralville, IA) according to published sequences (table S2).

Culture, adenoviral infection, and AR staining of floxed *IGF-1R* GPCs

Growth plate chondrocytes isolated from 2- to 4-day-old floxed *IGF-1R* mice (37) were cultured and infected with replication-deficient adenoviruses [~16 plaque-forming units (PFU)/cell] carrying cDNA encoding the bacterial Cre recombinase (Ad-Cre) or no insert (Ad-Cont) as described (38). RNA and cell lysates were isolated 48 to 72 hours postinfection to assess the expression of *IGF-1R* and $\alpha_1(X)$ as described above. Alizarin red staining was performed on infected cultures grown in medium containing 2.0 mM Ca^{2+} for 14 days to assess mineralization (8).

Statistics

Data from two groups were represented as mean ± the standard error of the mean and compared by unpaired Student's *t* test. Significance was assigned for $P < 0.05$ or $P < 0.01$.

REFERENCES AND NOTES

1. E. M. Brown, The calcium-sensing receptor: Physiology, pathophysiology and CaR-based therapeutics. *Subcell. Biochem.* **45**, 139–167 (2007).
2. E. M. Brown, R. J. MacLeod, Extracellular calcium sensing and extracellular calcium signaling. *Physiol. Rev.* **81**, 239–297 (2001).
3. W. Chang, D. Shoback, Extracellular Ca^{2+}-sensing receptors—an overview. *Cell Calcium* **35**, 183–196 (2004).
4. E. M. Brown, M. Bai, M. Pollak, Familial benign hypocalciuric hypercalcemia and other syndromes of altered responsiveness to extracellular calcium, in *Metabolic Bone Disease*, L. V. Avioli, S. M. Krane, Eds. (Academic Press, New York, 1998), pp. 479–499.
5. M. M. Dvorak, A. Siddiqua, D. T. Ward, D. H. Carter, S. L. Dallas, E. F. Nemeth, D. Riccardi, Physiological changes in extracellular calcium concentration directly control osteoblast function in the absence of calciotropic hormones. *Proc. Natl. Acad. Sci. U.S.A.* **101**, 5140–5145 (2004).
6. M. M. Dvorak, D. Riccardi, Ca^{2+} as an extracellular signal in bone. *Cell Calcium* **35**, 249–255 (2004).
7. W. Chang, L. Rodriguez, T. H. Chen, C. Tu, D. Shoback, Extracellular Ca^{2+}-sensing in cartilage. *J. Musculoskelet. Neuronal. Interact.* **4**, 410–411 (2004).
8. L. Rodriguez, Z. Cheng, T. H. Chen, C. Tu, W. Chang, Extracellular calcium and parathyroid hormone–related peptide signaling modulate the pace of growth plate chondrocyte differentiation. *Endocrinology* **146**, 4597–4608 (2005).
9. W. Chang, C. Tu, T. H. Chen, L. Komuves, Y. Oda, S. A. Pratt, S. Miller, D. Shoback, Expression and signal transduction of calcium-sensing receptors in cartilage and bone. *Endocrinology* **140**, 5883–5893 (1999).
10. C. Ho, D. A. Conner, M. R. Pollak, D. J. Ladd, O. Kifor, H. B. Warren, E. M. Brown, J. G. Seidman, C. E. Seidman, A mouse model of human familial hypocalciuric hypercalcemia and neonatal severe hyperparathyroidism [see comments]. *Nat. Genet.* **11**, 389–394 (1995).
11. S. C. Garner, M. Pi, Q. Tu, L. D. Quarles, Rickets in cation-sensing receptor-deficient mice: An unexpected skeletal phenotype. *Endocrinology* **142**, 3996–4005 (2001).
12. Q. Tu, M. Pi, G. Karsenty, L. Simpson, S. Liu, L. D. Quarles, Rescue of the skeletal phenotype in CasR-deficient mice by transfer onto the Gcm2 null background. *J. Clin. Invest.* **111**, 1029–1037 (2003).
13. C. H. Kos, A. C. Karaplis, J. B. Peng, M. A. Hediger, D. Goltzman, K. S. Mohammad, T. A. Guise, M. R. Pollak, The calcium-sensing receptor is required for normal calcium homeostasis independent of parathyroid hormone. *J. Clin. Invest.* **111**, 1021–1028 (2003).

RESEARCH ARTICLE

14. L. Rodriguez, C. Tu, Z. Cheng, T. H. Chen, D. Bikle, D. Shoback, W. Chang, Expression and functional assessment of an alternatively spliced extracellular Ca^{2+}-sensing receptor in growth plate chondrocytes. *Endocrinology* **146**, 5294–5303 (2005).

15. Y. Oda, C. L. Tu, W. Chang, D. Crumrine, L. Komuves, T. Mauro, P. M. Elias, D. D. Bikle, The calcium sensing receptor and its alternatively spliced form in murine epidermal differentiation. *J. Biol. Chem.* **275**, 1183–1190 (2000).

16. S. K. Libutti, J. S. Crabtree, D. Lorang, A. L. Burns, C. Mazzanti, S. M. Hewitt, S. O'Connor, J. M. Ward, M. R. Emmert-Buck, A. Remaley, M. Miller, E. Turner, H. R. Alexander, A. Arnold, S. J. Marx, F. S. Collins, A. M. Spiegel, Parathyroid gland-specific deletion of the mouse Men1 gene results in parathyroid neoplasia and hypercalcemic hyperparathyroidism. *Cancer Res.* **63**, 8022–8028 (2003).

17. F. Liu, H. W. Woitge, A. Braut, M. S. Kronenberg, A. C. Lichtler, M. Mina, B. E. Kream, Expression and activity of osteoblast-targeted Cre recombinase transgenes in murine skeletal tissues. *Int. J. Dev. Biol.* **48**, 645–653 (2004).

18. G. G. McGill, M. Horstmann, H. R. Widlund, J. Du, G. Motyckova, E. K. Nishimura, Y. L. Lin, S. Ramaswamy, W. Avery, H. F. Ding, S. A. Jordan, I. J. Jackson, S. J. Korsmeyer, T. R. Golub, D. E. Fisher, Bcl2 regulation by the melanocyte master regulator Mitf modulates lineage survival and melanoma cell viability. *Cell* **109**, 707–718 (2002).

19. K. M. Wiren, A. R. Toombs, A. A. Semirale, X. Zhang, Osteoblast and osteocyte apoptosis associated with androgen action in bone: Requirement of increased Bax/Bcl-2 ratio. *Bone* **38**, 637–651 (2006).

20. S. Pestka, C. D. Krause, D. Sarkar, M. R. Walter, Y. Shi, P. B. Fisher, Interleukin-10 and related cytokines and receptors. *Annu. Rev. Immunol.* **22**, 929–979 (2004).

21. S. J. Rodda, A. P. McMahon, Distinct roles for Hedgehog and canonical Wnt signaling in specification, differentiation and maintenance of osteoblast progenitors. *Development* **133**, 3231–3244 (2006).

22. D. A. Ovchinnikov, J. M. Deng, G. Ogunrinu, R. R. Behringer, Col2a1-directed expression of Cre recombinase in differentiating chondrocytes in transgenic mice. *Genesis* **26**, 145–146 (2000).

23. E. Nakamura, M. T. Nguyen, S. Mackem, Kinetics of tamoxifen-regulated Cre activity in mice using a cartilage-specific CreER(T) to assay temporal activity windows along the proximodistal limb skeleton. *Dev. Dyn.* **235**, 2603–2612 (2006).

24. Y. Maeda, E. Nakamura, M. T. Nguyen, L. J. Suva, F. L. Swain, M. S. Razzaque, S. Mackem, B. Lanske, Indian Hedgehog produced by postnatal chondrocytes is essential for maintaining a growth plate and trabecular bone. *Proc. Natl. Acad. Sci. U.S.A.* **104**, 6382–6387 (2007).

25. Y. Wang, S. Nishida, T. Sakata, H. Z. Elalieh, W. Chang, B. P. Halloran, S. B. Doty, D. D. Bikle, Insulin-like growth factor-I is essential for embryonic bone development. *Endocrinology* **147**, 4753–4761 (2006).

26. C. G. Bellows, H. Ishida, J. E. Aubin, J. N. Heersche, Parathyroid hormone reversibly suppresses the differentiation of osteoprogenitor cells into functional osteoblasts. *Endocrinology* **127**, 3111–3116 (1990).

27. T. Ishizuya, S. Yokose, M. Hori, T. Noda, T. Suda, S. Yoshiki, A. Yamaguchi, Parathyroid hormone exerts disparate effects on osteoblast differentiation depending on exposure time in rat osteoblastic cells. *J. Clin. Invest.* **99**, 2961–2970 (1997).

28. J. Liao, L. K. McCauley, Skeletal metastasis: Established and emerging roles of parathyroid hormone related protein (PTHrP). *Cancer Metastasis Rev.* **25**, 559–571 (2006).

29. J. C. Huang, T. Sakata, L. L. Pfleger, M. Bencsik, B. P. Halloran, D. D. Bikle, R. A. Nissenson, PTH differentially regulates expression of RANKL and OPG. *J. Bone Miner. Res.* **19**, 235–244 (2004).

30. M. K. Bergenstock, N. C. Partridge, Parathyroid hormone stimulation of noncanonical Wnt signaling in bone. *Ann. N. Y. Acad. Sci.* **1116**, 354–359 (2007).

31. O. Rahkonen, M. Savontaus, E. Abdelwahid, E. Vuorio, E. Jokinen, Expression patterns of cartilage collagens and Sox9 during mouse heart development. *Histochem. Cell Biol.* **120**, 103–110 (2003).

32. W. Chang, C. Tu, S. Pratt, T. H. Chen, D. Shoback, Extracellular Ca(2+)-sensing receptors modulate matrix production and mineralization in chondrogenic RCJ3.1C5.18 cells. *Endocrinology* **143**, 1467–1474 (2002).

33. W. Chang, C. Tu, R. Bajra, L. Komuves, S. Miller, G. Strewler, D. Shoback, Calcium sensing in cultured chondrogenic RCJ3.1C5.18 cells. *Endocrinology* **140**, 1911–1919 (1999).

34. M. J. McLeod, Differential staining of cartilage and bone in whole mouse fetuses by Alcian blue and alizarin red S. *Teratology* **22**, 299–301 (1980).

35. M. M. Dvorak, T. H. Chen, B. Orwoll, C. Garvey, W. Chang, D. D. Bikle, D. M. Shoback, Constitutive activity of the osteoblast Ca^{2+}-sensing receptor promotes loss of cancellous bone. *Endocrinology* **148**, 3156–3163 (2007).

36. W. Chang, S. Pratt, T. H. Chen, E. Nemeth, Z. Huang, D. Shoback, Coupling of calcium receptors to inositol phosphate and cyclic AMP generation in mammalian cells and *Xenopus laevis* oocytes and immunodetection of receptor protein by region-specific antipeptide antisera. *J. Bone Miner. Res.* **13**, 570–580 (1998).

37. M. Zhang, S. Xuan, M. L. Bouxsein, D. von Stechow, N. Akeno, M. C. Faugere, H. Malluche, G. Zhao, C. J. Rosen, A. Efstratiadis, T. L. Clemens, Osteoblast-specific knockout of the insulin-like growth factor (IGF) receptor gene reveals an essential role of IGF signaling in bone matrix mineralization. *J. Biol. Chem.* **277**, 44005–44012 (2002).

38. Z. Cheng, C. Tu, L. Rodriguez, T. H. Chen, M. M. Dvorak, M. Margeta, M. Gassmann, B. Bettler, D. Shoback, W. Chang, Type B gamma-aminobutyric acid receptors modulate the function of the extracellular Ca^{2+}-sensing receptor and cell differentiation in murine growth plate chondrocytes. *Endocrinology* **148**, 4984–4992 (2007).

Pilot Study 4:

Functional MRI of Emotional Memory in Veterans With and Without Post Traumatic Stress Disorder

Principal Investigator: Linda. L. Chao, Ph.D., Associate Adjunct Professor

ABSTRACT

The goal of this project is to use functional magnetic resonance imaging (fMRI) to examine the effects of posttraumatic stress disorder (PTSD) on neural modulation in a high-level visual processing area. Two groups of subjects will be studied: combat-exposed veterans with PTSD and combat-exposed veterans without PTSD. Blood-oxygen level dependent (BOLD) will be measured while subjects view pictures with and without combat-related content in "repeated" and "different" (i.e., novel) presentation conditions. The pattern of BOLD response in the lateral occipital complex (LOC), a high-level visual processing area, will be examined. Specifically, we will compare habituation of the BOLD response in the LOC to repeated presentations of combat-related and non-combat-related pictures. We hypothesize that veterans with PTSD will show less habituation of the BOLD response in the LOC to repeated presentations of combat-related pictures than to repeated presentations of non-combat-related pictures. In addition, we will compare habituation of the BOLD response in the LOC in this novel fMRI task to habituation of the acoustic startle response, a well-established finding in individuals with PTSD. If reduced BOLD habituation in the visual cortex is truly a robust and reproducible finding in PTSD, then it may prove to be a useful biomarker for validating self-reported measures of PTSD and PTSD treatment efficacy.

TABLE OF CONTENTS

INTRODUCTION

It is well established that individuals with posttraumatic stress disorder (PTSD) have enhanced physiological responses to trauma specific cues (1,2) and enhanced responses to acoustic startle (3-6). A recent functional magnetic resonance imaging (fMRI) study reported that PTSD subjects exhibited reduced habituation of the blood-oxygen level dependent (BOLD) response to repeated presentations of combat-related stimuli in a high-level visual processing area (7). Because impaired habituation and extinction have been proposed to play a prominent role in the pathogenesis of PTSD (8), it is tempting to conclude from the fMRI results of Hendler et al. (7) that subjects with PTSD have enhanced fear conditioning of traumatic experiences that is expressed as altered modulation of brain activity at the level of the sensory cortex. However, Hendler and colleagues only studied nine veterans with PTSD. Thus, it is unclear how robust or reproducible their finding is. The goal of this project is to replicate and extend, in a larger sample of PTSD subjects, the finding that PTSD reduces BOLD habituation in the visual cortex to combat-related stimuli. If reduced BOLD habituation in the visual cortex is truly a robust and reproducible finding in PTSD, then it may prove to be a useful biomarker for PTSD.

The goal of this project is to examine the effect of PTSD on neural modulation in the lateral occipital complex (LOC), a high-level visual processing region that is selectively activated by images of objects. To achieve this aim, we will test the hypothesis that habituation of the BOLD response in the LOC to repeated presentations of combat-related stimuli is reduced veterans with PTSD. In addition, we will compare habituation of the BOLD response in the LOC in this novel fMRI task to habituation of the acoustic startle response, a well-established phenomenon in individuals with PTSD (9).

BODY

To date, we have recruited and studied 7 veterans without PTSD and 10 veterans with PTSD. The subjects have all been male combat veterans of the Vietnam, Bosnia, and first Gulf War, as well as Operation Enduring Freedom and Operation Iraqi Freedom.

The table below describes the demographics of the subjects studied to date: There were no significant differences in age or years of education between subjects with and subjects without PTSD.

Table 1. Subject demographic data

	N	Age	Education
PTSD-	7	29.3 + 7.1	14.9 + 1.9
PTSD+	10	39.7 + 14.0	14.8 + 1.7

One of the first findings of this study is that the LOC responds more strongly to traumatic than to neutral images in subjects with and without PTSD (see Figure 1 below). Although the LOC is known to be an "object-responsive" region (i.e., a brain region that responds more strongly to images of objects than other types of images), no one to date has shown that traumatic images elicit a stronger response in this brain region than neutral images.

3

Based on the results of Hendler et al. (7) we had expected to find reduced fMR adaptation in the LOC to traumatic stimuli in subjects with PTSD compared to subjects without PTSD. Although we did find this pattern of results in some PTSD+ subjects (see Figure 1), we did not find it in all

Figure 1A. Example of lateral occipital complex (LOC) in a representative subject
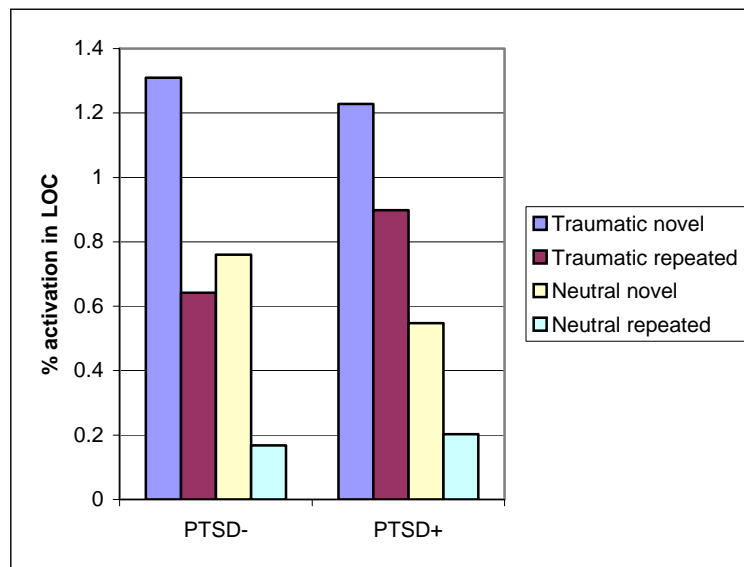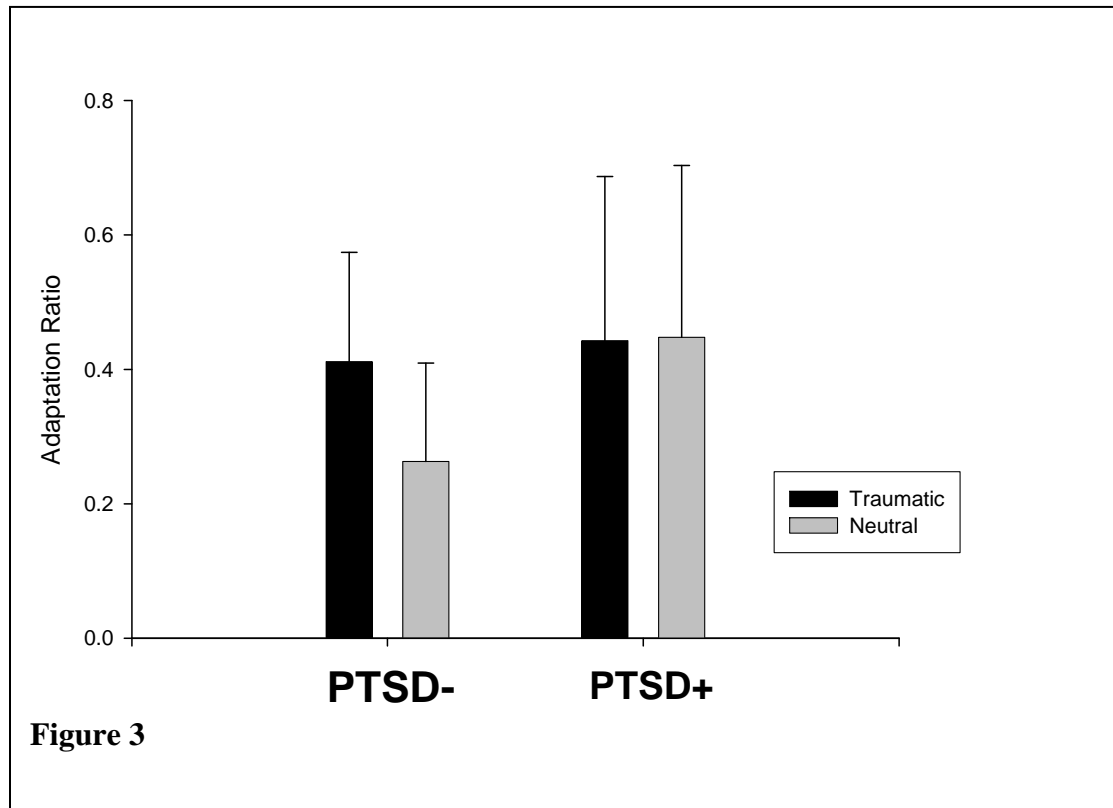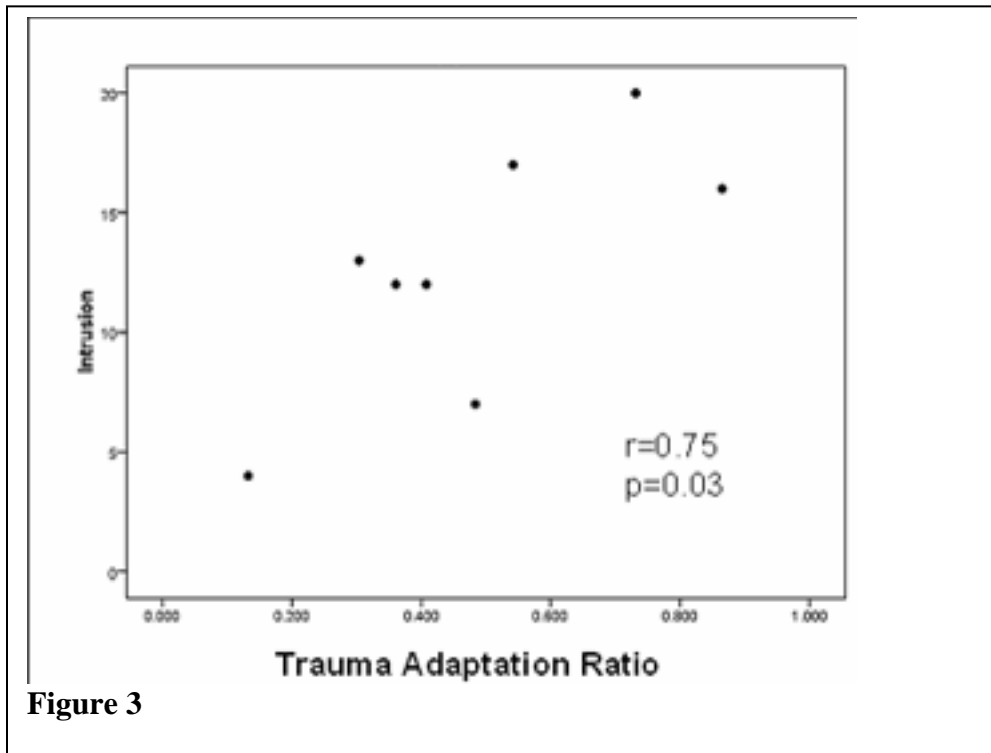

Figure 1B. Percent activation in the LOC to novel and repeated traumatic and neutral images in a PTSD- and PTSD+ subject. Note that both subjects show approximately the same amount of activation to novel traumatic images, but that the PTSD+ subjects shows greater activation to repeated traumatic images than the PTSD- subject.

PTSD+ subjects. Thus, we did not find any significant difference in the adaptation ratio to traumatic images in subjects with and without PSTD (see Figure 2). The adaptation ratio is a ratio of activation elicited by repeated and novel images. An adaptation ratio of 1 indicates no adaptation.

Figure 3

However, we did find that in PTSD+ subjects, the amount of adaptation in the LOC to traumatic images was positively correlated to the amount of intrusive symptoms they experienced (r=0.75, p=0.03). In other words, the more intrusive symptoms a PTSD+ subject reported, the less adaptation (or the higher the adaptation ratio) that subject showed to traumatic images (see figure 3). It should be noted that the Clinical-Administered PTSD Scale (CAPS) measures intrusion, avoidance, and arousal symptoms, but only intrusion correlated with the amount of adaptation to traumatic images in PTSD+ subjects.

Figure 3

KEY RESEARCH ACCOMPLISHMENTS
- We showed that the LOC responds more strongly to traumatic than neutral images in subjects with and without PTSD.
- We found that functional adaptation of the LOC to traumatic images is not merely a affected by PTSD but rather a by the amount of intrusive symptoms that a subject with PTSD experiences.

REPORTABLE OUTCOMES
No publications or abstracts have resulted from this study. However, we are planning to report our findings that the LOC responds more strongly to traumatic than neutral images in subjects with and without PTSD and the fact that functional adaptation of the LOC to traumatic images is related to how many intrusive symptoms a subject with PTSD experiences in an abstract soon.

CONCLUSION
The goal of this project is to examine the effect of PTSD on neural modulation in the LOC, a high-level visual processing region that is selectively activated by images of objects. Previous fMRI results from Hendler et al. (7) suggested that subjects with PTSD have enhanced fear conditioning of traumatic experiences that is expressed as altered modulation of brain activity at the level of the sensory cortex. Our results to date suggest that only PTSD+ subjects who experience many intrusive symptoms show altered modulation of brain activity at the level of the sensory cortex to traumatic images. T hese results suggest that reduced BOLD habituation in the visual association cortex is may be a useful biomarker for intrusive symptoms in PTSD.

REFERENCES

1. Orr SP, Pitman KR, Lasko NB, Herz LR. Psychophysiological assessment of posttraumatic stress disorder imagery in World War II and Korean combat veterans. J. Abnormal Psychol 1993;102:152-159.

2. Shalev AY, Orr SP, Pitman KR. Psychophysiologic assessment of traumatic imagery in Israeli civilian patients with posttraumatic stress disorder. Am. J. Psychiatry 1993;150:620-624.

3. Morgan CA, Grillon C, Lubin H, Southwick SM. Startle reflex abnormalities in women with sexual assault-related posttraumatic stress disorder. J. Am. Psychiatry 1997;154:1076-1080.

4. Morgan CA, Grillon C, Southwick SM, Davis M, Charney DS. Exaggerated acoustic startle reflex in Gulf War veterans with posttraumatic stress disorder. Am. J. Psychiatry 1996;153:64-68.

5. Shalev AY, Orr SP, Peri T, Schreiber S, Pitman R. Physiologic responses to loud tones in Israeli patients with posttraumatic stress disorder. Arch. Gen. Psychiatry 1992;49:870-875.

6. Pole N, Neylan TC, Best SR, Orr SP, Marmar CR. Effects of fear-potentiation on physiologic response to acoustic startle in urban police officers with posttraumatic stress symptoms. J Trauma Stress 2003;16:471-479.

7. Hendler T, Rotshtein P, Hadar U. Emotion-perception interplay in the visual cortex: "The eyes follow the heart". Cell Mol Neurobiol. 2001;21:733-752.

8. Newport DJ, Nemeroff CB. Neurobiology of posttraumatic stress disorder. Curr. Opin. Neurobiol. 2000;10:211-218.

9. Orr SP, Solomon Z, Peri T, Pitman RK, Shalev AY. Physiologic responses to loud tones in israeli veterans of the 1973 Yom Kippur War. Biol. Psychiatry 1997;41:319-326.

APPENDICES
N/A

SUPPORTING DATA
N/A

Pilot Study 5:

Novel Approach to Overcoming Psychological Stress-Induced Delays in Wound Healing by Inhibiting Stress Hormone (Glucocorticoid) Activities

Principle Investigator: Peter M. Elias M.D.

ABSTRACT

PURPOSE: To investigate the effects of specific effectors of the nuclear hormone receptor class, and the role of glucocorticoids, on the rate of skin wound healing during psychological stress. SCOPE: 1) To assess the effects of psychological stress on wound healing in normal and compromised skin; 2) To assess whether the psychological stress-induced delay can be attributed to enhanced glucocorticoid production; 3) To assess the basis for delayed skin wound healing in psychologically-stressed animals; and 4) To determine whether ligands of class II nuclear hormone receptors normalize skin wound healing in the face of psychological stress. MAJOR FINDINGS: Our initial results demonstrate a delay in the rate of skin wound healing in animals undergoing psychological stress compared with the rate of wound healing in control (non-stressed) animals. Demonstrated that skin wound healing in the psychological stress group is accelerated (normalized) when animals are removed from the psychological stress conditions. Initial studies to determine the extent to which pharmacologic activators of the liposensor subclass of class II nuclear hormone receptors (i.e., PPARα, PPARγ, PPARδ, and LXR) overcome psychological stress-induced delays in wound healing reveal that a specific PPAR agonist improves (overcomes) the psychological stress-induced delay in skin wound healing. SIGNIFICANCE: Studies to date suggest that specific nuclear hormone receptor agonists can improve the rate of wound healing following a full-thickness skin wound, while others can have deleterious effects on the rate of wound healing. Thus, activation of specific nuclear hormone receptor(s) may represent novel target pathways to alter the wound healing under conditions of psychological stress as experienced by combat military and non-military personnel. Increased rates of wound healing should improve outcomes for both military and non-military personnel experiencing combat-related injuries.

TABLE OF CONTENTS

INTRODUCTION

Whereas psychological stress (PS) is well-known to delay wound healing (WH), the responsible mechanisms have not yet been fully clarified. Our recent work on stressed rodent models, subjected to superficial injury, identifies a PS-induced increase in endogenous glucocorticoids (GC) as the responsible mechanism. Highly-increased PS is a defining feature of military service, particularly under combat conditions, which likely delays WH in wounded servicemen and women, particularly in those affected by post-traumatic stress disorder (PTSD). In a newly-developed rodent model, we will assess the role of increased endogenous GC in the PS-induced delay in WH. Since GC-mediated mechanisms operate in response to PS, we next will test which interventions that modify GC-mediated mechanisms are most effective in normalizing delayed WH. Finally, we will assess the ability of another class of therapeutic agents; i.e., activators of the liposensor subclass of class II nuclear hormone receptors, for their ability to accelerate WH. Our preliminary studies have shown that these agents not only accelerate WH after superficial epidermal insults, but they also override specific mechanisms that are suppressed by GC, such as epidermal barrier repair, mitogenesis, differentiation, and lipid synthesis. Together, these studies will determine the role of increased endogenous GC in delayed WH, and assess a variety of corrective approaches that could be applied quickly to benefit wounded military personnel and the general public.
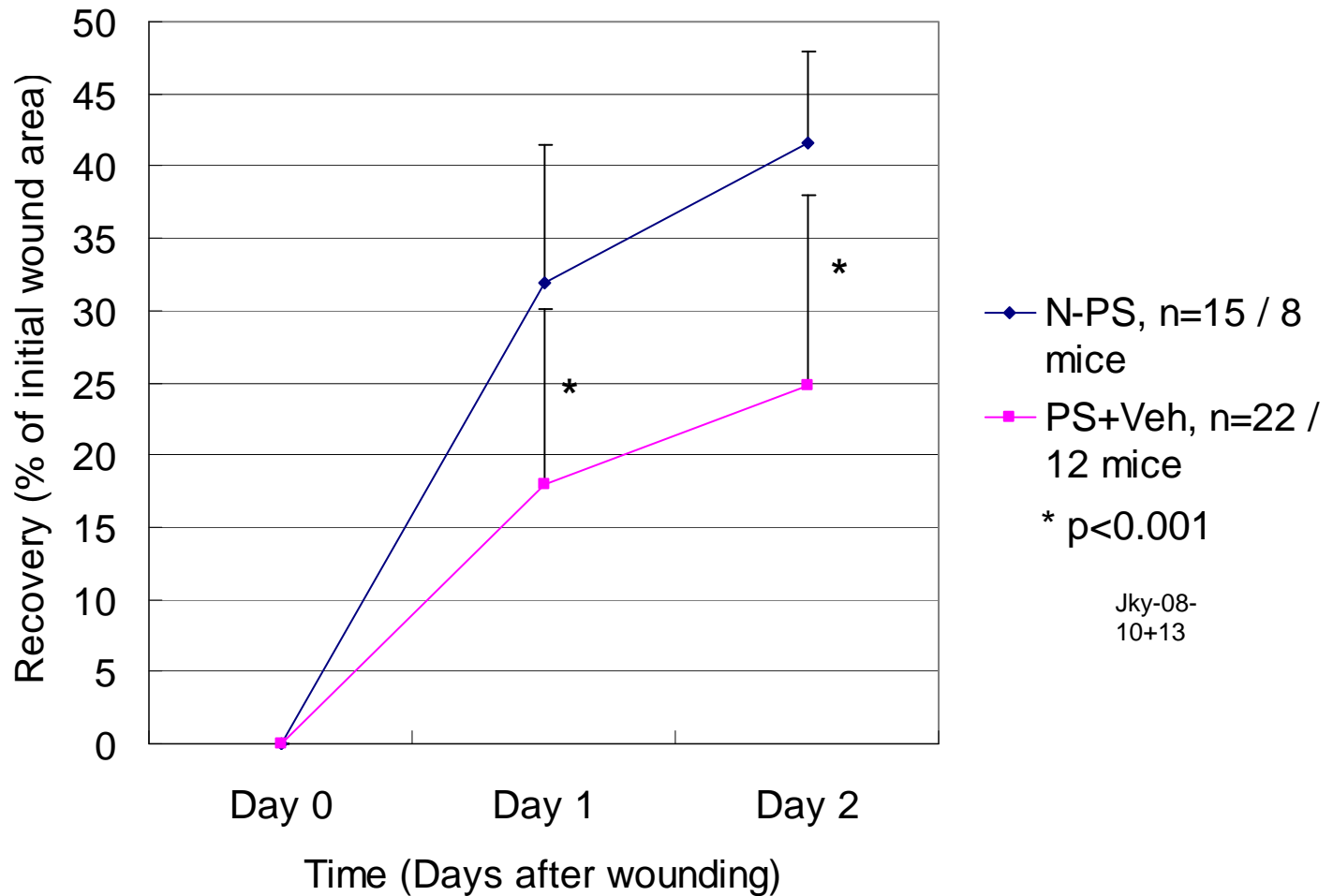
BODY

During the first full year of this grant, we have made significant progress toward the goals of this study. We have established and continue to optimize the animal model for stress-induced delay in wound healing. We have demonstrated a delay in wound healing in animals that are maintained in a stressed environment vs. those that are not similarly stressed (Controls: either food and water restricted, or allowed food and/or water access, to match the stressed-animal conditions). In this model, animals are placed in stress environment for 10-12 hrs per day (12-14 hrs non-stress) for three days prior to wounding, and for two-to-five days after wounding. Wounds (full-thickness biopsies) are obtained at day 0, and wound size is assessed digitally following daily photo-recording and integration of resultant of involved wound areas. Representative data are presented in Fig. 1, showing the rate of wound closure (percent of healing) vs. time after wounding, with a significant delay in wound repair for psychologically-stressed(PS) animals vs. food and water-restricted control animals.

We have obtained results with the test compounds proposed in these studies, including agonists of the nuclear hormone receptor (NHR) ligand families; i.e., PPARs and LXR agonists/ligands. Initial results (prior reported data) revealed that the treatment of animals topically (twice daily for 5 days after wounding) with the PPAR-alpha activator lead to improved wound healing vs. vehicle-treated (PGE) control animals. Repeat studies show now reveal no significant difference in wound healing repair with the topical application of the PPAR-alpha activator WY14643 immediately following wounding and during the initial wound repair period (Fig. 2).

Results with topical LXR agonist (TO) results: (Fig. 3 & 4): Similar topical treatment (as in Fig. 2) with the LXR-specific agonist (TO) resulted in a trend toward improved wound healing during psychological stress (Figs. 3 & 4), but differences did not reach statistical significance. Inter-animal variability has been an issue requiring further optimization of the wound healing/psychological stress model. In this regard, we are continuing to assess mechanisms to

reduce the variability in wound repair both between and within animals of the same grouping. A number of factors have been identified, including aggressive behavior of male (dominant) animals within groups, secondary scratch wounds to the biopsy site, as well as water restriction. We subsequently have modified the restraint housing containers to allow inclusion of gel packs (water source) during the PS period, housed mice separately following wounding, and performed PS wound repair studies using female mice. Additional experiments utilizing these modifications are being performed to further assess the effects of the LXR agonists on the psychological stress induced delay in wound healing.

To assess the role of glucocorticoids in the psychological stress induced delay in wound healing, the effects of Antalarmin (ATL) and RU486 were employed. Hairless mice were placed in stress environment, as described in Fig. 1, and treated (twice daily during initial psychological stress period, and for 2 days after wounding) with the glucocorticoid production inhibitor, Antalarmin, or the glucocorticoid receptor antagonist (RU486), or vehicle (Veh). Treatment with neither antalarmin nor RU486 resulted in inhibition of the psychological stress-induced delay in wound healing. Additional studies are ongoing using modified pretreatment regimens to further assess the mechanism by which restraint-induced psychological stress induces a delay in wound healing.

Figure 1:

Fig. 1: Psychological Stress delays wound healing in full-thickness cutaneous wounds:
Hairless mice were placed in stress environment (12 hrs per day;12 hrs non-stress) for three days
prior to wounding, and two days after wounding. Wounds (full-thickness biopsies) are obtained
at day 0, and wound size is assessed digitally following daily photo-recording of wound areas.
Representative preliminary/initial data show the rate of wound closure (percent of healing from
100% wound area) vs. time after wounding. Wound repair is delayed in stressed animals
(PS+Veh; propylene glycol:ethanol vehicle; lower/pink line) vs. non-psychologically-stressed,
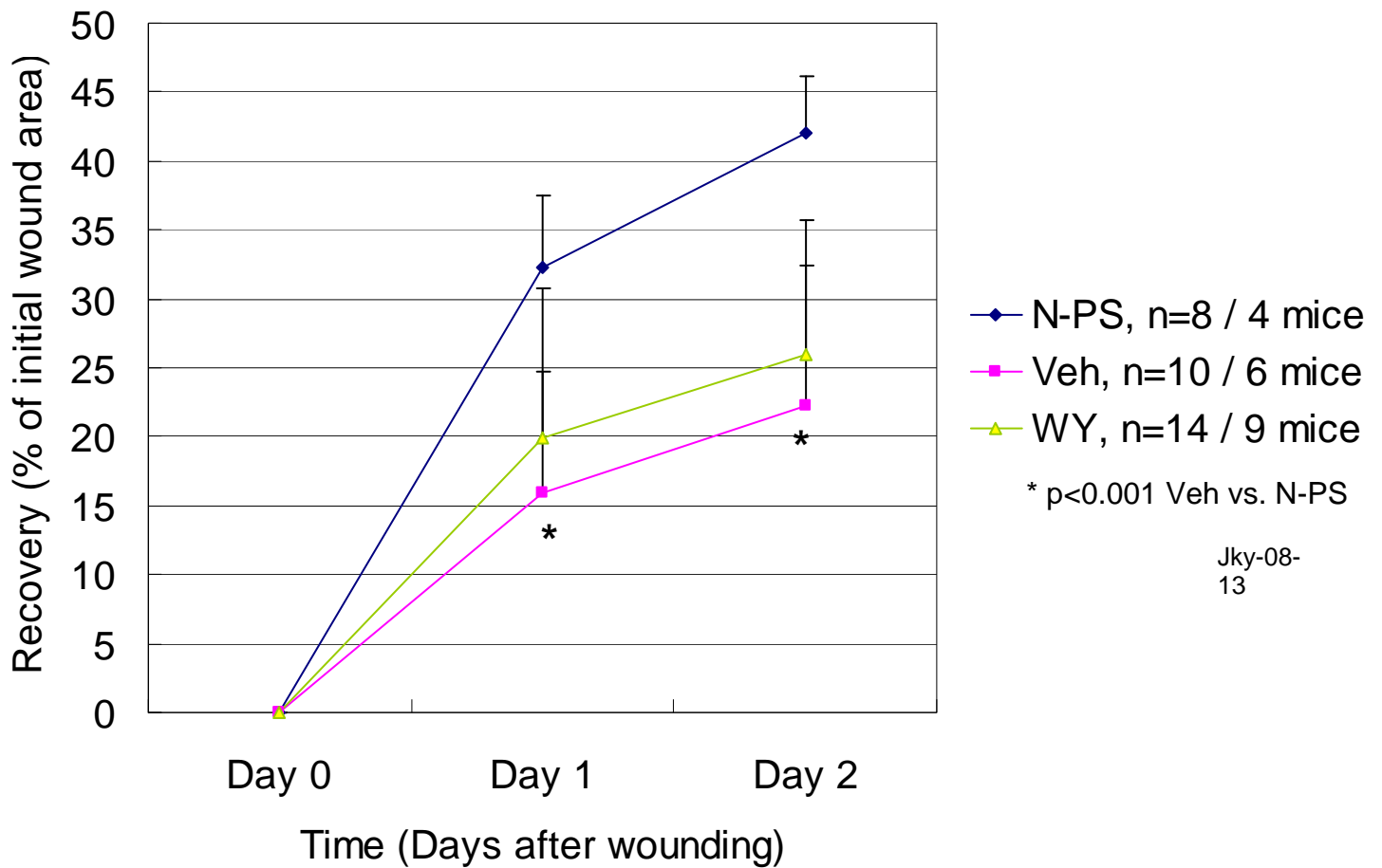food and water-restricted (N-PS Control animals; upper/blue line).

Figure 2:

Fig. 2: PPAR-alpha-specific ligand (WY) accelerates wound repair: Hairless mice were placed in stress environment, as described in Fig. 1, and treated topically (twice daily for 2 days after wounding) with the PPAR-alpha activator (WY) or vehicle (PGE) control. Treatment with PPAR-alpha agonist (WY) did not alter the rate of wound healing (middle/green line) vs. psychologically-stressed, vehicle-treated control(Veh) animals (lower/pink line); Psychologically-stressed animals (Veh) showed significantly delayed wound healing vs. Non-psychologically-stressed animals (N-PS; upper/blue line); *p<0.001.
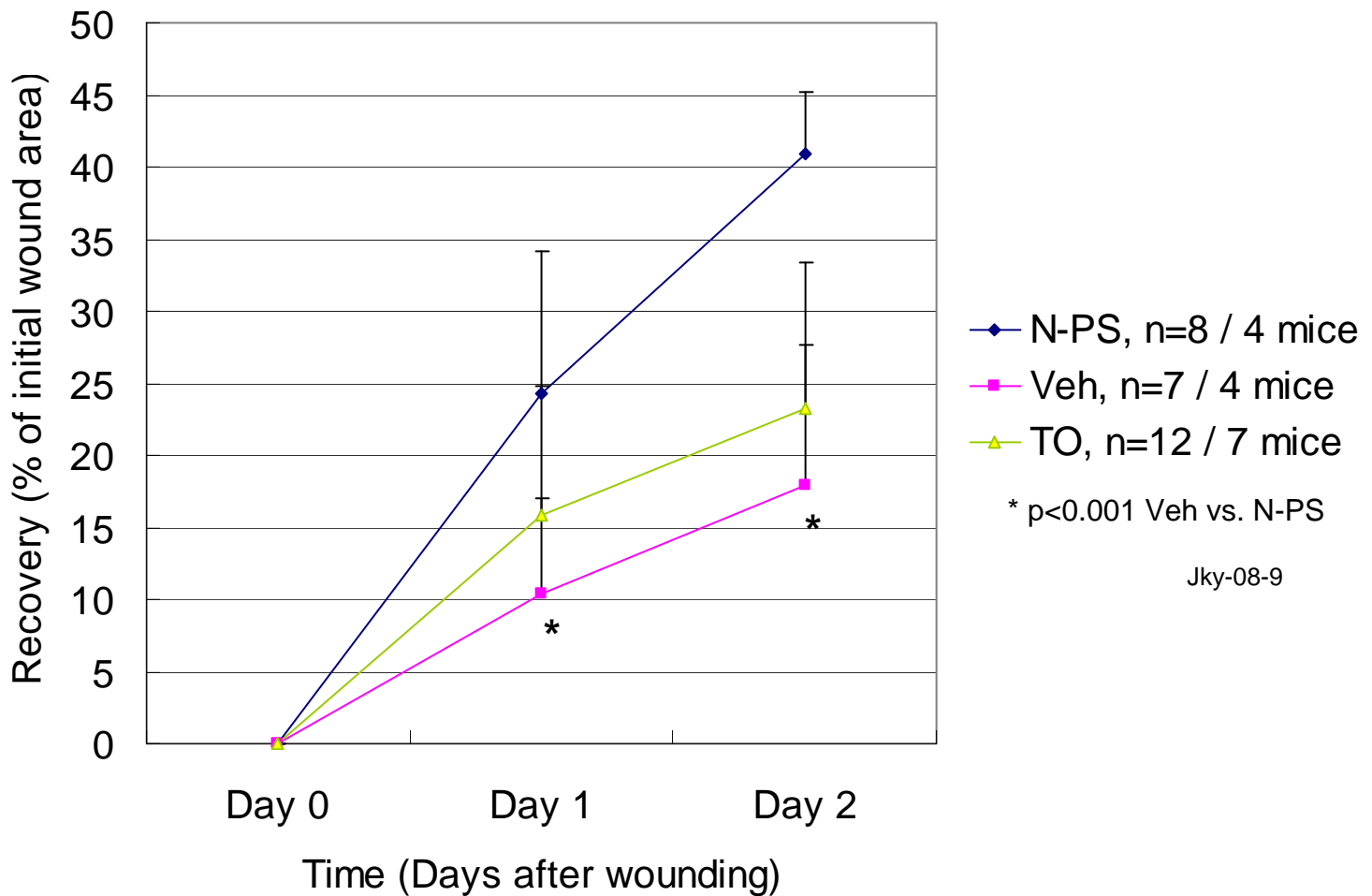
Figure 3:

Fig. 3: LXR-specific activator (TO) effect on psychologically-induced delay in wound repair: Hairless mice were placed in stress environment, as described in Fig. 1, and treated topically (twice daily for 2 days after wounding) with the LXR-specific activator (TO) or vehicle (DMSO) control. Treatment with the LXR-specific agonist (TO) showed a trend toward improved wound healing (middle/green line) relative to the appropriate psychologically-stressed, vehicle (DMSO)-treated (lower/pink line) control animals. Psychologically-stressed animals (Veh) showed significantly delayed wound healing vs. Non-psychologically-stressed animals (N-PS; upper/blue line); *p<0.001.
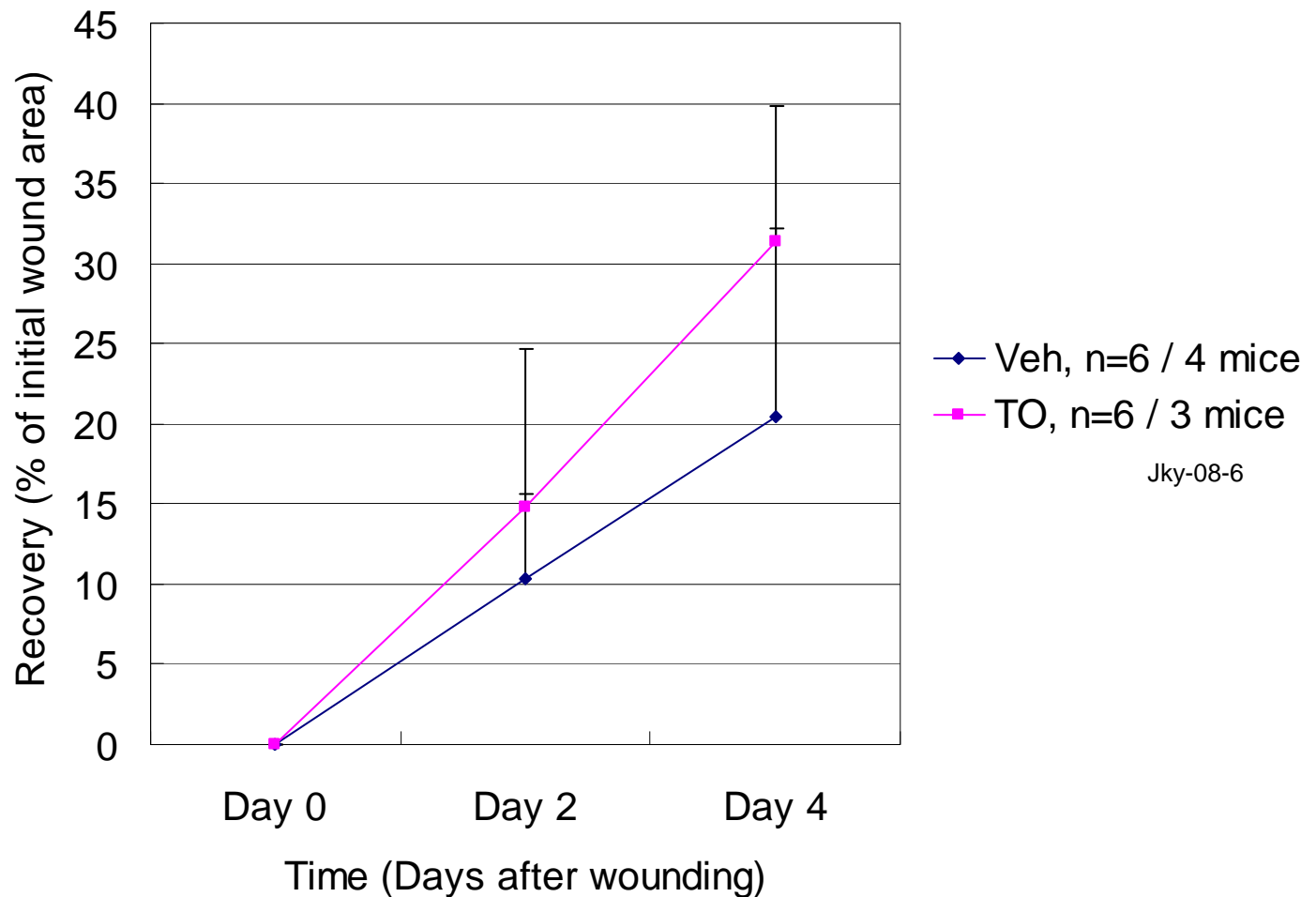
Figure 4:

Fig. 4: LXR-specific activator (TO) effect on psychologically-induced delay in wound

repair: Hairless mice were placed in stress environment, as described in Fig. 1, and treated topically (twice daily for 4 days after wounding) with the LXR-specific activator (TO) or vehicle (Veh; DMSO) control. Treatment with the LXR-specific agonist (TO) again showed a trend toward improved wound healing (upper/pink line) relative to the appropriate psychologically-stressed, vehicle (DMSO)-treated (lower/blue line) control animals, however differences were not statistically significant.
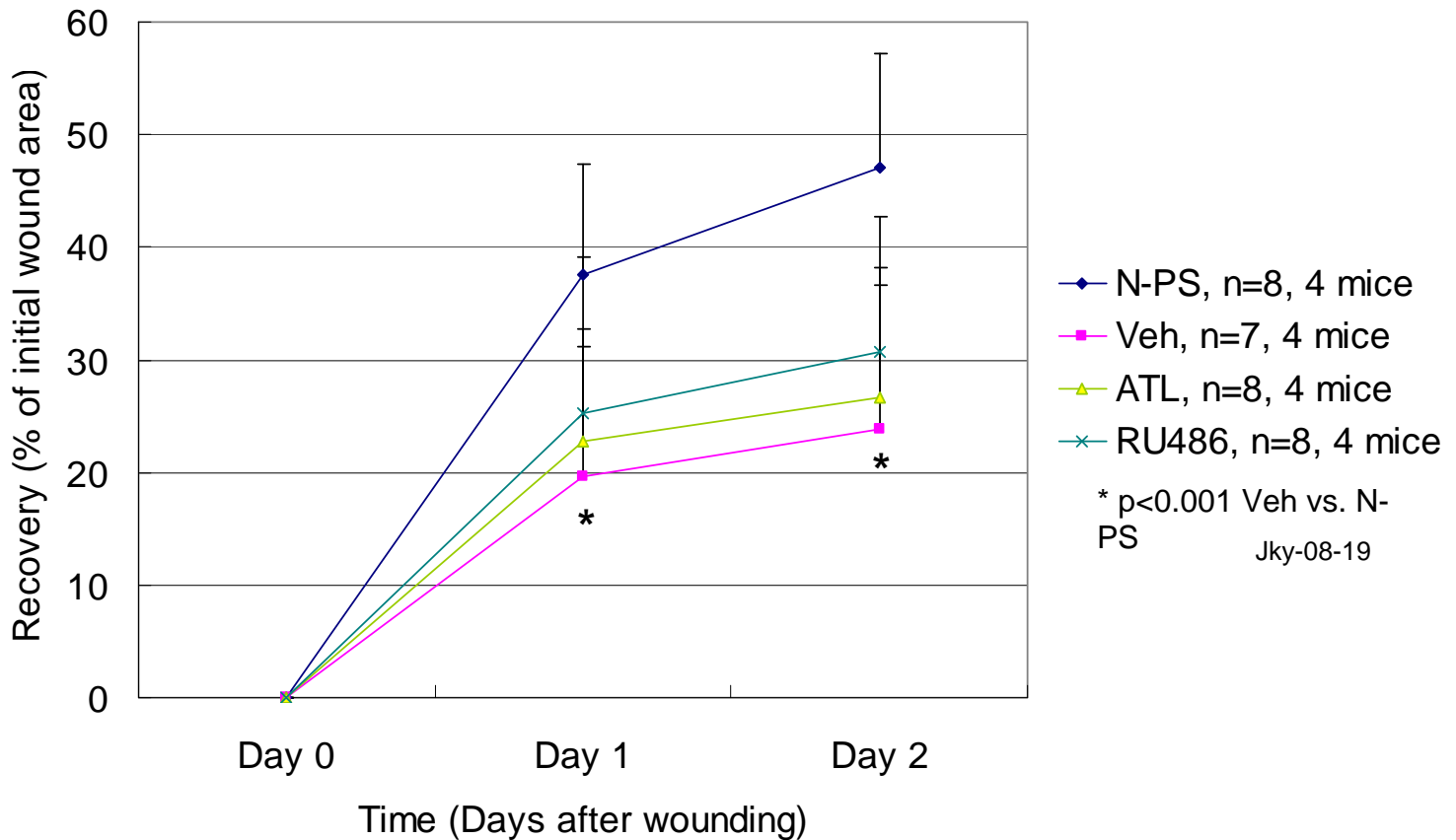
Figure 5:

Fig. 5: Effects of Antalarmin (ATL) and RU486 on Psychologically-Induced Delay in Wound Healing: Hairless mice were placed in stress environment, as described in Fig. 1, and treated topically (twice daily during and for 2 days after wounding) with the glucocorticoid production inhibitor, Antalarmin (ATL), or the glucocorticoid receptor antagonist (RU486), or vehicle (Veh). Treatment with neither antalarmin nor RU486 resulted in an inhibition of the psychological stress-induced delay in wound healing. Psychologically-stressed animals (Veh) showed significantly delayed wound healing vs. Non-psychologically-stressed animals (N-PS; upper/blue line); *p<0.001.

KEY RESEARCH ACCOMPLISHMENTS

1. Established the in vivo murine model for psychological stress, including animal husbandry conditions required to achieve the required psychological stress (PS).
2. Established the techniques required to produce the appropriate full-thickness wound (size & depth).
3. Established the techniques required to record and quantify the rate of wound healing following full-thickness wounding using a photo-based digital analysis system and requisite software.
4. Determined the rates of wound healing (WH) following full-thickness wounding in stressed and non-stressed animals.
5. Demonstrated that WH rates on the lower back of animals are distinct from the upper back area, requiring that lower back regions be excluded as study sites.
6. Demonstrated delay in WH rate in PS group animals (compared with the sham-treated control group).
7. Demonstrated that WH in the PS group is accelerated when animals are removed from the PS conditions.
8. Performed initial studies to determine the extent to which pharmacologic activators of the liposensor subclass of class II Nuclear Hormone Receptors (PPARα, PPARγ, PPARδ, and LXR) overcome PS-induced delays in WH.
9. Determined that a specific LXR agonist may improve the PS-induced delay in WH.

REPORTABLE OUTCOMES

An abstract describing these initial results will be submitted to the Society for Investigative Dermatology for presentation at the 2009 Annual Meeting of the Society for Investigative Dermatology, to be held May 6-9, 2009 in Montreal, Canada.

CONCLUSION

During this initial grant period, we have made significant progress toward the goals of this study. We have established the animal model for stress-induced delay in wound healing. In addition, initial results reveal that treatment with a PPAR-alpha activator improved/accelerated wound healing, while similar treatment with a LXR-specific agonist delayed wound healing relative to the appropriate vehicle-treated controls. These initial results strongly suggest that activators of the nuclear hormone receptors can alter wound healing under stress, with both positive and negative outcomes possible. Larger scale studies are underway to determine which of the nuclear hormone receptor agonists allows for optimal wound healing rates in this model of stress-induced wound healing.

REFERENCES
N/A

APPENDICES
N/A

SUPPORTING DATA
N/A

1) Pilot Study 6:

> **The Post-traumatic Syndrome of Blunt Head Injury: Noninvasive Neurochemical and Structural Assessment**

> **Principal Investigator: Grant Gauger, M.D.**

-- COMBINED WITH PILOT STUDY 13 --

2) Pilot Study 13:

> **High-Field Susceptibility-Weighted MRI and Volumetric Spectroscopic Imaging in Traumatic Brain Injury**

> **Principal Investigator: Wang Zhan, Ph.D.**

ABSTRACT

Blunt trauma of the human brain, occurring in the course of military operations of a wide variety, presents serious problems in assessment, treatment, and outcome prediction. Mild traumatic brain injury (TBI) is frequently followed by a clinical syndrome which is associated with serious disability, despite the absence of significant abnormalities on conventional radiologic imaging. Magnetic resonance spectroscopy has revealed changes in cerebral metabolite ratios in several sites, suggesting diffuse tissue damage. In a previous study using volumetric proton magnetic spectroscopic imaging (MRSI) at 1.5T, we have found significant changes in some brain regions for average values from all TBI subjects, with reduced N-Acetylaspartate (NAA)/Creatine (Cr), increased Choline (Cho)/Cr, and reduced NAA/Cho ratios. The results show evidence of widespread metabolic changes in regions that appear normal on diagnostic MR images. In order to clarify the extent and significance of such changes, we propose the study of a larger number of subjects, using the 4.0T system, with repeat testing at six months after injury. Moreover, the application of diffusion tensor imaging (DTI) to the study of white matter fiber systems in the brain permits an assessment of the relationship of metabolic changes in nuclear centers to the microstructural character of their connecting tracts. Data from both MRSI and DTI will be correlated with the results of neurocognitive and psychological testing. This correlation is anticipated to lead to improved understanding of the post-concussion syndrome, with early application to important decisions in the assessment and treatment of injured military personnel.

TABLE OF CONTENTS

INTRODUCTION

The purpose of this study is to determine the nature and extent of differences in metabolic measures between mild TBI patients and normal subjects, using 4 Tesla MRI imaging. Thisstudy is designed to test the hypothesis that the combination of metabolic
information, as measured with volumetric proton MRSI, and white matter connectivity, as measured by DTI, provides increased prognostic value in mild TBI, as compared to either measure alone. Furthermore, neuropsychological data will be correlated with the MRI findings to determine the underlying relationship between cognitive impairments and white matter integrity. 12 mTBI subjects and 6 normal controls are studied at 2 time points per year to evaluate post-injury changes in the brain over time.

BODY

Since the previous annual report on September 2007, 17 subjects have been recruited, and have undergone completion of the consent process at San Francisco General Hospital (SFGH). Both injured and control subjects have then completed the neurocognitive testing battery at SFGH, followed by spectroscopy, diffusion tensor imaging, and susceptibility weighted imaging at the San Francisco Veterans Affairs Medical Center (SFVAMC). A compromise of the recruiting process, caused by personnel changes at SFGH, and resulting in slowed acquisition, has been corrected by the designation of a new local coordinator.

The determination of the nature and extent of differences in metabolic measures between mild TBI patients and normal subjects, using the 4 Tesla magnet, will be accomplished upon completion of data acquisition from magnetic resonance spectroscopic study of both injured and control subjects, with repeat testing at a 6-month interval in determination of alterations of metabolic measures over time.

Voxel-based group analysis has been performed on the diffusion tensor imaging (DTI) data acquired from 14 injured subjects (Female=1, 29±7 yrs). Significant decreased fractional anisotropy (FA) ($p<0.01$) has been found in the intersection of the fornix and corpus callosum (See Fig.1, a), and in posterior cingulate cortex (b).
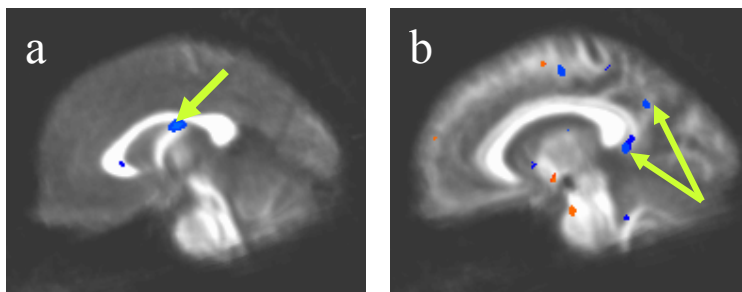

Fig.1: Reduced FA ($p<0.01$) in head injured subjects (N=13) compared with age and gender matched group.

White matter alterations in the trauma subjects have also been studied by correlation of DTI images with time after injury (7~46 days). Significant negative correlation between FA and time after injury was again found in cingulate (p<0.01), as shown in Fig.2.
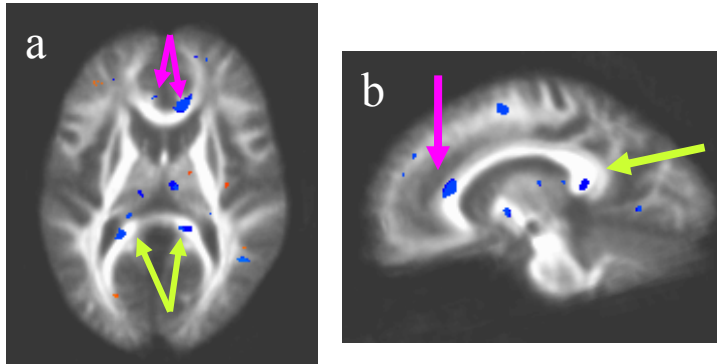

Fig.2: Negative correlation of FA with time after injury (p<0.01) in the injured subjects (N=13).

The correlation of MRSI and DTI data with neurobehavioral changes determined by the neurocognitive testing will be undertaken as soon as data acquisition and analysis permit.

KEY RESEARCH ACCOMPLISHMENTS

1. Successful and continuing advanced MR study of injured subjects and controls, and coordinated neurocognitive testing, including follow-up examinations.
2. Development of effective methodology to analyze the voxel-based diffusion tensor imaging data at group level.
3. Identification of patterns of white matter alteration in response to trauma, as demonstrated by changes in fractional anisotropy.

REPORTABLE OUTCOMES

N/A

CONCLUSION

The preliminary results of DTI investigation suggest the possibility of distinctive patterns of fractional anisotropy change in acute mild head injury subjects. We plan to perform correlation analysis with the results of both spectroscopic and neurocognitive examinations.

An improved understanding of the mechanisms of mild brain injury, including concussion and resulting impairment of cerebral function, will be dependent upon the correlation of biochemical, microstructural, and cognitive changes, and is the objective of the current study.

REFERENCES

N/A

APPENDICES

N/A

SUPPORTING DATA

N/A

Pilot Study 7:

> **Protect Dopamine Neurons from Neurotoxin-Inducted Degeneration by Targeting TGFβ Signaling**

Principal Investigator:

> **Eric J. Huang, M.D., Ph.D., Associate Professor of Pathology, UCSF & Attending Neuropathologist, San Francisco VA Medical Center**

ABSTRACT

Exposure to neurotoxins increases the risk of selective degeneration of midbrain dopamine (DA) neurons and has been postulated to be a major contributing factor to the pathogenesis of idiopathic Parkinson's disease. In addition, DA neurons have also been implicated in drug addiction and post-traumatic stress disorder. These important functions have inspired unremitting enthusiasm toward identifying neurotrophic factors that can promote the survival of midbrain DA neurons and protect them from toxin-induced degeneration. Our recent results indicate that, compared with the conventional neurotrophic factors, transforming growth factor beta (TGFβ) and its associated signaling molecules are highly potent in promoting survival of midbrain DA neurons during programmed cell death. However, it is unclear if similar mechanisms can protect DA neurons from toxin-induced injury. This research project aims to use both loss-of-function and gain-of-function approaches in a rodent model to determine if activation of TGFβ signaling protects DA neurons from neurotoxin-induced degeneration. Our long-term goal is to apply the success in this project to develop novel compounds that harness the protective effects of TGFβ signaling to prevent toxin-induced neurodegeneration during military combats and in civilian life.

TABLE OF CONTENTS

INTRODUCTION

The neural circuitries defined by the midbrain dopamine (DA) neurons control extrapyramidal movement and important cognitive functions. Perturbations to these pathways, caused by genetic mutations, neurotoxins in the environment or other unknown etiologies, have been implicated in many neuropsychiatric conditions, including Parkinson's disease, drug addiction, compulsive disorders, and possibly post-traumatic stress disorder (PTSD). Because of the important functions of DA neurons, a central goal of current research has been to identify compounds that can promote the survival of these neurons, or modulate dopamine synaptic transmission. Recent data from my lab provide strong genetic evidence that transforming growth factor beta (TGFβ) and its associated signaling molecule Smad3 and HIPK2 (homeodomain interacting protein kinase 2) are required for the survival of DA neurons during programmed cell death. Based on these results, we hypothesize that the robust neurotrophic function of TGFβ signaling pathway provides protective effects to DA neurons under the experimental paradigms of neurotoxin-induced degeneration. To test this hypothesis, we propose two specific aims to determine if (1) partial or complete loss of TGFβ signaling leads to selective vulnerability of DA neurons when exposed to neurotoxin MPTP, and (2) over-expression of HIPK2 bypasses the dependence on TGFβ and promotes the survival of DA neurons. Our goal is to achieve a thorough understanding of the TGFβ signaling pathway in protecting DA neurons from toxin-induced injury and to ultimately target this mechanism as potential therapeutic interventions for Parkinson's disease and related neurodegenerative conditions.

BODY

KEY RESEARCH ACCOMPLISHMENTS

We propose two specific aims to (1) determine if DA neurons in mice lacking one allele of $Tgf\beta3$ ($Tgf\beta3^{+/-}$) or two alleles of $Hipk2$ ($Hipk2^{-/-}$) are more susceptible to MPTP-induced toxicity, and (2) to determine if over-expression of HIPK2 using cell type-specific genetic approach could provide beneficial effects to the differentiation and survival of DA neurons in SNpc.

(1) Loss of HIPK2 leads to resistance to MPTP neurotoxicity in DA neurons
In the first Specific Aim, we injected wild type and $Hipk2^{-/-}$ mutants with PBS or MPTP (4mg/kg, daily for 10 days) and collect brain tissue to determine the number of DA neurons in SNpc and VTA. Consistent with published results, wild type mice treated with MPTP lost about 50% of DA neurons in SNpc and VTA. However, $Hipk2^{-/-}$ mutants treated with MPTP showed no further reduction in DA neurons in SNpc or VTA. These unexpected findings raised the question that loss of HIPK2 may render DA neurons more resistant to MPTP, probably due to the fact that MPTP treatment leads to constitutive activation of TGFβ signaling pathway. However, we cannot completely exclude the possibility that HIPK2-dependent DA neurons may be more sensitive to MPTP-induced cell death.

We used two approaches to further test the hypothesis that loss of HIPK2 leads to resistance to MPTP. First, we challenged wild type and $Hipk2^{-/-}$ mutants with higher dosages of MPTP treatment (e.g. 4 mg/kg, 4 times daily for 2 days) to determine if DA neurons in $Hipk2^{-/-}$ mutants remain resistant to MPTP. We reasoned that if DA neurons in both wild type and $Hipk2^{-/-}$ mutants show a similar reduction under higher dosages of MPTP, this outcome would favor the model that HIPK2-dependent DA neurons represent a subtype that is more sensitive to low dose MPTP treatment. Conversely, if DA neurons from $Hipk2^{-/-}$ mutants continue to be resistant to

high dosage of MPTP treatment, these results would favor the notion that HIPK2 may be required for MPTP-induced cell death. Our results indicated that, when exposed to a higher dose of MPTP, wild type mice showed further reduction in DA neurons. In contrast, only a smaller percentage of $Hipk2^{-/-}$ DA neurons were lost under the same treatment.

In the second approach, we examined JNK activation and c-Jun phosphorylation in DA neurons in response to MPTP treatment. Activation of JNK and c-Jun phosphorylation have been shown to be key mechanisms in activation of cell death in DA neurons following MPTP treatment. Our results indicate that both JNK phosphorylation and c-Jun phosphorylation are significantly reduced in tissue obtained from $Hipk2^{-/-}$ mutants. Taken together, these results support the notion that the increase in resistance to MPTP toxicity in the DA neurons from $Hipk2^{-/-}$ mutants may be due to the essential role of HIPK2 in the activation of JNK and c-Jun phosphorylation.

(2) Over-expression of HIPK2 increases MPTP neurotoxicity in a dose-dependent fashion

To determine if over-expression of HIPK2 influence MPTP toxicity, we established a conditional Hipk2 mutant allele (R26R^{HIPK2}) that express extra copies of HIPK2 specifically in DA neurons. Our results indicated that control mice that express one or two copies of R26R^{HIPK2} allele showed the same vulnerability to MPTP toxicity in DA neurons just like wild type mice. However, conditional mutants that express Cre recombinase in DA neurons (TH-IRES-Cre) and one or two copies of the conditional allele (TH-IRES-Cre;R26R$^{HIPK2/+}$ or TH-IRES-Cre;R26R$^{HIPK2/HIPK2}$) showed a gene dosage-dependent increase in neuron loss in substantia nigra (SNpc). These results are consistent with those from the loss of function analyses using $Hipk2^{-/-}$ mutants, and provide compelling genetic evidence that HIPK2 is a key component in the JNK signaling pathway in mediating MPTP-induced cell death in DA neurons.

To further investigate the underlying mechanism of HIPK2 in MPTP-induced cell death of DA neurons, we have began to perform a series of biochemical assays in HEK293 cells and SHSY5Y neuroblastoma cells. Our preliminary results indicate that HIPK2 interacts with JNK and activates c-Jun phosphorylation and the transcriptional activity of c-Jun.

REPORTABLE OUTCOMES

None.

CONCLUSIONS

1. Our results indicated that, when exposed to MPTP, wild type mice showed a dose-dependent reduction of DA neurons in ventral midbrain. In contrast, $Hipk2^{-/-}$ mutants showed no loss of DA neurons under low dose, chronic treatment with MPTP. Even at high dose treatment, only a smaller percentage of $Hipk2^{-/-}$ DA neurons were lost. These results are contrary to our hypothesis and support the notion that HIPK2 is required to activate cell death under MPTP treatment. Consistent with these results, both JNK phosphorylation and c-Jun phosphorylation are significantly reduced in brain tissue obtained from $Hipk2^{-/-}$ mutants.

2. Our results indicated that control mice that express one or two copies of R26R^{HIPK2} allele showed the same vulnerability to MPTP toxicity in DA neurons just like wild type mice. However, conditional mutants that express Cre recombinase in DA neurons (TH-IRES-

Cre) and one or two copies of the conditional allele (TH-IRES-Cre;R26R$^{HIPK2/+}$ or TH-IRES-Cre;R26R$^{HIPK2/HIPK2}$) showed a gene dosage-dependent increase in neuron loss in substantia nigra (SNpc). These results are consistent with those from the loss of function analyses using *Hipk2$^{-/-}$* mutants, and provide compelling genetic evidence that HIPK2 is a key component in the JNK signaling pathway in mediating MPTP-induced cell death in DA neurons.

3. To further investigate the underlying mechanism of HIPK2 in MPTP-induced cell death of DA neurons, we have began to perform a series of biochemical assays in HEK293 cells and SHSY5Y neuroblastoma cells. Our preliminary results indicate that HIPK2 interacts with JNK and activates c-Jun phosphorylation and the transcriptional activity of c-Jun. In addition, HIPK2 can also interact with ASK1 and such interaction can be induced under stress conditions.

REFERENCES
1. Bove, J., Prou, D., Perier, C. & Przedborski, S. Toxin-induced models of Parkinson's disease. NeuroRx 2, 484-94 (2005).
2. Oo, T. F., Kholodilov, N. & Burke, R. E. Regulation of natural cell death in dopaminergic neurons of the substantia nigra by striatal glial cell line-derived neurotrophic factor in vivo. J Neurosci 23, 5141-8 (2003).
3. Baquet, Z. C., Bickford, P. C. & Jones, K. R. Brain-derived neurotrophic factor is required for the establishment of the proper number of dopaminergic neurons in the substantia nigra pars compacta. J Neurosci 25, 6251-9 (2005).
4. Pu, L., Liu, Q. S. & Poo, M. M. BDNF-dependent synaptic sensitization in midbrain dopamine neurons after cocaine withdrawal. Nat Neurosci 9, 605-7 (2006).
5. Hynes, M. et al. Induction of midbrain dopaminergic neurons by Sonic hedgehog. Neuron 15, 35-44 (1995).
6. Otto, D. & Unsicker, K. Basic FGF reverses chemical and morphological deficits in the nigrostriatal system of MPTP-treated mice. J Neurosci 10, 1912-21 (1990).
7. Krieglstein, K. et al. Glial cell line-derived neurotrophic factor requires transforming growth factor-beta for exerting its full neurotrophic potential on peripheral and CNS neurons. J Neurosci 18, 9822-34 (1998).
8. Poulsen, K. T. et al. TGF beta 2 and TGF beta 3 are potent survival factors for midbrain dopaminergic neurons. Neuron 13, 1245-52 (1994).
9. Farkas, L. M., Dunker, N., Roussa, E., Unsicker, K. & Krieglstein, K. Transforming growth factor-beta(s) are essential for the development of midbrain dopaminergic neurons in vitro and in vivo. J Neurosci 23, 5178-86 (2003).
10. Krieglstein, K., Suter-Crazzolara, C., Fischer, W. H. & Unsicker, K. TGF-beta superfamily members promote survival of midbrain dopaminergic neurons and protect them against MPP+ toxicity. Embo J 14, 736-42 (1995).
11. Wiggins, A. K. et al. Interaction of Brn3a and HIPK2 mediates transcriptional repression of sensory neuron survival. J Cell Biol 167, 257-67 (2004).
12. Pho, V. et al. Essential role of HIPK2 in TGFbeta-dependent survival of midbrain dopamine neurons. (Submitted).
13. Sekito, A. et al. DJ-1 interacts with HIPK1 and affects H2O2-induced cell death. Free Radic Res 40, 155-65 (2006).

14. Rawson, J. M., Lee, M., Kennedy, E. L. & Selleck, S. B. Drosophila neuromuscular synapse assembly and function require the TGF-beta type I receptor saxophone and the transcription factor Mad. J Neurobiol 55, 134-50 (2003).

15. McCabe, B. D. et al. Highwire regulates presynaptic BMP signaling essential for synaptic growth. Neuron 41, 891-905 (2004).

16. Bezard, E., Dovero, S., Bioulac, B. & Gross, C. E. Kinetics of nigral degeneration in a chronic model of MPTP-treated mice. Neurosci Lett 234, 47-50 (1997).

17. Crocker, S. J. et al. Attenuation of MPTP-induced neurotoxicity and behavioural impairment in NSE-XIAP transgenic mice. Neurobiol Dis 12, 150-61 (2003).

18. Chytil, A., Magnuson, M. A., Wright, C. V. & Moses, H. L. Conditional inactivation of the TGF-beta type II receptor using Cre:Lox. Genesis 32, 73-5 (2002).

19. Lindeberg, J. et al. Transgenic expression of Cre recombinase from the tyrosine hydroxylase locus. Genesis 40, 67-73 (2004).

20. Soriano, P. Generalized lacZ expression with the ROSA26 Cre reporter strain. Nat Genet 21, 70-1 (1999).

APPENDICES

None.

SUPPORTING DATA
N/A

Pilot Study 8:

TLR4 Agonists as Neuroprotectants in Traumatic Brain Injury

Principal Investigator: Gary Jarvis, Ph.D.

ABSTRACT

To date more than 20,000 U.S. soldiers have been injured in the war in Iraq. The mortality from injury has declined in this war to its lowest rate ever due to greater use of body armor and advances in combat medicine [1]. The VA estimates that about 2/3s of the injuries were due to blasts from homemade bombs known as Improvised Explosive Devices (IEDs) [1, 2]. Walter Reed Army Medical Center estimates that 25% of those injured by IEDs have traumatic brain injury (TBI) [1]. Treatment of TBI focuses only on cardiopulmonary support, control of intracranial pressure and bleeding, and preventing complications [3]. A drug with few adverse side effects that could be used in the field to reduce the secondary inflammation and long-term disability due to TBI would be valuable in future conflicts, especially for blast injuries.

Overwhelming evidence shows that injury or ischemia to the brain or spinal cord causes an inflammatory response that further damages the CNS [4, 5]. Since there is a period of time before this secondary damage occurs, preventive therapeutic intervention is feasible. The administration of *E. coli* lipopolysaccharide (LPS) *before*, *during*, and even *after* injury has been shown to reduce the extent of ischemic, contusion, and other types of neuronal injury in cell culture models and in animal models of CNS injury. In particular, a recent study of *post-injury* administration of *E. coli* LPS for brain trauma reported that systemic delivery *2 hr after* injury in either of two animal models significantly reduced the inflammatory infiltration of leukocytes [6]. The activity of LPS is thought to be due to its binding to toll-like receptor 4 (TLR4), resulting in NF- B-mediated up-regulation of the expression of cytokines TNF and IFN which have been reported to be critical mediators of neuroprotection in these neuronal injury models [7]. In studies performed by our laboratory and others [8, 9], LPS from *Neisseria* induced higher levels of TNF and IFN expression in monocytic cells compared with that from *E. coli* suggesting that *Neisserial* LPS is a more potent TLR4 agonist and thus potentially a more potent neuroprotectant. In this proposal, we will test the hypothesis that administration of *Neisserial* LPS *post-injury* is beneficial for traumatic brain injury (TBI). In addition, our studies will add to our understanding of TLR4-mediated responses in the context of developing highly potent neuroprotectants. We propose two specific aims:

1) To compare the ability of *Neisserial* and *E. coli* LPS to protect cultured neuronal cells using an in vitro model of brain cell trauma with pre- and post-injury administration.
2) To determine the anti-inflammatory effect of *Neisserial* and *E. coli* LPS administered intravenously (iv) and intranasally (in) in a rat brain injury model, pre- and post-injury.

The research carried out to date over the previous two months has been aimed towards the first stated Specific Aim. Rodent C6 glial cell cultures have been utilized while primary neuronal cortical cultures are being established. The work carried out on the C6 cells has shown that the mechanical scratch injury method does indeed result in increased lactate dehydrodgenase being released into the culture media due to cell injury and subsequent death. Eight vertical scratches combined with 8 horizontal scratches produces a robust effect which can be adequately measured using a LDH cytotoxic assay. Incubation of the C6 culture cell with meningococcal strain 89I LPS at a concentration of 100ng/ml in both the presence and absence of the scratch injury has been shown to result in reduced LDH release from the cells, which is indicative of a reduction in death and injury in the LPS-treated cells as hypothesized.

TABLE OF CONTENTS

INTRODUCTION

Traumatic brain injury is a serious medical issue that 1-2 million people suffer from in the US each year with 70-90,000 sustaining a long-term disability with very high socio-economic costs [4]. Annually approximately 50,000 people in the U.S. die from TBI [3]. This number does not include military personnel who have been injured in the Iraq war, to date more than 20,000 U.S. soldiers have been injured. The VA has estimated that approximately 2/3s of these injuries were due to blasts from homemade bombs known as Improvised Explosive Devices (IEDs) [1, 2]. Walter Reed Army Medical Center estimates that 25% of those injured by IEDs have suffered a TBI [1]. Current treatment of traumatic brain injury (TBI) focuses on supporting vital functions and controlling intracranial pressure. Thus, there is a great need for new efficacious treatments. Injury to the brain or spinal cord causes an inflammatory response known as secondary damage that further damages the CNS.

Administration of *E. coli* lipopolysaccharide (LPS) *before*, *during*, and even *after* injury has been shown to reduce the extent of ischemic, contusion, and other types of neuronal injury in both cell culture and animal models of CNS injury. For treatment of trauma, administration of an agent *after the injury* to reduce the secondary damage is the most clinically relevant approach. In a study of post-injury administration of LPS, the systemic delivery of LPS either *2 hr after* contusion injury in a rat model of spinal cord injury or *2 hr after* injection of the brain injury-associated cytokine IL-1 into the brain of rats significantly reduced inflammatory leukocyte infiltration [6]. We have previously shown that *Neisserial* LPSs from various strains differ in their ability to induce production of inflammatory cytokines by human monocytic THP-1 cells [10], and are at present currently studying the structure/function relationships underlying this observation. In this current proposal, we will test the hypothesis that *post-injury* administration of *Neisserial* LPS is beneficial for TBI using both a cell culture and an animal model of trauma. Two specific aims are proposed:

1)   To compare the ability of *Neisserial* and *E. coli* LPS to protect cultured neuronal cells using an in vitro model of brain cell trauma with pre- and post-injury administration.
2)   To determine the anti-inflammatory effect of *Neisserial* and *E. coli* LPS administered intravenously (iv) and intranasally (in) in a rat brain injury model

BODY

Research for this grant commenced in July of 2008. The first Specific Aim set out in the proposal involved investigating and comparing the effect of different LPS on cultured neuronal cultures. Since generating primary neuronal cultures is a time-consuming and lengthy process, it was decided to initiated the development of the scratch injury model (inducing mechanical trauma to the cultures) using a neuronal cell line. To this end, rat C6 glioma cells were chosen and the cells were cultured in 6 well plates where they were grown to confluency. In order to assess the cytotoxic effect of the mechanical trauma, different numbers of scratches were made in each well ranging from 0 (negative control) up to 8 scratches in both horizontal and vertical directions before media was replaced and the cells left for a further 24 hours. In addition to investigating the cytotoxic effect on the cells of the scratching, we also investigated the effect of the media in which the cells were cultured for 24 hours. Serum in the media, which helps maintain healthy cell cultures, is known to contain innate lactate dehydrodgenase (LDH). The assay which we opted to use to determine the cytotoxic effect induced by the scratch method measures the amount of LDH released from cells during the process of cell death. Therefore, it

was imperative that the media in which the cells were cultured for the 24-hour time-period following scratch injury had as low of a background LDH level as possible. The basic media used to culture the cells was supplemented with different levels of sera (basic media alone was not sufficient to maintain healthy cells for a 24hr time period). The media was enhanced with either 1% Horse serum, 1% Fetal Bovine serum or with 1% both Horse and Fetal Bovine sera. The results from these experiments are shown in Figures 1 and 2.

Figure 1

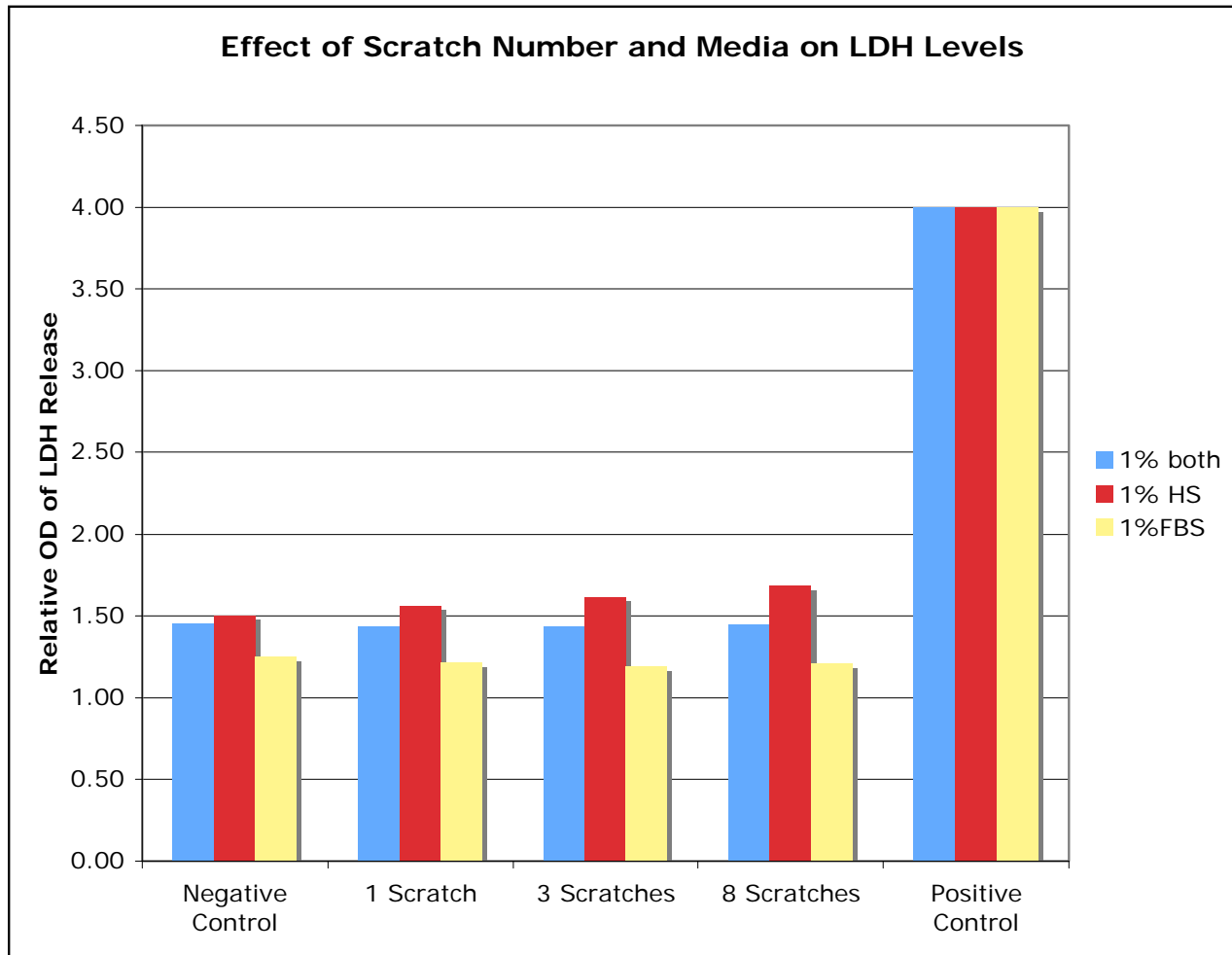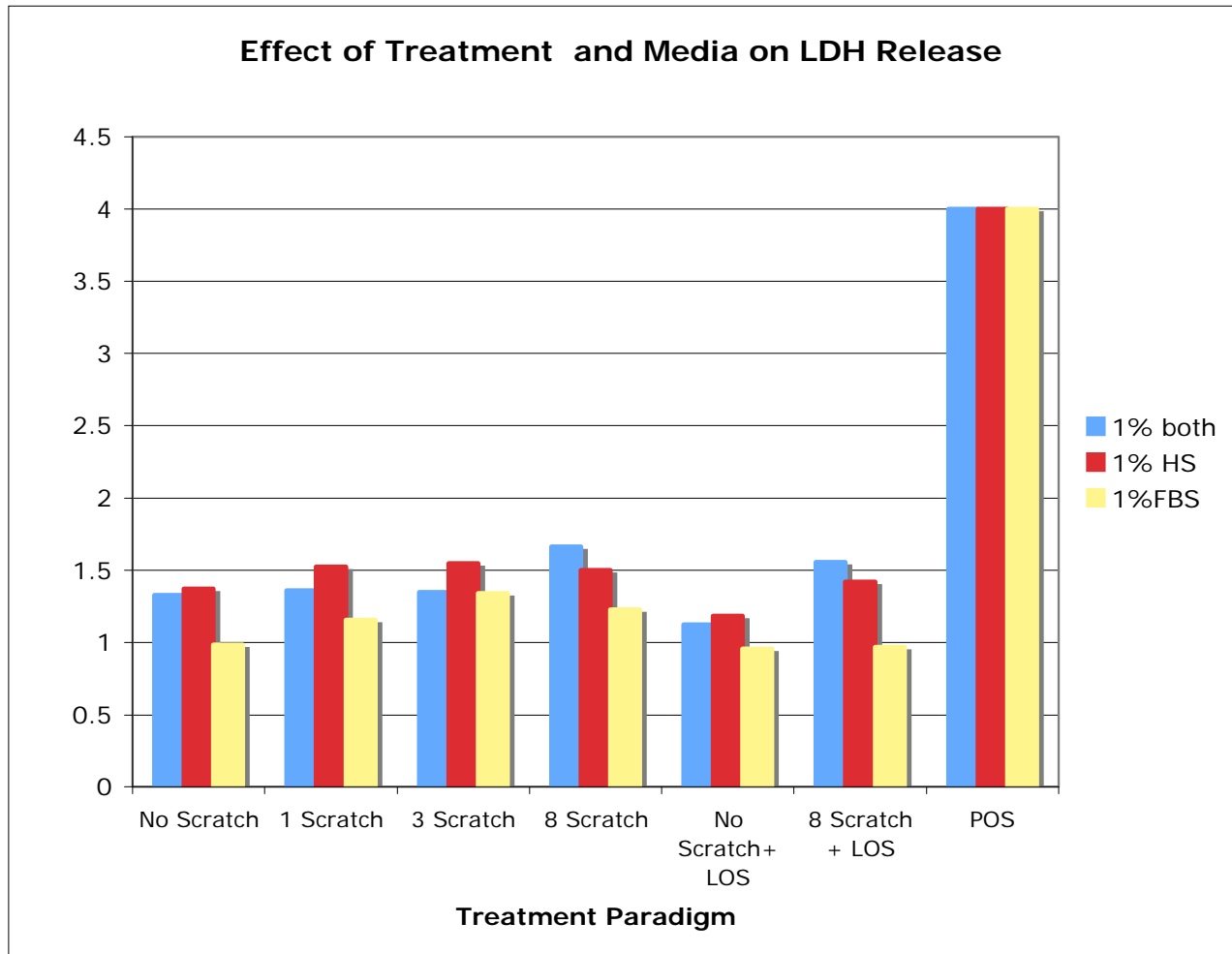**Effect of Scratch Number and Media on LDH Levels**

Figure 2

Note that the media which showed the least LDH reactivity in the negative control samples is the media containing 1%FBS. Regarding the effect of the scratch method on cytotoxicity, it was determined that the wells containing 8 horizontal and 8 vertical scratches resulted in the most reproducible injury as judged by increased LDH release.

The successful development of the rat C6 glioma cell culture model allowed us to begin work on Specific Aim 1 as proposed. Testing of the effect of LPS on cell viability following injury begin with treatment of confluent C6 cells with 100ng/ml of 89I LPS. The effect of the LPS was investigated both in cells not injured by scratching (negative control) as well as in scratched (injured) cells. The preliminary results of these on-going studies are shown in Figure 3.
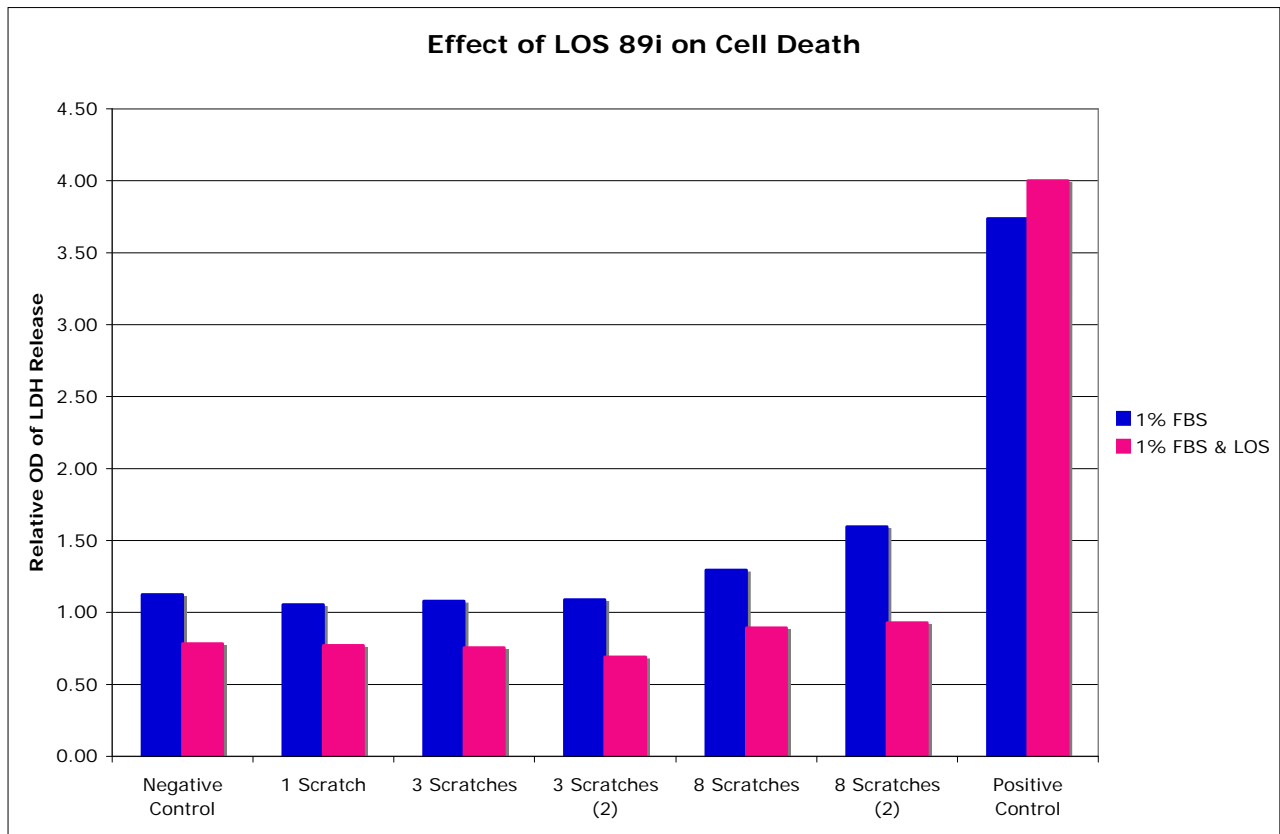
Figure 3

Effect of LOS 89i on Cell Death

Figure 3 demonstrates that treatment of C6 glioma cells with 89I LPS results in protection of the cells from normal cell death mechanisms as we found significantly less cell death in treated versus untreated cells. This neuroprotection was even more pronounced following cell injury, where it was found that cultures incubated with 89I LPS showed a significantly lower level of LDH in the media compared to non-LOS treated cells after being subjected to the scratch injury model of mechanical trauma.

The graphs all shown above are each representative of an n of 1. Therefore it is not currently possible to complete statistical analysis on these data sets. Due to these promising results more experiments are being carried out to increase the n number.

The primary neuronal cell culture work has also commenced and the technique used has proven to be successful to date, with work investigating the different effects of the LPSs on cell injury to begin in the next few weeks.

KEY RESEARCH ACCOMPLISHMENTS

- Established two rodent cell lines for use for the *in-vitro* research (C6 rat glioma cells and primary neuronal cortical cultures) as well as established the scratch injury model used to mimic traumatic brain injury in cell cultures.

- Set up the Lactate Dehydrodgenase Assay used to determine cytotoxic cell death.

- Determined that 89I LPS is neuroprotective against cellular death following scratch injury of C6 rat glioma cells.

REPORTABLE OUTCOMES

The reportable outcomes from the work which commenced in July 2008 are:

- Establishment of both the Rat Glioma C6 cell line as well as successful culture of rodent primary neuronal cultures from postnatal 1-day-old rat pups.

CONCLUSIONS

The research that has been carried out in our laboratory shows that when 89I LPS at a dose of 100ng/ml is administered to injured as well as non-injured C6 rat glioma cell cultures there is a significant reduction in lactate dehydrogenase released from the cells into the media. This suggests that the LPS is acting as a neuroprotectant in this rat glioma culture model. This was hypothesized by our laboratory and was part of our first Specific Aim. The next stage in the research is to determine the effect of the other LPS's (as stated in the proposal) on cytotoxic cell death in both the C6 rat glioma cell line and in primary rodent cortical neurons. Successful culture of the primary neurons has occurred and the cell line is currently being investigated.

REFERENCES

1. *The neurological burden of the war in Iraq and Afghanistan.* Ann Neurol, 2006. **60**(4): p. A13-5.
2. Warden, D., *Military TBI during the Iraq and Afghanistan wars.* J Head Trauma Rehabil, 2006. **21**(5): p. 398-402.
3. Chua, K.S., Y.S. Ng, S.G. Yap, and C.W. Bok, *A brief review of traumatic brain injury rehabilitation.* Ann Acad Med Singapore, 2007. **36**(1): p. 31-42.
4. Lenzlinger, P.M., M.C. Morganti-Kossmann, H.L. Laurer, and T.K. McIntosh, *The duality of the inflammatory response to traumatic brain injury.* Mol Neurobiol, 2001. **24**(1-3): p. 169-81.
5. Beattie, M.S., *Inflammation and apoptosis: linked therapeutic targets in spinal cord injury.* Trends Mol Med, 2004. **10**(12): p. 580-3.
6. Davis, A.E., S.J. Campbell, P. Wilainam, and D.C. Anthony, *Post-conditioning with lipopolysaccharide reduces the inflammatory infiltrate to the injured brain and spinal cord: a potential neuroprotective treatment.* Eur J Neurosci, 2005. **22**(10): p. 2441-50.

7. Stevens, S.L. and M.P. Stenzel-Poore, *Toll-like receptors and tolerance to ischaemic injury in the brain.* Biochem Soc Trans, 2006. **34**(Pt 6): p. 1352-5.

8. Zughaier, S.M., Y.L. Tzeng, S.M. Zimmer, A. Datta, R.W. Carlson, and D.S. Stephens, *Neisseria meningitidis lipooligosaccharide structure-dependent activation of the macrophage CD14/Toll-like receptor 4 pathway.* Infect Immun, 2004. **72**(1): p. 371-80.

9. Patrone, J.B. and D.C. Stein, *Effect of gonococcal lipooligosaccharide variation on human monocytic cytokine profile.* BMC Microbiol, 2007. **7**: p. 7.

10. Pridmore, A.C., G.A. Jarvis, C.M. John, D.L. Jack, S.K. Dower, and R.C. Read, *Activation of toll-like receptor 2 (TLR2) and TLR4/MD2 by Neisseria is independent of capsule and lipooligosaccharide (LOS) sialylation but varies widely among LOS from different strains.* Infect Immun, 2003. **71**(7): p. 3901-8.

APPENDICES

Primary Researcher Resume
Deborah Bingham PhD

9 Castro Street   Phone 415 828 7917
San Francisco   Email: **debsbingham@yahoo.com**
CA 94114
USA

Research and Professional Experience

2008- Present Staff Research Associate III, Northern Californian Institute for Research and Education, San Francisco Veterans Affair Medical Center, 4150 Clement Street, San Francisco CA 94121.

Current research involves determining the effect of intranasal lipooligosaccharides on traumatic brain injury (TBI) models, investigating both in vitro (injured primary cortical neuron cell cultures) as well as in vivo (stereotaxic injection of IL-1 into rodent brains) TBI models.

2007-2008 **Staff Research Associate III,** Northern Californian Institute for Research and Education, San Francisco Veterans Affair Medical Center, 4150 Clement Street, San Francisco CA 94121.

Research involved determining the effect of intranasal peptides as well as insecticides on rodent behavior. The behavioral monitoring system involved using telemetric cages and/or running wheels. Studies determined a significant increase in wheel turning behavior within 3 hours of intranasal Ouabain administration.

2005 - 2007 **Postdoctoral Research Fellow**, Ernest Gallo Clinic and Research Center, Emeryville, California, USA & Department of Neurology, University of California San Francisco, USA.

My research focused primarily on the influence of ethanol on the Ras pathway *in-vivo* and *in-vitro* in the striatum and cortex, with the long-term goal of determining the effect of disrupting the Ras pathway in an animal model of addiction.

Academic Qualifications

2000 – 2005   PhD, University of Glasgow, Glasgow, Scotland, UK
Supervisors Professor I.M. Macrae and Dr H.V.O. Carswell
Thesis Title: **The Influence of Estrogen on Ischemic Brain Damage.**

During my PhD I used an *in-vivo* experimental model of stroke in rats to investigate the effect of estrogen replacement therapy on ischemia. Contrary to current experimental results I showed a dose dependent increase in brain damage with estrogen replacement therapy. I subsequently investigated the mechanisms responsible involved in increased brain damage and the influence of ischemia on the animal's cognitive skills. The latter study was in collaboration with Prof. Richard Morris and Dr. Steven Martin from the University of Edinburgh. I presented my results at domestic and international meetings, submitted annual internal progress reports and attended postgraduate training courses.

1996-2000   BSc (Hons), University of Strathclyde, Glasgow, Scotland, UK
Supervisors: Dr D. Rotondo and Professor R. Plevin
Dissertation Title: The effect of verotoxin from *Escherichia Coli 0157:H7* on stress activated protein kinases.

Current Research Interests

o   Understand pathophysiology of neurodegenerative diseases
o   Investigate molecular and cellular mechanisms of neurodegeneration
o   Developing therapeutic and preventative treatments for such conditions

Awards

June 2005: Travel Award: For travel and poster presentation at the Brain '05 conference.
April 2002: William Ramsey Henderson Trust Traveling Scholarship: Awarded to enable travel to another neuroscience Institute to learn new techniques.
June 2000: BSc Immunology Class Award: Class award for highest marks in BSc undergraduate class.

Research Techniques and Skills

o   Intricate animal surgery e.g. highly reproducible model of stroke in rodents and stereotaxic surgery.
o   Intranasal dosing.
o   Quantitative histopathology and immunohistochemistry.
o   Microscopy and image analysis.
o   Brain Dissection, Western Blotting and immunoprecipitation.
o   Lipid raft isolation.
o   Radioligand Binding.

o Memory testing in rodents using the Morris water maze.
o Solid phase kinase assays and 17 -oestradiol radioimmunoassay.
o ELISA.
o Cell culture.
o Primary neuron cell culture.
o Assisted supervision of an undergraduate student (2003-2004).
o Provided technical advice and support to PhD students and technicians.
o Computer literate.

Publications

Bingham D., Macrae I.M. and Carswell H.V.O. Detrimental effects of 17 -oestradiol after permanent middle cerebral artery occlusion. Journal of Cerebral Blood Flow and Metabolism, 25(3): p414-420.

Carswell H.V.O., **Bingham D**., Wallace K., Nilsen M., Graham D.I., Dominiczak A.F. and Macrae I.M. Differential effects of 17 -oestradiol upon stroke prone and normotensive rats. Journal of Cerebral Blood Flow and Metabolism, (2004), 24 (3): p298-304.

Cameron P., **Bingham D**., Paul A., Pavelka M., Cameron S., Rotondo D. and Plevin R. Essential role for verotoxin in sustained stress-activated protein kinase and nuclear factor kappa B signaling, stimulated by *Escherichia coli 0157:H7* in Vero cells. Infection and Immunity, (2002), 70 (10), p5370-5380.

Bingham D., Martin S. J., Macrae I. M., Morris R. G. and Carswell H.V.O. Memory Acquisition and Retention Following Middle Cerebral Artery Occlusion in Rodents. Manuscript in preparation.
Selected Conference Presentation Abstracts

Bingham D., Martin S.J., Macrae I.M., Morris R.G.M and Carswell H.V.O. (2005) Unilateral Proximal Occlusion of the Middle Cerebral Artery has no Effect on Acquisition or retention of Spatial Memory. Brain '05, Abstract 601.

Bingham D., Macrae I.M. and Carswell H.V.O. (2002) Estrogen exacerbates brain damage after proximal occlusion of the middle cerebral artery in the rat. Society for Neuroscience, Abstract program 392.4.

SUPPORTING DATA
N/A

Pilot Study 9:

> **Biomimetic Scaffolds with Aligned Nanofibers for the Treatment of Segmental Nerve Injuries**

Principle Investigator: Hubert Kim, M.D., Ph.D.

ABSTRACT

A majority of combat related injuries involve penetrating trauma to the extremities (Patel el al, Ramalingam 2004). These injuries are frequently associated with peripheral nerve damage and segmental loss of neural tissue. At present, the best available treatment for segmental peripheral nerve injuries is nerve autografting. However, in the setting of battlefield injuries, sufficient nerve grafts may not be available. This surgical procedure is also associated with substantial donor site morbidity, and inconsistent clinical results. Biodegradable polymers can be useful scaffold materials for tissue repair and regeneration, and there is growing interest in their use for the treatment of nerve injuries. However, polymer scaffolds alone do not provide an acceptable environment for nerve repair and regeneration. The optimal environment also requires the presence of mechanical and chemical signals that direct and enhance neurite extension across the gap (Stoll et al. 1999). We hypothesized that combining aligned nanofiber scaffolds with adhesion and growth factors can provide a superior conduit for nerve repair and regeneration. To test this hypothesis, we synthesized electrospun biodegradable polymer nanofibers that mimic normal extracellular matrix (ECM) structure. We first tested the effect of nerve growth factor (NGF), Arg-Gly-Asp (RGD) peptides and other neurotropic factors on neurite growth of dorsal root ganglion explanted onto nanofiber scaffolds. The DRGs cultured on aligned nanofiber scaffolds had significantly longer neurite growth than those cultured on non-aligned nanofiber scaffolds. We also found that neurite outgrowth of DRGs was greatly enhanced by soluble NGF on aligned nanofiber scaffold. The effect of RGD was tested using fibronectin, an RGD peptide containing ECM protein. Fibronectin was found to be a potent promoter of neurite growth on nanofiber scaffolds, which is significant when considering that no other factor tested had activity close to NGF. These data validate the hypothesis that NGF and RGD both promote significantly enhanced neurite outgrowth on aligned nanofiber scaffolds, and lay the foundation for in vivo studies planned for year 2. In year 2, these conduits will be tested in a rat segmental sciatic nerve injury model and evaluated for their ability to enhance nerve repair/regeneration. If successful, this technology would provide a superior alternative to conventional nerve autografts for bridging peripheral nerve defects.

TABLE OF CONTENTS

INTRODUCTION

At present, the best available treatment for segmental peripheral nerve injuries is nerve autografting. Major problems with this surgical technique include limited graft availability, donor site morbidity, and inconsistent clinical results. Biodegradable polymers can be useful scaffold materials for tissue repair and regeneration, and there is growing interest in their use for the treatment of nerve injuries. However, polymer scaffolds alone do not provide an acceptable environment for nerve repair and regeneration. The optimal environment also requires the presence of mechanical and chemical signals that direct and enhance neurite extension across the gap (Stoll et al. 1999). We hypothesize that combining aligned nanofiber scaffolds with adhesion and growth factors can produce a superior conduit for nerve repair and regeneration. To test this hypothesis, we will synthesize electrospun biodegradable polymer nanofibers that mimic normal extracellular matrix (ECM) structure. Arg-Gly-Asp (RGD) peptides and nerve growth factor (NGF) will then be coupled to the nanofiber scaffold. We propose to test two specific hypotheses:

1. Biomimetic scaffolds will enhance Schwann cell function and dorsal root ganglion (DRG) axon outgrowth *in vitro*.
2. Biomimetic scaffolds will improve nerve repair and regeneration *in vivo*.

BODY

E.0. Procedures Common to Specific Aims 1 and 2

E.0.1 Fabrication of Scaffolds with Aligned Nanofibers

As previously described in our proposal, biodegradable polylactic acid (PLA; 20,000 Da-600,000 Da) was used to fabricate nanofibrous scaffolds by multiple-jet electrospinning technology (Zong et al., 2002). The voltage, flow rate and polymer concentration was modulated to control the deposition and formation of the electrospun polymer scaffold. Nanofibers were selectively oriented in either random (non-aligned) or longitudinal (aligned) direction. Longitudinal alignment was achieved by stretching the electrospun scaffolds at 60 ºC with a modified Instron 4400 tensile stretching apparatus, to yield a stretch ratio of 200%.

To endow bioactivity to the surface of nanofiber scaffolds, we had proposed to create a covalent bond between the carboxylic group on the PLA chains and the primary amine group of RGD peptide or at the N-terminus of the NGF using carbodiimide chemistry. Just recently, we successfully synthesized scaffolds with covalently bound RGD and have begun experiments with these scaffolds. In order to test bioactivity of RGD on the scaffolds in the interim period, we coated nanofiber scaffolds with fibronectin, an ECM protein that uses the RGD tripeptide to interact with integrins. Due to technical difficulties in covalent conjugation of NGF to the PLA chains, we are currently exploring alternative methods of immobilization of NGF. NGFs are known to possess low affinity binding to heparin, thus we fabricated heparin-bound nanofibers to immobilize NGF. This strategy has been successfully used to immobilize other bioactive factors such as FGFs and laminin (Patel et al., 2007).

E.1. Specific Aim 1: To test the hypothesis that biomimetic scaffolds will enhance Schwann cell function and dorsal root ganglia (DRG) axon outgrowth *in vitro*.

E1.1-3. Effects of Biomimetic Nanofiber Scaffolds on Schwann Cell and DRG Axon Growth

Doral root ganglia explants were harvested from CD-1 mouse pups (P5) and cultured on nanofiber scaffolds for three days. The previously proposed culture period of five days was reduced to three days after determining that the magnitude of growth after three days in culture was sufficient for analysis. DRG explants were cultured in basic media plus NGF, Fibronectin or heparin-activated scaffold surface and combinations of the previous treatments. Neurite growths from 15 to 20 DRG explants were tested for each treatment group. The degree of neurite outgrowth was quantified by a morphometric analysis of DRG cultures after staining with (1:100) Alexa Fluor Phalloidin-488. The originally proposed visualization method of neurofilament immunostaining was switched to Phalloidin-488 for its higher fluorescence signal after confirming its co-localization with neurofilament-H and neurofilament-M immunostaining (supplement fig. 1). Images were captured at 2.5x at 12-megapixel resolution (Zeiss). The amount of neurite growth was measured from the edge of the DRG (to control for variations in DRG size) to the edge of the longest axon in pixels using Photoshop (Adobe, CA). Measurements in pixels were converted to micrometers, and expressed as mean ±sem. Statistical significance of the values of different treatments was determined by two-tailed unpaired Student's *t* test.

The effect of nanofiber orientation on DRG neurite growth was first tested. These particular experiments were done on E14.5 DRGs before the harvesting techniques for pup DRGs were mastered. We found that embryonic DRGs are highly dependent on NGF for survival and growth, as embryonic DRGs grown without any NGF had minimal neurite growth(supplement Fig. 2). Neurite growth on random versus aligned nanofiber scaffolds were compared at two sets of NGF concentrations (5 ng/ml and 10 ng/ml). DRGs cultured on aligned nanofibers exhibited bipolar neurite extensions with parallel alignment to the nanofibers that closely resembled neurite outgrowth from DRG tissue *in vivo*. In contrast, DRGs grown on random nanofibers had unorganized neurite extensions that radiated in all directions from the DRG tissues (Fig. 1A, 1B). The DRGs cultured on aligned nanofiber scaffolds also had significantly longer neurite growth than those cultured on non-aligned nanofiber scaffolds by an average increase of 27.3% in 5 ng/ml of NGF and 26.7% in 10 ng/ml of NGF ($p<0.05$). Notably, neurite growth on aligned scaffolds in 5ng/ml of NGF was longer than neurite growth on non-aligned nanofiber in 10 ng/ml of NGF by an average increase of 13.5% (Fig. 1C **, $p<0.05$). Co-staining experiments verified that Schwann cell migration mirrored neurite outgrowth results (supplement fig. 1). The differences in length of growth measured in these conditions were all statistically significant. These data indicate that compared to non-aligned nanofiber scaffolds, aligned nanofiber scaffolds not only provide directional guidance to growing neurites but also support marked enhancement of neurite outgrowth.

We then characterized neurite outgrowth of P5 DRGs in response to increasing doses of soluble NGF on aligned nanofiber scaffolds. A clear dose response of neurite growth to NGF was observed (Fig. 2). DRGs cultured in basic media in the absence of NGF had an average neurite outgrowth of 666.35μm ±57.85. In presence of 1 ng/ml of NGF, neurite growth was

increased to 935.18 μm ±60.34, with statistically significant increases in growth up to 1284.12 μm ±59.88 at 10 ng/ml of NGF (Fig. 2).

To further probe the effects of growth factors on DRG neurite outgrowth, we tested whether or not the presence of another potential neurotrophic factor with NGF yields an additive effect on neurite outgrowth. The growth factors tested were Neurotrophin-3 (NT-3; Chemicon, CA), Neurotrophin-4 (NT-4; Chemicon, CA), Brain-derived Neurotrophic Factor (BDNF; Abcam Inc., MA), Acidic Fibroblast Growth Factor (Fgf-1; PeproTech, NJ) and Basic Fibroblast Growth Factor (FGF-2; Biosource, CA). Results showed only a marginal increase of 11.2% in neurite growth upon addition of 0.5 μg/ml of BDNF (Fig. 3, $p<0.05$). No statistically significant increases in neurite outgrowth were detected upon addition of other growth factors (Fig. 3, $p<0.05$). Our findings are in agreement with recent studies on the neurotrophic effect of NGF (Kapur et al. 2004), and have shown for the first time that NGF can be a potent promoter of neurite growth on PLA nanofiber scaffolds.

To determine the effect of fibronectin on DRG neurite outgrowth, fibronectin (Sigma, MO) from mouse plasma was coated onto aligned nanofiber scaffolds at four different concentrations (0.05, 0.5, 5.0 and 50 μg/ml). P5 DRGs were cultured on coated scaffolds in media containing 1 ng/ml of NGF. A clear dose response of neurite growth to fibronectin was observed (Fig. 4, $p<0.05$). Neurite growth on fibronectin-coated aligned scaffolds was significantly higher than on uncoated aligned scaffolds. Neurite growth was increased by 20.8% at 0.05μg/ml of fibronectin, 33.0 % at 5.0 μg/ml and 57.1% at 50 μg/ml of fibronectin (Fig. 4, $p<0.05$). Notably, neurite growth on even low concentrations of fibronectin-coated scaffolds showed equivalent or greater growth as compared to uncoated scaffolds with high NGF concentrations (Fig. 4). This observation suggests that fibronectin is a potent promoter of neurite growth, which is significant when considering that no other factor tested had activity close to NGF. We postulate that the enhanced neurite extensions were promoted by integrin-fibronectin (FN) interactions through the integrin-binding site that consists of RGD (Kokkoli et al, 2008). We will next test the specific effects of RGD-conjugated nanofiber scaffolds on neurite growth rate.

As previously described, heparin-conjugated nanofiber scaffolds were initially tested as an alternative approach to immobilize biochemical cues onto the scaffold surface. We tested whether heparin-conjugated aligned nanofibers can bind and immobilize NGF and promote greater neurite growth as compared to plain aligned nanofibers. Heparin (Sigma, MO) molecules were covalently attached to the free amines of the di-NH2-PEG molecules on PLA nanofibers via EDC and sulfo-NHS. Any remaining reactive sites on the nanofibrous scaffolds were blocked by incubating the samples in 10 % w/v glycine in phosphate-buffered solution (PBS). Then, both heparin-conjugated nanofiber membranes and plain-aligned nanofiber membranes were incubated with NGF to allow for binding. Membranes were lightly washed in PBS solution and P5 DRGs were explanted.

Results showed that heparin-conjugated nanofibers do not provide superior neurite growth as compared to plain-aligned nanofibers when pre-incubated with the same dose of NGF. Both heparin-conjugated nanofibers and unconjugated nanofibers supported similar but marginal increases in neurite growth when pre-incubated at progressively higher concentrations of NGF (Fig. 5). In addition, neurite growth in control conditions (0 ng/ml NGF) was significantly lower on heparin-conjugated nanofibers than on plain-aligned nanofibers by an average decrease of

42.9%. Similar findings were demonstrated in our preliminary experiments that compared E14.5 DRG neurite growth on heparin-conjuated aligned nanofibers versus plain-aligned nanofibers in soluble NGF (supplemental Fig. 2). These results suggest that the addition of heparin onto nanofiber scaffolds may have adverse effects on neurite outgrowth, although decreased growth rate can be compensated for by sufficient NGF stimulation. Currently, we are exploring other alternative methods of NGF immobilization to the scaffold surface. We are considering coupling biotinylated-NGF protein to an avidin-conjugated scaffold surface. Another possibility is the use of NGF containing hydrogels or fibrin gels as a coating for nanofiber scaffold surfaces.

E.2. Specific Aim 2: To test the hypothesis that biomimetic nerve scaffolds will improve nerve repair and regeneration in vivo.

As previously mentioned, we are in the process of optimizing conjugation strategies for RGD peptide and NGF to aligned nanofiber scaffolds. RGD peptide will be conjugated to the scaffold surface by using carbodiimide chemistry as originally proposed, and several alternative methods for NGF immobilization will be explored as previously described. In year 2, nerve conduits coupled with RGD-peptide and NGF protein will be tested in a rat segmental sciatic nerve injury model and evaluated for their ability to enhance nerve repair and regeneration. The surgical procedure for the implantation of nerve conduits has been optimized for our experiments. We have also established the use of CatWalk analysis(Noldus, VA) to assess functional recovery of the sciatic nerve which evaluates locomotor deficits and gait adaptations in voluntarily walking rats. Nerve conduction studies and electromyography studies will also be performed as part of the functional assessment of recovery.

KEY RESEARCH ACCOMPLISHMENTS AND FINDINGS:

- Assay conditions for in vitro analysis of bioactive nanofiber scaffolds, including "in house" isolation of DRGs used for testing, have been optimize. Results of these assays are now both highly consistent and reproducible.
- Aligned nanofiber scaffolds provide exceptional directional guidance to DRG neurite extensions while non-aligned nanofiber scaffolds do not.
- Aligned nanofiber scaffolds promote significantly enhanced DRG neurite outgrowth compared to non-aligned nanofiber scaffolds.
- Nerve Growth Factor (NGF) is a potent promoter of DRG neurite outgrowth on aligned nanofiber scaffolds.
- Fibronectin (RGD peptide surrogate) coating of aligned nanofiber scaffolds significantly enhances DRG neurite outgrowth.
- NT-3, NT-4, FGF-1, FGF-2 do not enhance DRG outgrowth on nanofiber scaffolds. BDNF had a small, but significant, effect on DRG outgrowth on nanofiber scaffolds. Of known neurotrophic factors, only NGF and fibronectin (RGD) were shown to be strong promoters of neurite outgrowth in our system.
- Heparin bound to nanofiber scaffolds has an unanticipated negative effect on DRG neurite outgrowth, precluding heparin affinity binding as a strategy for NGF immobilization.

REPORTABLE OUTCOMES

Shin B, Dang AC, Lee DJ, Weng K, Wang A, Li S, Kim HT. Enhanced DRG neurite outgrowth with aligned nanofiber scaffolds and neurotropins. Submitted to 55th Annual Meeting of the Orthopaedic Research Society. August 18, 2008.
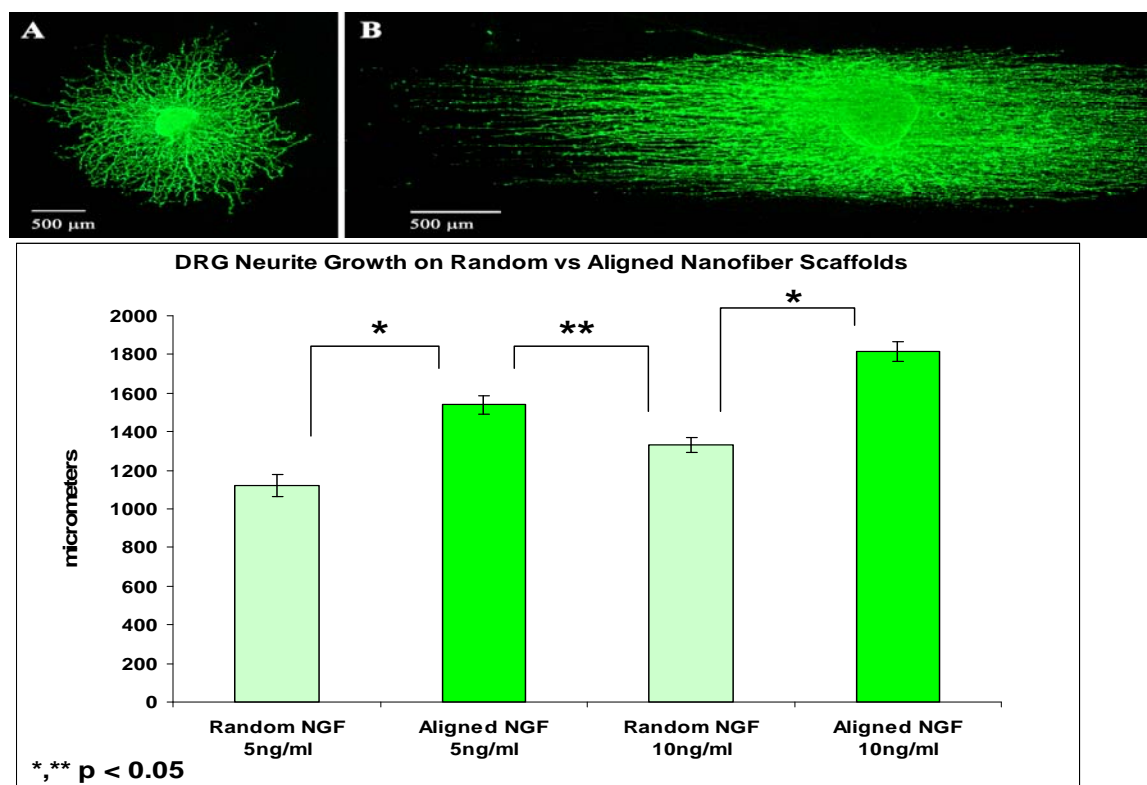
CONCLUSION

From our initial work, we have learned much about the response of DRGs to bioactive factors in conjunction with nanofiber scaffolds *in vitro*. We have shown the advantage of using aligned nanofiber scaffolds for unilateral directional guidance and enhanced neurite outgrowth. We have also shown that the use of additional biological factors can greatly increase the amount of neurite outgrowth from DRGs planted onto nanofiber scaffolds. Furthermore, we have identified NGF and RGD, out of six factors tested, as the most potent promoters of neurite outgrowth on nanofiber scaffolds. Taken together, we have shown that the combination of aligned nanofiber scaffolds with adhesion and growth factors does provide a superior conduit for neuronal growth *in vitro*, as we had hypothesized. This is important because it establishes a framework for understanding what factors are important for nerve regeneration when using synthetic conduits. This information will be critical in directing the construction of nanofiber scaffold conduits for use in our *in vivo* studies, which will begin shortly. A key challenge will be to find an alternative strategy to conjugate/deliver NGF, as two initial coupling strategies have been unsuccessful. If we are able to develop a conduit that has superior or even comparable results to nerve autografts, then this will be of great benefit to patients with segmental nerve defects.

REFERENCES

Craig JA et al. Effects of linker and spacer on the design of a fibronectin-mimetic peptide evaluated via cell studies and AFM adhesion forces. *Langmuir*. 2008; 10282-92.

Patel TH et al. A U.S. Army forward surgical team 's experience in operation Iraqi freedom. *J Trauma*. 2004; 57(2):201-7.

Patel TH et al. Bioactive nanofibers: synergistic effects of nanotopography and chemical signaling on cell guidance. *Nano Lett*.2007; 7(7):2122-8.

Stoll G et al. Nerve injury, axonal degeneration and neural regeneration: basic insights. *Brain Pathology*. 1999; 9(2):313-25.

Zong et al. Structure and process relationships in biodegradable nanofiber membrane by electro-spinning. *Polymer*. 2002; 43:4403-4412.
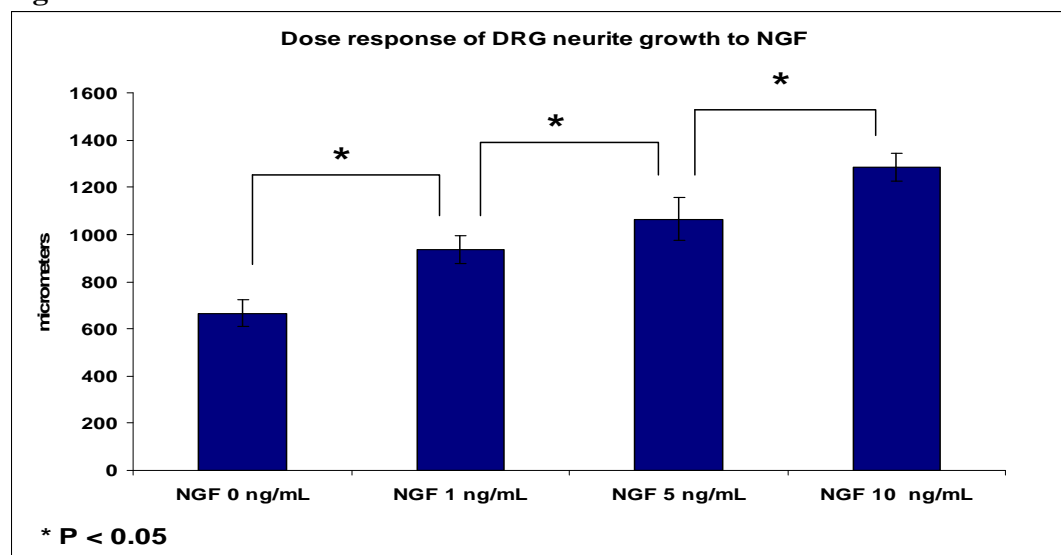
SUPPORTING DATA

Figure 1.

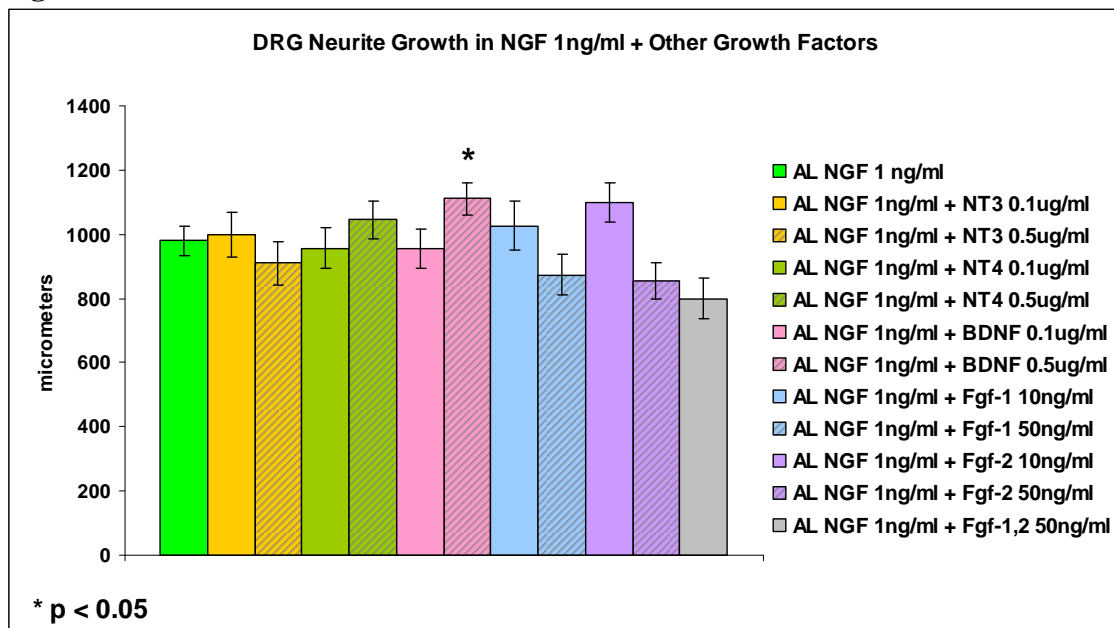**DRG Neurite Growth on Random vs Aligned Nanofiber Scaffolds**

(A, B) Phalloidin-FITC stain of DRG (in NGF 5ng/ml) grown on non-aligned and aligned nanofibers, respectively. (C) Comparison of neurite growth on non-aligned vs. aligned nanofibers at NGF concentrations of 5 and 10 ng/ml. Error bars represent s.e.m.
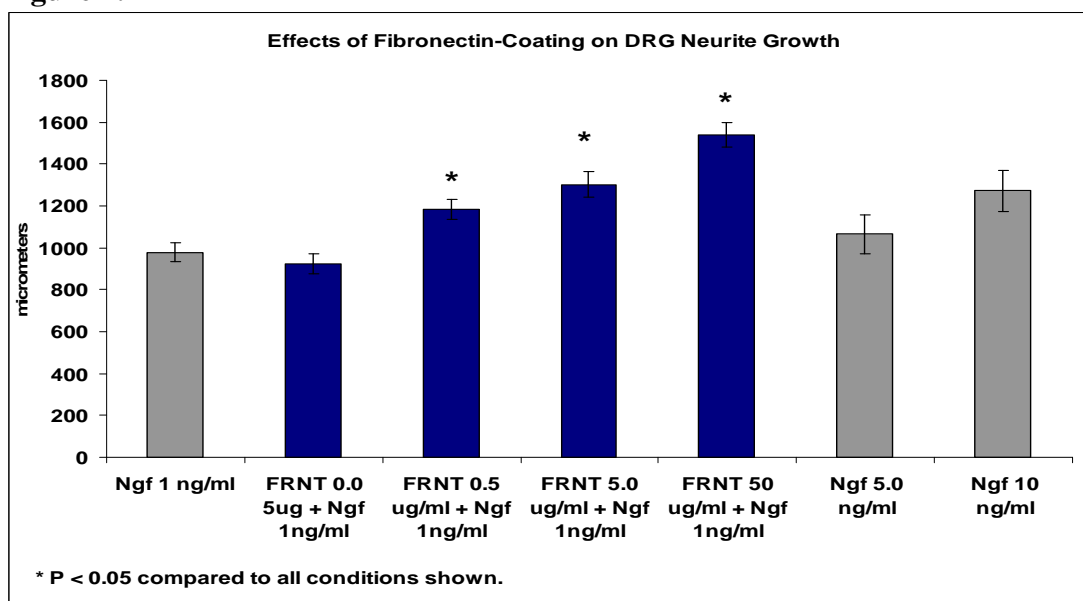
Figure 2.

Dose response of DRG neurite growth to NGF

Comparison of neurite growth with increasing concentration of NGF. A significant dose response of neurite growth to NGF is shown.
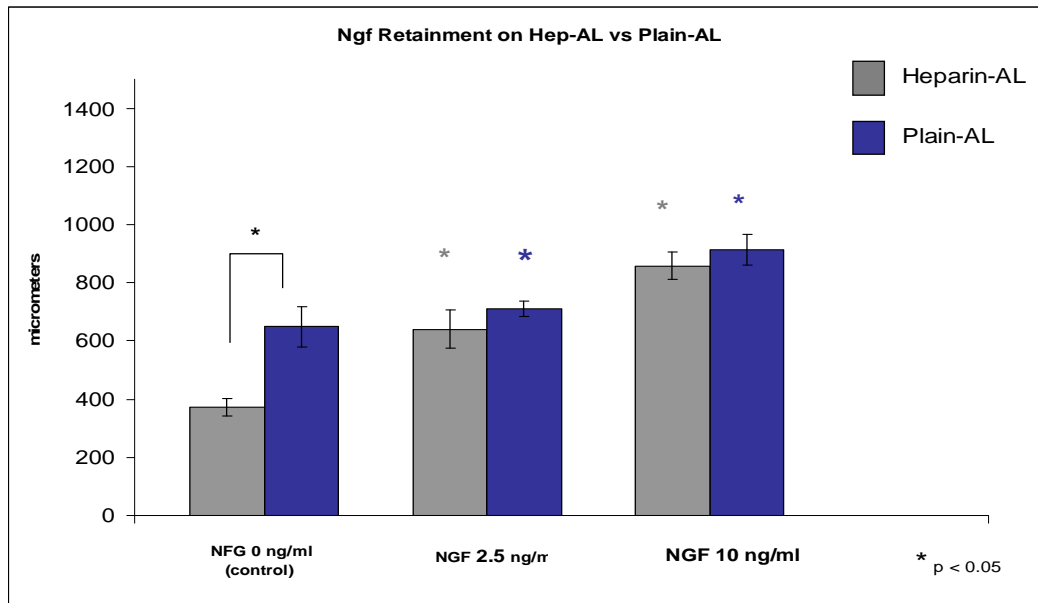
Figure 3.

Comparison of neurite growth in combination of NGF 1 ng/ml and an additional growth factor vs. NGF 1ng/ml alone.

Figure 4.

Comparison of neurite growth on fibronectin-coated nanofibers in NGF 1ng/ml vs. neurited growth in different concentrations of NGF alone. A significant dose response to Fibronectin-coating is observed. Neurite growth on fibronectin-coated nanofibers at and above 0.5 µg/ml is significantly greater than growth in NGF concentration of 1.0, 5.0 and 10.0 ng/ml alone.
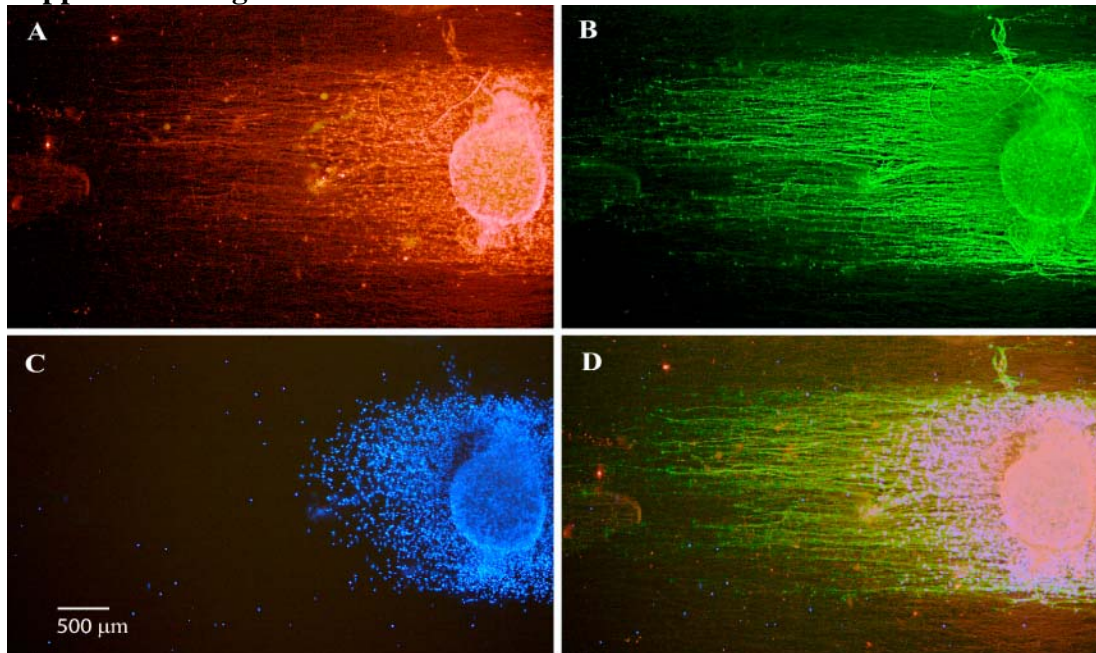
Figure 5.

Ngf Retainment on Hep-AL vs Plain-AL

Comparison of neurite growth on Heparin-conjugated aligned nanofibers and plain-aligned nanofibers after pre-incubation with NGF. Heparin-conjugation to nanofibers does not yield higher neurite growth than plain-aligned nanofibers.
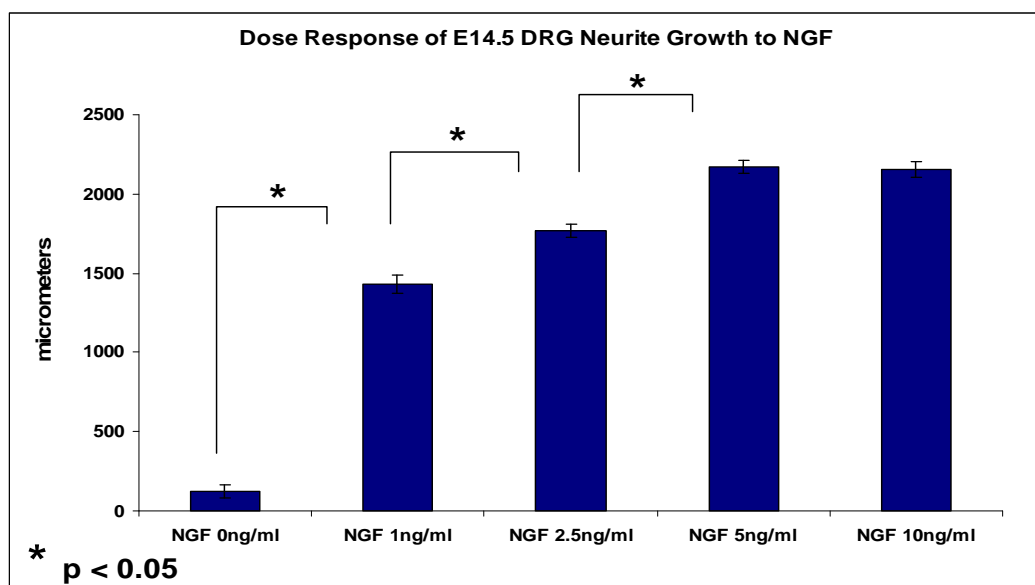
APPENDICES

Supplemental Figure 1.

Co-localization of Neurofilament –M immunostain and Alexa 488-Phalloidin stain on P5 DRGs cultured on aligned nanofiber scaffolds in 10 ng/ml of NGF.
(A) Immunostaining of Neurofilament-M (rabbit, Santa Cruz, Inc.) (B) Alexa 488-Phalloidin stain. (C) DAPI stain. (D) Overlay of all three channels 594, 488 and 258nm.

Supplemental Figure 2.

Dose Response of E14.5 DRG Neurite Growth to NGF

Comparison of embryonic (E14.5) DRG neurite growth with increasing concentration of NGF. E14.5 DRGs showed little to no growth in the absence of NGF. In presence of 1 g/ml of NGF, neurite growth was increased to 1429.69μg/ml ±57.49 (91.5 %) with statistically significant increase in growth up to 5 ng/ml of NGF.

Supplemental Figure 3.

Comparison of embryonic (E14.5) neurite growth on Heparin-conjugated aligned nanofiber scaffolds vs. plain-aligned nanofiber scaffolds in soluble NGF. Neurite growth on Heparin-conjugated aligned nanofibers is significantly compromised at every concentration of NGF tested.

Pilot Study 10:

Biological Pathways Expressed in PTSD

Principal Investigator: Thomas C. Neylan, M.D. Associate Prof. UCSF

ABSTRACT

Posttraumatic Stress Disorder (PTSD) is presently diagnosed with a constellation of clinical symptoms with no consistent marker of disease or pathogenic mechanism identified. The recent development of gene microarray technology has created the potential to identify novel pathways involved in the biology of PTSD which may lead to more targeted treatments. We have shown in preliminary experiments that PTSD is associated with a differential gene expression profile in immune reactive peripheral monocytes. Furthermore, genes that were significantly regulated were members of gene categories (e.g. gene ontologies) related to neurophysiological processes including dopamine and neurotransmitter metabolism, oxidative stress and neuropeptide signaling pathways. This data was collected from subjects with PTSD and controls that were well-characterized medication-free and age-matched controls. It is our overall hypothesis that subjects with chronic PTSD will have an altered expression of gene ontologies and proteins implicated in the regulation of brain function that are also expressed and detectable in peripheral monocytes. Our Specific Aims are 1) to determine monocyte gene expression profiles on male subjects with a clinical definition of PTSD compared to age matched trauma exposed male controls; 2) to verify the profile using qPCR (quanitative real-time PCR) and confirm protein expression by Western blotting. This study will recruit trauma exposed males with (N= 25) and without (N= 25) PTSD. This proposal involves a collaboration of 2 different laboratories focused on PTSD and neuroimmunology/molecular biology using new basic science technology and rigorous clinical parameters to clarify the biology of PTSD and reveal important information for diagnostic and treatment purposes. It is anticipated that 500,000 Americans will serve in Afghanistan and Iraq and recent reports estimate a prevalence of PTSD in 10-20% of men and women returning from service in Iran. There is a compelling need to understand the biological pathways related to PTSD and understand the pathogenesis of the disorder to develop more specific and effective treatments.

TABLE OF CONTENTS

INTRODUCTION

The purpose of the study is to identify biological pathways involved in the biology of PTSD. The study will test the hypothesis that subjects with chronic PTSD have an altered expression of gene ontologies and proteins that are expressed and detectable in peripheral blood mononuclear cells (PBMCs).

Our Specific Aims are:

1)To determine monocyte gene expression profiles on male subjects with a clinical definition of PTSD compared to age matched male controls who have experienced a traumatic life event.

2)To verify the profile using qPCR (quantitative real-time polymerase chain reaction) and confirm protein expression by Western blotting.

Hypothesis 1: Subjects with chronic PTSD will have an altered expression of gene ontologies and proteins implicated in the regulation of brain function that are also expressed and detectable in peripheral monocytes.

Hypothesis 2: Subjects with chronic PTSD will have an altered expression of gene ontologies, proteins (cytokines) associated with inflammation.

This study uses a case control design involving males with and without PTSD, ages 20-50, who will be recruited from a variety of different locations. Patients will be clinically assessed for inclusion exclusion criteria, have a screening laboratory blood draw, and will return for a second blood draw to compare group differences in expression of gene ontologies and proteins implicated in the regulation of brain and immune function that are expressed and detectable in peripheral blood mononuclear cells (PBMCs).

This proposal involves a collaboration of 2 different laboratories focused on PTSD and neuroimmunology/molecular biology using new basic science technology and rigorous clinical parameters to clarify the biology of PTSD and reveal important information for diagnostic and treatment purposes.

BODY

This study was initiated September 1, 2007. To date we have consented and assessed 29 potential participants, five were ruled out for not meeting eligibility criteria, and 24 were enrolled and completed the study (15 PTSD+ and 9 Controls). We have revised our subject selection criteria to expand enrollment beyond OEF/OIF combat veterans, thus to allow us to enroll both veteran and civilian males with and with out PTSD who have experienced a traumatic life event. This modification request was submitted to the IRB for review and received approval on July 2, 2008.

PLAN FOR NEXT YEAR

Continue to actively recruit and enroll males with and without PTSD and conduct the microarray analysis, gene ontology analysis, qPCR analysis, and western Blot analysis. Upon meeting out enrollment goals we will proceed to data analysis & manuscript preparation

KEY RESEARCH ACCOMPLISHMENTS

As we proceed into the second year of the study we continue to recruit and enroll participants. The data analysis phase has not started, thus there are no results to report to date.

REPORTABLE OUTCOMES

This congressional project/program titled, "Biological Pathways Expressed in PTSD," was selected to be reviewed at the Behavioral Health/PTSD Telemental Health Product Line Review (PLR) held on Tuesday, July 8, 2008 in Frederick, MD at the Morningside Inn. Dr. Thomas Neylan attended the PLR meeting and presented to the review panel.

CONCLUSION
The implications of this research project are currently not known because we are still acquiring data.

REFERENCES
N/A

APPENDICES
N/A.

SUPPORTING DATA
N/A

Pilot Study 11:

Parkinsonism as Model to Detect Neurodegeneration by High Field MRI

Principal Investigator: Norbert Schuff, Ph.D.

ABSTRACT

This is an annual progress report on this research project, which is funded from 1/18/7 to 1/17/9 to identify imaging markers of Parkinson's disease. The exact cause of Parkinson's Disease (PD) is still unknown, but there is increasing evidence that exposure to environmental toxins that can include nerve agents, pesticides, and herbicides as well as traumatic brain injury, can play a major role in the pathophysiology of PD. The main goal of this project is to accurately diagnose PD with the use of two novel MRI methods: 1) susceptibility weighted imaging (SWI), which can indirectly measure brain iron, a key player in the etiology of PD and 2) diffusion tensor imaging (DTI), which can detect subtle ultrastructural changes in brain tissue, such as disintegration of white matter fibers. Since the sensitivity of both SWI and DTI increases considerably with higher magnet field strength, the study will be conducted at 4 Tesla. The study is designed to test the following main hypotheses: 1) High field strength MRI can distinguish patients with PD from controls by increased phase evolution on SWI in the substantia nigra pars compacta and the striatum, reflecting increased iron deposition in these regions. 2) High field strength MRI can distinguish patients with PD from controls by decreased directionality of brain water diffusion on DTI in nigrostriatal and corticostriatal fibers, indicating disintegration of these fibers. The hypotheses will be tested initially on 40 patients with a diagnosis of idiopathic PD and 20 healthy subjects. It is expected that this study will help to identify new imaging markers, which will improve the diagnosis of PD, and potentially increase therapeutic options for the patient

Military relevance: Epidemiology studies suggest 1.5- to 7-fold increases in risk to develop PD for people with occupational exposure to environmental toxicants, including neuroagents, pesticides, and herbicides. In addition to toxicants, traumatic brain injury has also been associated with a higher risk to develop PD. Both exposures to toxicants and brain injuries increase considerably for military personnel on active duty. Furthermore, since age is another major risk factor, the incidence of PD may surge in the coming years when military personnel and veterans, who were deployed to Vietnam, the Persian Gulf, and Iraq, and other conflicts reach their 5th and 6th decades of life. The primary aim of this project is the identification of an imaging marker of PD that improves diagnosis of the disease, prognosis and response to pharmacological interventions. This emphasizes and establishes the strong military relevance of PD research in general and of this application in particular.

TABLE OF CONTENTS

INTRODUCTION

Parkinson's disease (PD) is associated with neuron loss and glial activation, especially in the substantia nigra pars compacta. Previous MRI studies of PD, however, yielded inconsistent results of brain tissue loss. Another major component of PD pathology seems to be increased iron. This project is using susceptibility weighted imaging (SWI), which can indirectly measure iron content in brain tissue by observation of signal phase evolutions, to detect iron abnormalities in PD. An increasing number of diffusion tensor imaging (DTI) studies in PD suggest abnormal measures of fractional anisotropy (FA), a directional diffusion measure thought to indicate decreased white matter integrity. We are using DTI to investigate the integrity of fiber bundles of the movement circuitry in PD. Overall, we aim to identify systematic abnormalities of SWI and DTI in PD that could be early markers of PD. Furthermore, we aim to investigate the extent to which SWI and DTI abnormalities correlate with PD severity.
Our aim was to explore if SWI could be a useful marker for PD that also tightly correlates with severity of the clinical symptoms. Specifically, we hypothesized that PD is associated with decreasing SWI phase in the movement controlling network, including the substantia nigra (SN), subthalamic nucleus (STN), globus pallidus (GP), putamen (PUT), and caudate nucleus (CAU) and furthermore that phase correlates with disease severity.

BODY

During the past year, we studied 18 male patients diagnosed with mild to moderate PD as measured using the Unified Parkinson's Disease Rating Scale (UPDRS) Part III motor score in the off-medication state and 10 male healthy controls of comparable age volunteered for this MRI study at 4Tesla (mean age 65 ± 6 years, UPDRS range from 3 to 52). All subjects received a comprehensive neurological evaluation to establish presence or absence of PD. The regions of SN, STN, GP, PUT and CAU were identified by a combination of automated labeling using nonlinear warping of the images to a brain atlas with Freesurfer software (http://surfer.nmr.mgh.harvard.edu/) and manual refinement by experienced readers blinded to all clinical information. The phase images of SWI were high-pass-filtered to remove low-spatial-frequency components. The final phase images appear on a scale from 0 to 4096, corresponding to $-\pi$ to $+\pi$. To evaluate the regional dispersion of the phase, we *evaluated the 2nd* order coincidences (co-occurrences) between pairs of phase values within the traced anatomical regions. For a region with a uniform phase distribution, the co-occurrences lie close to the diagonal of the co-occurrence matrix, whereas they appear off-diagonal for a heterogeneous distribution. We quantified co-occurrences by computing the entropy of the co-occurrence matrix, where greater entropy reflects increasing numbers of off-diagonal occurrences, equivalent to greater regional phase dispersion. The effect of PD on phase and phase entropy was statistically evaluated using ANOVA with age as co-factor. Correlations between UPDRS scores and phase or entropy were evaluated using Spearman Rank tests (α=0.05)

KEY RESEARCH ACCOMPLISHMENTS

1. Enrollment of subjects for this study began on January 8th, 2007 after we received final DoD IRB approval for the study.

3

2. During the past 12 months, we have recruited and studied 18 PD patients and 10 age and sex matched control subjects, which is close to our recruitment goal of enrolling 20 patients and 10 controls per year for this study. We are only a few subjects shy of reaching our total recruitment goals of 40 patients and 20 controls.

3. Processing of the MRI data is currently in progress. We obtained preliminary results from a small number of subjects including pilot data. The findings described in the next paragraph.
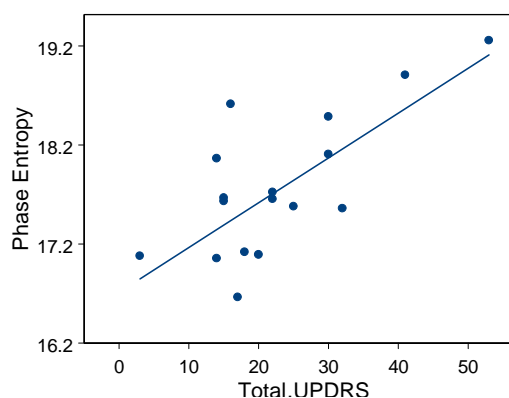
REPORTABLE OUTCOMES

SWI Results: SWI phase values (+/- SD) in PD and controls are listed in the table by regions. The most significant phase reductions, implying increased iron, occurred in the left STN (p = 0.01), right PUT (p = 0.01) and bilaterally in the CAU (p = 0.03), whereas differences in the SN and GP were not significant after accounting for age. The phase in the PUT significantly correlated with PD severity (left:p = 0.002; right: p = 0.01), whereas for STN and CAU these correlations were only a trend. Phase entropy was not significantly associated with PD in any region. However, phase entropy increased with increasing PD severity (higher UPDRS motor scores) in the CAU (p = 0.01), PUT (p = 0.007), and STN (p = 0.003), as depicted in the figure for the STN..

Region	Mean Phase		p- value
	PD	Control	
Substantia Nigra			
Right	2056 ± 139	2122 ± 184	n.s.
Left	2076 ± 135	2144 ± 219	n.s.
Subthalamic Nucleus			
Right	2077 ± 87	2108 ± 64	n.s.
Left	2056 ± 139	2173 ± 116	0.01
Globus Pallidus			
Right	2072 ± 28	2084 ± 39	n.s.
Left	2065 ± 26	2087 ± 48	n.s.
Putamen			
Right	2065 ± 18	2084 ± 27	0.01
Left	2056 ± 25	2100 ± 35	n.s.
Caudate Nucleus			
Right	2087 ± 21	2103 ± 25	0.02
Left	2093 ± 20	2113 ± 33	0.03

DTI Results: We also performed a group comparison for DTI: We found reduced FA (p<0.01) in PD compared to normal controls in various white matter regions. The DTI abnormalities in PD were primarily seen in proximity to the substantia nigra (SN), posterior striatum, as well as in frontal white matter and along projection fibers to the supplementary motor areas (SMA). **Correlation results:** In the PD patient group, negative correlations (p<0.01) between the FA and UPDRS scores were found close to the SN as shown in the Figure below. Moreover, the phase values of SWI in SN, presumably reflecting the regional iron levels, also correlated (p<0.01) with the FA in the WM tracts and projections to the SMA as illustrated in Fig.2 (b).

PD Severity in Terms of UPDRS and SWI Phase Entropy of Subthalamic Nucleus

Others:
1. Received invitation to speak at the 1st International Symposium on Neuroimaging in PD in Innsbruck Austria on high field MRI applications for PD studies.

2. Conference Proceedings: N. Schuff. Potential role of high field MRI for PD studies; 1st International Symposium on Neuroimaging in PD, Innsbruck Austria

3. Applied to the Michael J. Fox foundation for funding of a prospective study of PD that involves clinical evaluations and MRI scans at baseline and after one year. The proposed study will build on results of this DoD funded cross-sectional MRI study. However, since this DoD funded study has no prospective component to study PD progression, funds have been request for longitudinal studies of PD patients. Additional funds are requested to study a group of patients with MSA to determine the specificity of cross-sectional and longitudinal findings in PD.

CONCLUSION

Our preliminary findings indicate widespread brain deficits in PD along a regional profile that seems to be specific for PD (similar MRI measures in Alzheimer's disease and other dementias show different systematic patterns of abnormalities [1]). Furthermore, cortical deficits involving the SMA, may reflect dysfunctions of circuits for motor planning that may help differentiating between subtypes of PD, i.e. akinetic-rigid dominant versus tremor dominant types, which can differ in disease progression and responsiveness to treatment [2]. In short, these preliminary results support our hypothesis that PD is associated with a characteristic pattern of increased brain iron and fiber disintegration that can be detected with MRI.

Our plans for the coming year are to continue recruiting PD and control subjects and to process and analyze more data.

REFERENCES

1. Zhang Y, Schuff N, Jahng GH, Bayne W, Mori S, Schad L, Mueller S, Du AT, Kramer JH, Yaffe K, Chui H, Jagust WJ, Miller BL, Weiner MW. Diffusion tensor imaging of cingulum fibers in mild cognitive impairment and Alzheimer disease. Neurology 2007;68(1):13-19.

2. Mito Y, Yoshida K, Yabe I, Makino K, Tashiro K, Kikuchi S, Sasaki H. Brain SPECT analysis by 3D-SSP and clinical features of Parkinson's disease. Hokkaido Igaku Zasshi 2006;81(1):15-23.

APPENDICES (attached)

APPENDIX I   (1 page)

W. Zhan1, G. A. Kang, G. A. Glass, W. J. Marks2, Y. Zhang1, M. Nezamzadeh1, A. Ebel1, X. Zhu1, R. Millin1, D. McCoy1, M. W. Weiner1, and N. Schuff.   Voxel-Based DTI Analysis of White Matter Alterations in Parkinson's Disease. *Printed in the proceedings of the international society of magnetic resonance in medicine (ISMRM), meeting in Toronto, 2008*

APPENDIX II (1 page)

A. Ebel1,2, L. Stables3, G. A. Kang4, G. Glass3,4, R. Millin1,2, D. McCoy1,5, P. Lorenzen1,5, Y. Zhang1,5, W. Zhan1,5, M. W. Weiner1,5, W. Marks3,4, and N. Schuff. Abnormal Iron Content and Distribution in the Basal Ganglia in Parkinson's Disease: A Susceptibility-Weighted Imaging Study. *Printed in the proceedings of the international society of magnetic resonance in medicine (ISMRM), meeting in Toronto, 2008*

APPENDIX III (2 pages)

Gail A. Kang, M.D., Graham A. Glass, M.D., William Marks, M.D., Wang Zhan, Ph.D., Yu Zhang, M.D., Andres Ebel, Ph.D., Marzieh Nezamzadeh, Ph.D., Rachel Millin, B.S., Paul Dukarm, Ph.D., Norbert Schuff, Ph.D.   A Potential Role for Multi-Modal MRI as an Objective Diagnostic Tool and Surrogate Marker of Disease Progression in Parkinson's Disease. Poster.

SUPPORTING DATA
N/A

Voxel-Based DTI Analysis of White Matter Alterations in Parkinson's Disease

W. Zhan[1], G. A. Kang[2], G. A. Glass[2], W. J. Marks[2], Y. Zhang[1], M. Nezamzadeh[1], A. Ebel[1], X. Zhu[1], R. Millin[1], D. McCoy[1], M. W. Weiner[1], and N. Schuff[1]

[1]Radiology, University of California San Francisco, San Francisco, CA, United States, [2]VA Medical Center San Francisco, San Francisco, CA, United States

Introduction

As new potentially disease-modifying drugs for Parkinson's disease (PD) are being developed, there is increasing need for imaging markers to accurately diagnose PD and monitor progression. MRI-based techniques could play a particular role for drug studies of PD, because MRI measures do not rely on receptor binding, unlike radiotracer imaging with PET and SPECT [1-3]. In the present study, diffusion tensor imaging (DTI) [4] was applied to assess microscopic alterations of white matter (WM) tracts in PD. Specifically, we hypothesized that PD would be associated with fractional anisotropy (FA) reductions in brain regions known to be associated with PD, such as the substantia nigra (SN). Furthermore, we predicted that greater FA reductions in these regions would correlate with increased severity of PD symptoms.

Methods

Fourteen patients diagnosed with mild-moderate PD as measured by the Unified Parkinson's Disease Rating Scale (UPDRS) [5] (all males, age=68±8 yrs, UPDRS off-medication motor score=26.3±12.2), and 20 healthy male controls matched for age and education volunteered for this MRI study on a 4T scanner (Siemens). The scan protocol included DTI (EPI: TR/TE= 6s/77ms, voxel=2x2x3mm, GRAPPA=2, direction=6 at b=800s/mm^2, 4 repetitions), FLAIR (TR/TE/TI= 5000/355/2030ms), and T1 MPRAGE (TR/TE/TI= 2300/3.5/950 ms) images. Susceptibility-weighted images (SWI) were also collected to measure brain iron deposition [6]. All subjects received a comprehensive neurological evaluation to establish presence or absence of PD. Severity of PD was tested "off medication." Subjects were excluded if they had pathological diagnosis of any other neurological disorder, history of central nervous system infection, seizures, significant cognitive impairment (defined as MMSE < 26), or history of alcohol and/or drug abuse. MRI data showing strong motion artifact or WM lesions in raw images were also excluded from analysis. FSL (http://www.fmrib.ox.ac.uk/fsl/) was used for eddy current correction and DTI preprocessing offline. The tract-based spatial statistics (TBSS) technique [7] was implemented for DTI processing. One normal subject (age=65 yrs) was chosen as the "target" on which the FA maps of all subjects were nonlinearly co-registered, and non-FA DTI data were transformed by following the same pipeline. Aligned DTI data were then interpolated to 1x1x1mm resolution and spatially normalized into a T1 template in the Talairach space. A non-parametric permutation t-test was performed to provide the group comparisons with interpretable p values. An orthogonal linear regression algorithm was applied to estimate and remove age-related effects on a voxelwise basis. Pearson's cross-correlation coefficients between the DTI and UPDRS measurements were estimated for each voxel. No smoothing or clustering techniques were applied.

Fig 1: Abnormal DTI in PD compared to Controls

Results

Group comparisons: In Fig.1, reduced FA (p<0.01) in PD compared to normal controls is illustrated as blue clusters, superimposed on the mean FA map in normalized space. The DTI abnormalities in PD were primarily seen in proximity to the substantia nigra (SN), posterior striatum, as well as in frontal white matter and along projection fibers to the supplementary motor areas (SMA).

Correlation results: In the PD patient group, negative correlations (p<0.01) between the FA and UPDRS scores were found close to the SN as shown in Fig.2 (a). Moreover, the phase values of SWI in SN, presumably reflecting the regional iron levels, also correlated (p<0.01) with the FA in the WM tracts and projections to the SMA as illustrated in Fig.2 (b).

Discussions

Voxel-based DTI analysis revealed widespread decrease of FA in PD, primarily seen in WM close to the SN, as hypothesized, as well as in the posterior striatum, frontal lobe, and projections to the SMA, potentially indicating axonal degradation of neuronal pathways that play a role in movement planning and initiation [8]. Further support for an association between DTI alterations and PD comes from correlation analyses showing that the DTI abnormities in SN increased with the PD severity, and that the WM integrity in SMA is associated with changes of the iron level in SN. Taken together, these results suggest that DTI may help improve diagnosis and staging of PD.

Fig.2: Correlations results in the PD patients

References: [1] Faha S, N Engl J Med 2004; 351(24):2498. [2] Guttman M, Neurology 2001;56 (11):1559. [3] Ravina B, Neurology 2005;64 (2):208. [4] Le Bihan, JF, JMRI 2001; 13:534. [5] Mov Disord 2003;18 (7):738. [6] Haacke EM, MRM, 2004; 52 (3):612. [7] Smith SM, NeuroImage 2006, 31:1487. [8] Eric R. Principles of Neural Science. New York: McGraw-Hill; 2000.
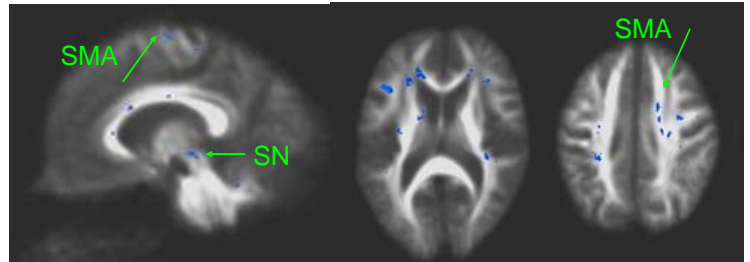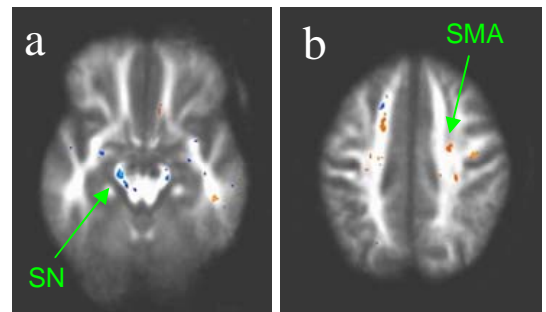
Abnormal Iron Content and Distribution in the Basal Ganglia in Parkinson's Disease: A Susceptibility-Weighted Imaging Study

A. Ebel[1,2], L. Stables[3], G. A. Kang[4], G. Glass[3,4], R. Millin[1,2], D. McCoy[1,5], P. Lorenzen[1,5], Y. Zhang[1,5], W. Zhan[1,5], M. W. Weiner[1,5], W. Marks[3,4], and N. Schuff[1,5]

[1]Center for Imaging of Neurodegenerative Diseases, San Francisco, CA, United States, [2]Northern California Institute for Research and Education, San Francisco, CA, United States, [3]Department of Neurology, University of California, San Francisco, CA, United States, [4]Parkinson's Disease Research, Education, and Clinical Center, VA Medical Center, San Francisco, CA, United States, [5]Department of Radiology, University of California, San Francisco, CA, United States

Background: Finding a robust MRI marker for Parkinson's disease (PD) is extremely important because of the difficulty of correctly diagnosing PD, especially at an early stage. Several MRI relaxation studies reported abnormal R2 and R2* values in PD in agreement with histopathological findings of increased iron deposition in the brain's nigrostriatal system. However, substantial problems remain to consistently and accurately quantify brain iron using MRI. An alternative MRI technique to measure brain iron is susceptibility-weighted imaging (SWI), which exploits the effect that subtle magnetic susceptibility differences alter the phase of the MRI signal. One advantage of SWI is that the phase should decrease linearly with brain iron concentration in contrast to R2 and R2* which show nonlinear changes (1). Moreover, since the phase is independent of the signal magnitude, phase is also more robust in the presence of noise (1). The aim of this study was to explore if SWI could be a useful marker for PD that also tightly correlates with severity of the clinical symptoms. Specifically, we hypothesized that PD is associated with decreasing SWI phase in the movement controlling network, including the substantia nigra (SN), subthalamic nucleus (STN), globus pallidus (GP), putamen (PUT), and caudate nucleus (CAU), and furthermore that phase correlates with disease severity.

Methods: Eighteen male patients diagnosed with mild to moderate PD as measured using the Unified Parkinson's Disease Rating Scale (UPDRS) Part III motor score in the off-medication state (mean age 65 ± 6 years, UPDRS range from 3 to 52) and 23 male healthy controls of comparable age volunteered for this MRI study at 4 Tesla. All subjects received a comprehensive neurological evaluation to establish presence or absence of PD. The scan protocol included 1 mm^3 T1 MPRAGE and FLAIR as well as 0.5 x 0.6 x 1.2 mm SWI (TR/TE=32/25 ms, courtesy of Dr. E.M. Haacke). The structural MRIs were co-registered to each other. The regions of SN, STN, GP, PUT, and CAU were identified by a combination of automated labeling using nonlinear warping of the images to a brain atlas with Freesurfer software (http://surfer.nmr.mgh.harvard.edu/) and manual refinement by experienced readers blinded to all clinical information. The phase images of SWI were high-pass-filtered to remove low-spatial-frequency components. The final phase images appear on a scale from 0 to 4096, corresponding to $-\pi$ to $+\pi$. To evaluate the regional dispersion of the phase, we evaluated the 2nd order coincidences (co-occurrences) between pairs of phase values within the traced anatomical regions. For a region with a uniform phase distribution, the co-occurrences lie close to the diagonal of the co-occurrence matrix, whereas they appear off-diagonal for a heterogeneous distribution. We quantified co-occurrences by computing the entropy of the co-occurrence matrix (2), where greater entropy reflects increasing numbers of off-diagonal occurrences, equivalent to greater regional phase dispersion. The effect of PD on phase and phase entropy was statistically evaluated using ANOVA with age as co-factor. Correlations between UPDRS motor scores and phase or entropy were evaluated using Spearman Rank tests (α=0.05).

Region	Mean Phase		
---	PD	Control	p-value
Substantia Nigra			
Right	2056 ± 139	2122 ± 184	n.s.
Left	2076 ± 135	2144 ± 219	n.s.
Subthalamic Nucleus			
Right	2077 ± 87	2108 ± 64	n.s.
Left	2056 ± 139	2173 ± 116	0.01
Globus Pallidus			
Right	2072 ± 28	2084 ± 39	n.s.
Left	2065 ± 26	2087 ± 48	n.s.
Putamen			
Right	2065 ± 18	2084 ± 27	0.01
Left	2056 ± 25	2100 ± 35	n.s.
Caudate Nucleus			
Right	2087 ± 21	2103 ± 25	0.02
Left	2093 ± 20	2113 ± 33	0.03

Results: SWI phase values (+/- SD) in PD and controls are listed in the table by regions. The most significant phase reductions, implying increased iron, occurred in the left STN (p = 0.01), right PUT (p = 0.01), and bilaterally in the CAU (p = 0.03), whereas differences in the SN and GP were not significant after accounting for age. The phase in the PUT significantly correlated with PD severity (left: p = 0.002; right: p = 0.01), whereas for STN and CAU these correlations were only a trend. Phase entropy was not significantly associated with PD in any region. However, phase entropy increased with increasing PD severity (higher UPDRS motor scores) in the CAU (p = 0.01), PUT (p = 0.007), and STN (p = 0.003), as depicted in the figure for the STN.
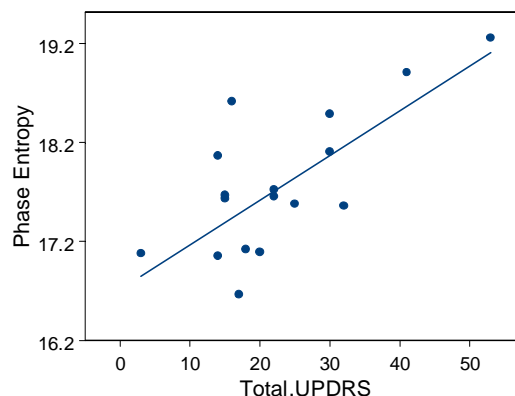
Conclusions: The findings support our a-priori hypotheses. The findings taken together suggest that SWI phase and entropy have potential value as markers for an objective diagnosis of PD, assessment of disease severity, as well as for response to disease-modifying interventions.

PD Severity in Terms of UPDRS and SWI Phase Entropy of Subthalamic Nucleus

References: (1) Haacke E.M. et al. Magnetic resonance imaging: Physical principles and sequence design. John Wiley & Sons, 1999; (2) Hadjidemetriou S. et al. Restoration of MRI data for field nonuniformities using high order neighborhood statistics. SPIE conference on medical imaging, San Diego, 2007.

ABSTRACT TO POSTER

Multimodal MRI Imaging of Parkinson's Disease

Kang[4], G. Glass[3,4], R. Millin[1,2], D. McCoy[1,5], P. Lorenzen[1,5], Y. Zhang[1,5], W. Zhan[1,5], M.W. Weiner[1,5], W. Marks[3,4], and N. Schuff[1,5].

Since the assessment of Idiopathic Parkinson's Disease (PD) is currently based primarily on symptoms and signs on clinical examination, an accurate diagnosis can be challenging especially at the initial stages of motoric involvement. However, an accurate diagnosis of IPD as well as disease progression has potential major implications for instituting effective neuroprotective strategies and for disease-modifying clinical trials. In this ongoing study, we are evaluating the utility of a multimodal MRI technique in distinguishing between PD patients and controls. In addition, we are assessing if there are any characteristic imaging changes seen with degree of disease severity. Some of the measurement tools available with this MRI technique include susceptibility-weighted imaging (SWI) which provides a measure of brain iron levels, diffusion tensor imaging (DTI) which assesses nerve fiber integrity and arterial spin labeling (ASL) MRI which measures cerebral blood flow.

18 PD (age range 55 – 82 years; 17 males/1 female) and 23 control subjects (age range 58-81 years; all male) have been evaluated. A significant correlation has been found between SWI phase and entropy measurements between the putamen (both left and right sides) and motoric severity (as assessed on UPDRS Part III) of PD subjects (right putamen: $p < 0.05$; left putamen: $p < 0.01$). There are similar findings for the caudate and subthalamic nucleus. In DTI analysis of a subset of these subjects (11 PD, 12 controls), there is a widespread decrease ($P < 0.01$) of fractional anisotropy in PD. These DTI abnormalities in PD were primarily seen in the posterior striatum as well as in the frontal white matter and supplementary motor area. ASL analysis in this same subset of subjects has shown significant reduction in blood flow in the frontal cortex in PD ($p < 0.001$). Our findings demonstrate widespread brain deficits in PD occurring in a regional distribution which appear to be specific for PD; a similar pattern of abnormalities have not been seen in other neurodegenerative disorders.

A Potential Role for Multi-Modal MRI as an Objective Diagnostic Tool and Surrogate Marker of Disease Progression in Parkinson's Disease

Gail A. Kang, M.D., Graham A. Glass, M.D., William Marks, M.D., Wang Zhan, Ph.D., Yu Zhang, M.D., Andres Ebel, Ph.D., Marzieh Nezamzadeh, Ph.D., Rachel Millin, B.S., Paul Dukarm, Ph.D., Norbert Schuff, Ph.D.

Center for Imaging of Neurodegenerative Diseases and
San Francisco Veterans Affairs Parkinson's Disease Research, Education, & Clinical Center (PADRECC)

Objective: To evaluate the utility of multimodal MRI in distinguishing between Idiopathic Parkinson's disease (PD) subjects and controls, using (1) normalized volume measurements of the basal ganglia and (2) susceptibility-weighted imaging (SWI) which provides measurement of iron levels. In addition, we determined if imaging characteristics correlate with disease severity and subtype of disease.

Background: The diagnosis of PD is based on clinical evaluation alone and an accurate diagnosis can be challenging. The establishment of an objective diagnostic tool and surrogate marker of disease progression has major implications for instituting effective neuroprotective strategies and in disease-modifying clinical trials.

Methods: Twenty-five PD and 23 control subjects met criteria to participate in the study and completed the MRI protocol. All potential subjects were evaluated by a movement disorders specialist who confirmed the clinical diagnosis of PD or in the case of control subjects, absence of PD. Unified Parkinson's Disease Rating Scale (UPDRS) scores were obtained with subjects in the "off" state (defined as having refrained from taking levodopa 12 hours prior to evaluation). Determination of PD subtype (akinetic-rigid, tremor dominant or mixed) was made according to the UPDRS data. Subjects were required to have a MMSE score of $\geq$ 26. A neuropsychological battery was also administered to rule out the presence of dementia.

Volume measurements were obtained of the right and left caudate, globus pallidus, and putamen and were normalized to intracranial volume to account for head size. Susceptibility weighted imaging processing was obtained for the substantia nigra and subthalamic nucleus.

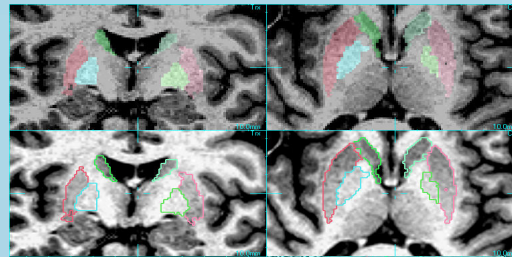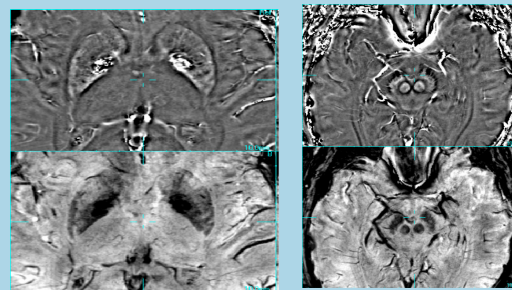## Figure 1: Example of Volume Measurements of the Basal Ganglia

Figure 2: Example of Susceptibility Weighted Imaging; Top Images: Phase only; Bottom Images: Phase and Magnitude Combined

Results:

Patient Demographics
• Mean age: PD subjects: 67.4 $\pm$1.27 years (range 55 – 82 years); control population: 66.83$\pm$1.29 (range: 58-81 years)
• PD subtypes: 17 akinetic-rigid, 7 tremor -dominant and 1 mixed
• UPDRS mean score 23; range 3 – 53; Hoehn and Yahr range 2 – 3

Volume Measurements (Figure 1)
•PD subjects had significantly smaller volume measurements of the left and right putamen (p< 0.05) in comparison to control subjects
•Significant negative correlations were found between UPDRS scores and volume measurements of the right caudate (R = -0.418; p < 0.05) and right globus pallidus (R= -0.51; p < 0.05)
•Tremor dominant subjects had significantly higher volume measurement of left putamen (p <0.05) in comparison to akinetic rigid subjects (p < 0.05)

Susceptibility Weighted Imaging (Figure 2)
•In comparison to controls, PD subjects had decreased mean SWI phase of the left subthalamic nucleus (p =0.055),and decreased mean SWI magnitude of the left substantia nigra (p=0.057) and right subthalamic nucleus (p=0.06)
•PD subjects had significantly lower entropy of the SWI magnitude in the right substantia nigra (p < 0.05) and the subthalamic nuclei bilaterally (p <0.05).
•Significant positive correlation was found between UPDRS scores and SWI phase entropy in the right subthalamic nucleus (R=0.45; p < 0.05)

Conclusions: Our findings demonstrate differences in imaging characteristics between PD and normal control subjects that involve alterations of both brain structure and increased iron deposition. Furthermore, the findings of correlations between these brain alterations and symptom severity indicates these changes may play a direct role in PD pathology. Further investigation of these MR imaging modalities as well as others that our group is concurrently studying will seek to further clarify if multimodal MRI is a valid objective tool in the diagnosis and monitoring of disease progression in PD.

Pilot Study 12:

The Neuropsychiatric Consequences of War: Investigating the Relationship between PTSD and Alcohol Abuse among Veterans Returning from Iraq and Afghanistan

Principal Investigator: Karen Seal, M.D., MPH
   Co-Director, OEF/OIF Integrated Care Clinic, San Francisco VA Medical Center
   Assistant Professor of Medicine and Psychiatry, University of California, San Francisco

ABSTRACT

A substantial proportion of veterans returning from Operation Enduring Freedom (OEF) and Operation Iraqi Freedom (OIF) suffer from one or more co-occurring mental health disorders. The VA has instituted an electronic clinical reminder to facilitate mental health post-deployment screening to rapidly assess symptoms of PTSD, depression and high-risk alcohol use among OEF/OIF veterans. The primary scientific aims of this DoD-funded study are to: 1) estimate the prevalence of positive screening tests for PTSD, depression and high-risk drinking, 2) among OEF/OIF veterans who screen positive for a mental health disorder, to determine the proportion who receive mental health treatment and the predictors of receiving mental health treatment, and 3) through rapid telephone assessment, using validated mental health screening instruments, to a) validate the VA post-deployment mental health screen and b) to determine barriers to mental health treatment. In a related study funded by the VA, we are piloting telephone-administered motivational interviewing (TAMI), a psychotherapeutic technique to enhance mental health treatment engagement among OEF/OIF veterans who screen positive for mental health disorders during the DoD-funded telephone survey. This work is relevant to the military and the VA because we will determine the effectiveness of mental health post-deployment screening to detect symptoms of mental illness and enhance follow-up mental health assessment of these symptoms. We will also ascertain specific barriers to mental health assessment and treatment among OEF/OIF veterans. In a related study, we will assess the effectiveness of telephone-administered motivational interviewing to overcome barriers to mental health care and enhance mental health treatment engagement among this high-risk population of OEF/OIF veterans. Our overall goal is to improve identification of mental health symptoms and enhance early intervention to prevent chronic mental illness and related disability.

TABLE OF CONTENTS

INTRODUCTION

Both the DoD and VA have instituted universal post-deployment mental health screening programs for returning military personnel and veterans of Operations Enduring Freedom (OEF) and Operation Iraqi Freedom (OIF), yet the effectiveness of these programs to increase mental health utilization among those screening positive for mental health symptoms has been questioned. [1, 2] This study evaluates the effectiveness of the VA post-deployment screen to increase mental health utilization among veterans screening positive for mental health symptoms. In addition, through telephone interviews with OEF/OIF veterans in Northern California, we will not only validate the VA post-deployment screen, but also explore barriers to mental health treatment and strategies to overcome these barriers. In a related randomized controlled trial funded by the VA, we are evaluating the effectiveness of telephone-administered motivational interviewing to increase engagement in mental health care among veterans screening positive for symptoms of mental health disorders. Our initial DoD funding was fundamental to securing additional funding from the VA and now forms the basis for four additional funded DoD/CDMRP grants. In addition, this initial DoD funding has directly and indirectly resulted in two published manuscripts, two manuscripts under review, one invited article, and several oral presentations at national and international conferences. The progress and products of the study are described below.

BODY (no SOW was required for the initial grant proposal)

In preparation to accomplish the stated aims of the DoD proposal (see below), we conducted the first national evaluation of the prevalence of mental health disorders among over 100,000 OEF/OIF veterans using VA healthcare. Using ICD-9 codes associated with visits to VA or VA-reminbursed facilities in the United States, we found that among 103,788 veterans of Iraq and/or Afghanistan, 32,010 (31%) received mental health and/or psychosocial diagnoses; the majority receiving multiple mental health diagnoses. The youngest group of returned veterans (18-24 years) were at greatest risk for receiving mental health or PTSD diagnoses compared to veterans aged $\geq$ 40 years [relative risk (RR)=3.32, 95% confidence interval (CI)=3.12-3.54] and PTSD (RR=5.04, 95% CI=4.52-5.62). Most initial mental health diagnoses originated from primary care settings. We concluded that targeted early detection and interventions beginning in primary care are needed to prevent chronic mental illness and disability. [3]

Aims 1 and 2:
1) To estimate the prevalence of positive screening tests for PTSD, depression and high-risk drinking and 2) among OEF/OIF veterans who screen positive for a mental health disorder, to determine the proportion who receive mental health treatment and the predictors of receiving mental health treatment.
We have completed the secondary data analyses associated with these aims and the article "Getting Beyond 'Don't Ask, Don't Tell': An Evaluation of VA Post-Deployment Mental Health Screening of Veterans Returning from Iraq and Afghanistan" was recently published in the American Journal of Public Health (2008). The abstract follows:

Objectives: To evaluate outcomes of the VA "Afghan and Iraq Post-Deployment Screen" for mental health symptoms.

Methods: Clinicians at one VA facility were encouraged to refer veterans of Iraq and Afghanistan who met the threshold for a positive screen for PTSD, depression and high-risk alcohol use to a VA mental health clinic. Univariate and multivariate methods were used to determine predictors of screening, the proportions screening positive for particular mental health problems, and predictors of attending a subsequent VA mental health appointment.

Results: From June 1, 2004 through June 30, 2006, of 750 Iraq and Afghanistan veterans seen, 338 underwent post-deployment screening; 233 (69%) met criteria for ≥ 1 positive mental health screens. Having been seen in primary care [adjusted odds ratio (AOR) =13.3, 95% CI=8.31-21.3] and at a VA community clinic (AOR=3.28, 95%CI=2.03-5.28) predicted screening, while African American veterans were less likely to be screened than Caucasian veterans (AOR=0.45, 95%CI=0.22-0.91). Of 233 veterans screening positive, 170 (73%) ultimately completed a mental health follow-up visit.

Conclusions: Based on data from one VA facility, post-deployment mental health screening increases mental health visits among returning veterans.

Two tables and two figures from the manuscript are shown below:

Table 1. Predictors of post-deployment screening among OIF/OEF veterans (n=645)[1,2]				
Characteristic	**Not Screened n (%)**	**Screened n (%)**	**Adjusted Odds Ratio (95% CI)**	**p-value**
Race/Ethnicity				
White	213 (51)	207 (49)	Ref	
Hispanic	54 (61)	34 (39)	0.83 (0.44 - 1.54)	0.55
Black	49 (71)	20 (29)	0.45 (0.22 - 0.91)	0.03
Other	40 (59)	28 (41)	0.83 (0.42 - 1.65)	0.60
Facility Type				
VA medical center	343 (63)	201 (37)	Ref	
VA community clinic	13 (13)	88 (87)	3.56 (1.78 - 7.11)	0.00
Any Visits to Primary Care				
No	257 (88)	36 (12)	Ref	
Yes	99 (28)	253 (72)	13.3 (8.31 – 21.3)	0.00
Any Visits to MH Clinic				
No	287 (69)	126 (31)	Ref	
Yes	69 (30)	163 (70)	3.28 (2.03 - 5.28)	0.00

[1] The population size was reduced from 750 to 645 to include only veterans with non-missing values for study variables.

[2] In addition to the predictor variables shown above, the multivariate model was adjusted for age, gender and total number of visits to the VA.

Figure 1: Of OIF/OEF veterans screening positive for mental health symptoms (n=233), the proportions of veterans screening positive for symptoms of PTSD, depression, high-risk alcohol use and co-morbid symptoms are shown below.
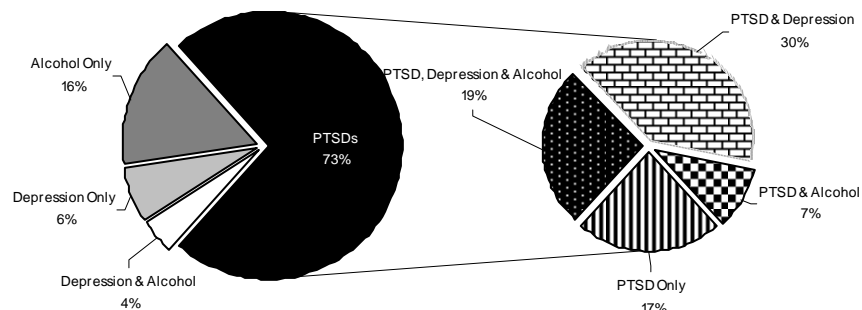

Figure 2: Mental health (MH) appointments scheduled and completed following post-deployment screening among 750 OEF/OIF veterans seen at a single VA medical center and associated community-based outpatient clinics (9/11/2001-6/30/06)
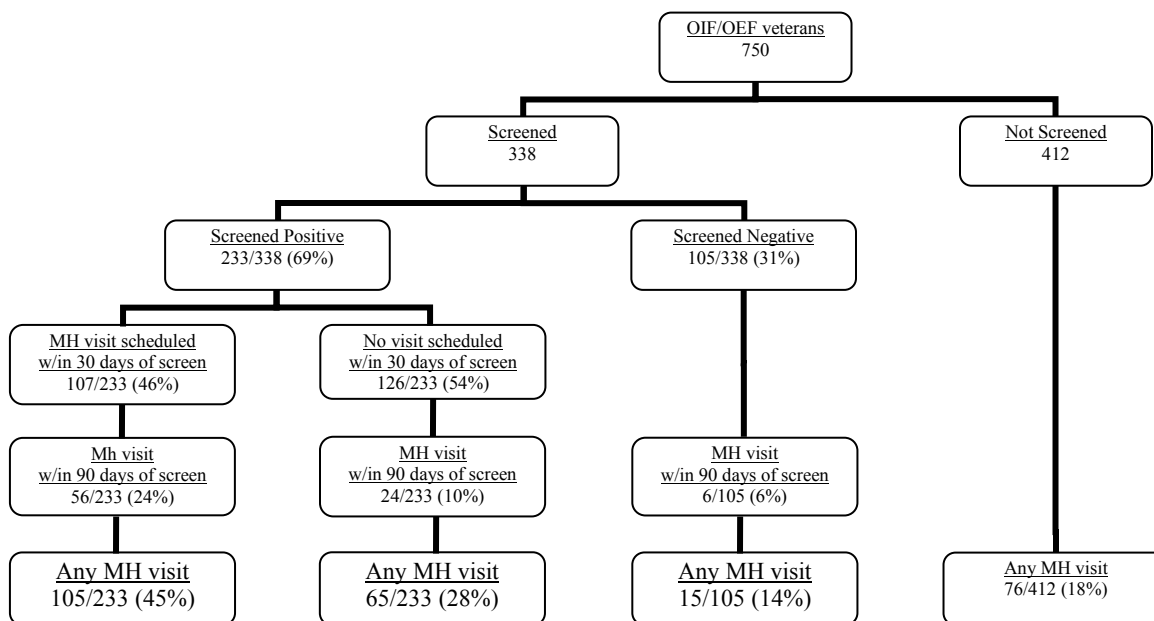
Table 2. Predictors of mental health visits within 90 days of screen among OEF/OIF veterans (n=159)[1]						
Characteristic	**MH visit w/in 90 days [2]**		**No MH visit w/in 90 days [2]**		**AOR (95% CI)**	**p-value**
	n (%)		**n (%)**			
PTSD screen						
Negative	8	(8)	91	(92)	Ref	
Positive	38	(63)	22	(37)	19.84 (6.16 - 63.9)	0.00
Depression screen						
Negative	17	(15)	96	(85)	Ref	
Positive	29	(63)	17	(37)	5.51 (1.79 - 17.0)	0.00
High-risk alcohol use						
Negative	27	(26)	78	(74)	Ref	
Positive	19	(35)	35	(65)	1.19 (0.39 - 3.61)	0.76
Gender						
Female	4	(31)	9	(69)	Ref	
Male	42	(29)	104	(71)	0.89 (0.07 - 10.8)	0.93
Age						
18-24	23	(36)	41	(64)	Ref	
25-29	11	(24)	35	(76)	0.85 (0.25 - 2.92)	0.80
30-39	10	(33)	20	(66)	4.18 (0.73 - 23.9)	0.11
40+	2	(11)	17	(89)	0.29 (0.02 - 3.34)	0.32
Race/Ethnicity						
White	32	(28)	81	(72)	Ref	
Hispanic	5	(28)	13	(72)	0.67 (0.12 - 3.87)	0.66
Black	5	(39)	8	(61)	4.79 (0.54 - 42.1)	0.16
Other	4	(27)	11	(73)	3.24 (0.49 - 21.7)	0.23
Component type						
National Guard/Reserve	15	(21)	55	(79)	Ref	
Active duty	31	(35)	58	(65)	2.23 (0.65 - 7.67)	0.20
Facility type						
VA medical center	22	(20)	87	(80)	Ref	
VA community clinic	24	(48)	26	(52)	6.08 (1.56 - 23.6)	0.01
Any visits to primary care						
No	1	(9)	10	(91)	Ref	
Yes	45	(30)	103	(70)	19.4 (1.30 - 290)	0.03
Number of non-MH visits						
Number of Visits (Mean, SD)[2]	14.5	16.2	12.2	12.1	1.03 (0.98 - 1.07)	0.26

[1] The population size was reduced to include only veterans with all three screens and no mental health visits prior to post-deployment screening and veterans with non-missing values for study variables.

[2] The column numbers represent numbers and percents for all characteristics except the "Number of non MH visits" where the column numbers represent the mean and SD of the column group.

Future Directions:
1) We are expanding this single center analysis of the effectiveness of post-deployment mental health screening to include multiple affiliated VA medical centers and community-based outpatient clinics in Northern California.
2) We were recently approved to submit a VA Merit proposal to investigate the effectiveness of VA traumatic brain injury (TBI) screening and health services utilization in veterans who screen positive for TBI.

Aims 3a and 3b:

3) Through rapid telephone assessment using validated mental health screening instruments, to a) validate the VA post-deployment mental health screen and b) to determine barriers to mental health treatment.

We initiated the third aim of this study 8/29/07 which was made possible through a companion VA MERIT grant (VA CSR&D 06S-VNIMH-03). We are in the second year of this grant and have conducted rapid telephone-administered mental health assessments in a total of over 130 Northern California-based OEF/OIF veterans. Standard, previously validated mental health screening measures are used to assess symptoms of PTSD (PCL-M), depression (PHQ-9), high-risk alcohol use (AUDIT) and illicit substance use (modified ASI). Among the majority of OEF/OIF veterans in this study who have already undergone VA post-deployment mental health screening, we will use the results of the standardized telephone screen to validate the VA post-deployment screening instrument. We will conduct the validation analysis (calculations of sensitivity and specificity) once we have 200 participants who have undergone both VA post-deployment screening and standardized mental health assessments through our current study to ensure adequate power. Recruitment has progressed more slowly because of the need for additional funding, staff turn-over and lower rates of recruitment than anticipated. Veterans who screen positive for mental health disorders but are not currently in mental health treatment are assessed for specific barriers to accessing mental health care and, if otherwise eligible, randomized to either an experimental motivational interviewing (MI) arm or a control arm. MI is a psychotherapeutic technique used to elicit the veteran's intrinsic motivation for positive change. In Phase 1 of this study, MI was compared to a control condition which was defined as psychoeducation balanced for time and attention to the intervention arm. Veterans in both study arms received referrals for VA or other mental health services. Over 6 months, we determined the effectiveness of MI versus control (psychoeducation) to (1) increase mental health treatment engagement (primary outcome) and (2) decrease mental health symptoms and improve functioning (secondary outcome).

We have made progress since our last report. We have hired a new project director, Ms. Kathleen McCartney, who started 4/1/08. We currently have 2 part-time interviewers and a full-time study coordinator all of whom have undergone rigorous training in motivational interviewing. We have a nationally-recognized motivational interviewing trainer/consultant (Steven Berg-Smith) who has provided the initial motivational interviewing training and now oversees the interviewers' MI sessions, providing additional training and feed-back as needed. We have hired two motivational interviewing coders who are blinded to group assignment and code each of the study interviews for MI fidelity. Below, we present some data from Phase 1 of our pilot motivational interviewing study which closed June 2008. During Phase 1, we enrolled 88 OEF/OIF veterans and conducted baseline assessments. We collected baseline information

on sociodemographics, military service and combat exposure. We also conducted baseline assessments for mental disorders and functional status, as well as perceived barriers to mental health treatment:

Table 1. Sociodemographics of OEF/OIF veterans (n=88)

	%
Age	
23-29	57
30-39	26
40-61	17
Sex	
Female	18
Male	82
Race	
White	57
Latino	14
Asian	14
African American	7
Other (Pacific Islander)	9
Education	
High School/GED	15
Some College	60
College Graduate	11
Post College	14
Marital Status	
Married/Domestic partner	38
Separated/Divorced	14
Never Married	48

Table 2. Military Service Characteristics of OEF/OIF veterans (n=88)

	%
Rank	
Enlisted	84
Officer	16
Service Branch	
Air Force	11
Army	36
Marine Corp	34
Navy	17
Service Component	
Active Duty	72
National Guard/Reserves	11
Reserves	17
Deployment Area	
OIF	68
OEF	10
Both	22
Number of Deployments	
0	6
1	50
2	26

> 2	18
Combat Exposure	
Low (0-1)	23
Medium (2-4)	35
High (5-6)	42

Table 3. Mental health (MH) screen results in OEF/OIF Veterans (n=88)

Mental Health Disorders[1]	% with positive screens
None	28
PTSD	34
Depression	50
Substance use disorders	40
Alcohol	41
Co-Morbid MH Disorders	
1 Screen Positive	24
2 Screens Positive	27
3 Screen Positive	16
4 Screens Positive	5

Table 4. Perceived functional status and barriers to mental health treatment in OEF/OIF veterans (n=88)

Perceived functional status	Mean score of 100 (SD)
Physical functioning	85 (26)
Physical limitations	80 (29)
Bodily Pain	79 (29)
General Health	67 (27)
Vitality	54 (31)
Social functioning	74 (31)
Emotional functioning	77 (30)
Mental Health	63 (24)
Perceived barriers* (n=80, missing 8)	**Percent**
Don't trust mental health professionals	10
Don't where to get help	8
Don't have transportation	8
Difficult to schedule appointment	26
Difficult to get time off from work	28
Mental health care costs too much	21
It would be too embarrassing*	23
It would harm career*	30
Peers might have less confidence in me*	25
Boss (superiors) might treat me differently*	28
Boss (superiors) might blame me*	9
I would be seen as weak*	31
Mental healthcare doesn't work	6
I don't have childcare	0

* Constitute "stigma" barriers

Of those undergoing baseline assessment, 63 (72%) screened positive for at least one mental health disorder and of these, 31 met inclusion criteria and were randomized for the trial: 17 participants were randomized to the MI arm and 14 participants were randomized to the control arm. Participants in the RCT were contacted again at 1 and 3 months for motivational interviewing versus control (psychoeducation) and again at 6 months for assessment only. (See Figure below.)

Phase 1: Enrollment, Randomization and Follow-up

103 Scheduled for phone baseline assessment

→ **15 No Show**

88 completed baseline assessment

57 excluded from RCT
• 32 current or past 60-day MH Tx
• 24 negative on MH assessment
• 1 moving within 6 months

31 enrolled in RCT

Psycho-education (n=14)	Motivational Interviewing (n=17)
1-month follow-up n=13 (93)	1-month follow-up n=13 (77)
3-month follow-up n=10 (71)	3-month follow-up n=11 (66)
6-month follow-up n=10 (71)	6-month follow-up n=12 (71)

Our preliminary analysis of the primary outcome, mental health treatment engagement, reveals that there was only a small (non-significant) difference between the intervention arm (MI) and control arm: 7/17 (41%) veterans in the MI and 5/14 (36%) veterans in the control arm had at least one VA or non-VA mental health visit during the 6-month follow-up period. While, our study was clearly under-powered, we determined that the effect size between intervention and control was not great enough and that the study needed modification to establish proof of concept for MI. felt that the trend toward increased mental health treatment engagement in the MI arm was not strong enough indicted that the study design needed to be modified.

We examined secondary outcomes, change in mental health symptoms and functioning, at two of the subsequent time points (3 and 6) using a repeated measures analysis (ANCOVA). At 6 months we found a borderline statistically significant improvement in PTSD symptoms (p=0.08) and in social (p=0.05) and mental health (p=0.03) functioning in the MI group compared to control. There were no other significant changes in symptom scores however between the two groups.

Based on these Phase 1 data, we have made several small, but important changes to the RCT study design. First, we have intensified and broadened the recruitment strategy to achieve aim 3. Second, we have intensified the MI intervention by re-training interviewers, opening MI with a psychoeducation component (normative feedback), adding an additional MI session, and lengthening each MI session. Third, we have deleted the psychoeducational component from control (too similar to MI), opting for brief neutral telephone check-in calls instead. Fourth, we have added more process outcomes to capture readiness to change or motivation to enter mental health treatment or to make other positive behavioral changes. Finally, we have broadened the

primary outcome to also include engagement in veterans' service organizations re-adjustment programs for OEF/OIF veterans. In May, 2008 we initiated Phase 2 and to date, have interviewed 43 OEF/OIF participants at baseline and 7 participants have entered the randomized controlled trial. With Phase 1 and 2 pilot data, in 2009 we will apply for an NIH grant to expand the MI RCT.

Current Related Studies:
Currently, we are using national-level VA clinical data to conduct several related secondary data analyses of this accruing population of OEF/OIF veterans with mental health disorders in collaboration with other SFVAMC investigators. We have recently submitted a manuscript describing trends in the prevalence of mental health disorders in OEF/OIF veterans from 2002-2008. Of 289,328 Iraq and Afghanistan veterans, 106,726 (36.9%) received mental health diagnoses; 62,929 (21.8%) were diagnosed with post-traumatic stress disorder (PTSD) and 50,432 (17.4%) with depression. Adjusted 2-year prevalence rates of PTSD increased 4-7 times after the invasion of Iraq. Active duty veterans < age 25 had the highest rates of PTSD, alcohol and drug use disorder diagnoses compared to active duty veterans > age 40 [adjusted relative risk (ARR) = 2.0-4.9]. Women were at higher risk for depression than men, while men were over twice the risk for drug use disorders. Proxies for greater combat exposure were associated with higher risk for PTSD in active duty veterans. A second manuscript is under review that compares medical health services utilization in OEF/OIF veterans with and without mental health disorders and PTSD. We have recently completed a third data analysis of VA mental health services utilization in OEF/OIF veterans with mental health and PTSD diagnoses and are preparing a manuscript for publication. Other active or planned analyses include: (1) the prevalence and predictors of mental health disorders in women OEF/OIF veterans and their unique patterns of mental health utilization (Dr. S Maguen-lead), (2) the prevalence of cardiovascular risk factors in OEF/OIF veterans (Dr. B Cohen-lead), and (3) the association of sleep disorders and PTSD in returning combat veterans (Dr. T Neylan-lead).

KEY RESEARCH ACCOMPLISHMENTS

We are very grateful for our original DoD pilot funding as this initial funding has resulted in additional funding and projects, manuscripts, national and international scientific presentations, several new related projects in development and participation in local and national committees

CURRENT FUNDING
1. W81XWH-05-2-0094 (PI)   09/06-08/08
    Department of Defense $143,000 direct/yr 1
    The Neuropsychiatric Consequences of War $286,000 direct/yrs 1-2
    among Veterans Returning from Combat in Iraq and Afghanistan

2. VA Career Development Transition Award (PI)   02/01/07-02/28/09
    Department of Veterans Affairs $195,200 direct/yr 1
    Facilitating Mental Health Treatment for OEF/OIF Veterans $390,400 direct/yrs 1-2

3. MN078889-01 (PI)   07/07-10/10
    VA CSR&D MERIT $150,000 direct/yr 1
    Motivational Interviewing to Engage OEF/OIF Veterans in $450,000 direct/yrs 1-3
    Mental Health Treatment

RECENTLY FUNDED OR APPROVED FOR FUNDING

4. PT-073238   (PI)   09/08-08/10
        Congressionally Directed Medical Research Program (CDMRP) $100,000 direct/yr 1
        Integrating Mental Health and Primary Care Services for $150,000 direct/yrs 1-1 ½
        OEF/OIF Combat Veterans with PTSD and Co-Morbid
        Disorders: Assessing the Evidence

5. PT-075369 (PI)   09/08-08/11
        Congressionally Directed Medical Research Program (CDMRP) $100,000 direct yr 1
        Does Integrating Primary Care and Mental Health Services $300,000 direct, yrs 1-3
        Improve Mental Health Services Utilization, Symptoms and
        Functioning among OEF/OIF Veterans?

6. PT-O73505   (Co-Investigator)   09/08-08/10
        Congressionally Directed Medical Research Program (CDMRP) $100,000 direct yr 1
        The Prevalence and Incidence of PTSD in OEF/OIF Women $150,000 direct yrs 1-1 ½
        Combat Veterans

7. NCIRE/DoD Neuroscience Center of Excellence, (Co-Investigator)   09/08-09/10
        Disentangling the Relationship between Traumatic Brain Injury,   150,000, direct yr 1
        PTSD, and Other Mental Health Disorders.   300,000, direct yrs 1-2

Scientific Manuscripts and Invited Articles:

Seal, KH, Bertenthal D, Miner CR, Sen S, Marmar C. Bringing the war back home: mental health disorders among 103,788 us veterans returning from Iraq and Afghanistan seen at VA facilities, Arch Intern Med. Mar 12;167 (5):476-82, 2007.

Seal KH, Bertenthal D, Maguen S, Gima K, Chu A, Marmar CR. Getting beyond 'don't ask, don't tell': an evaluation of VA post-deployment mental health screening of veterans returning from Iraq and Afghanistan. Am J Public Health. 98(4): 714-20, Apr 2008.

Seal KH, Maguen S, Bertenthal D, Gima K, Marmar CR. Response to Letter to the Editor by Rona. Am J Public Health. Sep 2008**;** 98: 1542 - 1543.

Seal KH, Metzler TJ, Gima K, Bertenthal D, Maguen S, Marmar CR. Growing burden of mental disorders among Iraq and Afghanistan veterans: Trends and risk factors for mental health diagnoses in new users of VA healthcare, 2002-2008. Manuscript under review.

Cohen BE, Kim S, Bertenthal D, Marmar CR, **Seal KH.** Higher rates of VA non-mental health services utilization in Iraq and Afghanistan veterans with PTSD. Manuscript under review.

Related National and International Presentations

• **Seal KH**, "Challenges to Detection and Management of PTSD and Other Mental Disorders in Primary Care", VA Integrated Primary Care Mental Health Care Conference, Seattle, WA, August, 2008.

- **Seal KH**, "Integrated Care for OEF/OIF Veterans: Building a New Clinic", VA Integrated Primary Care Mental Health Care Conference, Seattle, WA, August, 2008.

- **Seal KH**, "Success of Integrated Primary Care Mental Health Clinic for Iraq and Afghanistan Veterans with Co-Morbid PTSD and Traumatic Brain Injury, Brain at War Conference, SFVAMC, May 2008

- **Seal KH**, Metzler TJ, Gima K, Bertenthal D, Maguen S, Marmar CR. The Prevalence and Incidence of Mental Health Disorders Following the US Invasion of Afghanistan and Iraq in over 200,000 New Veterans Utilizing VA Healthcare, 2002-2007. Oral presentation at the <u>VA HSR&D National Conference</u>, February 15, 2008, Baltimore, MD.
.
- **Seal KH. "**Bringing the War Back Home: PTSD and Mental Health Problems among Veterans Returning from Iraq and Afghanistan. Invited presentation for the University of California, San Francisco "Iraq War Teach-In," May, 9. 2007.

- **Seal KH,** Bertenthal D, Chu A, Gima K, Marmar, C. VA Post-Deployment Screening for Mental Health Disorders among Veterans Returning from Iraq and Afghanistan- Are We Doing a Good Job? Oral presentation at <u>Society for General Internal Medicine</u> 30th Annual Meeting, Toronto, Canada, April 25-28, 2007.

- **Seal KH.** Suicide Risk in Primary Care: Assessment and Management. Grand Rounds Presentation <u>for National Suicide Prevention Awareness Day</u>, San Francisco VA Medical Center, March 26, 2007

- **Seal KH,** Bertenthal D, Chu A, Gima K, Marmar, C. OEF/OIF Veterans with PTSD are High Utilizers of Non-Mental Health VA Services. Poster presentation at <u>VA HSR&D National Conference</u>, February 23, 2007, Arlington, VA.

- **Seal KH.** Bringing the War Back Home: PTSD and Mental Health Disorders among Veterans Returning from Iraq and Afghanistan, Invited Presentation for <u>VA Research Week</u>, San Francisco VA Medical Center, May 5, 2006

- **Seal KH,** Bertenthal D, Miner CR, Sen S, Marmar C. Mental Health Disorders among Veterans of Operations Iraqi Freedom and Enduring Freedom. Plenary Talk at the <u>Society for General Internal Medicine Conference</u>, April, 2006, Los Angeles, California.

- **Seal KH,** Miner CR, Chu A, Bertenthal D. VA Post-Deployment Screening and Treatment Referral of OEF/OIF Veterans: How Well Are We Doing? Oral presentation at <u>VA HSR&D National Conference</u>, 2006, Arlington, VA.

Committee/Clinical Participation/Leadership:

- PTSD/TBI research working group VISN 21

- Operations Enduring Freedom/Operations Iraqi Freedom, SFVAMC Hospital Steering Committee (2007-current).

- National VA Substance Use Disorders QUERI-PTSD working group (2007-current).

REPORTABLE OUTCOMES

<u>**Mental health diagnoses in OEF/OIF veterans using VA facilities**</u>
1) Through September 30, 2005, in103,788 veterans of Iraq and/or Afghanistan, 32,010 (31%) received mental health and/or psychosocial diagnoses; the majority receiving multiple mental health diagnoses.

2) The prevalence of mental health diagnoses among OEF/OIF veterans continues to increase: through March 2008, 37% received mental health diagnoses; PTSD being the most common, followed closely by depression.

3) The youngest group of OEF/OIF veterans (18-24 years) reamin at greatest risk for receiving mental health diagnoses, including PTSD, alcohol or substance use disorder diagnoses compared to veterans aged $\geq$ 40 years. Women OEF/OIF veterans are significantly more likely to report depression than their male counterparts.

<u>**VA post-deployment mental health screening**</u>

4) From June 1, 2004 through June 30, 2006, among 750 Iraq and Afghanistan veterans, 338 (45%) underwent post-deployment screening. Having been seen in primary care and at a VA community clinic was associated with higher rates of screening, while African American veterans were less likely to be screened than Caucasian veterans.

5) Of 233 veterans screening positive, 170 (73%) ultimately completed a mental health follow-up visit. Based on data from one VA facility, post-deployment mental health screening increases mental health visits among returning veterans.

<u>**Motivational interviewing in OEF/OIF veterans to overcome barriers to care**</u>

6) Motivational interviewing shows promise as a technique to enhance mental health treatment engagement in OEF/OIF veterans who screen positive for mental health disorders.

CONCLUSIONS

The purpose of this DoD study is to describe the VA post-deployment screening process and to determine whether the national VA post-deployment screening program facilitates follow-up mental health assessment for OIF/OEF veterans screening positive for symptoms of mental health disorders. Our preliminary results indicate that a substantial proportion of OIF/OEF veterans screen positive for symptoms of co-occurring mental health problems, suggesting that the VA screens may help overcome a "don't ask, don't tell" climate surrounding stigmatized mental illness. Moreover, OIF/OEF veterans screening positive are far more likely than veterans screening negative or not screened at all to attend follow-up mental health appointments within 90 days of screening. Nevertheless, there are several areas for potential improvement in the screening program. First, fewer than half of OIF/OEF veterans seen at these VA facilities were screened, and efforts should be made to better understand differential screening rates. Second, a

high proportion of those screened were positive for co-occurring mental health symptoms, yet less than half received a scheduled appointment within 30 days and less than one-quarter attended a VA mental health clinic appointment within 90 days of the post-deployment screen. In sum, these preliminary results suggest that improvements are needed in the VA OIF/OEF post-deployment screening program with an emphasis on minimizing barriers to receiving psychological care.   Through telephone interviews with OEF/OIF veterans in Northern California, we will validate the VA post-deployment screen and will continue explore barriers to mental health treatment.   In a related randomized controlled trial funded by the VA, we will evaluate the effectiveness of telephone-administered motivational interviewing to increase engagement in mental health care among veterans screening positive for symptoms of mental health disorders.

REFERENCES

1.   Hoge CW, Auchterlonie JL, Milliken CS. Mental health problems, use of mental health services, and attrition from military service after returning from deployment to Iraq or Afghanistan. *Jama* 2006;295:1023-32.

2.   Seal KH BD, Maguen S, Gima K, Chu A, Marmar CR. Getting Beyond 'Don't Ask, Don't Tell': An Evaluation of VA Post-Deployment Mental Health Screening of Veterans Returning from Iraq and Afghanistan. *Am J Public Health* 2008; 98(4):714-20.

3.   Seal KH, Bertenthal D, Miner CR, Sen S, Marmar C. Bringing the war back home: mental health disorders among 103,788 US veterans returning from Iraq and Afghanistan seen at Department of Veterans Affairs facilities. *Arch Intern Med* 2007;167:476-82.

APPENDICES

Articles:

Appendix I: (Total 7 pages)
Seal KH, Bertenthal D, Miner CR, Sen S, Marmar CR. Bringing the War Back Home: Mental health Disorders among 103,788 Veterans returning from Iraq and Afghanistan Seen at VA Facilities. *Arch Intern Med.* 2007 Mar 12;167 (5):476-82.

Appendix II: (Total 2 pages)
Seal KH, Maguen S, Bertenthal D, Gima K, Marmar CR. Response to Letter to the Editor by Rona. Am J Public Health. Sep 2008**;** 98: 1542 - 1543.

Appendix III: (Total 7 pages)
Seal KH, Bertenthal D, Maguen S, Gima K, Chu A, Marmar CR. Getting Beyond 'Don't Ask, Don't Tell': An Evaluation of VA Post-Deployment Mental Health Screening of Veterans Returning from Iraq and Afghanistan. *Am J Public **Health**.* Apr 2008; 98: 714-720

SUPPORTING DATA
N/A

Bringing the War Back Home

Mental Health Disorders Among 103 788 US Veterans Returning From Iraq and Afghanistan Seen at Department of Veterans Affairs Facilities

Karen H. Seal, MD, MPH; Daniel Bertenthal, MPH; Christian R. Miner, PhD; Saunak Sen, PhD; Charles Marmar, MD

Background: Veterans of Operations Enduring Freedom and Iraqi Freedom (OEF/OIF) have endured high combat stress and are eligible for 2 years of free military service–related health care through the Department of Veterans Affairs (VA) health care system, yet little is known about the burden and clinical circumstances of mental health diagnoses among OEF/OIF veterans seen at VA facilities.

Methods: US veterans separated from OEF/OIF military service and first seen at VA health care facilities between September 30, 2001 (US invasion of Afghanistan), and September 30, 2005, were included. Mental health diagnoses and psychosocial problems were assessed using *International Classification of Diseases, Ninth Revision, Clinical Modification* codes. The prevalence and clinical circumstances of and subgroups at greatest risk for mental health disorders are described herein.

Results: Of 103 788 OEF/OIF veterans seen at VA health care facilities, 25 658 (25%) received mental health di-

agnosis(es); 56% of whom had 2 or more distinct mental health diagnoses. Overall, 32 010 (31%) received mental health and/or psychosocial diagnoses. Mental health diagnoses were detected soon after the first VA clinic visit (median of 13 days), and most initial mental health diagnoses (60%) were made in nonmental health clinics, mostly primary care settings. The youngest group of OEF/OIF veterans (age, 18-24 years) were at greatest risk for receiving mental health or posttraumatic stress disorder diagnoses compared with veterans 40 years or older.

Conclusions: Co-occurring mental health diagnoses and psychosocial problems were detected early and in primary care medical settings in a substantial proportion of OEF/OIF veterans seen at VA facilities. Targeted early detection and intervention beginning in primary care settings are needed to prevent chronic mental illness and disability.

Arch Intern Med. 2007;167:476-482

Author Affiliations:
Departments of Medicine (Dr Seal), Epidemiology and Biostatistics (Dr Sen), and Psychiatry (Dr Marmar), University of California, San Francisco, and Health Services Research and Development Research Enhancement Award Program (Mr Bertenthal), San Francisco VA Medical Center, San Francisco (Drs Seal, Miner, Sen, and Marmar).

RECENT MILITARY OPERATIONS in Iraq and Afghanistan represent the most sustained ground combat operations involving American forces since the Vietnam era.[1,2] The majority of military personnel experience high-intensity guerrilla warfare and the chronic threat of roadside bombs and improvised explosive devices.[1,2] Some soldiers endure multiple tours of duty, many experience traumatic injury, and more of the wounded survive than ever before.[3-5] Reports have suggested high rates of mental health disorders including posttraumatic stress disorder (PTSD), depression, and alcohol use disorders among active duty military personnel and veterans of Operation Iraqi Freedom (OIF) and, to a lesser extent, Operation Enduring Freedom (OEF).[3,5-7]

Separated OEF/OIF veterans are eligible for 2 years of free military service–

related health care through the Department of Veterans Affairs (VA). Nevertheless, there have been no recent detailed reports in the medical literature to describe the prevalence of single and co-occurring mental health diagnoses and psychosocial problems among OEF/OIF veterans seen at VA facilities after returning from Iraq and Afghanistan. This information is critical to developing targeted programs for early detection and intervention to prevent chronic mental illness among OEF/OIF veterans. The aim of this study was to (1) describe the proportion of OEF/OIF veterans seen in VA facilities who have received single or multiple mental health and/or psychosocial diagnoses and the timing and clinical setting of first mental health diagnoses and (2) identify subgroups of OEF/OIF veterans at high risk for receiving mental health diagnoses after returning from military service in Iraq and/or Afghanistan.

STUDY POPULATION

The present study includes OEF/OIF veterans who are new users of the VA health care system and included in the VA OEF/OIF Roster database (N = 165 351 as of November 1, 2005, when we accessed the OEF/OIF Roster).[8] For an OEF/OIF veteran to be included in the VA OEF/OIF Roster, the veteran must (1) be listed in the most recent enrollment file provided by the VA Health Eligibility Center or have had a VA clinic visit and/or (2) be included in the US Department of Defense, Defense Manpower Data Center database. The Defense Manpower Data Center database of the Department of Defense lists veterans separated from OEF/OIF service, and as of November 2005, 29% had accessed VA health care.[9] Approximately half of the VA OEF/OIF Roster derives from both sources (Defense Manpower Data Center and VA Health Eligibility Center), and about half derives from Defense Manpower Data Center only.

More than half (53%) of the veterans included in the roster lacked OEF/OIF service separation dates. Because we were interested in mental health diagnoses and psychosocial problems associated with military service in Iraq and Afghanistan, we defined our study population as veterans first seen at a VA facility after September 30, 2001 (the date of the US invasion of Afghanistan) through December 31, 2005, but excluded veterans listed in the VA OEF/OIF Roster if they (1) were listed in the VA Health Eligibility Center database only (n = 6369) (because OEF/OIF service could not be corroborated with Department of Defense data), (2) had a visit to a VA facility before September 30, 2001 (n = 24 172), or before to their OEF/OIF service separation date (n = 16 087), and (3) had not been seen at a VA facility by September 30, 2005 (n = 14 810). The study was approved by the Committee on Human Research, University of California, San Francisco, and the San Francisco VA Medical Center.

SOURCE OF DATA

The VA OEF/OIF Roster includes information on veterans' sex, race, date of birth, service separation date, and armed forces component (National Guard or Reserve vs active duty). Both components are voluntary, although active duty members join as full-time personnel, whereas members of the National Guard and Reserve join as part-time personnel who then become full-time when called to duty.

Encrypted social security numbers of 103 788 OEF/OIF veterans listed in the OEF/OIF Roster database were used to link to VA administrative and clinical data contained within the VA National Patient Care Database (NPCD) and Fee Basis records. National VA databases have been used extensively in epidemiological studies to describe patterns of disease and health care utilization among veterans.[10,11] Clinical data contained within the VA NPCD are derived from outpatient and inpatient visits to any of the nearly 1300 VA health care facilities nationwide, and fee basis records represent care rendered at other health care facilities reimbursed by the VA. For all VA visits, an electronic record is generated that includes the date of the visit, outpatient clinic or inpatient type, and the diagnosis(es) associated with the visit coded using the *International Classification of Diseases, Ninth Revision, Clinical Modification* (*ICD-9-CM*) codes. Mental health clinic visits were defined as all outpatient and inpatient visits to mental health and substance abuse services, while nonmental health visits were either outpatient visits or inpatient admissions to nonmental health services. Currently, available VA databases lacked data regarding income, education, duration of military service, military rank, branch, and pay grade for OEF/OIF veterans.

The *ICD-9-CM* codes associated with specific VA inpatient and outpatient visits were used to categorize mental health diagnoses as they accrued from the date of the first VA visit to December 31, 2005. We allowed for up to 10 distinct *ICD-9-CM* codes for each inpatient or outpatient encounter. Mental health diagnoses were defined as any *ICD-9-CM* diagnosis from 290.0 to 319.0, corresponding to the *Diagnostic and Statistical Manual of Mental Disorders, Fourth Edition, Revised* (*DSM-IV-R*).[12] In addition, we examined several individual *ICD-9-CM* mental health diagnostic categories that have been associated with military service[2,3,5,13]: anxiety disorders, PTSD, depressive disorders, substance use disorders (which included alcohol and illicit drug abuse and dependence but excluded nicotine dependence), acute stress reaction, adjustment disorders, and other mental health diagnoses. The category "other mental health diagnoses" comprised all *ICD-9-CM* mental health diagnoses excluding the military service–related categories listed previously. The category "psychosocial or behavioral problems" consisted of selected *ICD-9-CM* V-codes, a supplementary classification used to describe problems that are a focus for mental health treatment but are not considered mental health diagnoses.[14,15] Because *ICD-9-CM* codes may be considered provisional or "rule-out" diagnoses, we evaluated the proportion of diagnoses that were assigned on 2 or more separate clinical encounters. Also, if a mental health diagnosis was initially made in a nonmental health care setting, we determined the proportion that subsequently received the same mental health diagnosis at a follow-up mental health visit.

STATISTICAL ANALYSES

This was a descriptive analysis of the prevalence, clinical setting, and timing of mental health diagnoses among OEF/OIF veterans who were new users of VA health care. We also determined the relative risks (RRs) and 95% confidence intervals (CIs) of receiving mental health diagnoses associated with various sociodemographic and military service characteristics. Because of the large sample size, nearly all comparisons between subgroups were statistically significant, and for this reason, we examined effect sizes to determine what constituted clinically meaningful differences between subgroups. Moreover, because the measured demographic characteristics (eg, age) may serve as markers for other unmeasured characteristics (eg, combat exposure) and the relationships between measured and unmeasured covariates are complex, multivariable adjustment has the potential to mislead. Instead, we calculated stratum-specific RRs (using strata defined by combinations of observed characteristics), enabling us to identify subgroups of OEF/OIF veterans at increased risk for receiving mental health and PTSD diagnoses. All statistical analyses were conducted using STATA software, version 8.2 (StataCorp, College Station, Tex).

RESULTS

CHARACTERISTICS AND VA HEALTH SERVICES UTILIZATION OF OEF/OIF VETERANS

Table 1 gives the sociodemographic and military service-related characteristics of 103 788 OEF/OIF veterans seen at VA facilities nationwide. A substantial minority were women (13%); more than half were younger than 30 years (54%); nearly one third were members of ethnic minority groups; and nearly half were veterans of the National Guard or Reserve components.

Service separation data were available for 47% of the study population, and of these, the median time from OEF

Table 1. Characteristics of OEF/OIF Veterans Seen at VA Health Care Facilities

Characteristic	No. (%) of Veterans (n = 103 788)
Sex	
Male	90 117 (87)
Female	13 652 (13)
Age, y	
18-24	27 167 (26)
25-29	29 185 (28)
30-39	22 230 (22)
≥40	25 206 (24)
Race	
White	68 765 (69)
Black	18 165 (18)
Hispanic	11 410 (11)
Other*	2155 (2)
Marital status†	
Never married	35 249 (47)
Married	32 434 (43)
Divorced	7124 (10)
Separated or widowed	267 (0.4)
Service type	
Active duty	54 387 (52)
National Guard/Reserve	49 401 (48)
Service end date‡	
Oct 2001–Nov 2002	282 (0.6)
Nov 2002–Oct 2003	4803 (10)
Nov 2003–Oct 2004	24 239 (50)
Nov 2004–Oct 2005	19 165 (40)

Abbreviations: OEF/OIF, Operations Enduring Freedom and Iraqi Freedom; VA, Department of Veterans Affairs.

*Race categories in the OEF/OIF Roster are crude. "Other" refers to ethnic minority groups other than blacks and Hispanics.

†A total of 28 714 veterans (28%) lacked data for marital status.

‡A total of 55 299 veterans (53%) lacked data for service end date.

or OIF service separation to the first VA clinic visit was 2.9 months (intraquartile range [IQR], 1.3-6.0 months). Among all 103 788 OEF/OIF veterans, the median time in the VA system from the first VA clinic visit until the study end date (December 30, 2005) was 7.8 months (IQR, 2.9-14.5 months). Most (103 520 [99.7%]) had a clinic visit to a VA facility, while 9941 (10%) had visits to outside facilities reimbursed by the VA. Nearly all OEF/OIF veterans (103 734 [99%]) had an outpatient visit, while 3213 (3%) also had an inpatient visit.

MENTAL HEALTH SERVICES UTILIZATION AND TIME TO FIRST MENTAL HEALTH DIAGNOSIS

Of 103 788 OEF/OIF veterans, 25 396 (25%) had an outpatient mental health visit during the study period. Of note, 5059 OEF/OIF veterans (5%) were seen in mental health clinics but did not receive a mental health diagnosis. Of the 3213 OEF/OIF veterans with an inpatient visit, 1390 (43%) were admitted with the primary diagnosis of a mental health disorder. The median time from the first VA visit to the first mental health diagnosis was 13 days (IQR, 0-118 days). Of those receiving mental health diagnoses, 10 394 (41%) received mental health diagnoses on their first VA clinic visit.

MENTAL HEALTH DIAGNOSES AMONG OEF/OIF VETERANS SEEN AT VA FACILITIES

Table 2 gives the mental health diagnoses among 103 788 OEF/OIF veterans. Overall, 25 658 (25%) received 1 or more distinct mental health diagnoses. The median number of different diagnoses was 3 (IQR, 1-7); 44% had a single mental health diagnosis, 29% had 2 different diagnoses, and 27% had 3 or more different mental health diagnoses. Of those receiving mental health diagnoses, 18 582 (72%) had the same diagnosis made at 2 or more separate encounters. The single most common mental health diagnosis was PTSD, coded in 13 205 OEF/OIF veterans, representing 52% of those receiving mental health diagnoses and 13% of all OEF/OIF veterans in our study population. When we broadened our definition of "mental health problems" to include those with a mental health diagnosis and/or those receiving a V-code, representing a psychosocial problem, overall, 32 010 OEF/OIF veterans (31%) were coded as having "mental health problems."

CLINICAL SETTING OF MENTAL HEALTH DIAGNOSES AMONG OEF/OIF VETERANS

Table 2, columns 2 and 3, gives the proportions of veterans with mental health diagnoses and psychosocial problems (V-codes) that were assessed in mental health vs nonmental health settings. The majority of all mental health diagnoses (60%) were first made in nonmental health settings; 42% were made in primary care settings; and 18% were made in other settings.

Table 2, column 4, gives the proportions of veterans having a subsequent mental health visit if the initial mental health diagnosis occurred in a nonmental health setting. Column 5 shows the proportion of these subsequent mental health visits that resulted in the same mental health diagnosis as first assigned in the nonmental health setting. Overall, of veterans first receiving mental health diagnoses in nonmental health settings, the majority (61%) subsequently had a mental health visit, and 92% of these veterans received the same mental health diagnosis first made in the nonmental health setting.

PREDICTORS FOR RECEIVING MENTAL HEALTH DIAGNOSES

Table 3 shows that, with the exception of age subgroups, differences across subgroups of OEF/OIF veterans regarding risk for receiving mental health or PTSD diagnoses were minimal. **Figure 1** illustrates that the absolute mean difference among racial subgroups and between male and female veterans varied by no more than 2%. When stratified by component (active duty vs National Guard and Reserve), **Figure 2** shows that among veterans of active duty service, those in the younger age groups were at higher risk of receiving mental health and PTSD diagnoses compared with those in the oldest age group (≥40 years) (*P* value for trend, <.01). The youngest group of active duty veterans (age, 18-24 years) had a significantly higher risk of receiving 1 or more mental health diagnoses (RR, 3.32; 95% CI, 3.12-3.54) and PTSD

Table 2. Mental Health (MH) Diagnoses and Psychosocial/Behavioral Problems Among OEF/OIF Veterans Seen at VA Health Care Facilities*

Diagnosis	OEF/OIF Veterans (N = 103 788)	OEF/OIF Veterans With First MH Diagnosis in Non-MH Setting	MH Visit If First MH Diagnosis in Non-MH Setting	Same MH Diagnosis on MH Visit If First Diagnosis in Non-MH Setting
≥1 MH diagnosis(es)*†	25 658/103 788 (25)	15 347/25 658 (60)	9287/15 347 (61)	8543/9287 (92)
1 MH diagnosis	11 319 (44)	. . .	. . .	. . .
2 MH diagnoses	7342 (29)	. . .	. . .	. . .
≥3 MH diagnoses	6997 (27)	. . .	. . .	. . .
MH diagnosis‡		. . .	. . .	. . .
PTSD	13 205 (13)	5844 (44)	4198 (72)	3925 (94)
Anxiety disorder	6267 (6)	3131 (50)	2014 (64)	1897 (94)
Adjustment disorder	5936 (6)	1451 (24)	857 (59)	780 (91)
Depression	5405 (5)	1456 (27)	1018 (70)	966 (95)
Substance use disorder	4878 (5)	2419 (50)	1396 (58)	1310 (94)
Other MH diagnosis(es)§	12 447 (12)	8141 (65)	5157 (63)	4795 (93)
V-code diagnosis(es)‖	13 211 (13)	9333 (71)	3172 (34)	2683 (85)
Total with MH and/or V-code diagnoses	32 010 (31)	21 447 (67)	10 386 (48)	9302 (90)

Abbreviations: OEF/OIF, Operations Enduring Freedom and Iraqi Freedom; PTSD, posttraumatic stress disorder; VA, Department of Veterans Affairs.

*Data are given as number (percentage) of veterans. The first row shows denominators to demonstrate how the table is constructed. Column 1 gives MH diagnoses among 103 788 OEF/OIF versions. Column 2 gives row percentages to describe the proportion of OEF/OIF veterans who received their first MH diagnosis in a non-MH setting. The last 2 columns give row percentages to describe the proportion of OEF/OIF veterans who had a follow-up mental health visit if the first mental health diagnosis occurred in a nonmental health setting and the proportion of these who received the same mental health diagnosis as in the nonmental health setting.

†Based on *International Classification of Diseases, Ninth Revision, Clinical Modification* codes 290.0 to 319.0 that correspond to *Diagnostic and Statistical Manual of Mental Disorders, Fourth Edition, Revised* (*DSM-IV-R*) diagnostic codes for mental illness.

‡(1) "PTSD," 309.81; (2) "anxiety disorders," 300.00 to 300.09, 300.20 to 300.29, and 300.3; (3) "adjustment disorder," 309.0 to 309.9 (excluding 309.81); (4) "depressive disorders," 296.20 to 296.35, 296.50 to 296.55, 296.90, and 300.4; (5) "substance use disorders," 304 (drug dependence), 303 (alcohol dependence), and 305 (nondependent abuse of drugs and/or alcohol) (excludes codes for nicotine dependence).

§All MH diagnoses included in the *DSM-IV-R* other than the MH diagnoses listed in the double dagger footnote: "psychoses," 291 to 298 (11%); "schizophrenia," 295 (2%); "affective disorders," 924 (6%); "neurotic disorders," 300 (3%); "personality disorders," 301 (5%); "sexual disorders," 302 (7%); "depressive disorders not elsewhere classified," 311 (56%); and other mental health diagnoses (10%).

‖Includes V-codes (see "Source of Data" subsection of the "Methods" section) indicating a psychosocial or behavioral problem: V15.40 to V15.49; V60.0 to V60.2; V60.4; V61.0 to V61.22; V61.80 to V61.83; V61.90; V62.0; V62.2; V62.5; V62.80 to V62.89; V63.0; V63.9; V65.2; V65.5; V69.2 to V69.8; V70.1 to V70.2; V71.0 to V71.01; V71.5; V71.81; and V79.0 to V79.1.

(RR, 5.04; 95% CI, 4.52-5.62) compared with active duty veterans 40 years or older. Stratified RR analyses revealed that this inverse trend between age and risk for mental health and PTSD diagnoses persisted when veterans of active duty service were further stratified by race and sex, with the highest risk occurring in the youngest white male active duty veterans followed by the youngest black active duty male veterans, compared with veterans of each group 40 years or older (**Table 4**).

COMMENT

Of 103 788 OEF/OIF veterans first seen at VA health care facilities following OEF/OIF service, a quarter received mental health diagnoses, and more than half of these veterans were dually or multiply diagnosed. The most common military service–related mental health diagnosis was PTSD. When psychosocial problems were considered, overall, nearly a third of OEF/OIF veterans were classified as having either mental health diagnoses and/or psychosocial problems. Of veterans receiving mental health diagnoses, the majority were diagnosed on or within days of their first VA clinic visit. Most initial mental health diagnoses occurred in nonmental health settings, particularly in primary care settings. These results indicate a large burden of co-occurring mental health disorders associated with service in Iraq and Afghanistan. This burden will likely increase with time as new cases emerge and unresolved disorders become chronic, posing logistical and fiscal challenges for VA and non-VA mental health as well as primary care medical services.[16-18]

Roughly 29% of returned OEF/OIF veterans have already enrolled in VA health care, a historically high rate compared with 10% of Vietnam veterans.[9,19] Moreover, the median time from OEF or OIF service separation to the first VA clinic visit was short (<3 months) and from the first VA clinic visit to first mental health diagnosis even shorter (13 days). Of note, the majority of mental health diagnoses occurred in nonmental health settings, most commonly primary care settings. This relatively high rate of VA enrollment and the speed with which separated OEF/OIF veterans are seen and diagnosed provide the opportunity to implement early evidence-based interventions[20] in both mental health and primary care settings to decrease chronic military service-related mental illness and disability.

Central to effective early intervention, however, is early and accurate detection. Our results show that most initial mental health diagnoses among OEF/OIF veterans were made in nonmental health settings, particular in primary care. Of note, of the majority referred for mental health follow-up from a nonmental health setting, more than 90% received the same mental health diagnosis. The prevalence of mental health diagnoses among OEF/OIF

Table 3. Prevalence and Relative Risk of Receiving 1 or More MH and PTSD Diagnoses

Characteristic	≥1 MH Diagnoses, No. (%) of Veterans	RR (95% CI)	PTSD Diagnosis, No. (%) of Veterans	RR (95% CI)
Sex				
Female	3552 (26)	1 [Reference]	1550 (11)	1 [Reference]
Male	22 105 (25)	0.94 (0.91-0.97)	11 654 (13)	1.14 (1.08-1.10)
Age, y				
18-24	7558 (28)	1.47 (1.43-1.52)	4069 (15)	1.72 (1.63-1.80)
25-29	7525 (26)	1.37 (1.33-1.41)	3769 (13)	1.48 (1.41-1.56)
30-39	5827 (26)	1.39 (1.35-1.44)	3167 (14)	1.63 (1.55-1.72)
≥40	4748 (19)	1 [Reference]	2200 (9)	1 [Reference]
Race				
White	16 830 (25)	1 [Reference]	8597 (13)	1 [Reference]
Black	4574 (25)	1.03 (1.00-1.06)	2504 (14)	1.10 (1.06-1.15)
Hispanic	3034 (27)	1.09 (1.05-1.12)	1465 (13)	1.03 (0.98-1.08)
Other	529 (25)	1.00 (0.93-1.08)	294 (14)	1.09 (0.98-1.22)
Marital status				
Never married	10 813 (31)	1 [Reference]	5258 (15)	1 [Reference]
Married	9933 (31)	1.00 (0.98-1.02)	5537 (17)	1.14 (1.10-1.19)
Divorced	2572 (36)	1.18 (1.14-1.22)	1276 (18)	1.20 (1.14-1.27)
Separated or widowed	11 (44)	1.44 (1.26-1.65)	48 (18)	1.21 (0.93-1.56)
Component				
National Guard/Reserve	12298 (25)	1 [Reference]	6370 (13)	1 [Reference]
Active duty	13360 (25)	0.99 (0.97-1.01)	6835 (13)	0.98 (0.94-1.01)

Abbreviations: CI, confidence interval; MH, mental health; PTSD, posttraumatic stress disorder; RR, relative risk.

Figure 1. Posttraumatic stress disorder (PTSD) and mental health diagnoses by sex and race. OEF/OIF indicates Operations Enduring Freedom and Iraqi Freedom.

Figure 2. Posttraumatic stress disorder (PTSD) and mental health diagnoses by age group stratified by military component. OEF/OIF indicates Operations Enduring Freedom and Iraqi Freedom.

veterans reported herein is consistent with recent reports.[3,6] The frequency of *ICD-9-CM* PTSD diagnoses observed among OEF/OIF veterans in our study (13%) was only slightly lower than the current prevalence of PTSD several decades after returning from Vietnam as reported in the National Vietnam Veterans Readjustment Study (15.2%), but it was substantially higher than the 3.5% current prevalence reported in a recent national survey of a representative sample of the US population using standard assessments.[21,22]

We found minimal absolute differences between men and women, racial and ethnic subgroups, and component types regarding risk for receiving mental health and PTSD diagnoses. In contrast, similar to another recent study, we found both an absolute and statistically significant trend toward increased risk for mental health and

PTSD diagnoses with younger age, with the youngest group of OEF/OIF veterans (age, 18-24 years) at the highest risk compared with veterans 40 years or older.[23] This trend was magnified when the sample was first stratified by service component and further stratified by sex and race. Our analyses were limited by the fact that we lacked information on important potential confounders and/or effect modifiers of age such as military branch, rank, and combat exposure. Men serving in the active duty component are generally younger than members of the National Guard and Reserve. Because they are young, they are more likely to be of lower rank and more likely to have greater combat exposure than their older active duty counterparts. Degree of combat exposure has been associated with military service–related mental health disorders, particularly PTSD.[3,6,16,18,19] Our findings suggest

Table 4. Relative Risk of Receiving 1 or More MH or PTSD Diagnoses Among White and Black Male Veterans of Active Duty Service by Age Group*

Age, y	≥1 MH Diagnoses	PTSD Diagnosis
White active duty male veterans		
≥40	1 [Reference]	1 [Reference]
30-39	3.55 (3.20-3.94)	6.07 (5.05-7.28)
25-29	3.94 (3.59-4.33)	6.91 (5.82-8.21)
18-24	4.70 (4.28-5.16)	8.88 (7.49-10.54)
Black active duty male veterans		
≥40	1 [Reference]	1 [Reference]
30-39	1.90 (1.63-2.21)	2.17 (1.73-2.73)
25-29	2.07 (1.81-2.37)	2.47 (2.01-3.03)
18-24	2.18 (1.90-2.50)	2.64 (2.15-3.25)

Abbreviations: MH, mental health; PTSD, posttraumatic stress disorder; RR, relative risk.

*Data are given as relative risk (95% confidence interval).

that enhanced prevention, detection, and treatment should be targeted at the youngest OEF/OIF veterans younger than 25 years, particularly those in the active duty components.

Our findings are not generalizable to all veterans of OEF/OIF service. We had no data on veterans who have not accessed VA care. Furthermore, because we lacked service separation dates on half of the veterans listed in the VA OEF/OIF Roster, we restricted our study population to veterans listed in the VA OEF/OIF Roster who were new users of VA health care after the invasion of Afghanistan and/or who had accessed VA services after their OEF/OIF service separation date (among those with a separation date). We excluded veterans who had VA contact prior to OEF/OIF because our aim was to describe mental health disorders associated with OEF/OIF military service, not with prior military conflicts. Consequently, our results may overestimate the burden of mental health disorders because veterans with mental health disorders may be more likely to seek treatment at a VA facility than those without[19,24] and because we excluded more National Guard and Reserve and older veterans with prior VA contact who had the same or fewer mental health diagnoses than active duty and younger veterans (Table 1). Nevertheless, our findings, based on more than 100 000 OEF/OIF veterans who are new users of VA health care following OEF/OIF military service, may inform targeted prevention and treatment efforts within or outside the VA system.

Another limitation is that OEF/OIF veterans were not assessed systematically with validated self-report measures or structured diagnostic interviews. We captured clinical mental health diagnoses based on *ICD-9-CM* codes in VA administrative databases.[25] Thus, our results are subject to misclassification. Nevertheless, *ICD-9-CM* diagnostic codes have been found to be a valid proxy for estimating disease.[26,27] Furthermore, our own findings of a greater than 90% diagnostic concordance among veterans first diagnosed in nonmental health settings subsequently diagnosed in mental health settings, as well as the high proportion of veterans receiving the same mental health diagnosis on 2 or more clinical encounters, support our results based on the use of *ICD-9-CM* codes.

Our results signal a need for improvements in the primary prevention of military service–related mental health disorders, particularly among our youngest service members. Furthermore, early detection and evidence-based treatment in both VA and non-VA mental health and primary care settings is critical in the prevention of chronic mental illness, which threatens to bring the war back home as a costly personal and public health burden.

REFERENCES

1. Friedman MJ. Veterans' mental health in the wake of war. *N Engl J Med.* 2005;352: 1287-1290.
2. National Center for Post-Traumatic Stress Disorder and the Walter Reed Army Medical Center. *Iraq War Clinician Guide.* Washington, DC: Dept of Veterans Affairs; 2004.
3. Hoge CW, Castro CA, Messer SC, McGurk D, Cotting DI, Koffman RL. Combat duty in Iraq and Afghanistan, mental health problems, and barriers to care. *N Engl J Med.* 2004;351:13-22.
4. Gawande A. Casualties of war—military care for the wounded from Iraq and Afghanistan. *N Engl J Med.* 2004;351:2471-2475.
5. United States Army Surgeon General. Mental Health Advisory Team (MHAT-II): report. Washington, DC: Dept of the Army, Office of the Surgeon General; 2005: 1-30.
6. Kang HK, Hyams KC. Mental health care needs among recent war veterans. *N Engl J Med.* 2005;352:1289.

7. Hoge CW, Auchterlonie JL, Milliken CS. Mental health problems, use of mental health services, and attrition from military service after returning from deployment to Iraq or Afghanistan. *JAMA*. 2006;295:1023-1032.

8. OEF/OIF Roster (RMTPRD.MED.SAS.OEFOIF.ROSTER) [database online]. Washington, DC Department of Veterans Affairs. National Data Systems; 2005. Updated September 30, 2005.

9. Department of Veteran Affairs. Analysis of VA Health Care Utilization Among Southwest Asian War Veterans Combined—Operation Iraqi Freedom Operation Enduring Freedom. Washington, DC: VHA Office of Public Health and Environmental Hazards; February 14, 2006.

10. Ashton CM, Souchek J, Petersen NJ, et al. Hospital use and survival among Veterans Affairs beneficiaries. *N Engl J Med*. 2003;349:1637-1646.

11. Boyko EJ, Koepsell TD, Gaziano JM, Horner RD, Feussner JR. US Department of Veterans Affairs medical care system as a resource to epidemiologists. *Am J Epidemiol*. 2000;151:307-314.

12. American Psychiatric Association. *Diagnostic and Statistical Manual of Mental Disorders, Fourth Edition, Text Revision*. Washington, DC: American Psychiatric Association; 2000.

13. Schlenger WE, Caddell JM, Ebert L, et al. Psychological reactions to terrorist attacks: findings from the National Study of Americans' Reactions to September 11. *JAMA*. 2002;288:581-588.

14. Prophet S. V codes: supplementary classification of factors influencing health status and contact with health services. *J AHIMA*. 1996;67:16-25.

15. Hoge CW, Lesikar SE, Guevara R, et al. Mental disorders among U.S. military personnel in the 1990s: association with high levels of health care utilization and early military attrition. *Am J Psychiatry*. 2002;159:1576-1583.

16. Kessler RC, Sonnega A, Bromet E, Hughes M, Nelson CB. Posttraumatic stress disorder in the National Comorbidity Survey. *Arch Gen Psychiatry*. 1995;52:1048-1060.

17. Jordan BK, Schlenger WE, Hough R, et al. Lifetime and current prevalence of specific psychiatric disorders among Vietnam veterans and controls. *Arch Gen Psychiatry*. 1991;48:207-215.

18. Kang HK, Natelson BH, Mahan CM, Lee KY, Murphy FM. Post-traumatic stress disorder and chronic fatigue syndrome-like illness among Gulf War veterans: a population-based survey of 30,000 veterans. *Am J Epidemiol*. 2003;157:141-148.

19. Kulka RA, Schlenger WE, Fiarbank JA, et al. *Trauma and the Vietnam War Generation: Findings From the National Vietnam Veterans Readjustment Study*. New York, NY: Brunner/Mazel; 1990.

20. Watson PJ, Friedman MJ, Ruzek JI, Norris F. Managing acute stress response to major trauma. *Curr Psychiatry Rep*. 2002;4:247-253.

21. Kessler RC, Chiu WT, Demler O, Walters EE. Prevalence, severity, and comorbidity of 12-month *DSM-IV* disorders in the National Comorbidity Survey Replication. *Arch Gen Psychiatry*. 2005;62:617-627.

22. Dohrenwend BP, Turner JB, Turse NA, Adams BG, Koenen KC, Marshall R. The psychological risks of Vietnam for US veterans: a revisit with new data and methods. *Science*. 2006;313:979-982.

23. West AN, Weeks WB. Mental distress among younger veterans before, during, and after the invasion of Iraq. *Psychiatr Serv*. 2006;57:244-248.

24. Rosenheck R, Fontana A. Do Vietnam-era veterans who suffer from posttraumatic stress disorder avoid VA mental health services? *Mil Med*. 1995;160:136-142.

25. Maynard C, Chapko MK. Data resources in the Department of Veterans Affairs. *Diabetes Care*. 2004;27(suppl 2):B22-B26.

26. Movig KL, Leufkens HG, Lenderink AW, Egberts AC. Validity of hospital discharge *International Classification of Diseases* (*ICD*) codes for identifying patients with hyponatremia. *J Clin Epidemiol*. 2003;56:530-535.

27. Borzecki AM, Wong AT, Hickey EC, Ash AS, Berlowitz DR. Identifying hypertension-related comorbidities from administrative data: what's the optimal approach? *Am J Med Qual*. 2004;19:201-206.

LETTERS

SEAL ET AL. RESPOND

We appreciate Rona's concerns about population-based mental health screening of Iraq and Afghanistan veterans presenting to Department of Veterans Affairs (VA) medical facilities. The study population included veterans presenting to all outpatient clinics at 1 VA facility, not just primary care. Mental health screening may not have been a clinical priority during medical subspecialty visits, which may partially explain lower screening rates. Recently, in response to changes in national VA policy, postdeployment mental health screening rates in primary care have increased to more than 90%. Further, screening instruments used by the VA, specifically the primary care posttraumatic stress disorder (PTSD) screen, have demonstrated validity,[1] and brief screens for PTSD symptoms have been used successfully to detect cases of PTSD in primary care.[2]

When population-based postdeployment mental health screens were first introduced in VA facilities in 2004, the extent of mental problems stemming from the conflicts in Iraq and Afghanistan were just surfacing. Hoge et al. described stigma surrounding mental illness as a barrier to treatment for soldiers, highlighting that soldiers in greater distress were less likely to seek help.[3] Combat veterans might be more willing to disclose and accept treatment for mental health problems from the VA rather than the military. In addition, veterans may report mental health concerns months after returning home when at the VA, rather than immediately on their return when first screened by the military.

We concur that universal screening should not be conducted if there is inadequate follow-through of positive screens. In our study, 73% of combat veterans with positive screens attended mental health appointments, as opposed to 18% of veterans not screened. Unfortunately, the majority of mental health visits occurred more than 90 days after the positive screens. Since this study was conducted, however, the VA has greatly augmented its mental health capacity, hiring nearly 100 new psychologists.[4] Further, the VA has implemented a national model of integrated, collocated care in which mental health providers embedded in primary care conduct immediate assessment and triage of veterans who screen positive for mental health symptoms.[4] Preliminary data from one integrated clinic for Iraq and Afghanistan veterans demonstrated high use of mental health services within primary care. We cannot wait for a randomized controlled trial, as Rona suggests, to decide whether we should continue to screen veterans for combat-related mental disorders. If we don't ask, they may not tell, and we cannot afford the potential consequences of undetected mental illness in combat veterans. ∎

Karen H. Seal, MD, MPH
Shira Maguen, PhD
Daniel Bertenthal, MPH
Kristian Gima, BA
Charles R. Marmar, MD

About the Authors

Karen H. Seal, Shira Maguen, Daniel Bertenthal, Kristian Gima, and Charles R. Marmar are with the San Francisco VA Medical Center, San Francisco, CA. Karen H. Seal, Shira Maguen, and Charles R. Marmar are also with the University of California, San Francisco.

Requests for reprints should be sent to Karen H. Seal, MD, MPH, San Francisco VA Medical Center, 1450 Clement St, Box 111A-1, San Francisco, CA 94121 (e-mail: karen.seal@va.gov).

This letter was accepted May 1, 2008.
doi:10.2105/AJPH.2008.141333

References

1. Prins A, Ouimette P, Kimerling R, et al. The primary care PTSD screen (PC-PTSD): development and operating characteristics. *Prim Care Psychiatry.* 2004;9:9–14.

2. Kimerling R, Ouimette P, Prins A, et al. Brief report: utility of a short screening scale for DSM-IV PTSD in primary care. *J Gen Intern Med.* 2005.

3. Hoge CW, Castro CA, Messer SC, McGurk D, Cotting DI, Koffman RL. Combat duty in Iraq and Afghanistan, mental health problems, and barriers to care. *N Engl J Med.* 2004;351:13–22.

4. Zeiss AM, Karlin BE. Integration of mental health and primary care services in the Department of Veterans Affairs Health Care System. *J Clin Psychol Med Settings.* 2008;15:73–78.

Getting Beyond "Don't Ask; Don't Tell": an Evaluation of US Veterans Administration Postdeployment Mental Health Screening of Veterans Returning From Iraq and Afghanistan

| Karen H. Seal, MD, MPH, Daniel Bertenthal, MPH, Shira Maguen, PhD, Kristian Gima, BA, Ann Chu, MS, and Charles R. Marmar, MD

High levels of exposure to combat have characterized the conflicts principally in Iraq and Afghanistan—Operation Iraqi Freedom (OIF) and Operation Enduring Freedom (OEF). Improvised explosive devices and frequent, unexpected mortar attacks have brought the "front line" to most OIF and OEF military service personnel.[1] In the Vietnam and Persian Gulf wars, level of combat exposure was strongly associated with posttraumatic stress disorder (PTSD), depression, and substance use disorders.[2,3] Similarly, an epidemic of mental health disorders is emerging among veterans of OIF and OEF.[4,5] Early intervention with evidence-based mental health treatment has been shown to prevent chronic mental illness and associated disability.[6] Mental health screening of combat veterans has the potential to increase early detection of symptoms and early intervention.

Since World War I, the US military has conducted mass mental health screening primarily to exclude psychologically vulnerable recruits from service, yet these programs have failed to reduce the incidence of psychological casualties.[7] This experience, coupled with high rates of psychiatric disorders in the aftermath of the Vietnam and Persian Gulf wars, shifted the focus of screening to the detection of mental health symptoms during and after deployment.[8] Recent reports have indicated that service members are more likely to report mental health problems 3 to 4 months after returning from deployment, and delayed presentations of mental health disorders have been documented years after military service.[9,10] Accordingly, in June 2004, the Veterans Administration (VA) issued a national directive to initiate the Afghan and Iraq Post-Deployment Screen.[11] The screen consists of brief, previously validated instruments to detect symptoms of

Objectives. We sought to evaluate outcomes of the Veterans Administration (VA) Afghan and Iraq Post-Deployment Screen for mental health symptoms.

Methods. Veterans Administration clinicians were encouraged to refer Iraq or Afghanistan veterans who screened positive for posttraumatic stress disorder, depression, or high-risk alcohol use to a VA mental health clinic. Multivariate methods were used to determine predictors of screening, the proportions who screened positive for particular mental health problems, and predictors of VA mental health clinic attendance.

Results. Among 750 Iraq and Afghanistan veterans who were referred to a VA medical center and 5 associated community clinics, 338 underwent postdeployment screening; 233 (69%) screened positive for mental health problems. Having been seen in primary care (adjusted odd ratio [AOR] = 13.3; 95% confidence interval [CI] = 8.31, 21.3) and at a VA community clinic (AOR = 3.28; 95% CI = 2.03, 5.28) predicted screening. African American veterans were less likely to have been screened than were White veterans (AOR = 0.45; 95% CI = 0.22, 0.91). Of 233 veterans who screened positive, 170 (73%) completed a mental health follow-up visit.

Conclusions. A substantial proportion of veterans met screening criteria for co-occurring mental health problems, suggesting that the VA screens may help overcome a "don't ask, don't tell" climate that surrounds stigmatized mental illness. Based on data from 1 VA facility, VA postdeployment screening increases mental health clinic attendance among Iraq and Afghanistan veterans. (*Am J Public Health.* 2008;98:714–720. doi:10.2105/AJPH.2007.115519)

PTSD, depression, and high-risk alcohol use among veterans of OIF and OEF who seek VA healthcare. Veterans Administration clinicians are expected to complete the screen and to assess whether veterans who meet screening criteria for depression and high-risk alcohol use require a mental health referral. Veterans Administration clinicians are encouraged to refer patients who meet screening criteria for PTSD for further mental health assessment and treatment.

Clinicians at 1 VA medical center and its affiliated community-based clinics were encouraged to refer Iraq and Afghanistan veterans who met screening criteria for PTSD, depression, or high-risk drinking for follow-up mental health assessment. Based on data from this facility, we sought to determine (1) the

frequency and predictors of implementation of the VA postdeployment screen; (2) the proportion of veterans with positive screens for PTSD, depression, or high-risk alcohol use; and (3) the proportion of veterans who were seen in a VA mental health clinic within 90 days of screening and beyond.

METHODS

The Veterans Administration Afghan and Iraq Post-Deployment Screen

Veterans of OIF and OEF are eligible to receive 2 years of free military service–related health care through the VA healthcare system. Since 2002, 33% of eligible OEF and OIF veterans have sought VA healthcare. When veterans of OIF or OEF present to a

VA healthcare facility, clinicians are asked to complete the 10- to 15-minute Afghan and Iraq Post-Deployment Screen, which appears in the Computerized Patient Record System as a clinical reminder. Although this screen is intended solely for OIF and OEF veterans, clinicians are initially prompted to complete this clinical reminder for all veterans with a service separation date after September 11, 2001. The first question of the screen asks about location of military service, and if a veteran denies having served in OIF or OEF, the screen is terminated. For veterans who endorse OIF or OEF service, VA clinicians are expected to complete the screen and, in so doing, clear the clinical reminder.

Veterans Administration clinicians are monitored to determine the proportion of veterans seen for whom they have cleared the post-deployment screen reminder. Clinicians are encouraged to assess veterans with positive screens and to offer a VA mental health referral for those whom they determine would benefit from further assessment.[11] Nevertheless, ultimately, whether a patient accepts a mental health referral or attends a mental health follow-up appointment is based on the patient's interest, preferences, and willingness—information we did not have for our study.

The Afghan and Iraq Post-Deployment Screen includes 3 standard, previously validated, brief mental health screens to assess for symptoms of PTSD, depression, and high-risk alcohol use. Posttraumatic stress disorder is assessed with a 4-item yes-or-no screening instrument—the Primary Care PTSD Screen developed by the National Center for PTSD.[12] The stem of the screening questions read, "Have you ever had any experience that was so frightening, horrible, or upsetting that in the last month you. . . ." The 4 questions cover the 4 main symptom clusters of PTSD: re-experiencing trauma, numbing, avoidance, and hyperarousal. Initially, endorsement of any 2 of the 4 screen items constituted a positive screen.[12] In the second quarter of fiscal year 2005, the VA increased the threshold for a positive screen to 3 "yes" responses.[13] Two separate blinded validation studies found that the use of cut-off scores of either 2 or 3 "yes" responses to indicate a positive screen resulted in sensitivities of 0.73 and 0.78 and specificities of 0.88 and 0.87, respectively.[9,12,14]

Symptoms of depression are assessed in the VA postdeployment screen with the 2-item Patient Health Questionnaire, which screens for depressed mood and anhedonia (little interest or pleasure in doing things).[15,16] A "yes" answer to either question constitutes a positive screen for depression. In a sample of veterans seen in primary care, the 2-item Patient Health Questionnaire was found to have a sensitivity of 0.96 and specificity of 0.57.[15] The 4-item Alcohol Use Disorders Identification Test assesses high-risk alcohol use. A score of 4 or more points for men and 3 or more points for women is considered a positive screen. In a large primary care practice, these thresholds resulted in a sensitivity of 0.86 among men and 0.73 among women and a specificity of 0.89 among men and 0.91 among women.[17]

Study Population

From June 1, 2004, through September 30, 2006, 1178 veterans with military service separation dates after September 11, 2001, presented for care to a VA medical center or 1 of its 5 associated VA community-based clinics. Because our aim was to assess predictors and clinical outcomes of postdeployment screening among OIF and OEF veterans, we excluded from the final study population veterans who denied prior military service in Iraq, Afghanistan, or surrounding regions (n=358) and those who were not included in the VA National OIF/OEF Roster database (n=42). Further, we excluded 5 veterans who were missing data on each of the 3 individual screens and 23 veterans whose initial VA visit was within 90 days of the study end date, which allowed inadequate follow-up time. Consequently, the final study population consisted of 750 OIF or OEF veterans.
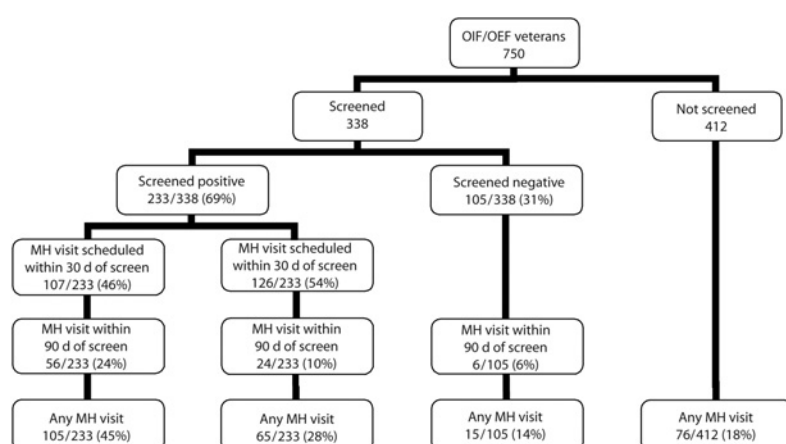
Source and Definitions of Data Used

The Veterans Health Information Systems and Technology Architecture database was used to extract postdeployment screen results for symptoms of depression, PTSD, and high-risk alcohol use, and the date of and specific clinic in which postdeployment screening occurred. The Veterans Health Information Systems and Technology Architecture database was also used to determine the date when an initial mental health clinic visit was scheduled and the date when an initial mental health

visit occurred. A mental health clinic visit was defined as a clinical visit to any mental health, alcohol, or substance abuse clinic at the medical center or associated VA community-based outpatient clinics. We defined our outcome as mental health clinic visits scheduled within 30 days and completed within 90 days of the postdeployment screen date to maximize the likelihood that scheduling and appointment attendance were related to the postdeployment screening program. In addition, to allow informal comparisons of all mental health follow-up visits between veterans who were screened and not screened, we determined the number of all mental health visits beyond 90 days of screening, although these visits may not have been related to postdeployment screening. Local VA Health Information Systems and Technology Architecture data were linked to the VA National OIF/OEF Roster to identify and confirm veterans' OIF or OEF military service. In addition, data derived from the VA National Patient Care Database were used to augment and confirm local sociodemographic, military service, and clinical visit information.

Statistical Analyses

This was a retrospective descriptive study. Predictors of having received postdeployment screening were evaluated with a multivariate logistic regression model adjusted for gender, race/ethnicity, age, and other predictor variables associated with postdeployment screening in univariate analysis. After we determined the proportion of OIF and OEF veterans who screened positive for symptoms of single or comorbid PTSD, depression, or high-risk alcohol use, we determined the proportion (screened vs unscreened and screen-positive vs screen-negative) who were scheduled for and completed a mental health appointment within 30 and 90 days of postdeployment screening, respectively. Among screen-positive veterans without a VA mental health clinic visit prior to screening, multivariate logistic regression analysis was used to determine whether screening positive for specific mental health symptoms was independently associated with completion of 1 or more follow-up VA mental health clinic visits. All analyses were conducted with Stata software version 8.2 (StataCorp LP, College Station, TX).

Notes. OIF/OEF = Operation Iraqi Freedom or Operation Enduring Freedom; MH = mental health.

FIGURE 1—Mental health appointments scheduled and completed following postdeployment screening among 750 veterans of Operation Iraqi Freedom or Operation Enduring Freedom seen at the San Francisco Veterans Administration Medical Center and associated community-based outpatient clinics: September 11, 2001, to June 30, 2006.

RESULTS

Clinicians at 1 VA facility initiated the VA Afghan and Iraq Post-Deployment Screen for 748 of the 1178 (64%) veterans for whom the screening instrument appeared in the electronic medical record triggered by their post–September 11, 2001, service separation dates. Of these, 358 (48%) of the 748 veterans denied prior OIF or OEF military service, and thus, their screens were terminated. Of the 750 OEF or OIF veterans in the final study population, 11% were women 35% were racial/ethnic minorities the median age was 27 years (range = 19–60 years), and 41% were veterans of the US National Guard or Reserve forces. The majority (85%) had been seen primarily at the VA medical center, and 74% had attended 4 or more VA outpatient visits during the study period.

Postdeployment Screening

Of the 750 OIF or OEF veterans who presented for VA outpatient care during the study period, 338 underwent postdeployment screening (Figure 1). The median time to postdeployment screening from service separation was 9 months (intraquartile range [IQR] = 4–16 months) and the median time

to screening from the first VA outpatient visit was 29 days (IQR = 0–175 days). The majority (73%) was screened during a VA primary care medical visit, 17% at a mental

health visit, 9% at other outpatient visits (e.g., dental), and 1% at a social services visit. Postdeployment screening was more likely in veterans who had a primary care visit versus other settings (72% vs 12%; adjusted odds ratio [AOR] = 13.3; 95% confidence interval [CI] = 8.31, 21.3) and for those seen at a VA community clinic rather than at the medical center (87% vs 37%; AOR = 3.56; 95% CI = 1.78, 7.11). African American veterans of OIF or OEF were less likely to be screened than were White veterans (29% vs 49%; AOR = 0.45; 95% CI = 0.22, 0.91) (Table 1).

Results of Postdeployment Screening

Of the 338 individuals who were screened, the majority, 233 (69%), screened positive for 1 or more mental health disorders (Figure 1); most (61%) screened positive for co-occurring mental health symptoms. A positive screen for PTSD was the most common, occurring in 171 (50% of all veterans screened) and in 73% of those with positive screens (Figure 2). Of note, after June 2005 when the threshold for a positive PTSD screen increased from 2 to 3 items positive

TABLE 1—Predictors of Postdeployment Mental Health Screening Among Veterans of Operation Iraqi Freedom and Operation Enduring Freedom (n = 645) Seen at the San Francisco Veterans Administration Medical Center and 5 Associated Community Clinics: June 1, 2004, to September 30, 2006

Characteristic	Not Screened, No. (%)	Screened, No. (%)	AOR (95% CI)	P
Race/ethnicity				
White (Ref)	213 (51)	207 (49)	1.00	
Hispanic	54 (61)	34 (39)	0.83 (0.44, 1.54)	.55
Black	49 (71)	20 (29)	0.45 (0.22, 0.91)	.03
Other	40 (59)	28 (41)	0.83 (0.42, 1.65)	.60
Facility type				
VA medical center (Ref)	343 (63)	201 (37)	1.00	
VA community clinic	13 (13)	88 (87)	3.56 (1.78, 7.11)	<.001
Any visits to primary care				
No (Ref)	257 (88)	36 (12)	1.00	
Yes	99 (28)	253 (72)	13.3 (8.31, 21.3)	<.001
Any visits to mental health clinic				
No (Ref)	287 (69)	126 (31)	1.00	
Yes	69 (30)	163 (70)	3.28 (2.03, 5.28)	<.001

Notes. AOR = adjusted odds ratio; CI = confidence interval; VA = Veterans Administration. The population size was reduced from 750 to 645 to include only veterans with nonmissing values for study variables. In addition to the predictor variables shown here, the multivariate model was adjusted for age, gender, and total number of visits to the VA medical center or associated community clinics.

TABLE 2—Predictors of Mental Health Visit Among Veterans of Operation Iraqi Freedom and Operation Enduring Freedom (n = 159) Within 90 Days of Postdeployment Mental Health Screen at the San Francisco Veterans Administration Medical Center and 5 Associated Community Clinics: June 1, 2004, to September 30, 2006

Characteristic	Mental Health Visit Within 90 Days,[a] No. (%)	No Mental Health Visit Within 90 Days,[a] No. (%)	AOR (95% CI)	P
PTSD screen				
Negative (Ref)	8 (8)	91 (92)	1.00	
Positive	38 (63)	22 (37)	19.84 (6.16, 63.9)	<.001
Depression screen				
Negative (Ref)	17 (15)	96 (85)	1.00	
Positive	29 (63)	17 (37)	5.51 (1.79, 17.0)	<.001
High-risk alcohol use				
Negative (Ref)	27 (26)	78 (74)	1.00	
Positive	19 (35)	35 (65)	1.19 (0.39, 3.61)	.76
Gender				
Women (Ref)	4 (31)	9 (69)	1.00	
Men	42 (29)	104 (71)	0.89 (0.07, 10.8)	.93
Age, y				
18–24 (Ref)	23 (36)	41 (64)	1.00	
25–29	11 (24)	35 (76)	0.85 (0.25, 2.92)	.80
30–39	10 (33)	20 (66)	4.18 (0.73, 23.9)	.11
≥40	2 (11)	17 (89)	0.29 (0.02, 3.34)	.32
Race/ethnicity				
White (Ref)	32 (28)	81 (72)	1.00	
Hispanic	5 (28)	13 (72)	0.67 (0.12, 3.87)	.66
Black	5 (39)	8 (61)	4.79 (0.54, 42.1)	.16
Other	4 (27)	11 (73)	3.24 (0.49, 21.7)	.23
Component type				
National Guard/Reserve (Ref)	15 (21)	55 (79)	1.00	
Active duty	31 (35)	58 (65)	2.23 (0.65, 7.67)	.20
Facility type				
VA medical center (Ref)	22 (20)	87 (80)	1.00	
VA community clinic	24 (48)	26 (52)	6.08 (1.56, 23.6)	.01
Any visits to primary care				
No (Ref)	1 (9)	10 (91)	1.00	
Yes	45 (30)	103 (70)	19.4 (1.30, 290)	.03
Number of non–mental health visits, mean (SD)	14.5 (16.2)	12.2 (12.1)	1.03 (0.98, 1.07)	.26

Notes. AOR = adjusted odds ratio; CI = confidence interval; PTSD = posttraumatic stress disorder; VA = Veterans Administration. The population size was reduced to include only veterans with all 3 screens and no mental health visits prior to postdeployment screening and veterans with nonmissing values for study variables.
[a] The column numbers represent numbers and percentages for all characteristics except the number of non–mental health visits, where the column numbers represent the mean and SD of the column group.

out of 4 items, there was a moderate decrease (from 58% to 47%; *P*=.05) in the proportion who met criteria for a positive PTSD screen. A positive screen for PTSD most commonly co-occurred with a positive screen for depression (30%), followed by the triad of positive screens for PTSD, depression, and high-risk alcohol use (19%; Figure 2). Overall, of screen-positive OIF and OEF veterans, 59% screened positive for depression, and 46% screened positive for high-risk alcohol use.

Mental Health Referrals and Appointments

As shown in Figure 1, of the 233 OIF or OEF veterans with 1 or more positive screens, 107 (46%) had a VA mental health clinic visit scheduled within 30 days of the screen and about half of these, or 24% of veterans who screened positive, completed a scheduled mental health visit within 90 days of the screen date. Overall, of the 338 veterans who underwent postdeployment screening, 56 completed a scheduled mental health appointment, most likely as a result of screening, compared with 30 veterans who completed a mental health visit within 90 days of screening despite not having been scheduled for an appointment (n=24) or despite having screened negative (n=6). When the follow-up period was extended beyond 90 days of screening, 73% of screen-positive veterans completed a mental health appointment any time during the study period compared with 32% of veterans who screened negative or who were not screened at all (Figure 1).

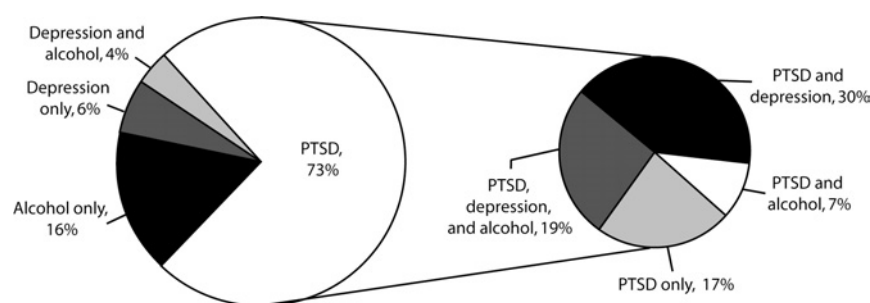## Predictors of Mental Health Appointments After Screening

After the exclusion of veterans with mental health visits prior to postdeployment screening, multivariate analyses adjusted for age, race/ethnicity, gender, VA facility type, number of VA visits, and visits to primary care revealed that veterans who screened positive for PTSD and depression were independently more likely to complete a follow-up mental health visit within 90 days of screening. There was no significant association between screening positive for high-risk alcohol use and mental health appointment attendance. The same analysis also revealed that the likelihood of a follow-up mental health visit within 90 days of screening was increased for veterans who were seen in a VA community clinic versus the medical center (AOR=6.08; 95% CI=1.56, 23.6) and for those seen in primary care versus another outpatient setting (AOR=19.4; 95% CI=1.30, 290).

DISCUSSION

We sought to describe the VA postdeployment screening program at 1 VA medical center and its 5 associated community-based

Note. PTSD = posttraumatic stress disorder. The proportions presented are those of veterans seen at the San Francisco Veterans Administration Medical Center and associated community-based outpatient clinics who screened positive for mental health symptoms (n = 233).

FIGURE 2—The proportions of veterans of Operation Iraqi Freedom or Operation Enduring Freedom who screened positive for symptoms of posttraumatic stress disorder, depression, high-risk alcohol use, and comorbid symptoms: September 11, 2001, to June 30, 2006.

clinics from 2004 to 2006. We also sought to determine whether screening facilitated follow-up mental health assessment for veterans of OIF or OEF who screened positive for mental health disorders. Our results indicated that a substantial proportion of OIF and OEF veterans met screening criteria for co-occurring mental health problems, which suggested that the VA screens may help overcome a "don't ask; don't tell" climate that surrounds stigmatized mental illness. Moreover, veterans of OIF or OEF who screened positive were far more likely than were veterans who screened negative or who were not screened at all to attend follow-up mental health appointments within 90 days of screening.

Veterans Administration Postdeployment Screening Process

Based on data from 1 VA facility, we found that postdeployment screening was administered to the minority of OIF and OEF veterans and it was administered differentially on the basis of clinic and facility type and racial/ethnic group. These results suggest that the postdeployment screen may not have been acceptable to some clinicians or patients. Our data are limited in that we lack individual-level facility, provider, and patient data as to why the majority of screens were not performed. The OIF and OEF post-deployment screen is not a VA performance measure; thus, competing clinical priorities may take precedence. If the screen were a performance measure, completion rates and uniform screening practices would likely improve.[18] Further, formal staff

in-servicing as to how to administer psychological screening and provide feedback of sensitive test results would likely increase screening rates. Finally, making provisions for extra clinician time or ancillary clinic staff to conduct the 10- to 15-minute screening interview would likely increase screening rates in busy clinical settings. Indeed, since this study was conducted, several of these changes were implemented at the medical center and the rate of postdeployment screening in primary care now exceeds 90%.

High Proportion of Positive Mental Health Screens

Notably, an extremely high proportion (69%) of OIF and OEF veterans who underwent postdeployment screening at this VA facility screened positive for PTSD, depression, or high-risk alcohol use. By contrast, a recent study of a US military postdeployment screening program showed that among more than 300 000 military service personnel, only 15% reported a mental health concern.[19] Most veterans who access VA care are separated from military service and, thus, may feel less stigma than military personnel might about disclosing mental health symptoms and less concern about a negative impact on their military careers.[4] In addition, veterans who have been home longer may develop symptoms they did not have or recognize previously.[20] Further, some of the screening instruments may be even less specific in combat veterans than reported in other studies because they have not yet been validated in this population.

Mental Health Follow-Up for Positive Screens

For veterans with mental health symptoms, early evidence-based intervention has been shown to prevent chronic mental illness.[6,21] Cognitive–behavioral therapy and selective serotonin reuptake inhibitors are first-line therapies for combat-related PTSD and depression.[22,23] Our results from 1 VA facility, similar to those of other studies, found that a minority of those who screened positive attended a mental health follow-up appointment as a direct result of screening.[19,24] Hoge et al. found that although 31% of OIF service personnel had at least 1 mental health appointment, only 8% of these were referred through the official screening program.[19] Our data are limited in that we were not able to determine the proportion of veterans offered referrals who declined nor the details of why some screen-positive veterans did not accept referrals or attend mental health clinic appointments.

This finding is consistent with other studies, however, that have found that even after mental health referrals were made, military personnel and civilians did not always follow through.[4,19,25] Of note, when we extended our follow-up period beyond 90 days, we found that the majority (73%) of veterans who screened positive ultimately attended a mental health appointment. This may reflect the importance of mental health screening within the context of a longer-term relationship with a primary care provider who may, over time, help patients overcome their reluctance to accept mental health treatment.

Overcoming Barriers to Mental Health Care

Barriers to mental health care are crucial to address in the planning of a mental health screening program. A central challenge is that, by design, most veterans are screened in primary care, which requires a referral to a mental health clinic for those who screen positive. Barriers to accessing mental health care are myriad—patient stigma regarding mental health treatment[4]; geographic barriers; family, work, or school obligations; avoidance; low motivation; and denial—all features of depression, PTSD, and alcohol-use disorders.[6,26] In addition, unlike the mandate to provide pre- and

posttest counseling for HIV screening, there is no precedent for provision of pre- and posttest counseling for mental health screening, which carries intense stigma for many. This may be a missed opportunity for early intervention as the empathetic feedback of test results is a core element of motivational interviewing, a psychotherapeutic technique used to enhance mental health treatment engagement and behavioral change.[27]

Of note, the VA has been a leader in pioneering a collaborative care model for the integration and co-location of mental health and primary care,[26] removing the barrier of making a separate mental health appointment at some time in the future in a different location. Formal integrated primary and mental health care did not exist at these VA facilities during the study period. Because the VA community clinics are small, primary care is naturally closer in proximity to mental health, facilitating communication. This may explain why a greater proportion of screen-positive veterans seen at the VA community clinics had follow-up mental health appointments compared with veterans screened at the medical center. To bridge the gap between primary care and mental health, in April 2007, an integrated, co-located primary care and mental health care clinic was established at the medical center specifically for veterans of Iraq and Afghanistan. To date, of 42 veterans of OEF and OIF seen, 35 (83%) were seen by a mental health specialist immediately following their primary care visit. In the future, expanded telephone and Internet-based mental health treatment options may help to overcome additional barriers to care among OIF and OEF veterans.

Study Limitations

Our study had some limitations. Most importantly, this study was conducted at a single VA medical center and its 5 associated VA community clinics; thus, our results may not generalize to all VA facilities in other geographic areas. Specifically, the referral of veterans who met criteria for a positive screen for follow-up mental health services may have differed from the national standard. For instance, at many VA facilities, veterans who screen positive for mental health problems in primary care may be further assessed and treated within primary care. Finally, because we had no data on non–VA mental health encounters, we do not know whether veterans were receiving mental health treatment outside the VA system, which would likely decrease their acceptance of a referral to a VA mental health clinic.

Conclusions

Our results from a single VA facility indicated that the postdeployment mental health screening of combat veterans has the potential to overcome a "don't ask; don't tell" environment that surrounds stigmatized mental illness, to efficiently detect mental health symptoms, and to facilitate early intervention to prevent chronic mental illness. Our early experience has led to important improvements in our screening process. In addition to achieving higher screening rates through universal screening of OEF and OIF veterans who presented to primary care, integrating and co-locating mental health specialists within primary care has increased mental health clinic attendance and decreased wait times. Further innovations tailored to the needs of this new generation of veterans may further improve mental health treatment adherence beyond initial engagement. ■

About the Authors

Karen H. Seal, Charles R. Marmar, and Shira Maguen are with the San Francisco Veterans Administration Medical Center and the University of California, San Francisco, and are affiliated with the San Francisco Veterans Administration Health Services Research and Development Research Enhancement Award Program. Daniel Bertenthal, Kristian Gima, and Ann Chu are with the San Francisco Veterans Administration Medical Center.

Requests for reprints should be sent to Karen H. Seal, MD, MPH, San Francisco VA Medical Center, Division of General Internal Medicine, Box 111A-1, 4150 Clement St, San Francisco, CA 94121 (e-mail: karen.seal@ucsf.edu).

This article was accepted August 21, 2007.

Contributors

The study was originated and designed by K.H. Seal, C.R. Marmar, and D. Bertenthal. The data were acquired by D. Bertenthal and A. Chu and were analyzed by K. Gima and K.H. Seal. Data were interpreted by all authors and the article was drafted by K.H. Seal and S. Maguen with final editing by C.R. Marmar. K.H. Seal obtained funding that supported the study.

Human Participant Protection

This study was approved by the Committee on Human Research, University of California, San Francisco, the San Francisco Veterans Administration Medical Center, and the US Department of Defense.

References

1. Friedman MJ. Veterans' mental health in the wake of war. *N Engl J Med.* 2005;352:1287–1290.

2. Kang HK, Natelson BH, Mahan CM, Lee KY, Murphy FM. Post-traumatic stress disorder and chronic fatigue syndrome-like illness among Gulf War veterans: a population-based survey of 30,000 veterans. *Am J Epidemiol.* 2003;157:141–148.

3. Kulka RA, Schlenger WE, Fairbank JA, et al. *Trauma and the Vietnam War Generation: Findings From the National Vietnam Veterans Readjustment Study.* New York, NY: Brunner/Mazel; 1990.

4. Hoge CW, Castro CA, Messer SC, McGurk D, Cotting DI, Koffman RL. Combat duty in Iraq and Afghanistan, mental health problems, and barriers to care. *N Engl J Med.* 2004;351:13–22.

5. Seal KH, Bertenthal D, Miner CR, Sen S, Marmar C. Bringing the war back home: mental health disorders among 103,788 US veterans returning from Iraq and Afghanistan seen at Department of Veterans Affairs facilities. *Arch Intern Med.* 2007;167:476–482.

6. Friedman MJ. Posttraumatic stress disorder among military returnees from Afghanistan and Iraq. *Am J Psychiatry.* 2006;163:586–593.

7. Jones E, Hyams KC, Wessely S. Screening for vulnerability to psychological disorders in the military: an historical survey. *J Med Screen.* 2003;10:40–46.

8. Kang HK, Mahan CM, Lee KY, Magee CA, Murphy FM. Illnesses among United States veterans of the Gulf War: a population-based survey of 30,000 veterans. *J Occup Environ Med.* 2000;42: 491–501.

9. Bliese PWK, Adler A, Thomas J. Research report 2004–002: validation of the 90–120 day postdeployment screen. Available at: http://www.usamru-e.hqusareur.army.mil. Accessed March 28, 2007.

10. Solomon Z, Mikulincer M. Trajectories of PTSD: a 20-year longitudinal study. *Am J Psychiatry.* 2006;163:659–666.

11. VHA directive: 2004–015: Implementation of the New National Clinical Reminder, the "Afghan and Iraq Post-Deployment Screen." Washington, DC: Department of Veterans Affairs, Veterans Health Administration; 2004.

12. Prins A, Ouimette P, Kimmerling R, et al. The primary care PTSD screen (PC-PTSD): development and operating characteristics. *Prim Care Psychiatry.* 2004;9:9–14.

13. Revised implementation of national clinical reminder for Afghan and Iraq post-deployment screening. Washington, DC: Department of Veterans Affairs, Veterans Health Administration; 2005.

14. Bliese PWK, Adler A, Thomas J, Hoge C. Screening for traumatic stress among re-deploying soldiers: US Army Medical Research Unit–Europe. Washington, DC: Walter Reed Army Institute of Research; 2004.

15. Whooley MA, Avins AL, Miranda J, Browner WS. Case-finding instruments for depression. Two questions are as good as many. *J Gen Intern Med.* 1997;12:439–445.

16. Kroenke K, Spitzer RL, Williams JB. The Patient Health Questionnaire-2: validity of a two-item depression screener. *Med Care.* 2003;41:1284–1292.

17. Bradley KA, DeBenedetti AF, Volk RJ, Williams EC, Frank D, Kivlahan DR. AUDIT-C as a brief screen for alcohol misuse in primary care. *Alcohol Clin Exp Res.* 2007;31:1208–1217.

18. Fung CH, Woods JN, Asch SM, Glassman P, Doebbeling BN. Variation in implementation and use of computerized clinical reminders in an integrated healthcare system. *Am J Manag Care.* 2004;10(11 pt 2):878–885.

19. Hoge CW, Auchterlonie JL, Milliken CS. Mental health problems, use of mental health services, and attrition from military service after returning from deployment to Iraq or Afghanistan. *JAMA.* 2006;295:1023–1032.

20. Grieger TA, Cozza SJ, Ursano RJ, et al. Posttraumatic stress disorder and depression in battle-injured soldiers. *Am J Psychiatry.* 2006;163:1777–1783.

21. Gray MJ, Maguen S, Litz BT. Acute psychological impact of disaster and large-scale trauma: limitations of traditional interventions and future practice recommendations. *Prehosp Disaster Med.* 2004;19:64–72.

22. Foa E, Davidson J, Frances A. The expert consensus guideline series: treatment of post-traumatic stress disorder. *J Clin Psychiatry.* 1999;61.

23. Monson CM, Schnurr PP, Resick PA, Friedman MJ, Young-Xu Y, Stevens SP. Cognitive processing therapy for veterans with military-related posttraumatic stress disorder. *J Consult Clin Psychol.* 2006;74:898–907.

24. Wright KM, Thomas JL, Adler AB, Ness JW, Hoge CW, Castro CA. Psychological screening procedures for deploying U.S. Forces. *Mil Med.* 2005;170:555–562.

25. Grunebaum M, Luber P, Callahan M, Leon AC, Olfson M, Portera L. Predictors of missed appointments for psychiatric consultations in a primary care clinic. *Psychiatr Serv.* 1996;47:848–852.

26. Hedrick SC, Chaney EF, Felker B, et al. Effectiveness of collaborative care depression treatment in Veterans' Affairs primary care. *J Gen Intern Med.* 2003;18:9–16.

27. Miller W, Rollnick S. *Motivational Interviewing. Preparing People for Change.* 2nd ed. New York, NY: Guilford Publications; 2002.

1) Pilot Study 13:

> **High-Field Susceptibility-Weighted MRI and Volumetric Spectroscopic Imaging in Traumatic Brain Injury**

> **Principal Investigator: Wang Zhan, Ph.D.**

-- COMBINED WITH PILOT STUDY 6 --

2) Pilot Study 6:

> **The Post-traumatic Syndrome of Blunt Head Injury: Noninvasive Neurochemical and Structural Assessment**

> **Principal Investigator: Grant Gauger, M.D.**

ABSTRACT

Blunt trauma of the human brain, occurring in the course of military operations of a wide variety, presents serious problems in assessment, treatment, and outcome prediction. Mild traumatic brain injury (TBI) is frequently followed by a clinical syndrome which is associated with serious disability, despite the absence of significant abnormalities on conventional radiologic imaging. Magnetic resonance spectroscopy has revealed changes in cerebral metabolite ratios in several sites, suggesting diffuse tissue damage. In a previous study using volumetric proton magnetic spectroscopic imaging (MRSI) at 1.5T, we have found significant changes in some brain regions for average values from all TBI subjects, with reduced N-Acetylaspartate (NAA)/Creatine (Cr), increased Choline (Cho)/Cr, and reduced NAA/Cho ratios. The results show evidence of widespread metabolic changes in regions that appear normal on diagnostic MR images. In order to clarify the extent and significance of such changes, we propose the study of a larger number of subjects, using the 4.0T system, with repeat testing at six months after injury. Moreover, the application of diffusion tensor imaging (DTI) to the study of white matter fiber systems in the brain permits an assessment of the relationship of metabolic changes in nuclear centers to the microstructural character of their connecting tracts. Data from both MRSI and DTI will be correlated with the results of neurocognitive and psychological testing. This correlation is anticipated to lead to improved understanding of the post-concussion syndrome, with early application to important decisions in the assessment and treatment of injured military personnel.

TABLE OF CONTENTS

INTRODUCTION

The purpose of this study is to determine the nature and extent of differences in metabolic measures between mild TBI patients and normal subjects, using 4 Tesla MRI imaging. Thisstudy is designed to test the hypothesis that the combination of metabolic
information, as measured with volumetric proton MRSI, and white matter connectivity, as measured by DTI, provides increased prognostic value in mild TBI, as compared to either measure alone. Furthermore, neuropsychological data will be correlated with the MRI findings to determine the underlying relationship between cognitive impairments and white matter integrity. 12 mTBI subjects and 6 normal controls are studied at 2 time points per year to evaluate post-injury changes in the brain over time.

BODY

Since the previous annual report on September 2007, 17 subjects have been recruited, and have undergone completion of the consent process at San Francisco General Hospital (SFGH). Both injured and control subjects have then completed the neurocognitive testing battery at SFGH, followed by spectroscopy, diffusion tensor imaging, and susceptibility weighted imaging at the San Francisco Veterans Affairs Medical Center (SFVAMC). A compromise of the recruiting process, caused by personnel changes at SFGH, and resulting in slowed acquisition, has been corrected by the designation of a new local coordinator.

The determination of the nature and extent of differences in metabolic measures between mild TBI patients and normal subjects, using the 4 Tesla magnet, will be accomplished upon completion of data acquisition from magnetic resonance spectroscopic study of both injured and control subjects, with repeat testing at a 6-month interval in determination of alterations of metabolic measures over time.

Voxel-based group analysis has been performed on the diffusion tensor imaging (DTI) data acquired from 14 injured subjects (Female=1, 29±7 yrs). Significant decreased fractional anisotropy (FA) (p<0.01) has been found in the intersection of the fornix and corpus callosum (See Fig.1, a), and in posterior cingulate cortex (b).

Fig.1: Reduced FA (p<0.01) in head injured subjects (N=13) compared with age and gender matched group.

White matter alterations in the trauma subjects have also been studied by correlation of DTI images with time after injury (7~46 days). Significant negative correlation between FA and time after injury was again found in cingulate (p<0.01), as shown in Fig.2.
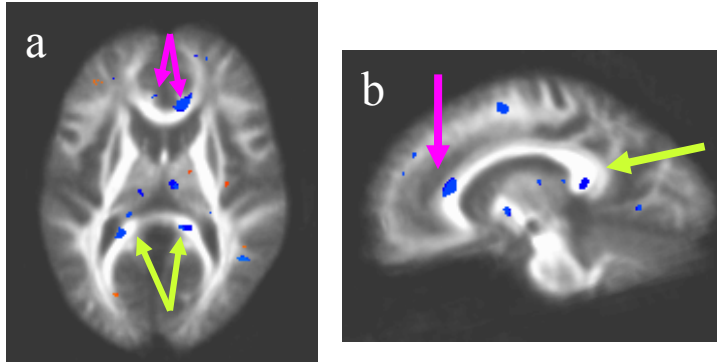

Fig.2: Negative correlation of FA with time after injury
(p<0.01) in the injured subjects (N=13).

The correlation of MRSI and DTI data with neurobehavioral changes determined by the neurocognitive testing will be undertaken as soon as data acquisition and analysis permit.

KEY RESEARCH ACCOMPLISHMENTS:

1. Successful and continuing advanced MR study of injured subjects and controls, and coordinated neurocognitive testing, including follow-up examinations.
2. Development of effective methodology to analyze the voxel-based diffusion tensor imaging data at group level.
3. Identification of patterns of white matter alteration in response to trauma, as demonstrated by changes in fractional anisotropy.

REPORTABLE OUTCOMES

N/A

CONCLUSION

The preliminary results of DTI investigation suggest the possibility of distinctive patterns of fractional anisotropy change in acute mild head injury subjects. We plan to perform correlation analysis with the results of both spectroscopic and neurocognitive examinations.

An improved understanding of the mechanisms of mild brain injury, including concussion and resulting impairment of cerebral function, will be dependent upon the correlation of biochemical, microstructural, and cognitive changes, and is the objective of the current study.

REFERENCES

N/A

APPENDICES

N/A

SUPPORTING DATA

N/A

Pilot Study 14:   <u>Final Report</u> **(funding period 04/01/06 – 06/30/08)**

Improve Function of Spinal Cord Injury-included Neurogenic Bladder

Principal Investigator: Rajvir Dahiya, Ph.D.

ABSTRACT

The **<u>main goal</u>** of this proposal was to investigate a novel strategy to improve the function of spinal cord injury mediated neurogenic bladder using grafting of acellular bladder matrix (BAMG). The rationale for this study is that spinal cord injury mediated neurogenic bladder is a common problem associated with our combat veterans. The treatment for this type of combat-related injury is limited. Our laboratory and others have developed an animal model for spinal cord injury mediated neurogenic bladder. We used this model to improve bladder function using grafting of acellular bladder matrix to enhance bladder capacity and compliance. There are two specific aims of this project. Under aim 1, we investigated whether grafting of acellular matrix can improve the function of neurogenic bladder in a spinal cord injury model. Under aim 2, we investigated whether administration of growth factors can stimulate *in vivo* function of matrix-directed regeneration of neurogenic bladders. The results of these experiments suggest that acellular matrix can enhance the bladder capacity and compliance of spinal cord injury induced neurogenic bladder. Nerve growth factor (NGF) has a significant synergistic effect on the development, differentiation and functional restoration of the acellular matrix when administered with vascular endothelial growth factor (VEGF) in neurogenic bladder. Our results indicate that NGF may be a useful cytokine for enhancing the regeneration of a functional bladder following acellular matrix grafting in neurogenic rat model. This project has high military relevance because spinal cord injury mediated neurogenic bladder is a common problem among our combat veterans. The treatment for such combat-related injury is limited. The data generated from this project presents an entirely new strategy for bladder reconstruction that eliminates many of the disadvantages inherent in earlier models.

TABLE OF CONTENTS

INTRODUCTION

The <u>main goal</u> of this proposal was to investigate a novel strategy to improve the function of spinal cord injury mediated neurogenic bladder using grafting of acellular bladder matrix. The hypothesis is that spinal cord injury mediated neurogenic bladder can be regenerated when grafted with acellular bladder matrix. The cellular and molecular mechanisms for regeneration of acellular bladder matrix in neurogenic model may be through activation of various cytokines such as growth factors that will accelerate the regeneration of acellular matrix bladder when grafted onto neurogenic rat bladder. Two specific aims have been proposed to test this hypothesis. Specific Aim # 1: To investigate whether grafting of acellular matrix can improve the function of neurogenic bladder in a spinal cord injury model. Under this specific aim, we will investigate whether grafting of acellular bladder matrix can regenerate a functional bladder using a spinal cord injury induced neurogenic rat model. Our laboratory and others have developed an animal model (rat) for spinal cord injury mediated neurogenic bladder. We will use this model to improve bladder function by grafting of acellular bladder matrix to enhance bladder capacity and compliance in neurogenic bladder. The following experiments will be conducted to investigate: (a) epithelial migration; (b) smooth muscle cell migration and growth; (c) neovascularization and nerve growth; (d) *in vivo* function of regenerated neurogenic bladder by urodynamic studies. Specific Aim # 2: To investigate whether administration of growth factors can stimulate *in vivo* function of matrix-directed regeneration of neurogenic bladders.

BODY

There were two specific aims of this project. Under aim 1, we investigated whether grafting of acellular matrix can improve the function of neurogenic bladder in a spinal cord injury model. Under this aim, we used female rats to induce spinal cord injury (SCI) by transection of the spinal cord at the lower thoracic level. Eight weeks following spinalization, bladder augmentation using BAMG was performed after hemicystectomy of the hypertrophic bladder. Cystometrography was performed at 8 weeks after spinalization and again at 8 weeks after augmentation. Several urodynamic parameters were measured and the grafted bladder was histologically evaluated. Urodynamic parameters showed improvement in some bladder functions in both hyperreflexic and underactive bladders after augmentation. In addition, bladder compliance was increased in hyperreflexic bladders and decreased in underactive bladders. Bladder augmentation decreased bladder capacity in high-capacity rats and increased it in low-capacity rats. Histological evaluation showed complete regeneration of BAMG in SCIinduced neurogenic bladder at 8 weeks after augmentation. This is the first report suggesting that the voiding function in SCI-induced neurogenic bladder can be improved by augmentation using BAMG. Improved voiding function was accompanied by histological regeneration of BAMG. We published these findings in World J. Urology (25: 207-213, 2007).

Specific Aim # 2: To investigate whether administration of growth factors can stimulate *in vivo* function of matrix-directed regeneration of neurogenic bladders. Under this aim, we used female, Sprague-Dawley rats. At eight weeks after spinalization surgery (neurogenic bladder), they were divided into five groups consisting of untreated controls and those whose bladders were injected with no either growth factor, NGF (2 μg/rat), VEGF (2 μg/rat) or both at partial BAMG replacement surgery. After eight weeks, bladder function was assessed by urodynamic studies and bladders were harvested for histological examination. Smooth muscle induction, collagen and nerve fiber regeneration were assessed immunohistochemically using antibodies to smooth muscle actin (α-actin), Masson's Trichrome and protein gene product 9.5 (PGP 9.5) respectively. Bladder capacity and compliance were significantly increased in all BAMG groups 8 weeks after surgery compared with that before bladder replacement surgery. Bladder capacity and compliance were much higher in VEGF and NGF combined group than in controls, or NGF and VEGF alone groups. This is the first report demonstrating that NGF has a significant synergistic effect on the development, differentiation and functional restoration of the BAMG when administered with VEGF in neurogenic bladder. Our results indicate that NGF may be a useful cytokine for enhancing the regeneration of a functional bladder following acellular matrix grafting in neurogenic rat model. All these experiments are completed and got accepted for publication (Kikuno et al, 2008).

KEY RESEARCH ACCOMPLISHMENTS

The major findings of this project are the followings: First, grafting of acellular matrix on spinal cord injury-induced neurogenic bladder can enhance both histological and functional parameters and thus resulting in increased in bladder capacity and compliance. Second, nerve growth factor (NGF) has a significant synergistic effect on the development, differentiation and functional restoration of the acellular matrix when administered with vascular endothelial growth factor (VEGF) in neurogenic bladder. Our results indicate that NGF may be a useful cytokine for enhancing the regeneration of a functional bladder following acellular matrix grafting in neurogenic rat model. This project has high military relevance because spinal cord injury mediated neurogenic bladder is a common problem among our combat veterans. The treatment for such combat-related injury is limited. The data generated from this project presents an entirely new strategy for bladder reconstruction that eliminates many of the disadvantages inherent in earlier models.

REPORTABLE OUTCOMES

Urakami S, Shiina H, Enokida H, Kawamoto K, Kikuno N, Fandel T, Vejdani K, Nunes L, Igawa M, Tanagho EA, Dahiya R. Functional improvement in spinal cord injury-induced neurogenic bladder by bladder augmentation using bladder acellular matrix graft in the rat. World J Urol. 25(2):207-13, 2007.

Kikuno N, Kawamoto, Hiroshi Hirata H, Vejdani K, Kawakami K, Fandel T, Nunes L, [1], Urakami S, Shiina H, Igawa M, [2], Tanagho E, and Dahiya R. Nerve growth factor (NGF) combined with vascular endothelial growth factor (VEGF) enhances regeneration of bladder acellular matrix graft in spinal cord injury-induced neurogenic rat bladder. Brit. J. Urology (accepted for publication, 2008).

CONCLUSIONS

In summary, the results of this project suggest that grafting of acellular matrix on spinal cord injury-induced neurogenic bladder can enhance both histological and functional parameters and thus resulting in increased in bladder capacity and compliance. Second, nerve growth factor (NGF) has a significant synergistic effect on the development, differentiation and functional restoration of the acellular matrix when administered with vascular endothelial growth factor (VEGF) in neurogenic bladder. This project has high military relevance because spinal cord injury mediated neurogenic bladder is a common problem among our combat veterans. The treatment for such combat-related injury is limited. The data generated from this project presents an entirely new strategy for bladder reconstruction that eliminates many of the disadvantages inherent in earlier models.

REFERENCES

Urakami S, Shiina H, Enokida H, Kawamoto K, Kikuno N, Fandel T, Vejdani K, Nunes L, Igawa M, Tanagho EA, Dahiya R. Functional improvement in spinal cord injury-induced neurogenic bladder by bladder augmentation using bladder acellular matrix graft in the rat. World J Urol. 25(2):207-13, 2007.

Kikuno N, Kawamoto, Hiroshi Hirata H, Vejdani K, Kawakami K, Fandel T, Nunes L, [1], Urakami S, Shiina H, Igawa M, [2], Tanagho E, and Dahiya R. Nerve growth factor (NGF) combined with vascular endothelial growth factor (VEGF) enhances regeneration of bladder acellular matrix graft in spinal cord injury-induced neurogenic rat bladder. Brit. J. Urology (accepted for publication, 2008).

APPENDICES

Two manuscripts:

Appendix I (7 pages total)

Urakami S, Shiina H, Enokida H, Kawamoto K, Kikuno N, Fandel T, Vejdani K, Nunes L, Igawa M, Tanagho EA, Dahiya R. Functional improvement in spinal cord injury-induced neurogenic bladder by bladder augmentation using bladder acellular matrix graft in the rat. World J Urol. 25(2):207-13, 2007.

Appendix II (27 pages total)

Kikuno N, Kawamoto, Hiroshi Hirata H, Vejdani K, Kawakami K, Fandel T, Nunes L, [1], Urakami S, Shiina H, Igawa M, [2], Tanagho E, and Dahiya R. Nerve growth factor (NGF) combined with vascular endothelial growth factor (VEGF) enhances regeneration of bladder acellular matrix graft in spinal cord injury-induced neurogenic rat bladder. Brit. J. Urology (accepted for publication, 2008).

SUPPORTING DATA
N/A

ORIGINAL ARTICLE

Functional improvement in spinal cord injury-induced neurogenic bladder by bladder augmentation using bladder acellular matrix graft in the rat

**Shinji Urakami · Hiroaki Shiina · Hideki Enokida · Ken Kawamoto ·
Nobuyuki Kikuno · Thomas Fandel · Kaveh Vejdani · Lora Nunes ·
Mikio Igawa · Emil A. Tanagho · Rajvir Dahiya**

Abstract Spinal cord injury (SCI) rostral to the lumbo-sacral level causes bladder hyperreflexia and detrusor-sphincter dyssynergia (DSD), which are accompanied by bladder hypertrophy. We hypothesize that bladder augmentation using a bladder acellular matrix graft (BAMG) can improve the function of SCI-mediated neurogenic bladder. In female rats ($n = 35$), SCI was induced by transection of the spinal cord at the lower thoracic level. Eight weeks following spinalization, bladder augmentation using BAMG was performed after hemicystectomy of the hypertrophic bladder. Cystometrography was performed at 8 weeks after spinalization and again at 8 weeks after augmentation. Several urodynamic parameters were measured and the grafted bladder was histologically evaluated. Thirty one rats were alive 8 weeks after spinalization. Twenty two (71%) rats developed hyperreflexic bladders and nine (29%) rats had underactive bladders before bladder augmentation. Twenty six rats survived until 8 weeks after augmentation. Urodynamic parameters showed improvement in some bladder functions in both hyperreflexic and underactive bladders after augmentation. In addition, bladder compliance was increased in hyperreflexic bladders and decreased in underactive bladders. Bladder augmentation decreased bladder capacity in high-capacity rats and increased it in low-capacity rats. Histological evaluation showed complete regeneration of BAMG in SCI-induced neurogenic bladder at 8 weeks after augmentation. This is the first report suggesting that the voiding function in SCI-induced neurogenic bladder can be improved by augmentation using BAMG. Improved voiding function was accompanied by histological regeneration of BAMG.

Keywords Bladder acellular matrix graft ·
Bladder augmentation · Spinal cord injury ·
Neurogenic bladder · Tissue engineering

S. Urakami · H. Shiina · H. Enokida · K. Kawamoto ·
N. Kikuno · T. Fandel · K. Vejdani · L. Nunes ·
E. A. Tanagho · R. Dahiya (✉)
Department of Urology, Veterans Affairs Medical Center,
University of California, 4150 Clement Street,
San Francisco, CA 94121, USA
e-mail: RDahiya@urology.ucsf.edu

S. Urakami · H. Shiina · N. Kikuno · M. Igawa
Department of Urology, Faculty of Medicine,
Shimane University, Izumo 693-8501, Japan

H. Enokida · K. Kawamoto
Department of Urology, Graduate School of Medical
and Dental Sciences, Kagoshima University,
Kagoshima 890-8520, Japan

Introduction

Voluntary micturition is regulated by a complex mechanism in the spinal and supraspinal neural pathways. Spinal cord injury (SCI) rostral to the lumbosacral level eliminates the voluntary control of micturition [1, 2]. After the initial SCI-induced areflexic bladder, the bladder becomes hyperreflexic and bladder sphincter coordination is impaired, leading to detrusor-sphincter dyssynergia (DSD). This causes urinary retention and bladder overdistension, and increases the workload of the bladder leading to hypertrophy of the bladder muscle. Lower urinary tract dysfunction including heavy trabeculation and diverticular formation of the bladder causes various problems, such as urinary incontinence, urinary tract infection and upper urinary tract damage.

Standard treatment for neurogenic bladder after SCI is usually limited to urinary drainage by catheterization, which can lead to repeated urinary tract infection and lower quality of life. Surgical options for neurogenic bladder that has failed to respond to conservative treatments are augmentation cystoplasty. This technique can potentially solve the problems associated with bladder capacity. However, urinary tract infection, mucus production, urolithiasis and absorptive disadvantage related to the usage of bowel segments are increased since this type of enterocystoplasty cannot guarantee detrusor function which is necessary for physiological micturition [3, 4].

Recently, we have demonstrated the applicability of bladder replacement using bladder acellular matrix graft (BAMG) as a scaffold for complete regeneration of smooth muscle, urothelium, blood vessels and nerves in normal rats [5–8]. The bladder capacity and compliance of the grafted bladder were improved as compared to controls. The grafted bladder had restored function for emptying and served as a low-pressure reservoir. Thus, bladder replacement using BAMG may be an alternative surgical option to augmentation enterocystoplasty for refractory neurogenic bladder. We hypothesize that bladder replacement using BAMG in SCI-induced neurogenic bladder will restore normal bladder function. Since SCI rats and humans exhibit similar lower urinary tract dysfunction [2], this study was conducted with SCI rats to evaluate whether BAMG replacement could show functional and histological improvement of SCI-mediated neurogenic bladder.

Materials and methods

Animals

For this study we used 35 female Sprague–Dawley rats (Charles River, Montreal, QC, Canada) weighing 200 to 250 g. The animals were maintained and treated according to our institutional guidelines. The local Animal Care Committee approved the experimental protocol.

Bladder acellular matrix grafts

The BAMG was prepared from bladders harvested from 4-month-old female Sprague–Dawley rats, and it was prepared as described previously in our laboratory [5–8]. In brief, bladders were washed with PBS and then treated with 0.1 M sodium chloride solution containing DNase for 2 days to lyse all the cells. The bladders were then treated with 4% sodium deoxycholate overnight. The BAMG size was almost same, and acellularity was confirmed by light microscopy using H&E and methyl green pyronin staining before grafting.

Spinalization surgery

Rats were anesthetized by inhalation of 2% isoflurane. A midline dorsal incision was made over lower thoracic vertebra to expose the vertebral spines and paravertebral muscles. A laminectomy of the T10 spinal vertebrae was performed and the spinal cord was completely transected at the lower thoracic level. Postoperatively the bladder was manually emptied twice daily until reflex voiding recovered after SCI. Furthermore, additional 10 rats also underwent spinalization surgery as SCI-control rats without bladder replacement.

Bladder wall replacement surgery

After 8 weeks the spinalized rats were prepared for bladder replacement surgery. Rats were anesthetized by inhalation of 2% isoflurane. The urinary bladder was exposed via a small suprapubic incision and partial cystectomy (50%) was performed. The BAMG was then anastomosed to the host bladder with running and interlocking 7–0 absorbable sutures. The bladder was irrigated with normal saline to test the anastomosis for leakage.

Cystometrography

Cystometrography was done before grafting and repeated 8 weeks after bladder replacement. All rats underwent cystometrography under ketamine anesthesia (100 mg/kg) [9]. Cystometrography was performed according to previously published methods [10]. After the bladder was emptied, saline was infused into the bladder at 0.2 ml/min. The variables recorded during saline infusion included resting bladder pressure, threshold bladder volume (bladder capacity), threshold voiding pressure, bladder compliance, voided volume, residual urine volume (RUV), voiding efficacy, frequency of uninhibited detrusor contractions (UIC), maximal amplitude of UIC and infused saline volume at the first UIC. Bladder compliance was calculated by dividing the bladder capacity by the threshold voiding pressure. Voiding efficacy was estimated using the formula, (voided volume/bladder capacity) $\times 100$. A contraction of 15 cm of H_2O or greater was considered an UIC. The presence of UIC in this model of neurogenic

bladder was categorized as a hyperreflexic-bladder, whereas the absence of UIC indicated an underactive-bladder. Cystometrography was performed on 10 normal rats serving as controls.

Histologic evaluation

After completion of all procedures, the bladder was filled with a 10% formalin solution and removed. The bladder specimens were embedded in paraffin wax. Deparaffinized sections (4 μm) were used for staining with hematoxylin and eosin (H&E) and Masson's trichrome. Immunohistochemical staining was performed using anti-smooth muscle actin (α-actin) (Sigma, St Louis, MO) and anti-Desmin (Santa Cruz Biotechnology, Santa Cruz, CA) to confirm the presence of smooth muscle fibers. Immunostaining of anti-CD31 (Santa Cruz Biotechnology, Santa Cruz, CA) was used to assess endothelial cell regeneration and anti-protein gene product 9.5 (PGP 9.5) (Biogenesis, Poole, UK) was used to detect nerve fibers.

Statistical analysis

The relationship between pre- and post-augmentation in urodynamic parameters was analyzed using a Wilcoxon signed-rank test. Other statistical analysis was performed using the Mann–Whitney test. A P-value of less than 0.05 was considered to be statistically significant.

Results

Mortality and morbidity of spinalization and bladder replacement

Suprasacral spinalization surgery was performed on 35 rats. Four rats (11.4%) died before bladder replacement surgery. Eleven rats (31.4%) had gross hematuria after spinalization. Overdistention of the bladder was assumed to be the cause of hematuria. Six rats (17.1%) developed urinary tract infections. Eight weeks after spinalization 31 rats (88.6% survival rate) underwent bladder replacement surgery after cystometrography. However, five animals (16.1%) died due to urine leakage at the site of anastomosis. Twenty-six rats (83.9%) survived to 8 weeks after replacement and had cystometrography at this time. Nine rats (34.6%) were found to have vesical stones at bladder harvest after cystometrography. Some stones had formed on the absorbable or non-absorbable sutures. Ten rats (38.7%) developed urinary tract infection after replacement.

Sixteen rats (61.5%) had hematuria after replacement. The causes for hematuria were urinary tract infection early after replacement and stone-formation at later times.

Cystometrography

All 10 normal control rats showed a stable cystometrogram with no UIC (Fig. 1a). However, of the 31 surviving SCI rats, 22 rats (71.0%) developed hyperreflexic bladders with UIC and 9 (29.0%) had underactive bladders with no UIC 8 weeks after spinalization (Fig. 1b, c). In these nine rats with underactive bladders, 8 (88.9%) had gross hematuria after spinalization. The average bladder capacity and RUV of SCI rats (4.2 ± 2.3, 1.5 ± 1.6 ml, respectively) was significantly higher than that of normal rats (0.5 ± 0.1, 0.05 ± 0.02 ml, respectively) ($P < 0.05$). All SCI rats had a grossly hypertrophied, thick bladder wall prior to bladder replacement.

In addition, SCI-control rats without bladder replacement showed similar urodynamic data at 8 weeks and 16 weeks after spinalization (data not shown). In other words, condition including symptom and data will stabilize 8 weeks after SCI in rats. Therefore, we compared urodynamic parameters between 8 weeks after spinal cord injury (as pre-replacement) and 8 weeks after bladder replacement surgery (as post-replacement). Urodynamic data after replacement was obtained from 26 rats. The RUV after replacement significantly decreased as compared to that before replacement and voiding efficacy also significantly improved ($P < 0.0001$, both) (Fig. 2a, b). Seventeen rats developed hyperreflexic bladders before replacement and had a significantly decreased UIC after replacement ($P < 0.002$) (Fig. 2c). In the nine underactive-bladder rats, bladder compliance significantly decreased after replacement ($P < 0.02$) (Fig. 2d) and bladder capacity showed a trend toward a reduction ($P < 0.1$). Of 17 hyperreflexic bladders, 9 were low-capacity (≥ 5 ml) and 8 were high-capacity ≥ 5.0 ml) bladders. In the hyperreflexic, low-capacity bladders, the bladder capacity and compliance were significantly increased after replacement ($P < 0.03$, both) (Fig. 3a, b). Also, the frequency of UIC during the first 10 minutes and maximum amplitude of UIC significantly decreased after replacement ($P < 0.03$, $P < 0.03$, respectively) (Fig. 3c, d). In contrast, the hyperreflexic, high-capacity bladders showed a significant decrease of capacity after replacement ($P < 0.02$) (Fig. 3e). The frequency of UIC during the first 10 minutes and maximum amplitude of UIC did not change after replacement.
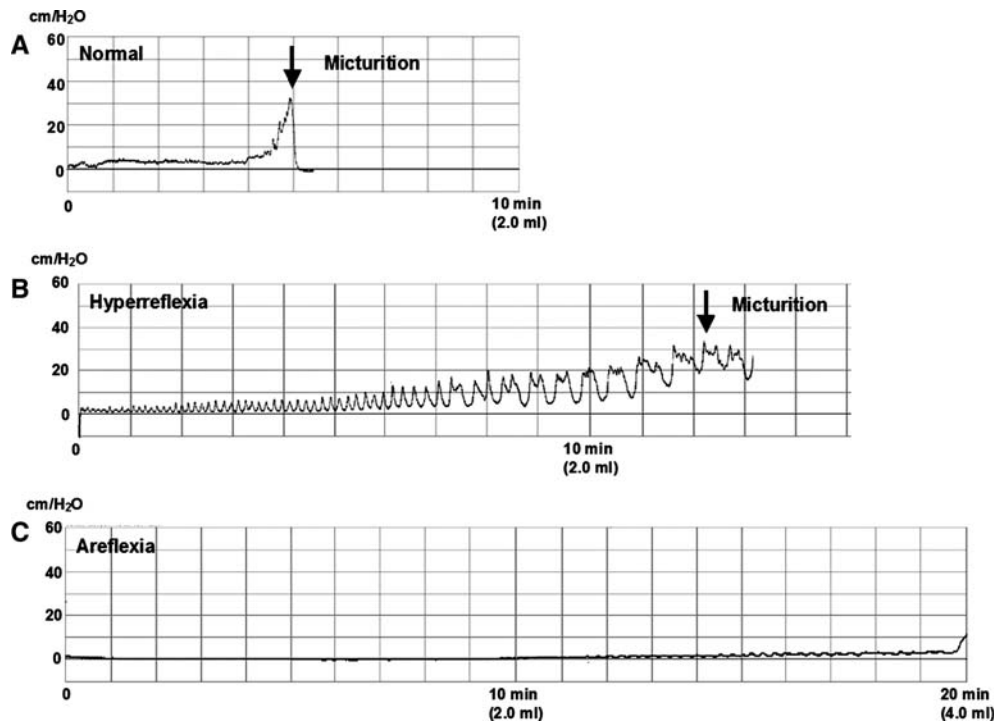
Fig. 1 **a** Typical cystometrogram of normal bladder: this normal rat showed stable cystometrogram with no uninhibited contractions. The bladder capacity was 1.0 ml and the peak amplitude of the voiding contractions is 31.0 cm/H_2O. **b** Typical cystometrogram of SCI-induced hyperreflexic-bladder (hyperreflexia): this spinalized rat showed many and large uninhibited non-voiding contractions (more than 15 cm/H_2O) during saline infusion. The size of the contractions increased with time. Bladder capacity was approximately 2.5 ml, threshold pressure was 33.5 cm/H_2O, and bladder compliance was 0.075. **c** Typical cystometrogram of SCI-induced underactive-bladder (areflexia): this spinalized rat showed no uninhibited contractions during saline infusion. The bladder capacity was more than 4.0 ml, and bladder compliance was very high

Histologic evaluation

Rats which did not survive the full 8 weeks after replacement were histologically evaluated. Two days after bladder replacement, there was a monolayer of urothelial lining on the BAMG and a number of mesenchymal infiltrating cells (Fig. 4a). At 2 weeks, the lumen of the BAMG was covered with multiple layers of urothelium (Fig. 4b). At 4 weeks, spindle-shaped smooth muscle bundles positive for α-actin staining were observed in the sub-urothelium (Fig. 4c, d). As for the rats that did survive, at 8 weeks, aggregated bundles of smooth muscle were observed underneath the urothelium and a well-defined detrusor layer was identified (Fig. 4e–g). However, α-actin expression and collagen fibers were significantly less apparent than in the hypertrophied host bladder. In submucosal regions of the BAMG, densely arranged collagen fibers were also observed by Masson's trichrome staining (Fig. 4h). Vascular endotheliums were immunostained with anti-CD31 antibodies (Fig. 4i). Nerve cells were observed with PGP9.5 staining at 8 weeks (Fig. 4j).

Discussion

When the spinal cord above the sacral segment is damaged in rats, the SCI produces an initial period of bladder areflexia that lasts for several days. After this period, rats usually develop hyperreflexic bladders. However, there are some exceptions to this rule, particularly in human patients with lesions of the thoracolumbar vertebral junction where the sacral cord is located. Our results with rats indicated that 30% had underactive bladders after suprasacral spinalization involving the thoraco-lumbar region. In fact, detrusor areflexia has been reported in 30% of human patients with suprasacral SCI or disease [11, 12]. The cause for this is hypothesized to be the coexistence of a second sub-clinical lesion at a different level, a post-traumatic vascular involvement of distal spinal segments, a variability in cord-to-column correlation, myogenic detrusor damage due to bladder overdistension, and a disordered integration of afferent activity at the sacral root or cord level [12, 13]. In our study, the coexistence of hematuria with bladder distention was related to the development of an underactive bladder. Therefore,

Fig. 2 Urodynamic parameters before and after replacement. In all rats, the residual urine volume (**a**) significantly decreased and voiding efficacy (**b**) significantly improved after augmentation as compared with those before augmentation ($P < 0.0001$, both). The rats with hyperreflexic-bladder showed that the maximum amplitude of UIC significantly decreased after augmentation ($P < 0.002$) (**c**). Furthermore, in underactive-bladder rats, bladder compliance was significantly decreased after augmentation ($P < 0.02$) (**d**)
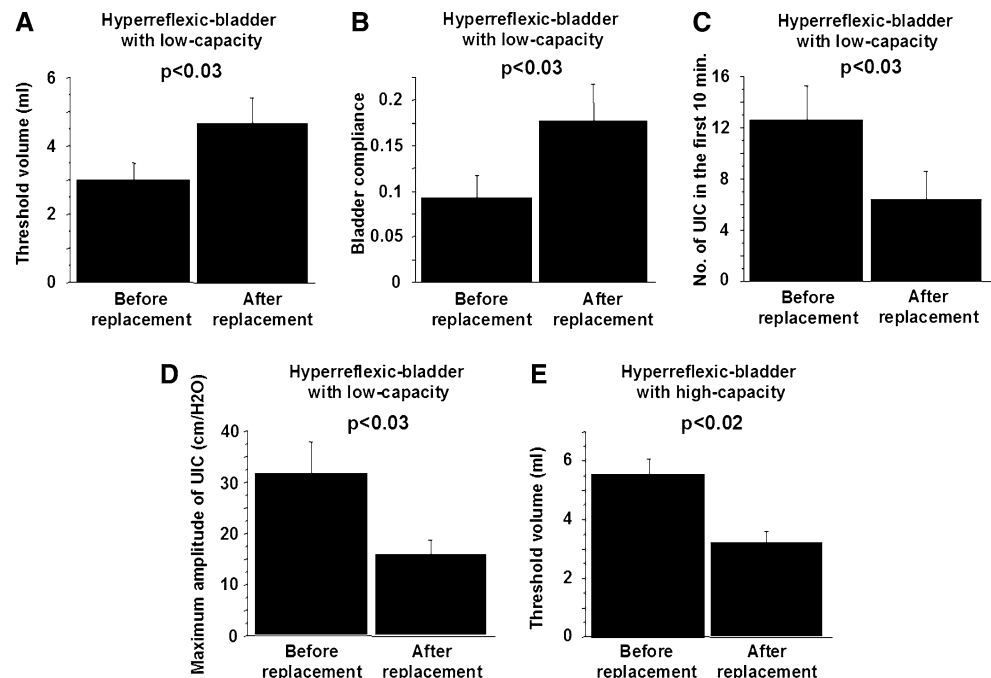

Fig. 3 In hyperreflexic-bladder rats with low-capacity, the bladder capacity (**a**) and bladder compliance (**b**) significantly increased after augmentation as compared with those before augmentation ($P < 0.03$, both). The number of UIC in the first 10 min (**c**) and maximum amplitude of UIC (**d**) significantly decreased after augmentation ($P < 0.03$, $P < 0.03$, respectively). On the other hand, the hyperreflexic-bladder rats with high capacity showed a significant decrease of bladder capacity after augmentation ($P < 0.02$) (**e**)

myogenic detrusor damage due to bladder overdistension during the areflexia phase may influence the urodynamic pattern of SCI-induced neurogenic bladder involving the thoraco-lumbar junction.

Our experience with bladder replacement using BAMG has been very encouraging. We investigated the functional and histological restoration of SCI-induced

neurogenic bladder grafted with BAMG. Initially, the urodynamics showed improved bladder function such as voiding efficacy for both hyperreflexic and underactive bladders after replacement. In addition, UICs were inhibited in hyperreflexic bladders. Moreover, bladder replacement decreased bladder capacity in high-capacity rats and in contrast, increased the

Fig. 4 a Representative H&E staining of BAMG at 3 days after grafting (×100): a monolayer of urothelium (*black arrows*) covered the BAMG surface. A diffuse infiltration of mesenchymal cells was observed in the suburothelium. **b** Representative H&E staining of BAMG at 2 weeks after grafting (×100): the lumen of the BAMG was covered with multi-layers of urothelium (*black arrows*). Sparse thin smooth muscle fibers (*asterisks*) were noted in the suburothelium along with blood vessels. **c** Representative H&E staining of BAMG 4 weeks after grafting (×100): Smooth muscle fibers were increased and aggregated into small bundles. **d** Representative immunostaining of α-actin in the BAMG 4 weeks after grafting (×100): Spindle-shaped smooth muscle cells with α-actin positive staining were observed in the suburothelium. **e** Representative H&E staining of the BAMG 8 weeks after grafting (×100): Small smooth muscle bundles were increased and aggregated into organized thick bundles. **f** Representative immunostaining of α-actin in the BAMG 8 weeks after grafting (×100): Organized smooth muscle bundles in the BAMG show strong staining for α-actin. **g** Representative immunostaining of Desmin in the BAMG 8 weeks after grafting (×200): Smooth muscle bundles with Desmin positive staining were observed. **h** Representative Masson's trichrome staining of the BAMG 8 weeks after grafting (×100): Collagen, muscle fibers and nuclei are shown as blue, red and black, respectively. In submucosal regions, densely arranged collagen and muscle fibers were observed. **i.** Representative immunostaining of CD31 in the BAMG 8 weeks after grafting (×200): vascular endotheliums were immunostained with anti-CD31 antibodies. **j.** Representative immunostaining of PGP9.5 in the BAMG 8 weeks after grafting (×200): nerve cells and bundles (*asterisks*) were observed around smooth muscle bundles

bladder capacity in low-capacity rats. This functional improvement in both hyperreflexic and underactive bladders, demonstrates that the regenerated BAMG in neurogenic bladders can work not only as a low-pressure reservoir (storage of urine), but also as a functional bladder tissue with contractile activity. In addition, histological evaluation showed a complete histological regeneration of BAMG including neovascularity, smooth muscle and urothelium regeneration and re-innervation in SCI-induced neurogenic bladder 8 weeks after replacement. This was comparable to our previous findings in normal rats [5–8]. In addition, we have reported that normal histological and functional regeneration of BAMG was observed in the rat chemical cystitis model [14]. Therefore, bladder replacement using BAMG can lead to functional and histological

improvement over diseased host bladder. In addition, bladder hyperreflexia after SCI is induced by increased excitability of C-fiber bladder afferent nerves [15]. Bladder C-fiber afferent nerve activation may continue to induce DSD and cause a hypertrophied bladder to redevelop in a successfully regenerated BAMG. Therefore, treatment of DSD with bladder replacement may also require external sphincterotomy or desensitization of the C-fiber afferent nerves with intravesical vanilloids [16, 17].

Augmentation surgery is an invasive treatment method. Nonsurgical treatment is the mainstay of therapy for hyperreflexic bladder, and available options include bladder training, electrical stimulation, pharmacotherapy, and a combination of these options [18]. There is no doubt that the antimuscarinic drugs cur-

rently used in clinical practice (oxybutynin, tolterodine, trospium, solifenacin and darifenacin) are effective in reducing the symptoms of hyperreflexic bladder [19]. However, augmentation surgery should be reserved for severe problems recalcitrant to pharmacologic and behavioral therapeutic endeavors.

Conclusions

In this study, we investigated the functional and histological restoration of SCI-mediated neurogenic bladder grafted with BAMG. The results indicate that bladder replacement using BAMG can be an effective treatment option for SCI-induced neurogenic bladder.

References

1. Kruse MN, Belton AL, de Groat WC (1993) Changes in bladder and external urethral sphincter function after spinal cord injury in the rat. Am J Physiol 264:R1157–1163
2. Shaker H, Mourad MS, Elbialy MH, Elhilali M (2003) Urinary bladder hyperreflexia: a rat animal model. Neurourol Urodyn 22:693–698
3. Kashif KM, Holmes SA (1998) The use of small intestine in bladder reconstruction. Int Urogynecol J Pelvic Floor Dysfunct 9:275–280
4. Shekarriz B, Upadhyay J, Demirbilek S, Barthold JS, Gonzalez R (2000) Surgical complications of bladder augmentation: comparison between various enterocystoplasties in 133 patients. Urology 55:123–128
5. Piechota HJ, Dahms SE, Nunes LS, Dahiya R, Lue TF, Tanagho EA (1998) In vitro functional properties of the rat bladder regenerated by the bladder acellular matrix graft. J Urol 159:1717–1724
6. Piechota HJ, Dahms SE, Probst M, Gleason CA, Nunes LS, Dahiya R, Lue TF, Tanagho EA (1998) Functional rat bladder regeneration through xenotransplantation of the bladder acellular matrix graft. Br J Urol 81:548–559
7. Piechota HJ, Gleason CA, Dahms SE, Dahiya R, Nunes LS, Lue TF, Tanagho EA (1999) Bladder acellular matrix graft: in vivo functional properties of the regenerated rat bladder. Urol Res 27:206–213
8. Wefer J, Sievert KD, Schlote N, Wefer AE, Nunes L, Dahiya R, Gleason CA, Tanagho EA (2001) Time dependent smooth muscle regeneration and maturation in a bladder acellular matrix graft: histological studies and in vivo functional evaluation. J Urol 165:1755–1759
9. Dahms SE, Piechota HJ, Dahiya R, Gleason CA, Hohenfellner M, Tanagho EA (1998) Bladder acellular matrix graft in rats: its neurophysiologic properties and mRNA expression of growth factors TGF-alpha and TGF-beta. Neurourol Urodyn 17:37–54
10. Youssif M, Shiina H, Urakami S, Gleason C, Nunes L, Igawa M, Enokida H, Tanagho EA, Dahiya R (2005) Effect of vascular endothelial growth factor on regeneration of bladder acellular matrix graft: histologic and functional evaluation. Urology 66:201–207
11. Blaivas JG (1982) The neurophysiology of micturition: a clinical study of 550 patients. J Urol 127:958–963
12. Pesce F, Castellano V, Finazzi Agro E, Giannantoni A, Tamburro F, Vespasiani G (1997) Voiding dysfunction in patients with spinal cord lesions at the thoracolumbar vertebral junction. Spinal Cord 35:37–39
13. Light JK, Faganel J, Beric A (1985) Detrusor areflexia in suprasacral spinal cord injuries. J Urol 134:295–297
14. Cayan S, Chermansky C, Schlote N, Sekido N, Nunes L, Dahiya R, Tanagho EA (2002) The bladder acellular matrix graft in a rat chemical cystitis model: functional and histologic evaluation. J Urol 168:798–804
15. de Groat WC, Kawatani M, Hisamitsu T, Cheng CL, Ma CP, Thor K, Steers W, Roppolo JR (1990) Mechanisms underlying the recovery of urinary bladder function following spinal cord injury. J Auton Nerv Syst 30 Suppl:S71–77
16. Barton CH, Khonsari F, Vaziri ND, Byrne C, Gordon S, Friis R (1986) The effect of modified transurethral sphincterotomy on autonomic dysreflexia. J Urol 135:83–85
17. de Seze M, Wiart L, de Seze MP, Soyeur L, Dosque JP, Blajezewski S, Moore N, Brochet B, Mazaux JM, Barat M, Joseph PA (2004) Intravesical capsaicin versus resiniferatoxin for the treatment of detrusor hyperreflexia in spinal cord injured patients: a double-blind, randomized, controlled study. J Urol 171:251–255
18. Khullar V, Chapple C, Gabriel Z, Dooley JA (2006) The effects of antimuscarinics on health-related quality of life in overactive bladder: a systematic review and meta-analysis. Urology 68:38–48
19. Finney SM, Andersson KE, Gillespie JI, Stewart LH (2006) Antimuscarinic drugs in detrusor overactivity and the overactive bladder syndrome: motor or sensory actions? BJU Int 98:503–507

Dear Dr. Rajvir Dahiya

Nerve growth factor (NGF) combined with vascular endothelial growth factor VEGF) enhances regeneration of bladder acellular matrix graft in spinal cord injury-induced neurogenic rat bladder.

Thank you for sending your Manuscript to the BJU International.

I am pleased to inform you that your paper has been reviewed and has been accepted to appear in the Journal in print and as an Online Early publication.

OnlineEarly articles are complete, full-text articles published online in advance of their publication in a printed issue.

OnlineEarly articles are complete and final. They have been fully reviewed, revised and edited for publication, and the authors' final corrections have been incorporated. Because they are in final form, no changes can be made after online publication. Please make sure you have carefully checked your proofs before confiming that you have no changes to make to the production team.

As OnlineEarly articles do not yet have volume, issue or page numbers, they cannot be cited in the normal way and are, therefore, given a Digital Object Identifier (DOI). This allows the article to be cited and tracked before it is allocated to an issue. After print publication, the DOI remains valid and can continue to be used to cite and access the article, or the normal reference can be used.

It is very important that we have received the 3 forms that can allow us to process your paper. If you have not yet done so, please print the Submission, Exclusive Licence Form and Conflict of Interest forms. They can be found by clicking the 'Instructions and Forms' button at the top right hand corner of the Manuscript Central screen and should be faxed to us immediately at + 353 1 803 4389.

Please note the Copyright Assignment Form has now changed to an Exclusive Licence Form, E.L.F.. This means that you, the Author, is required to licence copyright in your paper to Blackwell Publishing. Since 01st November 2005 Copyright Licensing is a condition of publication in the BJUI, and papers will not be passed to the publisher for production unless the E.L.F. has been received.

To minimise publication time of your manuscript it is important that all electronic artwork is supplied in the correct format and resolution. I recommend that you consult the Illustration guidelines at http://www.blackwellpublishing.com/bauthor/illustration.asp if you need advice on any aspect of preparing your artwork.

On a future date the Technical Editors will ensure that your manuscript conforms to editorial policy and if there are any discrepancies you will be contacted directly by them.

Proofing your manuscript is done via "e-proofing". You will receive an e-mail from the typesetter when your article is ready for proofing, normally within 6 weeks of the acceptance letter, along with instructions about how to download your paper and return your corrections.

You will receive instructions for ordering offprints/reprints when you are notified that your proofs are ready for review.

Yours sincerely,

John M Fitzpatrick MCh, FRCSI, FC Urol (SA), FRCSGlas, FRCS
Editor
BJU International

BJUI

BJU INTERNATIONAL

FOR REVIEW

Nerve growth factor (NGF) combined with vascular endothelial growth factor VEGF) enhances regeneration of bladder acellular matrix graft in spinal cord injury-induced neurogenic rat bladder.

harvested for histological examination. Smooth muscle induction, collagen and nerve fiber regeneration were assessed immunohistochemically using antibodies to smooth muscle actin (α-actin), Masson's Trichrome and protein gene product 9.5 (PGP 9.5) respectively.

RESULTS: Bladder capacity and compliance were significantly increased in all BAMG groups 8 weeks after surgery compared with that before bladder replacement surgery. Bladder capacity and compliance were much higher in the VEGF and NGF combined group than in controls, or NGF and VEGF alone groups. There was no significant difference in the residual volume ratio among all groups.

CONCLUSIONS: This is the first report demonstrating that NGF has a significant synergistic effect on the development, differentiation and functional restoration of the BAMG when administered with VEGF in neurogenic bladder. Our results indicate that NGF may be a useful cytokine for enhancing the regeneration of a functional bladder following acellular matrix grafting in neurogenic rat model.

Nerve growth factor (NGF) combined with vascular endothelial growth factor VEGF) enhances regeneration of bladder acellular matrix graft in spinal cord injury-induced neurogenic rat bladder.

Nobuyuki Kikuno[1], Ken Kawamoto[1], Hiroshi Hirata[1], Kaveh Vejdani[1], Kazumori Kawakami[1], Thomas Fandel[1], Lora Nunes[1], Shinji Urakami[2] Hiroaki Shiina[2], Mikio Igawa[2], Emil Tanagho[1] and Rajvir Dahiya[1]

Authors' Affiliations:

1 Department of Urology, Veterans Affairs Medical Center and University of California, San Francisco, San Francisco, California.

2 Department of Urology, Shimane University School of Medicine, Izumo, Japan

Running title: Function of growth factors on regeneration of BAMG in neurogenic bladder

Key words: NGF, VEGF, BAMG, neurogenic bladder

Correspondence to:

Rajvir Dahiya, Ph.D., D.Sc.

Professor and Director

Urology Research Center (112F)

Veteran Affairs Medical Center and University of California, San Francisco,

4150 Clement Street, San Francisco, CA 94121.

Phone: 415-750-6964; Fax: 415-750-6639;

E-mail: rdahiya@urology.ucsf.edu

ABSTRACT

OBJECTIVE: The purpose of this study was to determine the combined effects of nerve growth factor (NGF) and vascular endothelial growth factor (VEGF) on regeneration of the bladder acellular matrix graft (BAMG) in spinal cord injury (SCI)-mediated neurogenic bladder in rats.

MATERIALS AND METHODS: For this study we used 40 female, Sprague-Dawley rats. At eight weeks after spinalization surgery (neurogenic bladder), they were divided into five groups consisting of untreated controls and those whose bladders were injected with either no growth factor, NGF (2 μg/rat), VEGF (2 μg/rat) or both at partial BAMG replacement surgery. After eight weeks, bladder function was assessed by urodynamic studies and bladders were harvested for histological examination. Smooth muscle induction, collagen and nerve fiber regeneration were assessed immunohistochemically using antibodies to smooth muscle actin (α-actin), Masson's Trichrome and protein gene product 9.5 (PGP 9.5) respectively.

RESULTS: Bladder capacity and compliance were significantly increased in all BAMG groups 8 weeks after surgery compared with that before bladder replacement surgery. Bladder capacity and compliance were much higher in the VEGF and NGF combined group than in controls, or NGF and VEGF alone groups. There was no significant difference in the residual volume ratio among all groups.

CONCLUSIONS: This is the first report demonstrating that NGF has a significant synergistic effect on the development, differentiation and functional restoration of the BAMG when administered with VEGF in neurogenic bladder. Our results indicate that

NGF may be a useful cytokine for enhancing the regeneration of a functional bladder following acellular matrix grafting in neurogenic rat model.

INTRODUCTION

Neurogenic bladder has recently become a common indication for augmentation surgery in clinical situations. Augmentation enterocystoplasty is suitable for selected patients with overactive or end-stage bladder disorders that have failed to respond to conservative therapies [1-3]. Although this technique can potentially solve the problems associated with bladder capacity, the potential surgical complications such as dysbolism, urolithiasis, and absorptive disadvantage related to the usage of bowel segments, and cancer induction have limited its application [1-3]. Recently, we and other investigators have demonstrated the applicability of bladder replacement using bladder acellular matrix graft (BAMG) as one of the alternatives to augmentation enterocystoplasty in normal or spinal cord injury (SCI)-induced neurogenic bladder rats [4, 5]. Nevertheless, these promising results have not yet become clinically relevant [6]. One major problem in these studies is the lack of a clear distinction between native and regenerated bladder in total bladder function after augmentation. Another crucial problem is the absorption and shrinkage of larger grafts, which may result from insufficient vascular supply and smooth muscle regeneration [6]. Several growth factors are believed to play an important role in organogenesis [7, 8]. Vascular endothelial growth factor (VEGF) is a multifunctional cytokine that functions as an inducer of vascular permeability and endothelial cell-specific mitogen [9]. In addition to its angiogenic function, VEGF also serves as an inhibitor of apoptosis in smooth muscle [10], and endothelial cells [11] and as a neurotrophic factor involved in nerve regeneration [12]. In contrast, nerve growth factor (NGF) is the first and best-characterized member of the neurotrophin family. NGF supports the survival and maintenance of peripheral sensory

4

and autonomic neurons, during development and adult stages [13, 14]. Exogenous NGF exogenous administration in developing animals prevents or reduces peripheral neuropathies induced by chemical and surgical insult [15-17]. However, the optimal choice and combination of growth factors to be added and the specific contribution of each growth factor to tissue regeneration remain unclear. We have previously reported that VEGF could enhance BAMG regeneration at early but not late periods after grafting in normal rats [18].

In the current study, we investigated whether NGF has a synergistic effect with VEGF on the development and differentiation of the BAMG for partial bladder replacement and whether the effect of NGF continues until the late periods after grafting in a SCI-induced neurogenic rat bladder.

MATERIAL S AND METHODS

For this study we used 40 female, Sprague-Dawley rats (Charles River, Montreal, Quebec, Canada). The animals were divided into the following five groups: Group 1 received only spinalization surgery. Group 2 received BAMG surgery without any growth factors at 8 weeks after the spinalization surgery. Group 3 and 4 received NGF or VEGF. In group 5, both NGF and VEGF were injected into the host bladder. The animals were maintained and treated according to our institutional guidelines. The local Animal Care Committee approved the experimental protocol.

The bladder from adult healthy rats were harvested and decellularized by sequential 48-hour treatments with DNase (400 U/40mL of 2M NaCl, Sigma, St. Louis), ammonium hydroxide (0.05 mM), and sodium deoxycholate (2%), followed by extensive washes with distilled water for 5 days. Acellularity was confirmed by light microscopy using H&E and methyl green pyronin staining before grafting.

Rats were anesthetized by inhalation of 2% isoflurane. A midline dorsal incision was made over lower thoracic vertebra to expose the vertebral spines and paravertebral muscles. A laminectomy of the T10 spinal vertebrae was performed and the spinal cord was completely transected at the lower thoracic level. Postoperatively the bladder was manually emptied three times daily until reflex voiding recovered after SCI.

After 8 weeks the spinalized rats were prepared for bladder replacement surgery. Under

anesthesia, 50% partial cystectomy was performed and 50% of the acellular scaffold was stitched to the bladder using absorbable 7-0 PDS running sutures. The bladder was irrigated with normal saline to test the anastomosis for leakage. Non-absorbable 6-0 Nylon marking sutures were placed at 4 points immediately under the PDS suture line. In the groups that received growth factors, a total of 2 μg of each growth factor was injected at 4 points into the bladder submucosa after partial cystectomy.

Open-abdomen cystometrography was done before grafting and repeated 8 weeks after bladder replacement. All rats underwent cystometrography under ketamine anesthesia (100 mg/kg) [19]. Cystometrography was performed according to previously published methods [18]. After the bladder was emptied, saline was infused into the bladder at 0.2 ml/min. The variables recorded during saline infusion included resting bladder pressure, threshold bladder volume (bladder capacity), threshold voiding pressure, bladder compliance, voided volume, residual urine volume (RUV), leak pointed pressure, voiding efficacy, maximal amplitude of uninhibited detrusor contractions (UIC). Voided volume and residual volume mean the amount which was leaked from the meatus around the tube and which was drained by the tube after the leakage, respectively. A contraction of 15 cm of H_2O or greater was considered an UIC. Bladder compliance was calculated by dividing the bladder capacity by the threshold voiding pressure. The presence of UIC in this model of neurogenic bladder was categorized as a hyperreflexic-bladder, whereas the absence of UIC indicated an underactive-bladder.

7

After completion of all procedures, the bladder was filled with a 10% formalin solution and removed. The bladder specimens were embedded in paraffin wax. Deparaffinized sections (4 μm) were used for staining with hematoxylin and eosin (H&E) and Masson's trichrome. Immunohistochemical staining was performed using anti-smooth muscle actin (α-actin) (Sigma, St Louis, MO) to confirm the presence of smooth muscle fibers. Immunostaining of anti-protein gene product 9.5 (PGP 9.5) (Biogenesis, Poole, UK) was used to detect nerve fibers.

The relationship between pre- and post-augmentation in urodynamic parameters was analyzed using a Wilcoxon signed-rank test. Other statistical analysis was performed using the Mann–Whitney test. A *P*-value of less than 0.05 was considered to be statistically significant.

RESULTS

All SCI-control rats without bladder replacement (group 1) showed similar urodynamic data at 8 weeks and 16 weeks after spinalization. In other words, bladder functions stabilized at 8 weeks after SCI. Therefore, we compared the urodynamic parameters at 8 weeks after spinal cord injury (as pre-replacement) and 8 weeks after bladder replacement surgery (as post-replacement) in each group. Of the 40 SCI rats, 27 rats (67.5%) developed hyperreflexic bladders with UIC and 8 (20.0%) had underactive bladders with no UIC 8 weeks after spinalization (Fig. 1). Urodynamic data after replacement was obtained from 23 rats. The bladder capacity and compliance were significantly increased in the BAMG groups 8 weeks after surgery compared to those before bladder replacement surgery. As mentioned previously, there was no significant difference in these parameters in group 1 between 8 weeks and 16 weeks after spinalization. Furthermore, both capacity and compliance were much higher in the VEGF and NGF combined group (group 5) than in the control (group 2), NGF alone (group 3) or VEGF alone (group 4) (Fig. 2). There was no significant difference in the recorded parameters between pre- and post-augmentation except for bladder capacity and compliance.

H&E and Masson's trichrome stains showed regeneration of the urothelium, blood vessels, smooth muscle, and nerve fibers into the acellular collagen scaffold at 8 weeks in all groups. The luminal surface of the implanted BAMG was completely covered with urothelium 8 weeks after grafting with no significant difference between the groups. Aggregated bundles of smooth muscle were observed underneath the urothelium and a well-defined detrusor

9

layer was identified in all groups. Smooth muscle content as determined by alpha-actin

staining was significantly greater in group 5 (VEGF and NGF combined group) than in

other groups at all points. Specific nerve cell staining using PGP9.5 showed regeneration of

nerve fiber in the groups with growth factors. PGP9.5 positive nerve fibers were observed

most abundantly in group 5 (Fig. 3). There was no harmful effect of growth factors on

bladder regeneration.

DISCUSSION

  Our data demonstrates that BAMG combined with administration of NGF and VEGF improves bladder capacity and compliance in SCI-induced neurogenic rat bladder accompanied by aggregated bundles of smooth muscle and regeneration of nerve fibers. These results indicate that NGF has a significant synergistic effect on the development, differentiation and functional restoration of the BAMG when administered with VEGF and that the combination may be useful for enhancing the regeneration of a functional bladder following grafting. There could be other factors that may also contribute to the bladder regeneration.

  When the spinal cord above the sacral segment is damaged in rats, the SCI produces an initial period of bladder areflexia that lasts for several days. After this period, rats usually develop hyperreflexic bladders [4]. On the other hand, it has been reported that detrusor areflexia happens in 30% of human patients with suprasacral SCI or disease [20, 21]. Based on these previous reports, our data that hyperreflexic bladder was induced in 67.5% of rats and underactive bladder in 20% at 8 weeks after spinalization surgery is close to previously reported values. There were no differences among the groups with regard to complications such as gross hematuria, UTI or vesical stone formation 8 weeks following spinalization surgery. However, these complications were more prevalent in rats with underactive bladders compared to the rats with hyperreflexic bladders at 8 weeks after spinalization surgery.

  We and several other investigators have already demonstrated the histological and functional regeneration of healthy and SCI-induced neurogenic bladders augmented with

11

BAMG in a rat model [4, 5]. We have also shown a favorable effect of VEGF on bladder

regeneration using BAMG at the early period in the healthy rat model [18]. However, the

effects of NGF and VEGF on regeneration of neurogenic bladder have not been

investigated. We believe that bladder regeneration using BAMG could become an effective

approach if it was adopted to treat specific pathological conditions such as sphincteric

deficiency, muscle hypertrophy and fibrosis, weak detrusor, or impaired innervations of the

bladder. In the present study, we investigated whether bladder augmentation surgery using

BAMG combined with additional cytokines can effect bladder regeneration and

development of tissues at early and late periods in order to enhance functional restoration of

SCI-induced neurogenic bladders. As autonomic neural modulation has been a major target

for both neurogenic and non-neurogenic bladder dysfunction, the restoration of neural

function may represent a major aspect of functional bladder regeneration [6].

  Recent studies provide mounting evidence for a direct involvement of NGF in the

angiogenic process, in addition to the well-established "classical" angiogenic growth

factors such as VEGF and basic FGF. For example, NGF induces *in vitro* proliferation of

umbilical cord [22] and brain capillaries [23]. The few studies in animal models to date

indicate that NGF up-regulates VEGF production [24, 25] and induces reparative

neoangiogenesis, arteriogenesis, and wound healing [26-29]. Whether these processes occur

cumulatively, directly via NGF-induced angio/arteriogenesis or indirectly via the induction

of classical "angiogenic factors" such as VEGF remains to be clarified. However, these

previous reports indicate that NGF could enhance the potential effect of VEGF.

  The current study shows that both bladder capacity and compliance were significantly

12

improved at 8 weeks after BAMG when either NGF or VEGF alone or in combination were

administered before augmentation surgery compared to no growth factor. Furthermore, the

grafted BAMG of NGF/VEGF (+/+) rats immunohistochemically had numerous

alpha-actin-positive spindle cells and PGP9.5-positive nerve cells when compared to the

other groups of rats (Fig.3). These findings support the hypothesis that the combined

administration of NGF and VEGF can accelerate the process of angiogenesis and

neurogenesis in the grafted BAMG and keep them stable until the late phase, leading to

aggregation of smooth muscle bundles and enhancement of bladder function in the BAMG.

  Although additional studies are necessary to elucidate the precise mechanism of how NGF

functions synergistically with VEGF in BAMG, our results indicate that NGF may be a

useful cytokine for enhancing the regeneration of a functional bladder following grafting.

CONCLUSION

In the present study, NGF has a significant synergistic effect on the development,

differentiation and functional restoration of the BAMG when administered with VEGF. Our

results indicate that NGF may be a useful cytokine for enhancing the regeneration of a

functional bladder following grafting.

ACKNOWLEDGMENTS

REFERENCES

1. Blaivas JG, Weiss JP, Desai P, Flisser AJ, Stember DS and Stahl PJ: Long-term followup of augmentation enterocystoplasty and continent diversion in patients with benign disease. J Urol 2005; **173:** 1631.

2. S.M. Gilbert and T.W. Hensle: Metabolic consequences and long-term complications of enterocystoplasty in children: a review. J Urol 2005; **173:** 1080.

3. Hasan ST, Marshall C, Robson WA and Neal DE: Clinical outcome and quality of life following enterocystoplasty for idiopathic detrusor instability and neurogenic bladder dysfunction. Br J Urol 1995; **76:** 551.

4. Urakami S, Shiina H, Enokida H *et al*. Functional improvement in spinal cord injury-induced neurogenic bladder by bladder augmentation using bladder acellular matrix graft in the rat. World J Urol 2007; **25:** 207.

5. Obara T, Matsuura S, Narita S, Satoh S, Tsuchiya N and Habuchi T: Bladder acellular matrix grafting regenerates urinary bladder in the spinal cord injury rat. Urology 2006; **68:** 892.

6. Kanematsu A, Yamamoto S and Ogawa O. Changing concepts of bladder regeneration. International Journal of Urology 2007; **14:** 673.

7. Baskin LS, Hayward SW, Sutherland RA, DiSandro MS, Thomson AA and Cunha GR: Cellular signaling in the bladder. Front Biosci 1997; **2:** d592.

8. Kanematsu A, Yamamoto S, Noguchi T, Ozeki M, Tabata Y and Ogawa O. Bladder regeneration by bladder acellular matrix combined with sustained release of exogenous growth factor. J Urol 2003; **170:** 1633.

9. Ferrara N and Davis-Smyth T. The biology of vascular endothelial growth factor. Endocr Rev 1997; **18:** 4.

10. Yamanaka M, Shirai M, Shiina H, Shirai M, Tanaka Y, Fujime M *et al*. Loss of anti-apoptotic genes in aging rat crura. J Urol 2002; **168:** 2296.

11. Gerber HP, Dixit V and Ferrara N. Vascular endothelial growth factor induces expression of the antiapoptotic proteins Bcl-2 and A1 in vascular endothelial cells. J Biol Chem 1998; **273:** 13313.

12. Sondell M, Sundler F and Kanje M. Vascular endothelial growth factor is a neurotrophic factor which stimulates axonal outgrowth through the flk-1 receptor. Eur J Neurosci 2000; **12:** 4243.

13. Barde YA. The nerve growth factor family. Prog Growth Factor Res 1990; **2:** 237.

14. Levi-Montalcini R. The nerve growth factor 35 years later. Science 1987; **237:** 1154.

15. Abe T, Morgan DA and Gutterman DD. Protective role of nerve growth factor against postischemic dysfunction of sympathetic coronary innervation. Circulation 1997; **95:** 213.

16. Aloe L and Levi-Montalcini R. Nerve growth factor induced overgrowth of axotomized superior cervical ganglia in neonatal rats. Similarities and differences with NGF effects in chemically axotomized sympathetic ganglia. Arch Ital Biol 1979; **117:** 287.

17. Apfel SC, Arezzo JC, Lipson L and Kessler JA. Nerve growth factor prevents experimental Cisplatin neuropathy. Ann Neurol 1992; **31:** 76.

18. Youssif M, Shiina H, Urakami S, Gleason C, Nunes L, Igawa M *et al.* Effect of vascular endothelial growth factor on regeneration of bladder acellular matrix graft: histologic

and functional evaluation. Urology 2005; **66:** 201.

19. Dahms SE, Piechota HJ, Dahiya R, Gleason CA, Hohenfellner M and Tanagho EA: Bladder acellular matrix graft in rats: its neurophysiologic properties and mRNA expression of growth factors TGF-alpha and TGF-beta. Neurourol Urodyn 1998; **17:** 37.

20. Blaivas JG: The neurophysiology of micturition: a clinical study of 550 patients. J Urol 1982; **127:** 958.

21. Pesce F, Castellano V, Finazzi Agro E, Giannantoni A, Tamburro F and Vespasiani G. Voiding dysfunction in patients with spinal cord lesions at the thoracolumbar vertebral junction. Spinal Cord 1997; **35:** 37.

22. Cantarella G, Lempereur L, Presta M, Ribatti D, Lombardo G, Lazarovici P *et al*. Nerve growth factor-endothelial cell interaction leads to angiogenesis in vitro and in vivo. FASEB J 2002; **16:**1307.

23. Moser KV, Reindl M, Blasig I and Humpel C. Brain capillary endothelial cells proliferate in response to NGF, express NGF receptors and secrete NGF after inflammation. Brain Res 2004; **1017:** 53.

24. Calza L, Giardino L, Giuliani A, Aloe L and Levi-Montalcini R. Nerve growth factor control of neuronal expression of angiogenetic and vasoactive factors. Proc Natl Acad Sci U S A 2001; **98:** 4160.

25. Manni L, Antonelli A, Costa N and Aloe L. Stress alters vascular-endothelial growth factor expression in rat arteries: Role of nerve growth factor. Basic Res Cardiol 2005; **100:** 121.

26. Emanueli C, Salis MB, Pinna A, Graiani G, Manni L and Madeddu P. Nerve growth

    factor promotes angiogenesis and arteriogenesis in ischemic hindlimbs. Circulation

    2002; **106:** 2257.

27. Graiani G, Emanueli C, Desortes E, Van Linthout S, Pinna A, Figueroa CD *et al*. Nerve

    growth factor promotes reparative angiogenesis and inhibits endothelial apoptosis in

    cutaneous wounds of Type 1 diabetic mice. Diabetologia 2004; **47:** 1047.

28. Lambiase A, Manni L, Bonini S, Rama P, Micera A and Aloe L. Nerve growth factor

    promotes corneal healing: structural, biochemical, and molecular analyses of rat and

    human corneas. Invest Ophthalmol Vis Sci 2000; **41:** 1063.

29. Yoo MH, Kim JT, Rhee CH, Park MJ, Bae IJ, Yi NY *et al*. Reverse effects of

    tetraarsenic oxide on the angiogenesis induced by nerve growth factor in the rat cornea.

    J Vet Med Sci 2004; **66:** 1091.

Figure legends

Figure 1

A. Typical cystometrogram of SCI-induced hyperreflexic-bladder (hyperreflexia): this
spinalized rat showed many large uninhibited non-voiding contractions (more than 15
cm/H_2O) during saline infusion. The size of the contractions increased with time.
Bladder capacity was approximately 3.4 ml, threshould pressure was 43.5 cm/H_2O, and
bladder compliance was 0.078.

B. Typical cystometrogram of SCI-induced underactive-bladder (areflexia): this spinalized
rat showed no uninhibited contractions during saline infusion. The bladder capacity was
approximately 4.7 ml, threshould pressure was 28.0 cm/H_2O, and bladder compliance
was 0.168

Figure 2

Bladder capacity (A) and compliance (B) at 8 weeks and 16 weeks after spinalization
surgery in group 1 (G1) and before and after BAMG replacement surgery in group 2-5
(G2-5). The (pre) and (post) means before and after BAMG replacement in group 2-5,
respectively. Asterisk (*) indicates the statistical difference of bladder capacity and
compliance between pre-BAMG replacement and post-BAMG replacement in each group.
The mark (#) indicates the statistical difference of bladder capacity and compliance
between post-BAMG replacement of G2 and G5.

Figure 3

G1. Representative H&E, Masson's trichrome, α-actin, and PGP9.5 staining of native

bladder at 16 weeks after spinalization surgery in group 1 (×200).

G2-5. Representative H&E, Masson's trichrome, α-actin, and PGP9.5 staining of BAMG at

8 weeks after grafting in group 2-5 (×200).

Fig. 1

A   **Hyperreflexia bladder**
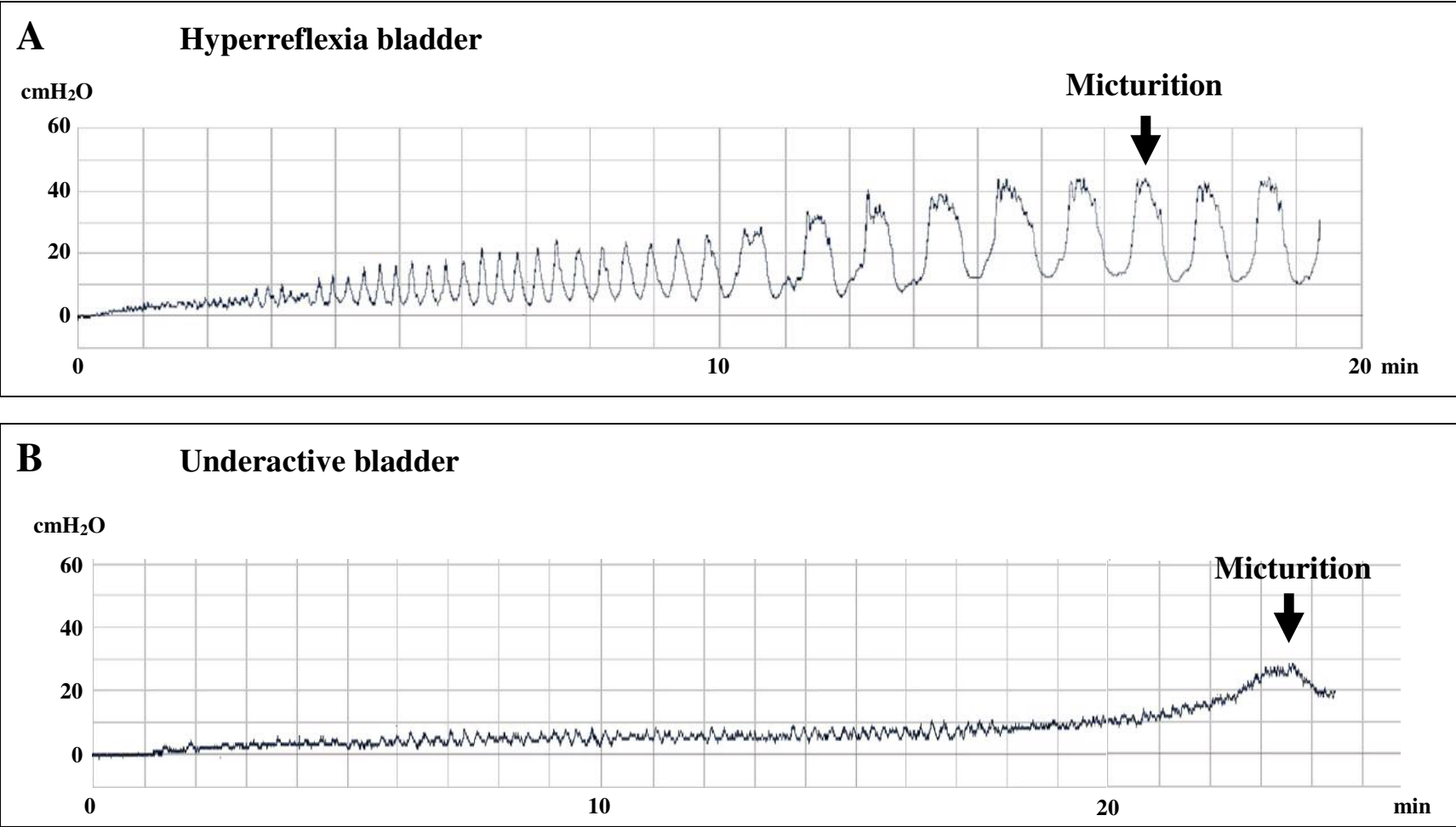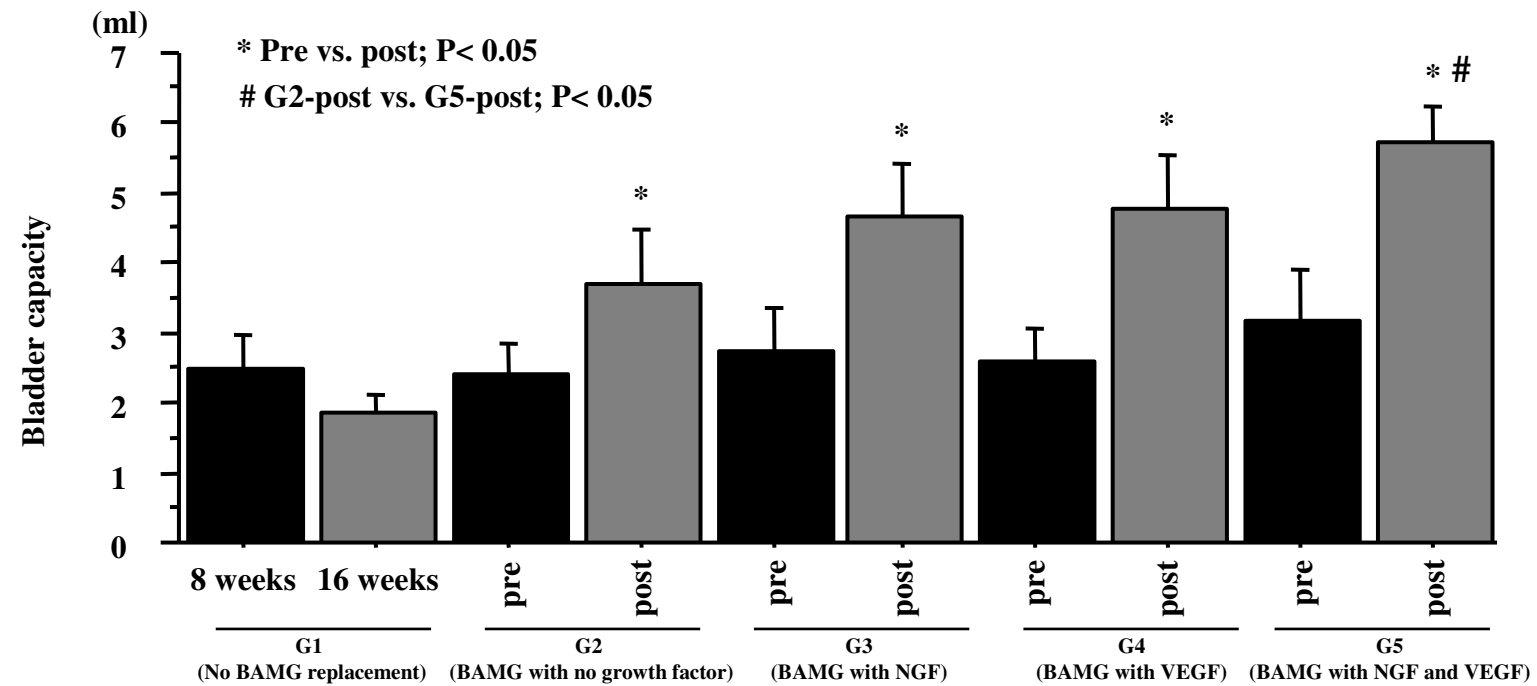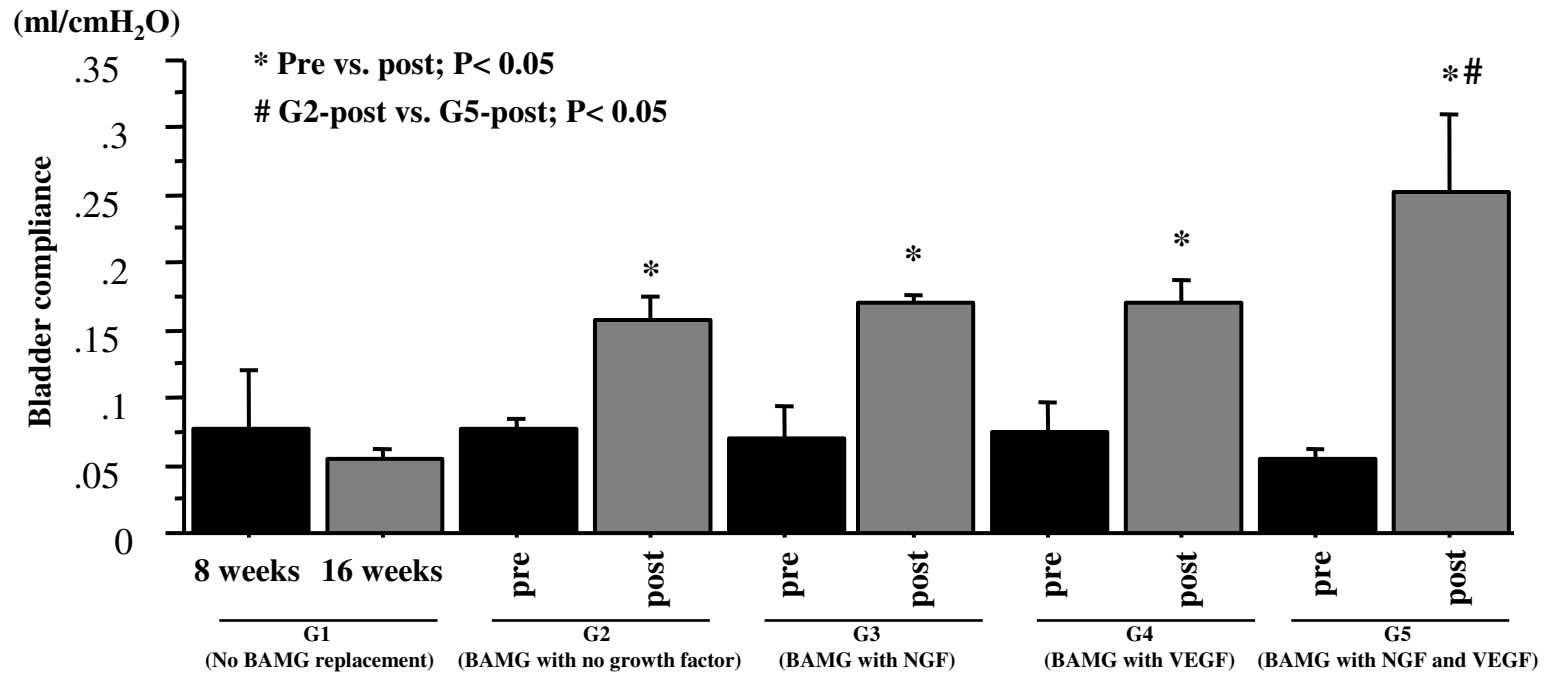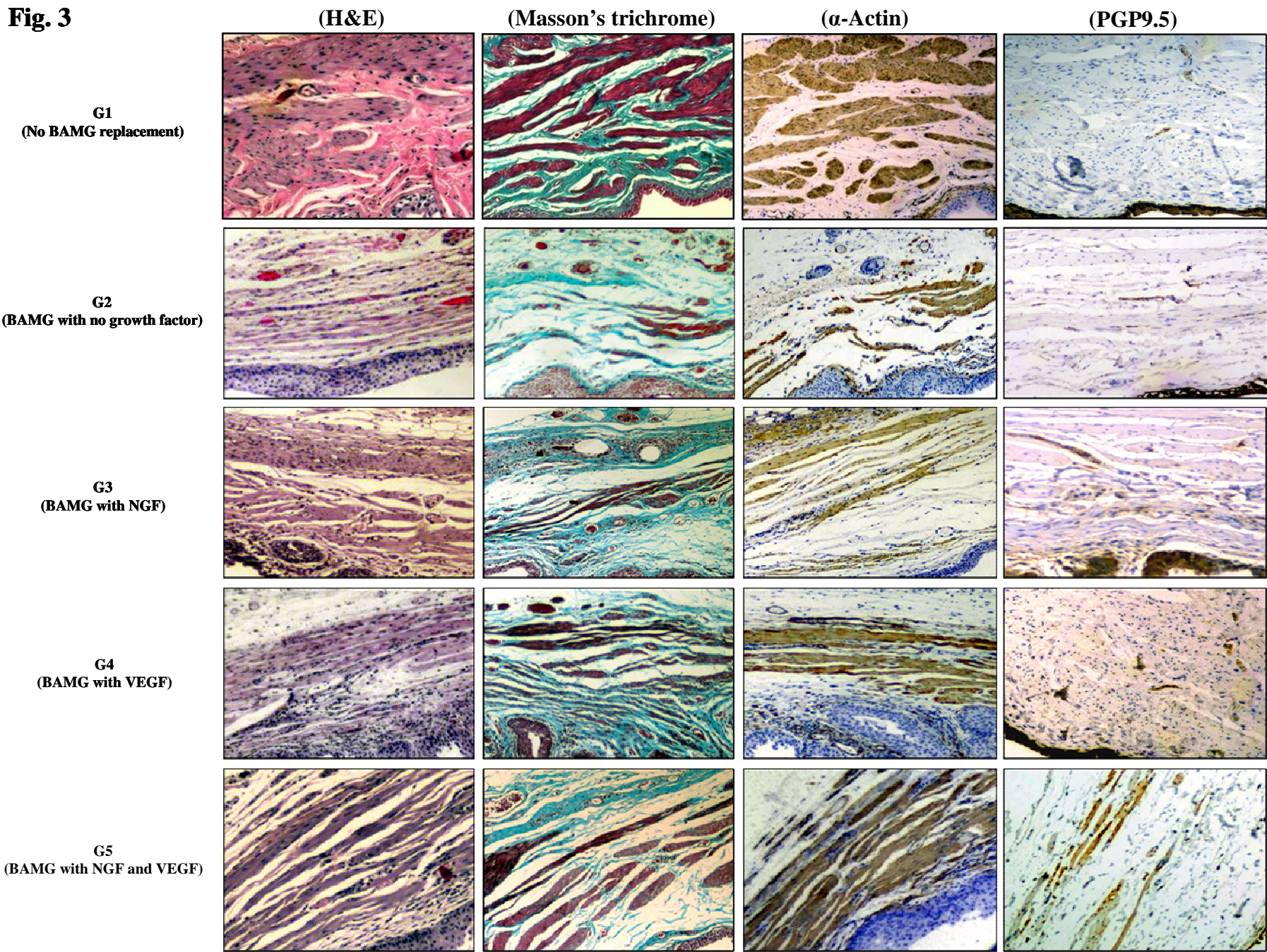
Micturition

cmH$_2$O

B   **Underactive bladder**

Micturition

cmH$_2$O

Fig. 2

Fig. 3

| | (H&E) | (Masson's trichrome) | (α-Actin) | (PGP9.5) |

G1
(No BAMG replacement)

G2
(BAMG with no growth factor)

G3
(BAMG with NGF)

G4
(BAMG with VEGF)

G5
(BAMG with NGF and VEGF)

Pilot Study 15:   <u>Final Report</u> **(funding period: 10/01/05-09/30/08)**

**Novel Neuroprotective and Regenerative Agents for Head and Spinal
Cord Injury**

Principle Investigator: Stephen Massa, M.D., Ph.D.

ABSTRACT

PURPOSE: To investigate the effects of several small molecule agonists of the neurotrophin receptors TrkB and p75NTR on outcomes of traumatic brain injury.

SCOPE: 1. Determine whether the compounds decrease the cell degeneration and death that occurs in traumatic brain injury in rats. Determine whether the compounds decrease memory and motor deficits in that model. 2. Determine the pharmacokinetics of the compounds access to the central nervous system.

MAJOR FINDINGS: In this period, we confirmed that the p75NTR ligand LM11A-31 decreases neural cell degeneration, as indicated by FluoroJadeB staining, in the hippocampus and cortex following TBI. In detailed dose-response studies, we determined that 10-100 nM LM11A-31 caused maximal proliferation of adult hippocampal neural progenitor cells and activation of AKT and upregulation of polysialylated NCAM, a marker of neuronal differentiation; the compound was also found not to decrease cell death in these cultures, suggesting that increases in cell number were due principally to increased cell division. LM11A-31 was found to be well absorbed orally and rapidly crosses the blood-brain barrier

SIGNIFICANCE: Studies to date suggest that LM11A-31 has protective effects in a traumatic brain injury model. Thus, compounds of this class may be important leads in the development of new TBI therapies.

TABLE OF CONTENTS

INTRODUCTION

In several models of CNS trauma, administration of a neurotrophin (e.g. BDNF, NGF) protects tissues acutely and promotes longer term recovery. However, the neurotrophins are poor drugs as they are labile, exhibit poor CNS penetration and may augment pain pathways. These properties are due to their polypeptide composition, and the stimulation of intersecting signalling pathways through the activation of multiple receptors. To address these problems, we have previously identified, and extensively characterized in vitro, several small, stable, non-peptidyl drug-like compounds that potently promote neuronal survival through selective interactions with the neurotrophin receptors p75NTR and TrkB. The p75NTR-directed compounds also inhibit the action of proNGF, which has been implicated in the apoptotic death of oligodendrocytes in the spinal cord and corticospinal tract neurons in the brain following trauma. In the previous period we established an injury system using a electromagnetic impactor to produce cortical injury, and delivered compounds intranasally. We found that the p75 ligand LM11A-31 and the TrkB ligand LM22A-4 significantly improved motor performance and upregulated survival signaling, and LM11A-31 improved memory performance, and preliminarily was found to decrease hippocampal cell death, and increase neural progenitor cell survival and/or proliferation, and promotes neuronal differentiation. In this period we have quantified and confirmed the effects of LM11A-31 on hippocampal and cortical cell death, studied effects on neuronal precursors in vivo, and extended observations on the mechanisms of compound effects on neural progenitor cells in culture.

BODY

In previous studies using fluorescent flow (FACscan) analysis of cells dissociated from hippocampi, we found that LM11A-31 reduced death of neuronal cells following TBI. These results were confirmed and extended with *in situ* with counting of FluoroJade B (FJB) positive cells in the hippocampus and cortex (Fig.1).
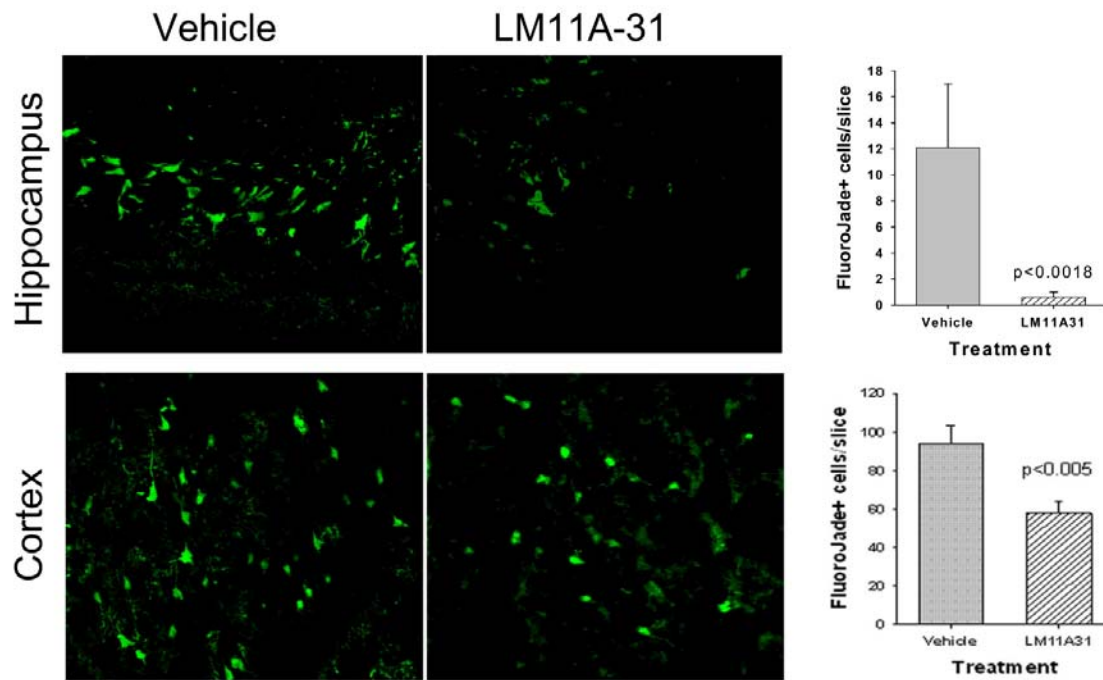

Fig. 1. LM11A-31 decreases neuronal degeneration in the hippocampus and cortex following CCI. 24 hrs following injury/dosing brains were sectioned through the area of injury (~70 slices) and every fifth section counted for numbers of FJB+ cells in the area of interest. Cortical positive cells were in the areas surrounding the impact site. Hippocampal FJB+ cells were seen in CA3 (shown above), CA1 and the dentate gyrus. Left panels, representative sections; right graphs, quantitation of numbers of FJB+ cells/slice. N=35-45 slices/condition, from 3 animals/condition. Qualitatively similar results are seen in a fourth animal not yet quantitated.

Preliminary observations suggest that the number of cells labeled with BrdU and expressing Tuj1 is increased *in vivo* in the perilesional area with LM11A-31 treatment (Fig 2); quantification is ongoing as is a repetition of the experiment.
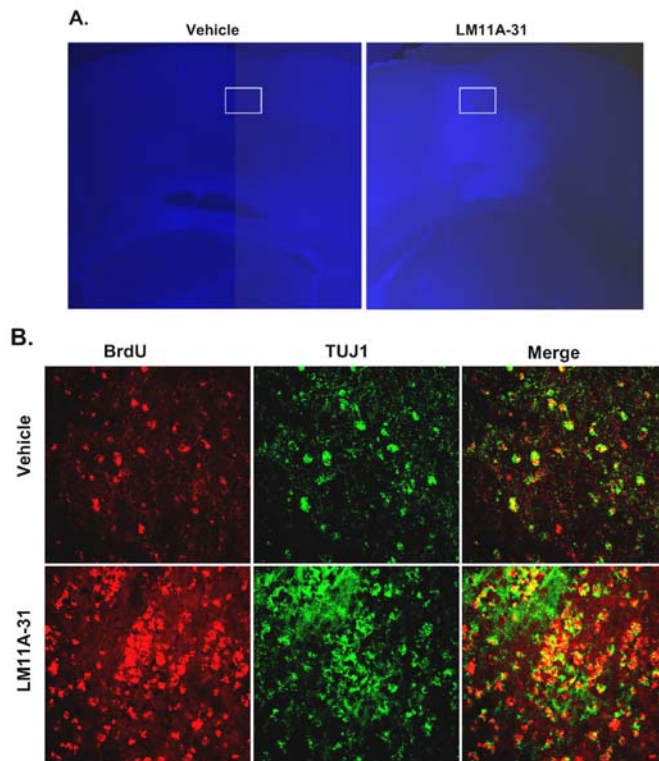

Fig. 2. Adult Sprague-Dawley rats were subjected to unilateral CCI and administered BrdU and LM11A-31 or vehicle immediately following the procedure. BrdU administration continued for 7 days, and LM11A-31/vehicle for 2 weeks, at which time they were sacrificed and immunostained for BrdU and Tuj1. **A.** DAPI staining of sections through equivalent regions at the edge of the injury cavity, showing increased cellularity in animals treated with LM11A-31. No such area of increased cellularity is observed in any animal treated with vehicle. Regions encompassed by white squares were examined with confocal microscopy. **B.** Confocal colocalization of BrdU and Tuj1 immunofluorescence in regions adjacent the injury. LM11A-31 treatment is associated with increases of both BrdU and Tuj1 signal, though whether the proportion of Tuj1-1 positive cells is different from control has not yet been determined. A similar pattern has been observed in 4 of 4 animals examined thus far.
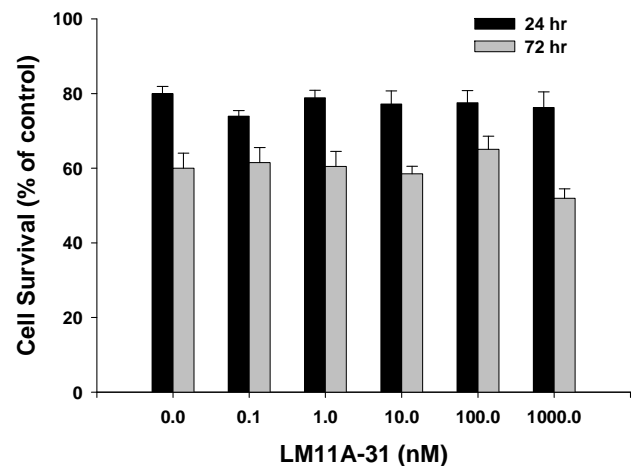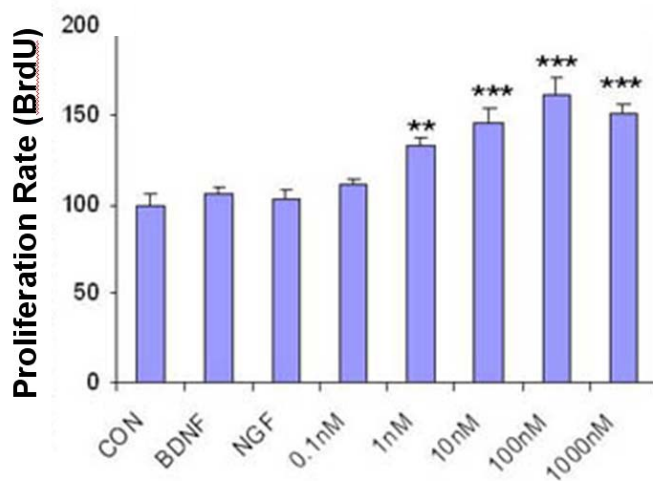

Fig. 3. LM11A-31 increases proliferation of adult hippocampal NPCs and does not prevent cell death during differentiation. **A.** Proliferating neurospheres were treated with LM11A-31 and BrdU incorporation measured with the Roche cell proliferation ELISA method. *, $P<0.02$; **, $P<0.005$, ***, $P<0.001$; N=16 per treatment drawn from one culture; repeated x3 with similar results. **B.** NPCs under differentiation conditions treated with LM11A-31 as indicated and assayed for cell survival using MTT at 24 and 72 hrs after treatment. N=8 per treatment drawn from one culture.

LM11A-31 treatment of adult hippocampal NPCs causes significant increases in proliferation beginning at 1 nM, with a maximum at ~100 nM (Fig 3A). Under differentiation conditions (removal of EGF and FGF, low serum) cells begin to die, with ~40% loss over 72 hrs. LM11A-31 does not interfere with cell death under these conditions (Fig 3B).
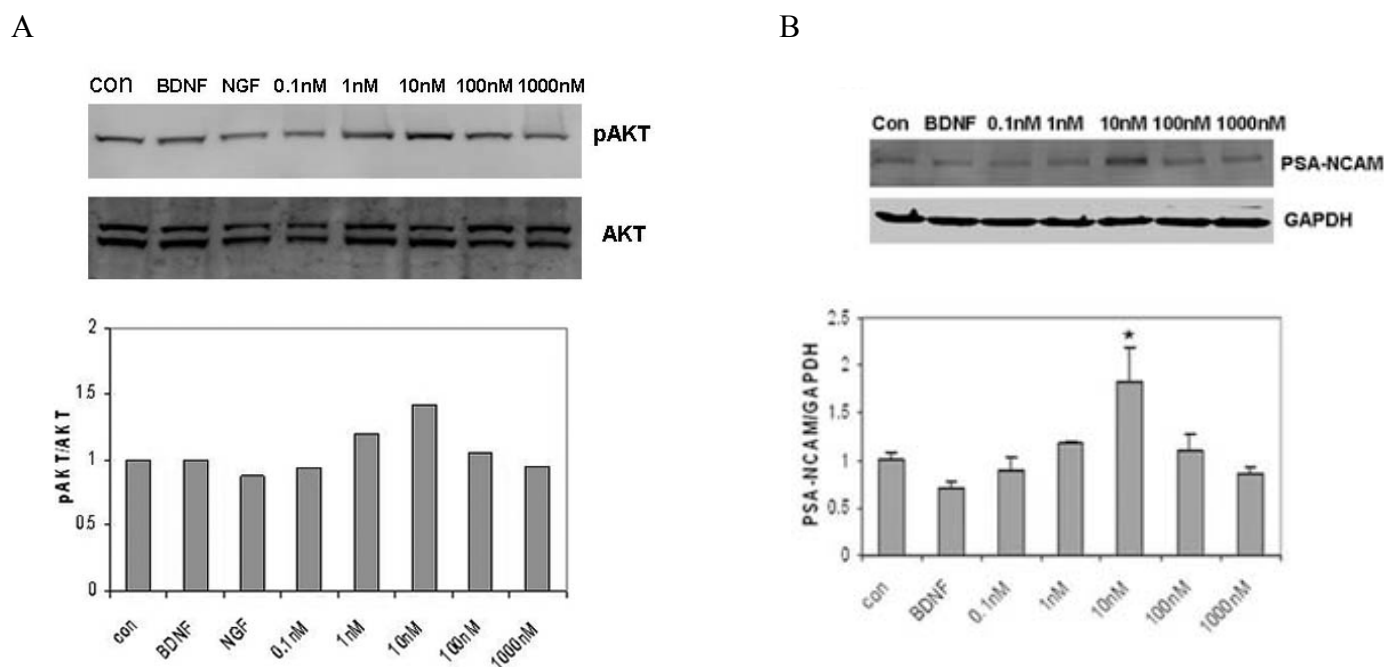
A

B

Fig. 4. LM11A-31 increases AKT activation and PSA-NCAM expression of adult hippocampal NPCs. **A.**Differentiating neurospheres were treated with LM11A-31, and AKT activation (A) and PSA-NCAM levels (B) determined; repeated x3 with similar results.

The PI3K/AKT pathway is associated neuronal differentiation of NPCs; LM11A-31 causes a modest constitutive increase in AKT activation (Fig 4A), and promotes differentiation as indicated by an increase in polysialylated-NCAM (Fig 4B), a neuronal marker. This latter increase is inhibited by LY294001, a PI3K inhibitor (not shown), implicating the PI3K/AKT pathway. Preliminary data also suggests that the effect of LM11A-31 is inhibited by blocking p75NTR antibody, confirming its action through the receptor.

Finally, in collaboration with Dr. F. Longo, we have obtained detailed pharmacokinetic data on LM11A-31 distribution in brain and plasma following iv and oral administration. As shown in Fig 5, LM11A-31 is rapidly absorbed when given orally, achieving high levels in <15 min and reaching a maximum at ~ 30 min. The t1/2 in brain is 2-3 hours, while the plasma level drops more quickly. We have also found that LM11A-31 is not metabolized significantly by human hepatic microsomes, nor does it interact with any of 50 known receptors in a CEREP screen.
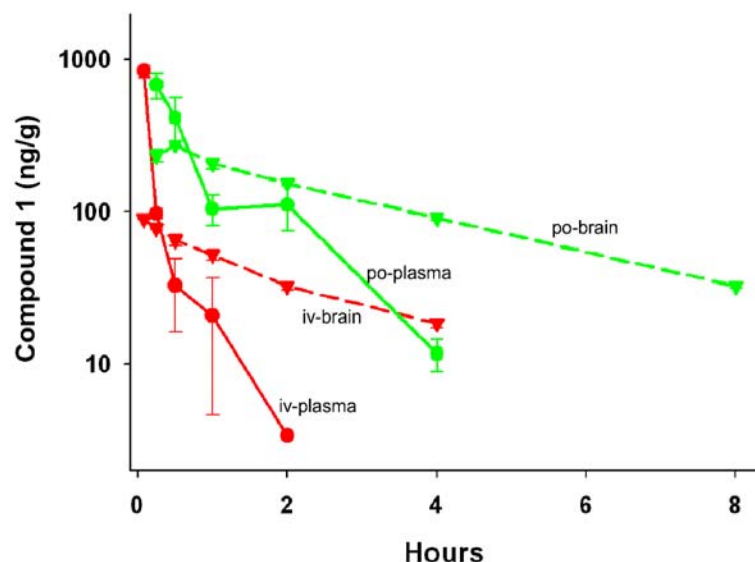
Fig. 5. Brain and plasma levels of LM11A-31 (determined by LC-MS/MS) following a single 5 mg/kg dose iv or 50 mg/kg po dose in male CD-1 mice (N=3 per time point). Concentrations in brain at 15 min following po dosing correspond to ~900 nM (if distributed throughout the water content and may be higher if confined to the extracellular space), falling to ~ 120 nM at 8 hrs. Following oral administration, the half-life in brain is 2-3 hours.

KEY RESEARCH ACCOMPLISHMENTS

1. Demonstrated LM11A-31-mediated increased survival of neurons in the hippocampus and cortex following TBI.
2. Demonstrated increased Tuj1+ cells with LM11A-31 treatment in situ following injury.
3. Demonstrated increased proliferation and differentiation of hippocampal progenitor cells with compound treatment; preliminarily found this to be dependent on PI3K/AKT pathway activation.
4. Demonstrated rapid oral uptake of the compound and transit of the blood brain barrier; the apparent half life in the brain is 2-3 hours.

REPORTABLE OUTCOMES
N/A

CONCLUSION

We have established and characterized a model of rat head injury and studied the effects of compounds from two new classes of neurotrophic compounds on post injury behavioral, cellular and biochemical parameters. Previous results suggested that a p75NTR ligand improved motor and memory behavioral outcomes, and promoted cell survival and neural progenitor growth and differentiation. In this period we have further confirmed the effects on cell survival, examined the dose response and mechanisms of effects on progenitor cell proliferation and differentiation, and examined pharmacokinetic parameters. Further studies are planned to expand on these observations and include memory testing with TrkB ligand treatment. These compounds could represent important leads in the development of new therapies for preserving and recovering tissue and function following brain and spinal cord trauma.

REFERENCES
N/A

APPENDICES
N/A

SUPPORTING DATA
N/A

Pilot Study 16:   <u>**Final Report**</u> **(funding period 05/01/06 – 09/30/08)**

Role of TREM-2 in the Microglial Response to Injured Neurons

Principal Investigator: William Seaman, M.D., Staff Physician WOC

ABSTRACT

This is a final report on this research project, which was funded from 05/01/2006 to 09/30/2008.

Brain injury can follow trauma, ischemia, or inflammation. In response to neuronal injury, microglia can initiate repair by phagocytosing dead neurons without eliciting further inflammation. Alternatively, microglia may be activated to elicit a damaging inflammatory response. Thus, like macrophages, microglia may develop into functionally diverse subsets. Prior evidence has demonstrated that phagocytosis is promoted and inflammation is inhibited when microglia express the cell surface receptor TREM2 (triggering receptor expressed by myeloid cells-2). Our studies were designed to test the hypothesis that this effect of TREM2 is promoted by the interaction of TREM2 with ligands (TREM2-L) on neurons. As evidence that neuronal cells express TREM2-L, we find that TREM2-Fc fusion protein directly stains Neuro2A neuroblastoma cells as well as cultured cortical and dopamine neurons, and apoptosis of neurons increases their expression of TREM2-L. By using a reporter cell assay, we demonstrate that neurons, especially apoptotic neurons, directly stimulate TREM2, and an anti-TREM2 mAb blocks this stimulation.   To further examine the role of TREM2 and TREM2-L in phagocytosis by microglia, we have studied BV2 microglial cells, which like freshly cultured microglia express TREM2. We find that apoptotic Neuro2A cells are phagocytosed by BV2 microglia, and engulfment is reduced by one of our anti-TREM2 mAb but not others, suggesting the presence of a functional site on TREM2 that is blocked by the antibody. TREM2 and TREM2-L interactions provide a pathway for microglial interactions with apoptotic neurons that may promote clearance of neuronal debris and allow brain repair. Our work is relevant to the military because it addresses the cellular mechanisms behind injury and recovery from traumatic brain injury. Promotion of TREM2 expression in microglia and/or of TREM2-L on neurons would promote healing without damaging inflammation.

TABLE OF CONTENTS

INTRODUCTION

The consequences of brain injury are highly regulated by microglia, brain cells of macrophage lineage. Microglia monitor the brain environment, support neuronal function, remove damaged neurons by phagocytosis, and can initiate inflammation. In response to injury, microglia release TNF-α and IL-6, as well as nitric oxide and other reactive oxygen species (ROS) (*1*). The ensuing inflammatory response is important to combat infection and as a response to injury, but it can also augment damage to the brain.

TREM2 is an immunoglobulin-like orphan receptor of the TREM family that is expressed on immature dendritic cells, activated macrophages, osteoclasts, and microglia (*2*). TREM2 and its signaling adapter molecule DAP12 are critical in maintaining homeostasis of the CNS, as demonstrated by the finding that mutations in TREM2 or DAP12 lead to a fatal neurodegenerative disease, Nasu-Hakola disease. One function of TREM2/DAP12 is to attenuate inflammatory cytokine responses of macrophages that have been stimulated by toll-like receptor (TLR) ligands (*3-5*). Furthermore, TREM2 expression in microglia impairs expression of TNFα and NOS2 even as it increases phagocytosis in response to apoptotic neurons (*6*). In mice with experimental autoimmune encephalitis (EAE), treatment with TREM2-expressing myeloid cells reduces inflammation and improves disease (*5, 7*). In all, these findings support a model in which TREM2 suppresses inflammation and promotes tissue repair through removal of apoptotic cells. Phagocytosis of apoptotic cells is important to prevent leakage of noxious contents, and to suppress unwanted immune responses (*8*).

Although clinical and experimental studies demonstrate the importance of TREM2 in the brain, ligands for TREM2 have not been characterized, and the cellular interactions required to activate the TREM2/DAP12 complex have not been defined. We therefore tested the hypothesis that ligands for TREM2 are expressed on neurons, especially apoptotic neurons, and that expression of TREM2 ligands on neurons promotes their phagocytosis by microglia and can affect the cytokine expression of microglia.

BODY

Our central hypothesis is that regulatory effects of TREM2 on microglial cell function require engagement with ligands on neuronal cells. Our secondary hypothesis is that this response is altered in the presence of bacterial lipopolysaccharide (LPS). Our <u>Specific Aims</u> are:

1. Determine the expression of TREM2 ligand on freshly prepared neurons by staining with soluble TREM2 fusion protein, both before and after induction of apoptosis in the neurons.
2. Directly demonstrate the response of TREM2 to ligands on neuronal cells by using a reporter cell line specific for engagement of TREM2.
3. Using freshly prepared microglia, examine the consequences of blocking ligand recognition by TREM2 on the microglial response to healthy and apoptotic neurons, as assessed by both phagocytosis and cytokine release.
4. By crosslinking biotinylated F(ab')$_2$ anti-TREM2 mAb on microglia, define the responses by microglia to TREM2 alone and in combination with LPS.
5. Test the consequences of exposure to LPS on the microglial response to healthy and apoptotic neurons, with or without blocking of TREM2.

Results

Specific Aim 1. Determine the expression of TREM2 ligand on freshly prepared neurons by staining with soluble TREM2 fusion protein, both before and after induction of apoptosis in the neurons.

Neurons express potential ligands for TREM2 that are increased by apoptosis

Because TREM2 on microglia has been shown to be important for the phagocytosis of apoptotic neurons, we tested the hypothesis that TREM2 recognizes a ligand on neurons that facilitates engulfment. To address this, we studied both the neuronal cell line, Neuro2A, as well as primary cultured mouse cortical and ventral midbrain neurons. We first examined these cells for the expression of TREM2 ligands (TREM2-L) by staining them with a TREM2-Fc fusion protein or, as a control, a TREM1-Fc control fusion protein. The chimeric proteins consist of the extracellular domains of the TREM receptor fused to the Fc domain of human IgG1, mutated to reduce binding to Fc receptors. By cytochemistry, staining with these soluble receptors demonstrated that both Neuro2A cells and fresh neuronal cells bind to TREM2-Fc but not TREM1-Fc (Figure 1). These data suggest that multiple cultured neuronal cells express a potential ligand for TREM2.

To assess the effects of apoptosis on the expression of TREM2-L by neuronal cells, we used flow cytometry to stain Neuro2A cells with soluble TREM2-Fc before and after induction of apoptosis by staurosporine. Consistent with our cytochemistry data, Neuro2A cells bound TREM2-Fc but not TREM1-Fc (Figure 2A). Notably, induction of apoptosis in Neuro2A cells with staurosporine resulted in a doubling of the median fluorescence intensity (MFI) of TREM2-Fc binding to the Annexin V^{hi} Neuro2A cells. These data provide evidence that apoptosis increases the expression of TREM2-L on neurons, presenting a potential mechanism for enhancing their clearance by $TREM2^+$ microglia.

Specific Aim 2. Directly demonstrate the response of TREM2 to ligands on neuronal cells by using a reporter cell line specific for engagement of TREM2.

TREM2-L on neuronal cells activate the TREM2/DAP12 receptor complex

To determine if TREM2-L on neuronal cells can functionally engage TREM2 and initiate intracellular signaling, we utilized a TREM2 reporter cell line. This was constructed from BWZ cells, a thymoma expressing the gene for β-galactosidase under the control of multiple copies of the NFAT promoter element.   We expressed both TREM2 and DAP12 in this line (BWZ.TREM2/DAP12 cells), anticipating that functional perturbation of TREM2 by ligands would lead to the phosphorylation of DAP12 and the consequent activation of the NFAT reporter and production of β-galactosidase.

We first looked at stimulation of the BWZ.TREM2/DAP12 reporter line by healthy or apoptotic Neuro2A cells.   Untreated Neuro2A cells stimulated the BWZ.TREM2/DAP12 reporter cell above the PMA alone control (Figure 2B). Strikingly, however, Neuro2A cells treated with neurotoxins, such as MPP^+ (1-methyl-4-phenylpyridinium), or subjected to serum-starvation, stimulated the reporter cell line even more (apoptotic vs. untreated Neuro2A, *p*-value = 0.0001), to a level comparable to maximal excitation by PMA and ionomycin. This response was specifically mediated by TREM2 as assessed by two means. First, BWZ cells lacking

TREM2 and DAP12 did not respond to healthy or apoptotic neuronal cells. Second, stimulation of the TREM2/DAP12 reporter cells by Neuro2A or apoptotic Neuro2A cells was partially blocked by one of our anti-TREM2 mAb (Clone 78.18) (black bars), but stimulation was unaffected by an isotype control mAb (rat IgG1) (gray bars) (*p*-values of blockade < 0.05). Stimulation of the reporter cells with the anti-TREM2 antibody alone did not induce activation (not shown). We also attempted to block TREM2 by using other anti-TREM2 mAbs in our panel, but only Clone 78.18 inhibited TREM2 activation (data not shown). These results suggest that the 78.18 mAb may specifically block a binding site engaged by TREM2-L. Alternatively, this mAb may inactivate TREM2 in a manner not mimicked by our other mAbs.

We next tested whether primary neurons, and particularly apoptotic primary neurons, could also activate TREM2. Ventral midbrain neurons (VMN) activated TREM2 and this activity was fully impaired by the anti-TREM2 mAb (Figure 2B). Healthy cortical neurons (CN) had less effect on TREM2 stimulation, although activation was completely inhibited with the anti-TREM2 mAb (p-values < 0.005) (Figure 2B). Like apoptotic Neuro2A cells, apoptotic primary neurons, either cortical or from the ventral midbrain, more effectively activated the TREM2/DAP12 reporter cells, and this activation was fully impaired by the anti-TREM2 mAb (*p*-values < 0.05) (Figure 4B). None of the neuronal cells activated the parental BWZ cell line (Figure 2B, results for ventral midbrain neurons are shown). In addition, reporter cell activation required cell-cell contact, because supernatants from apoptotic neuronal cells did not activate the BWZ.TREM2/DAP12 reporter (not shown). Thus, apoptotic neuronal cells bind to TREM2, and they activate signal transduction through the TREM2-DAP12 complex.

Specific Aim 3. Using freshly prepared microglia, examine the consequences of blocking ligand recognition by TREM2 on the microglial response to healthy and apoptotic neurons, as assessed by both phagocytosis and cytokine release.

Phagocytosis of neuronal cells requires TREM2

As a model for microglial phagocytosis of neurons, we studied the uptake of Neuro2A neuroblastoma cells by BV2 microglial cells. For these studies, Neuro2A cells were labeled with the fluorescent dye CM-DiI and apoptosis was induced by treatment with staurosporine, a kinase inhibitor. After 1 h, about 30% of BV2 microglial cells engulfed fluorescent material from the Neuro2A cells (Figure 3A). This did not reflect non-specific binding, because pretreatment of the BV2 cells with 2 µM cytochalasin D, a cytoskeletal inhibitor, abrogated phagocytosis. To confirm by microscopy the uptake of fluorescent cell particles by BV2 microglia, images were taken of the effector cells (labeled with CMFDA, green) following coincubation with CM-DiI-labeled Neuro2A cells. Untreated BV2 cells showed uptake of CM-DiI$^+$ particles, but BV2 cells treated with cytochalasin D did not (Figure 3A).

It has previously been shown that TREM2 expression on microglia promotes phagocytosis (*6*). To confirm this in our system, we used RNAi to reduce TREM2 expression in BV2 cells and compared phagocytosis by these cells to phagocytosis by BV2 cells transduced with a control lentivirus expressing only GFP. Transduction of BV2 microglial cells with shRNA targeted to TREM2 successfully reduced the surface expression of TREM2 by 84% as detected by flow cytometry (Fig 3B). BV2 cells infected with the TREM2 shRNA lentivirus demonstrated a dramatic reduction in phagocytosis compared to empty-virus infected BV2 cells (Figure 3B). In BV2 cells with reduced expression of TREM2, the percentage of cells with detectable phagocytosis dropped to 7.5±0.9% compared to untreated BV2 cells, which had 28.5±1.9%, or 26.8±2.8% for BV2 cells transduced with empty virus (*p* values <0.0001 and

equal to 0.0006, respectively), indicating that TREM2 is important for the clearance of apoptotic neuronal cells by BV2 cells (Figure 3B).

Phagocytosis of neurons by microglia is inhibited by an anti-TREM2 mAb

To determine if the interaction of TREM2 with putative TREM2-L on neuronal cells is important for the phagocytic function of microglia, we performed phagocytosis assays using BV2 microglial cells in the presence of the blocking TREM2 mAb or with an isotype control mAb. BV2 cell uptake of CM-DiI-labeled apoptotic Neuro2A cells was diminished in the presence of the TREM2 mAb, but not with the isotype control (Figure 4). Representative flow cytometric histograms are shown in Figure 4A, and a summary of multiple experiments (n=6) examining the effect of blocking TREM2 and TREM2-L interactions on phagocytosis is shown in Figure 4B. Untreated BV2 cells or isotype control BV2 cells showed comparable levels of phagocytosis, 38.8±2.9% and 36.7±2.1%, respectively. Pretreatment of the BV2 cells with the anti-TREM2 blocking mAb decreased the number of cells in which phagocytosis could be detected to 23.7±0.9%, which is 32% less than untreated cells and 35% less than cells treated with control mAb (*p* values = 0.0049 and 0.0002, respectively). Blockade of phagocytosis by an anti-TREM2 mAb supports the hypothesis that direct recognition by TREM2 of its ligands on neuronal cells is important for efficient phagocytosis by microglial cells. Blockade of phagocytosis by the anti-TREM2 mAb is incomplete, however. This may be partially explained by the inability of the antibody to completely block the activation of TREM2 by its ligands on Neuro2A cells as shown in the reporter cell assays (Figure 4B). Alternatively, other interactions may contribute to microglial phagocytosis of apoptotic neuronal cells in a manner that is independent of TREM2.

Specific Aim 4. By crosslinking biotinylated F(ab')$_2$ anti-TREM2 mAb on microglia, define the responses by microglia to TREM2 alone and in combination with LPS.

Crosslinking anti-TREM2 on the surface of microglia does not elicit a cytokine response and does not modulate the response to LPS.

Results from these studies were negative. We first attempted to crosslink anti-TREM2 with rabbit and goat antibodies to rat Ig. Here we encountered the problem that the secondary antibody alone stimulated the production of TNFa, even when we used F(ab')$_2$ fragments to avoid crosslinking Fc receptors. We therefore instead biotinylated anti-TREM2 mAb and crosslinked it on the cell surface using either soluble avidin or avidin coupled to beads. This solved the problem of background—avidin alone did not stimulate microglia—but we found little or no cytokine response to anti-TREM2, and anti-TREM2 did not affect TNFa production in response to LPS.

6

Specific Aim 5. Test the consequences of exposure to LPS on the microglial response to healthy and apoptotic neurons, with or without blocking of TREM2.

TNFa production from microglia in response to LPS, and this is suppressed by apoptotic but not fresh neuronal cells in a manner that appears independent of TREM2

To determine whether TREM2 affected production of the proinflammatory cytokine TNFa, we compared cytokine production from wildtype microglia and microglia derived from TREM2 knockout mice (an approach that became possible only at the end of the grant period, when we obtained these mice from Marco Colonna at Washington University, St. Louis). Purified microglia were cocultured with either apoptotic Neuro2A cells or untreated Neuro2A cells for 8h, and supernatants were assessed for TNFa production using Bioplex cytokine assays. Apoptotic neuronal cells alone did not stimulate TNF responses, whereas untreated neuronal cells induced low levels TNFa response (Figure 5).

LPS (1mg/ml) induced microglia to secrete TNFa and, interestingly, apoptotic neuronal cells partially suppressed this response at 8h, whereas normal neuronal cells amplified the TNF response (results not shown). Apoptotic cells thus attenuate the inflammatory response by microlgia to LPS. This effect seemed independent of TREM2, as similar results were obtained using microglia from mice genetically deficient in TREM2 This result was unexpected, since previous reports have shown that TREM2 inhibits TNFa transcription, and that TREM2 in macrophages diminishes the TNFa response following TLR stimulation. It is possible that multiple receptors recognize apoptotic neurons and may be redundant in their ability to suppress the inflammatory response..

KEY RESEARCH ACCOMPLISHMENTS

1. Neurons, especially apoptotic neurons, express functional ligands for TREM2.
2. Recognition of TREM2 ligands on apoptotic neurons facilitates efficient phagocytosis by microglia.

REPORTABLE OUTCOMES

Manuscript: Hsieh, CL, M Koike, S Spusta, E Niemi, M Yenari , MC Nakamura, and WE Seaman. Manuscript submitted. **"**A Role for TREM2 Ligands in the Phagocytosis of Neuronal Cells by Microglia"

Grant: These studies provided the preliminary data for a grant to Dr. Seaman in response to USAMRMC proposal PT075679. The grant is "The Role of Microglial Subsets in Regulating Traumatic Brain Injury," Award Number W81XWH-08-2, funded July 1, 2008 to June 30, 2012.

CONCLUSION

Our studies indicate that expression of TREM2 on microglia facilitates the phagocytosis of neuronal cells through the direct recognition of TREM2-L on apoptotic neuronal cells. When neuronal cells undergo apoptosis, they increase the expression of TREM2-L with a corresponding increase in their phagocytosis by BV2 cells, which is blocked at least in part by antibody to TREM2.

The engulfment of apoptotic cells is essential in the CNS to clear cell debris without eliciting an inflammatory response (*8*). Our colleagues and others have shown that TREM2 on macrophages can inhibit inflammatory responses induced by TLR ligands or during EAE (*3, 9*). In microglia, it has been demonstrated that TREM2 promotes phagocytosis without upregulation of antigen presentation molecules or TNFα transcripts (*6*). Taken together, these data suggest that in the CNS, TREM2 on microglia mediates a phenotype characterized by phagocytosis and non-inflammatory effect. We show here that the promotion of phagocytosis by TREM2 is controlled in part by TREM2 ligands that are upregulated on apoptotic neurons. We have not found, however, that recognition of TREM2 ligands on apoptotic neurons is necessary for their suppression of the inflammatory response by microglia.

Beyond the implications of our findings for traumatic brain injury, the control of microglial responses by TREM2-L could also have important implications for regulating inflammation and its associated damage in Parkinson's disease, Alzheimer's disease, and multiple sclerosis. With regard to Alzheimer's disease, TREM2 was found to be specifically upregulated in amyloid plaque-associated microglia in APP23 transgenic mice. Further studies are warranted to examine the function of microglia, TREM2, and TREM2-L in Alzheimer's disease (*10*).

In sum, our data suggest that TREM2 is a phagocyte receptor that is stimulated by an unknown "eat-me" signal on apoptotic neurons. The nature of the ligands for TREM2 on apoptotic neurons, however, has not yet been identified. Characterization of TREM2-L will greatly facilitate studies about TREM2 and its role in the CNS. In the meantime, understanding the mechanisms by which TREM2-L regulate microglial activity may prove important to ameliorate brain injury as well as inflammatory neurodegenerative diseases.

REFERENCES

1.	F. Aloisi, *Glia* **36**, 165 (Nov, 2001).
2.	M. Colonna, *Nat Rev Immunol* **3**, 445 (Jun, 2003).
3.	J. A. Hamerman *et al.*, *J Immunol* **177**, 2051 (Aug 15, 2006).
4.	J. A. Hamerman, N. K. Tchao, C. A. Lowell, L. L. Lanier, *Nat Immunol* **6**, 579 (Jun, 2005).
5.	L. Piccio *et al.*, *Eur J Immunol* **37**, 1290 (May, 2007).
6.	K. Takahashi, C. D. Rochford, H. Neumann, *J Exp Med* **201**, 647 (Feb 21, 2005).
7.	K. Takahashi, M. Prinz, M. Stagi, O. Chechneva, H. Neumann, *PLoS Med* **4**, e124 (Apr, 2007).
8.	K. S. Ravichandran, U. Lorenz, *Nat Rev Immunol* **7**, 964 (Dec, 2007).
9.	I. R. Turnbull *et al.*, *J Immunol* **177**, 3520 (Sep 15, 2006).
10.	S. Frank *et al.*, *Glia* **56**, 1438 (Oct, 2008).

SUPPORTING DATA
N/A

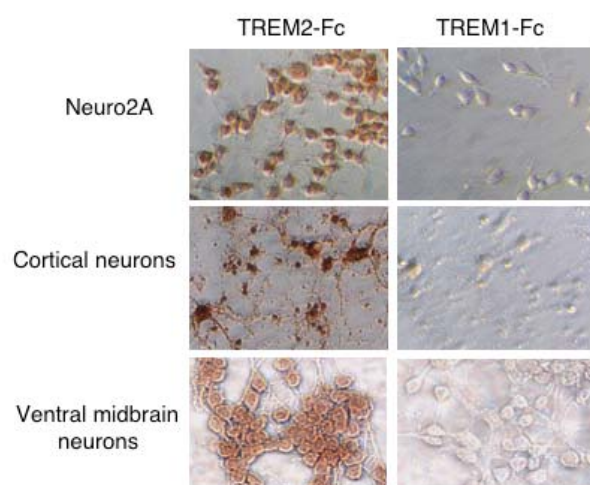**APPENDICES** (figures attached)

Figure 1. *Neuronal cells express a potential ligand for TREM2.*
Neuro2A (top), primary cortical neurons (middle), and primary ventral midbrain neurons (bottom) were cultured and stained for TREM2-L expression by cytochemistry, using a soluble TREM2-Fc fusion protein. All neuronal cells examined express putative ligands for TREM2 (brown), but not for TREM1 (right column).
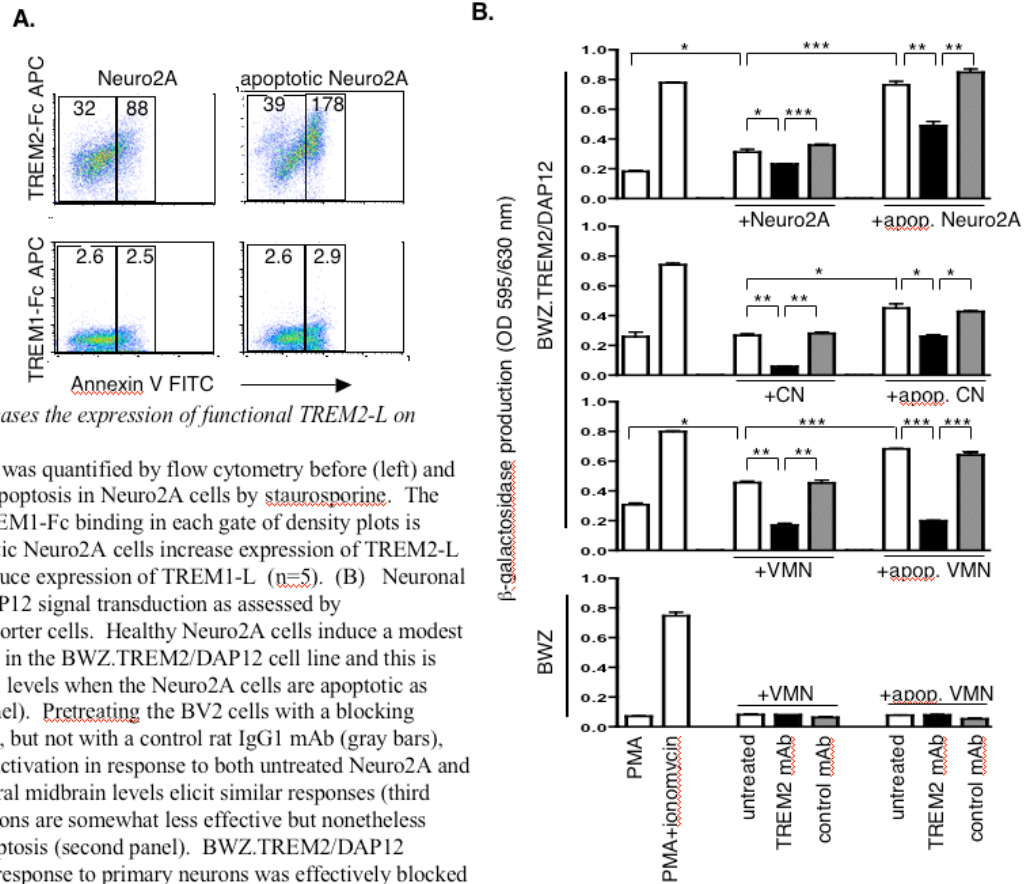
A.

B.

Figure 2. *Apoptosis increases the expression of functional TREM2-L on neuronal cells.*

(A) TREM2-L expression was quantified by flow cytometry before (left) and after (right) induction of apoptosis in Neuro2A cells by staurosporine. The MFI of TREM2-Fc or TREM1-Fc binding in each gate of density plots is shown at the top. Apoptotic Neuro2A cells increase expression of TREM2-L by 3-4 fold, but do not induce expression of TREM1-L ($n=5$). (B) Neuronal cells activate TREM2/DAP12 signal transduction as assessed by BWZ.TREM2/DAP12 reporter cells. Healthy Neuro2A cells induce a modest level of cellular activation in the BWZ.TREM2/DAP12 cell line and this is increased to near-maximal levels when the Neuro2A cells are apoptotic as induced by MPP$^+$ (top panel). Pretreating the BV2 cells with a blocking TREM2 mAb (black bars), but not with a control rat IgG1 mAb (gray bars), partially reduces cellular activation in response to both untreated Neuro2A and apoptotic Neuro2A. Ventral midbrain levels elicit similar responses (third panel), while cortical neurons are somewhat less effective but nonetheless stimulatory following apoptosis (second panel). BWZ.TREM2/DAP12 reporter cell activation in response to primary neurons was effectively blocked with the TREM2 mAb. None of the neuronal cells activate the parental BWZ reporter cell line (representative results for ventral midbrain neurons are shown in the bottom graph). (*p-value <0.05, **p-value < 0.005, ***p-value < 0.0005).
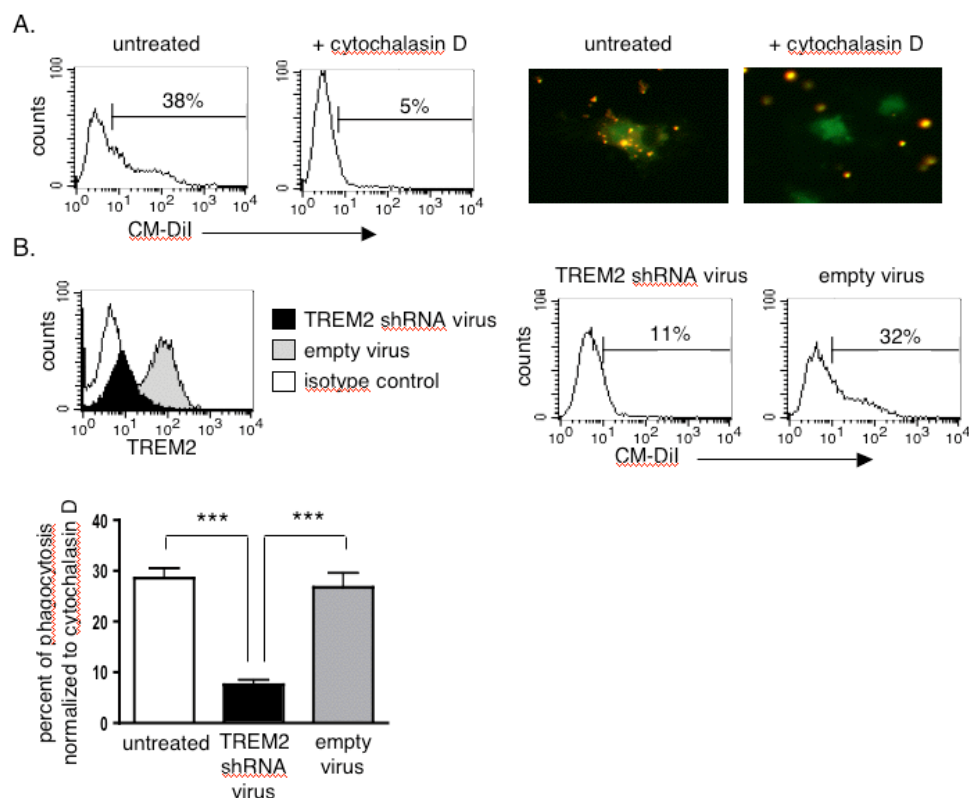
Figure 3. *Efficient phagocytosis of neuronal cells requires TREM2.*
(A) Phagocytosis of apoptotic Neuro2A cells (>50% Annexin V+) by BV2 cells, assessed by flow cytometry (left two panels) or fluorescence microscopy (right two panels). BV2 cells are labeled with CMFDA (green) and cocultured with apoptotic Neuro2A cells (red-yellow). Phagocytosis is inhibited by cytochalasin D in both assays. (B) Phagocytosis of Neuro2A cells is reduced in BV2 cells following lentiviral-mediated RNAi against TREM2. RNAi reduces the expression of TREM2 by 84% (left) and reduces the percent of cells with detectable phagocytosis to 11% from 32% for cell transduced with empty virus as shown by representative histograms (right). Quantification of 3 experiments shows that phagocytosis by BV2 cells deficient in TREM2 is reduced to 7.5 ± 0.9% from 28.5 ± 1.9% for untreated cells and from 26.8 ± 2.8% for cells transduced with empty virus (***p-value ≤ 0.0006) (bottom).
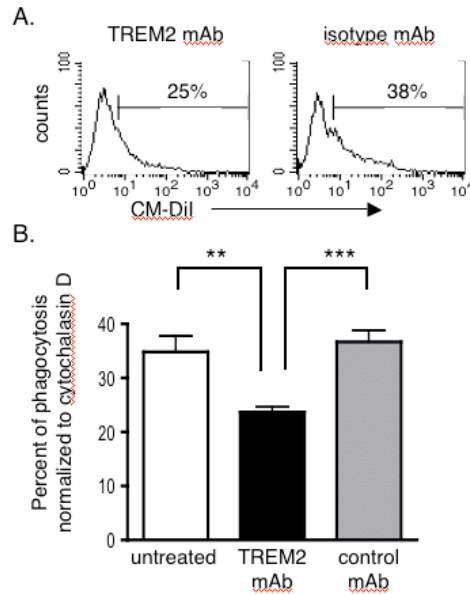
A.

B.

Figure 4. *Efficient phagocytosis of neuronal cells requires TREM2-L recognition.*
A mAb to TREM2 partially inhibits phagocytosis of apoptotic Neuro2A cells by BV2 microglia. (A) An example of the effect of anti-TREM2 on phagocytosis, showing a reduction of cells with detectable phagocytosis from 38% to 25%. (B) Summary of 6 experiments, showing a reduction to 23.7 ± 0.9% of effector cells engulfing targets compared to untreated (34.8 ± 2.9%) and control mAb (36.7 ± 2.1%) treated BV2 cells. The TREM2 mAb partially decreases phagocytosis by 32-35%. (**p-value =0.005, ***p-value=0.0002).
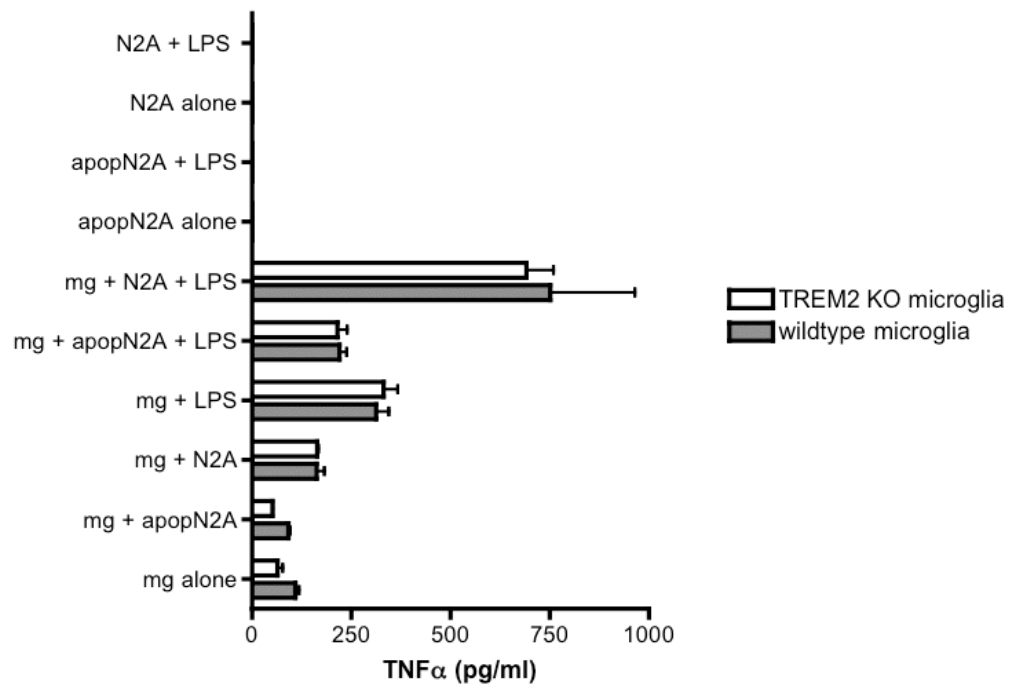

Figure 5. *Apoptotic neuronal cells suppress TNF secretion from LPS-treated microglia..*
Neonatal microglia isolated from wildtype C57BL/6 mice or from TREM2-/- were cocultured with apoptotic Neuro2A (apopN2A), untreated Neuro2A (N2A), or in combination with LPS (1 μg/ml). Supernatants were obtained after 8h and measured for TNF using a Bioplex cytokine assay. In the presence of LPS, apopN2A suppressed TNF secretion, while normal N2A cells amplified the cytokine response. The suppression of TNF by apopN2A is independent of TREM2 since no significant differences between wildtype and TREM2-deficient microglia were detected.

12